APPENDIX A

2012 GEORGIANA SLOUGH NON-PHYSICAL BARRIER STUDY ACOUSTIC TAG SYSTEM DATA COLLECTION

2012 GEORGIANA SLOUGH NON-PHYSICAL BARRIER STUDY
ACOUSTIC TAG SYSTEM DATA COLLECTION

Draft Report

HTI Project 3292

Prepared for

California Department of Water Resources
1416 Ninth St, Room 252-35
P.O. Box 942836
Sacramento, CA 94236-0001

Prepared by

Hydroacoustic Technology, Inc.
715 NE Northlake Way
Seattle, WA 98105
(206) 633-3383
consulting@htisonar.com

December 17, 2012

TABLE OF CONTENTS

page

1.0 INTRODUCTION A-1
1.1 Study Area Description A-1

2.0 Objectives…… A-5

3.0 METHODS…… A-5
3.1 Acoustic Tag System Overview A-5
3.2 System Components A-5
3.3 Monitoring Equipment Deployment and Hydrophone Array Design A-12
3.4 Data Collection/Back-up Procedures A-14
3.5 System Testing Procedures A-14

4.0 References…… A-19

Appendix A. Summary of Releases during the GSNPB Study, 2012 ..... A1

LIST OF FIGURES

page

Figure 1. Location of Hydrophone Array and Non-Physical Barrier (NPB) installed in the Sacramento River at the divergence of the Georgiana Slough, 2012 (Adapted from Department of Water Resources). 2

Figure 2. Basic components of the Non-Physical Barrier (NPB) installed at Georgiana Slough, 2012. (Adapted from Bowen and Bark 2010). 3

Figure 3. Conceptual Layout of the Georgiana Slough NBP (data provided by Fish Guidance Systems and adapted by AECOM). 4

Figure 4. Pulse-rate interval also referred to as the “Tag Period” or “ping” rate is the interval between each tag transmission. 6

Figure 5. Tag Pulse Length is the amount of time the tag transmits its pulse. The interval between transmissions is the tag period. 6

Figure 6. Example graphic from the data collection program showing the primary (tag period) and secondary (subcode) transmit signal returns from a *Model 795 Acoustic Tag*. 7

Figure 7. Acoustic Tag Receiver signal processing procedures. 9

Figure 8. An echogram of detected signals using time window 1100ms (vertical scale) shown in *MarkTags*. 11

Figure 9. Positioning of an acoustic tag in three dimensions with a four-hydrophone array. 11

Figure 10. Location of the 34 hydrophones as deployed at Georgiana Slough NPB 2012. 13

Figure 11. Results of a "ping-around" test in *MarkTags* program. 16

Figure 12. *MarkTags* marked signals (yellow) received from a transmitting hydrophone, included in the ping around analysis. 17

LIST OF TABLES

page

Table 1. Acoustic tags used for the GSNPB study in 2012. 6

Table 2. Acoustic tag subcodes used for Chinook, steelhead, and predators at GSNPB study in 2012. 7

1.0 INTRODUCTION

The Sacramento River Delta is a complex network of natural and man-made channels connecting the Sacramento River with San Francisco Bay (Nichols et al 1986). The decline of Chinook salmon (*Oncorhynchus tshawytscha*) stocks emigrating from its tributaries are likely attributable to the cumulative effect of a number of anthropogenic and natural changes in the Delta. Efforts to protect and restore salmon stocks are guided by scientific findings outlined in the June 2009, National Marine Fisheries Service (NMFS) Jeopardy Biological Opinion (BO) on the operation of the State Water Project (SWP) and Central Valley Project (CVP).

The NMFS BO recognized that operations at the CVP/SWP jeopardize populations of several federally listed species, including Chinook salmon. Recent studies have indicated that operations at the CVP/SWP can affect juvenile Chinook salmon migration rates, vulnerability to predation, feeding success growth rates and overall survival (Perry et al 2011). Studies using hydroacoustic sampling indicated that juvenile Chinook salmon migrating downstream in the Sacramento River have an increased potential for entering the interior Delta via the Georgiana Slough and other pathways (Horn and Blake 2004). One of the Reasonable and Prudent Alternatives to Jeopardy under the NMFS BO required evaluation of potential engineering solutions to prevent emigrating juvenile salmonids from entering Georgiana Slough and the interior Delta from the Sacramento and San Joaquin Rivers.

Based on preliminary results from studies of a non-physical barrier (NPB) installed to keep Chinook salmon from entering the Old River (Bowen et al. 2009, Bowen and Bark 2010), a similar configuration to prevent emigrating juvenile salmonids from entering Georgiana Slough was installed in 2011 (California Department of Water Resources 2012). The Georgiana Slough Non-Physical Barrier (GSNPB) is intended to protect out-migrating salmon and steelhead smolts by keeping them in the Sacramento River and preventing them from entering the central and south Delta with the goal of increasing the survival rate of salmon as they move through the Sacramento River to San Francisco Bay. DWR re-installed the GSNPB in late winter/early spring 2012 to continue the experimental evaluations of barrier performance.

The 2012 GSNPB study was conducted under the authorization of AECOM Task Order No. 6, Project DWR GSNPB 2012 Study Implementation, 60247108 Task 4.2. This document is submitted as fulfilment of the HTI Task 2 Draft Data Collection Report called for in the Scope of Work. This report contains materials and methods implemented for collecting, processing and storing the 3-D tracked fish data. The final study results of this and other components of the study will be presented in the Draft and Final Project Report entitled “2012 Effectiveness of a Non-Physical Fish Barrier at the Divergence of the Sacramento River and Georgiana Slough (CA)”. The processed data, including the electronic EonFusion database, processed data, and raw data, will also be included as appendices to the Final Project Report.

1.1 Study Area Description

Hydroacoustic Technology Inc. (HTI) monitored and collected data at an acoustic fish tracking system, with the hydrophone array installed by AECOM, California Department of Water Resources (DWR), and the US Geologial Survey (USGS) at the NPB located in the Sacramento River at the divergence of the Georgiana Slough near the town of Walnut Grove, CA (Figure 1). The physical installation of the NPB occurred primarily in February 2012. The 2102 GSNPB installation was similar to the configuration that was deployed and tested at the site in 2011, which in turn was based on the NPB installed previously at Old River in 2010 (Bowen and Bark 2010). Designed by Fish Guidance Systems and also called the “Bio-Acoustic Fish Fence”, or BAFF, the structure is an alternative to a solid physical fish barrier which allows free flow of water and does not obstruct boat traffic (Welton et al. 2002). The GSNPB components included sound projectors, an air bubble curtain, and strobe lights (Figure 2). The air bubble curtain constrains the sound signal to create a more coherent sound source to guide fish. The GSNPB was attached to pilings and installation was completed by March 5, 2012 (Figure 3).

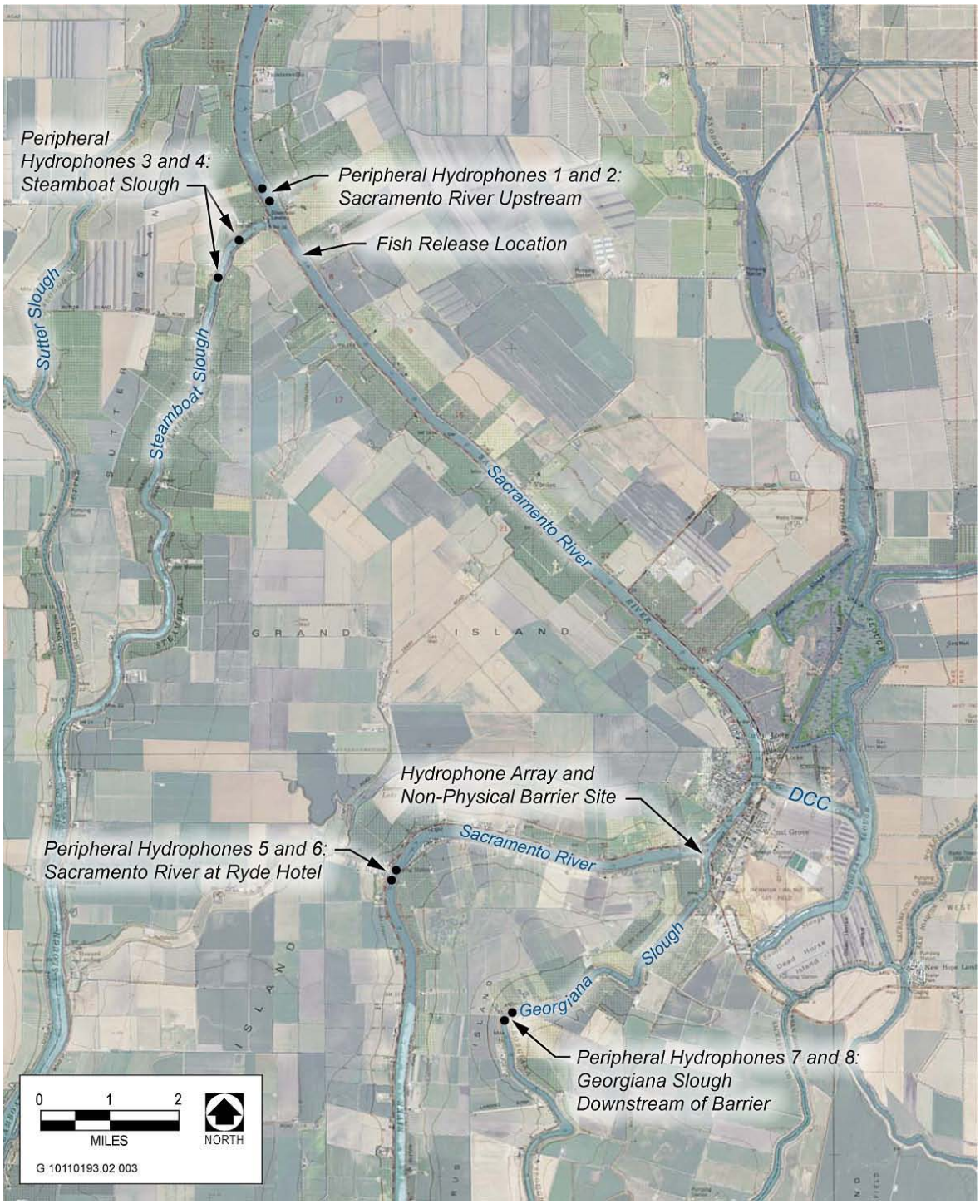

Figure 1. Location of Hydrophone Array and Non-Physical Barrier (NPB) installed in the Sacramento River at the divergence of the Georgiana Slough, 2012 (Adapted from Department of Water Resources).

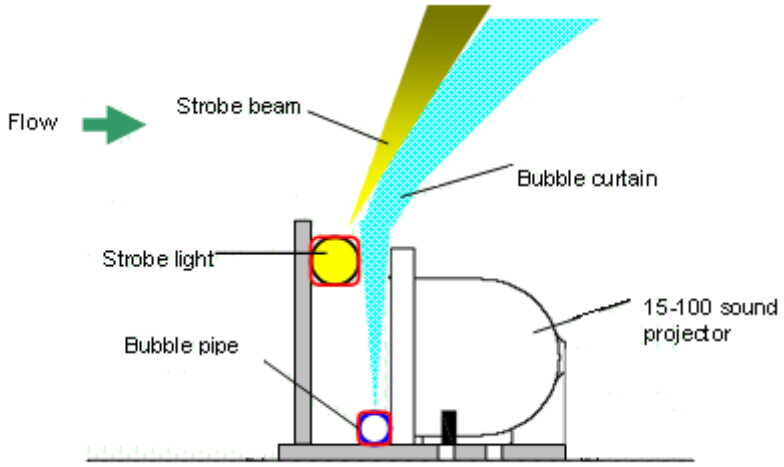

Figure 2. Basic components of the Non-Physical Barrier (NPB) installed at Georgiana Slough, 2012. (Adapted from Bowen and Bark 2010).

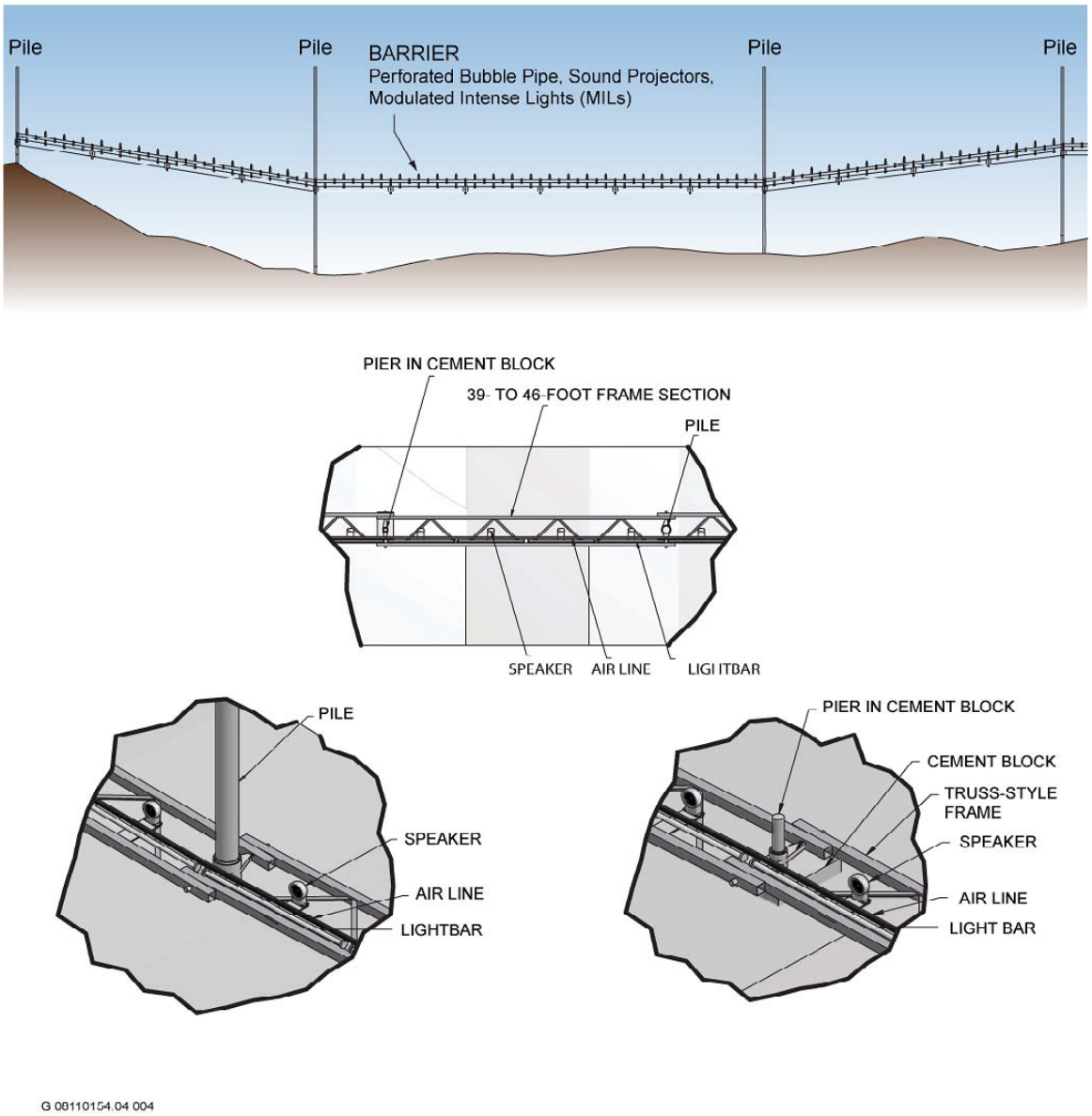

Figure 3. Conceptual Layout of the Georgiana Slough NBP (data provided by Fish Guidance Systems and adapted by AECOM).

2.0 OBJECTIVES

The objective of this component of the study was to collect data that would allow tracking of the movement of fish implanted with acoustic tags within the array of hydrophones installed in the vicinity of the GSNPB.

3.0 METHODS

3.1 Acoustic Tag System Overview

Acoustic tag tracking was performed using the system developed by Hydroacoustic Technology, Inc. (HTI), Seattle, Washington. The HTI *Acoustic Tag Tracking System* (ATS) uses a fixed array of underwater hydrophones to track movements of fish implanted with acoustic tags. As fish approached the study area, the transmitted signal from each tag was detected and the arrival time recorded at several hydrophones. The difference in tag signal arrival times at each hydrophone was used to calculate a two or three-dimensional position. The ATS includes the following hardware and software components:

- A tag programmer that activates and programs the tag.
- Acoustic tags each transmitting a pulse of sound at regular intervals.
- Hydrophones that function like underwater microphones, listening within a defined volume of water.
- Cables connecting hydrophones to tag receivers.
- Tag receivers connected to a computer that receives the tag signal from the hydrophones, conditions the signal and using specialized software, outputs the data into a format that can be stored in data files.

3.2 System Components

Acoustic Tags

All tags used in this study operated at a frequency of 307 kHz and were encapsulated with a non-reactive, inert, low toxicity resin compound (Table 1). The tags utilized “pulse-rate encoding” which provided increased detection range, improved the signal-to-noise ratio and pulse-arrival resolution, and decreased position variability when compared to other types of acoustic tags (Ehrenberg and Steig 2003). Pulse-rate encoding uses the interval between each transmission to detect and identify the tag (Figure 4). Each tag was programmed with a unique pulse-rate to track movements of individual tagged fish.

The pulse-rate is measured from the leading edge of one pulse to the leading edge of the next pulse in sequence. By using slightly different pulse-rates, tags can be individually identified. The timing of the start of each transmission is precisely controlled by a microprocessor within the tag. Each tag was programmed to have its own tag period to uniquely identify between tags. Test tag periods ranged between 2.007-4.086 s with beacon tag intervals of 13.011-13.095 s. The amount of time that the tag actively transmits is the pulse length (or pulse duration) (Figure 5). For this study, the transmit pulse length was 3.0 ms.

Table 1. Acoustic tags used for the GSNPB study in 2012.

Model Number	Diameter (mm)	Length (mm)	Weight in Air (g)	Tagged Species	Number Released
795Lm	6.5	16.5	0.65	Chinook smolt	1,501
795LD	6.5	18	1.0	Steelhead smolt	299
795LG	11	25	4.5	Predator	50

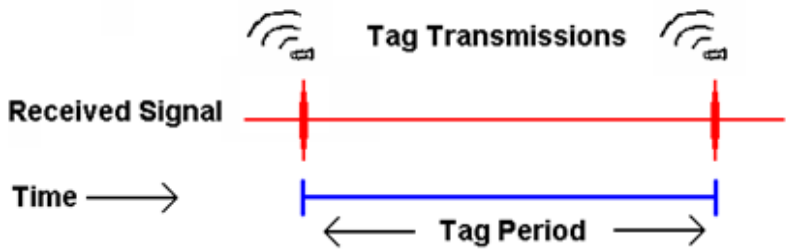

Figure 4. Pulse-rate interval also referred to as the "Tag Period" or "ping" rate is the interval between each tag transmission.

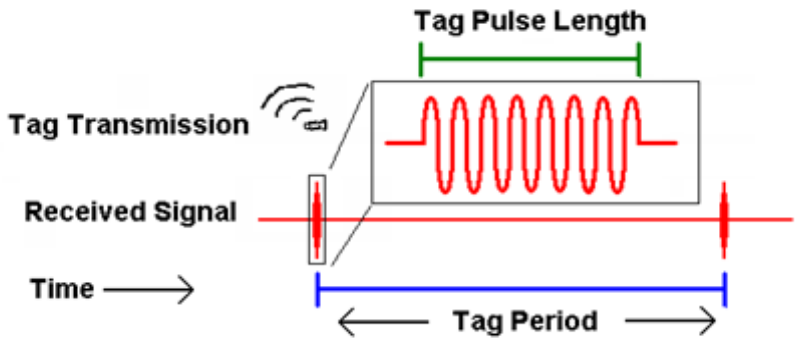

Figure 5. Tag Pulse Length is the amount of time the tag transmits its pulse. The interval between transmissions is the tag period.

In addition to the tag period, the HTI tag double-pulse mode or "subcode" option can be used to increase the number of unique tag ID codes available. Using this tag coding option, each tag is programmed with a defined primary tag period, and also with a defined secondary transmit signal, called the subcode. This

subcode defines a precise elapsed time period between the primary and secondary tag transmissions (Figure 6). There are 31 different subcodes possible for each tag period, resulting in over 100,000 total unique tag ID codes. Twenty-one subcodes were used for the GSNPB study in 2012 (Table 2).

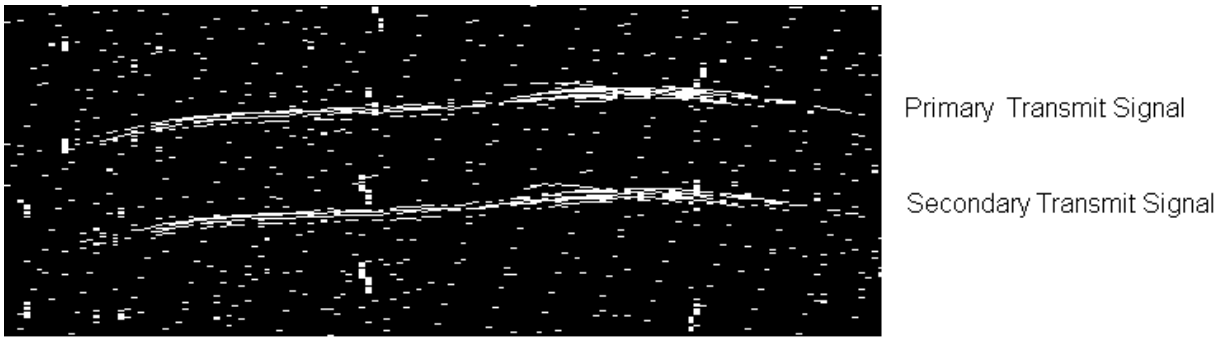

Figure 6. Example graphic from the data collection program showing the primary (tag period) and secondary (subcode) transmit signal returns from a *Model 795 Acoustic Tag*.

Table 2. Acoustic tag subcodes used for Chinook, steelhead, and predators at GSNPB study in 2012.

Subcodes	Species	No. Released	Start date	End date
15	Predatory fish	50	2/26/12 10:49	5/12/12 15:38
4	Chinook	98	3/6/12 15:01	4/7/12 0:01
10	Chinook	58	3/6/12 15:01	4/23/12 20:56
13	Chinook	94	3/6/12 15:01	3/22/12 6:00
17	Chinook	93	3/6/12 15:01	3/22/12 6:00
31	Chinook	97	3/6/12 15:01	3/22/12 6:00
29	Chinook	75	3/12/12 9:02	3/22/12 6:00
23	Steelhead	99	3/18/12 12:06	4/15/12 3:00
12	Chinook	99	3/22/12 9:03	4/3/12 17:58
19	Chinook	99	3/22/12 9:03	4/3/12 17:58
25	Chinook	99	3/22/12 9:03	4/3/12 17:58
28	Chinook	98	3/22/12 9:03	4/3/12 17:58
22	Chinook	99	3/22/12 21:03	4/22/12 18:00
2	Chinook	100	4/7/12 9:02	4/10/12 5:59
27	Chinook	98	4/10/12 9:05	4/13/12 9:06
11	Steelhead	99	4/11/12 6:02	4/13/12 3:03
18	Steelhead	100	4/13/12 3:03	4/15/12 3:00
7	Steelhead	1	4/13/12 9:05	4/13/12 9:05
1	Chinook	100	4/13/12 9:06	4/16/12 12:01
20	Chinook	97	4/16/12 12:01	4/19/12 11:57
26	Chinook	97	4/19/12 15:00	4/23/12 9:02

Hydrophones

A thirty-four node array of hydrophones was installed for this study. The *Model 590* hydrophones operated at 307 kHz and included a low-noise preamplifier and temperature sensor. Hydrophone directional coverage was approximately 330 degrees, with equivalent sensitivity in all directions except for a 30 degree limited sensitivity cone directly behind the hydrophone where the cable was attached. The hydrophone sensor element tips were encapsulated in specially treated rubber with acoustic impedance close to that of water to ensure long-term reliability. The hydrophone and connector housing were made of corrosion resistant aluminum-bronze alloy. Cables were twisted pair wire and double shielded for noise reduction. Individual cable lengths ranged from 50 to 500 ft.

The hydrophone preamplifier circuit provided signal conditioning and background noise filtering for transmission over long cable lengths and in acoustically noisy environments. A calibration circuit in the preamplifier provided a method for field testing hydrophone operation and was used to measure the signal time delays between all hydrophones within the array. The *Model 590* hydrophones included temperature sensors to measure water temperature variations, which impact the velocity of the tag signal transmission in water.

To measure signal time delays, the calibration circuit for each hydrophone is set to transmit ("ping") while all other hydrophones are set to receive. This procedure is repeated for all hydrophones in the array. Data from each hydrophone are processed to measure the time delay and water temperature from each hydrophone. Accurate measurement of signal time delays between hydrophones will provide the position data to locate the array in UTM or Lat/Lon coordinates and provides the resolution necessary for sub-meter two- and three-dimensional positioning.

Acoustic Tag Receiver

Three HTI *Model 290 Acoustic Tag Receivers* (ATR) were used to monitor at the GSNPB. Each ATR is designed to receive up to 16 separate channels; with one channel assigned to each hydrophone. Each ATR was connected to a personal computer used to analyze and store the acoustic data. The three ATR's were synchronized utilizing an internal GPS in each of the receivers. An individual raw data file was created for each sample hour, at each ATR. Filters in the acoustic tag receiver were set to identify the acoustic tag sound pulse and discriminate tags from the ambient background noise.

When the tag signal is received by the ATR, a series of signal processing steps are completed (Figure 7). The envelope detector receives the signal and outputs the positive "envelope" with the carrier frequency removed. This detected echo envelope is then digitized at a rate of 12 kHz. A real-time adaptive noise threshold is set based on a 1 second window of the background noise level for each hydrophone independently which is updated every 0.083 msec. The pulse width of each pulse that exceeds a predetermined threshold is measured at the -3, -6, and -12 dB points and the pulse peak amplitude is located and measured.

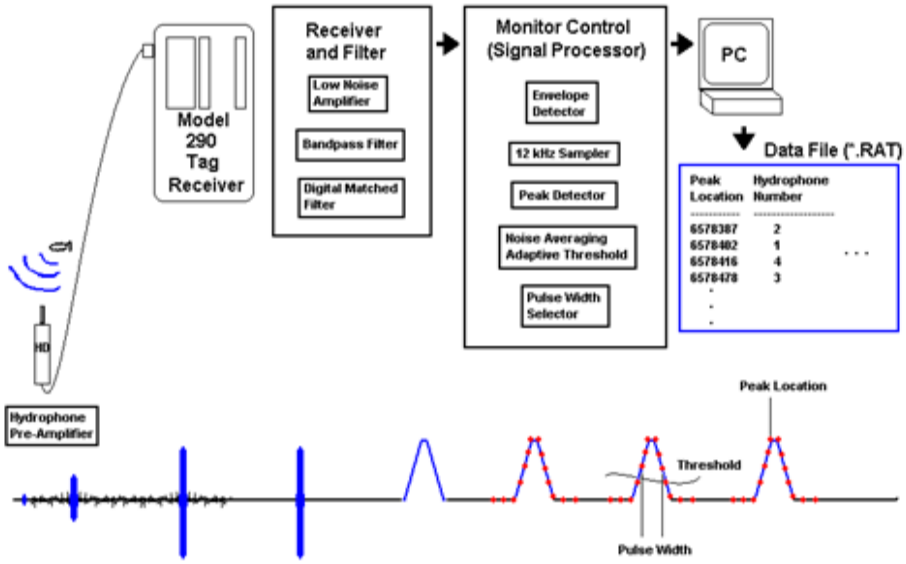

Figure 7. Acoustic Tag Receiver signal processing procedures.

The ATR pulse measurements are reported for each single echo from each hydrophone and written to Raw Acoustic Tag files (*.RAT) using the *AcousticTag* program. Each *.RAT file contains header information for data acquisition settings followed by the raw echo data. Each raw echo data file contains all acoustic signals detected during the time period, including signals from tagged fish as well as some additional unfiltered acoustic noise.

Software – *MarkTags* and *AcousticTag*

Two separate programs were used to collect and process the acoustic tag data; *AcousticTag* and *MarkTags*. *AcousticTag* was used initially to both acquire data from the ATR and to store the data in raw acoustic echoes files. *MarkTags* reads the raw acoustic echo files, identifies tag signals and creates acoustic tag files. These acoustic tag files are used again in *AcousticTag* to position the tags in two- and three-dimensional space.

AcousticTag acquires data and stores it in *.RAT files. It is important to note that these raw echoes are not associated with any specific Tag ID or spatial positioning. Depending on the project site and environmental conditions, many echoes found within these files are not tag data but derived from secondary sources (i.e. ambient noise, multipath). Thus, the first important phase of post processing is to select the acoustic echoes that have been received directly from tags, and to assign the unique Tag ID to these echoes.

The echo selection process is completed in the *MarkTags* program (Figure 8). The procedure for isolating the signals from a given tag follows from the method used for displaying the signals themselves. Each vertical scan in the plot shows the detected arrivals in the time window equal to the pulse-rate encoding of a particular tag (Ehrenberg and Steig 2003). In this example, only signals from the tag programmed with this 1100 ms period will fall along the straight line. The results of the tag selection process completed in *MarkTags* is written to tracked acoustic tag files (*.TAT file). These files contain the individual raw acoustic echoes which have been assigned a Tag ID but no spatial positioning has yet been assigned. *AcousticTag* performs the triangulation calculations and provides a database of point locations for each fish.

Tag Programmer

The HTI *Model 490-LP* Acoustic Tag Programmer and the *TagProgrammer* application software are used to set the individual settings when programming a tag.

Hydrophone Placement Geometry and Position Calculation

Detection on one hydrophone confirms the presence of an acoustic tag, but to be accurately positioned in three-dimensions a tag must be detected on at least four hydrophones (Figure 9). Similarly, to be positioned in two-dimensions a tag must be detected on at least three hydrophones. Three-dimensional tag coordinates with sub-meter accuracy are achieved using hydrophones located in known positions, at different vertical planes and within direct line of sight of the tag. As an acoustic tag passed through the four beams, the difference in the arrival time of each pulse was used to triangulate the exact location of the tag. In this way, a swimming path for each tagged fish could be mapped and presented in a three-dimensional display.

The principle that is used for determining acoustic tag positions is the same principle that accurately determines positions using the Global Position Satellites (GPS). The acoustic tag transmits a signal which is received by at least four hydrophones. By knowing the positions of the four hydrophones and measuring the relative signal arrival times at the hydrophones, the locations of the tagged fish can be estimated. In particular, if h_{ix}, h_{iy}, h_{iz} specify the x,y,z location of the ith hydrophone and let F_x, F_y, F_z specify the unknown x,y,z locations of the tagged fish.

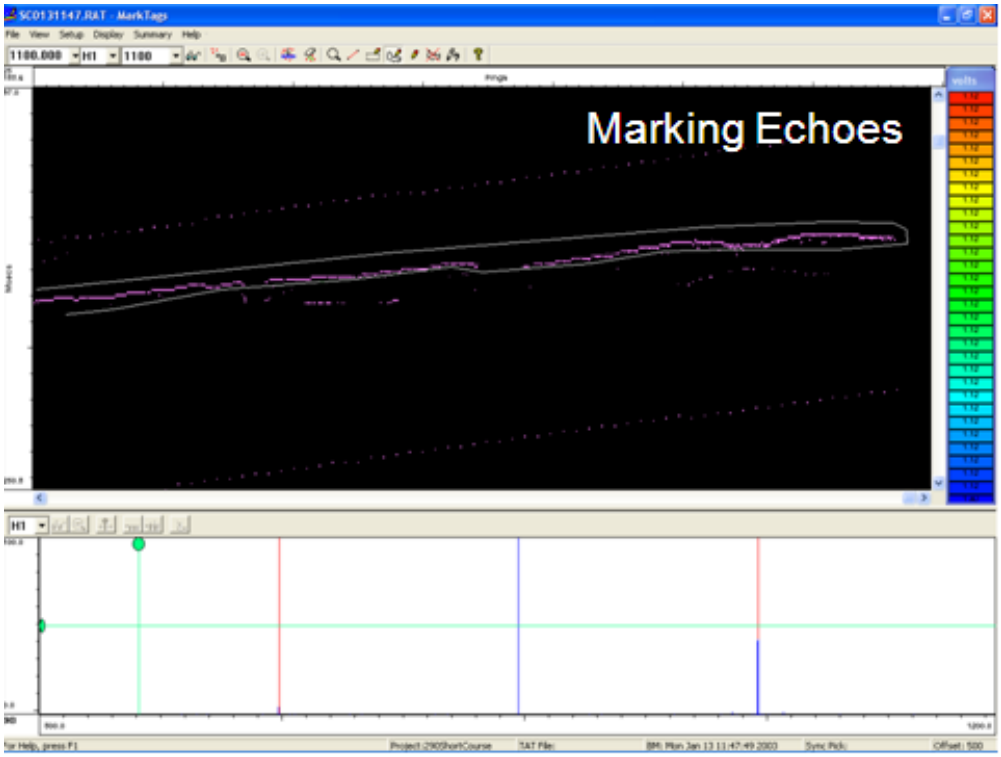

Figure 8. An echogram of detected signals using time window 1100ms (vertical scale) shown in *MarkTags*.

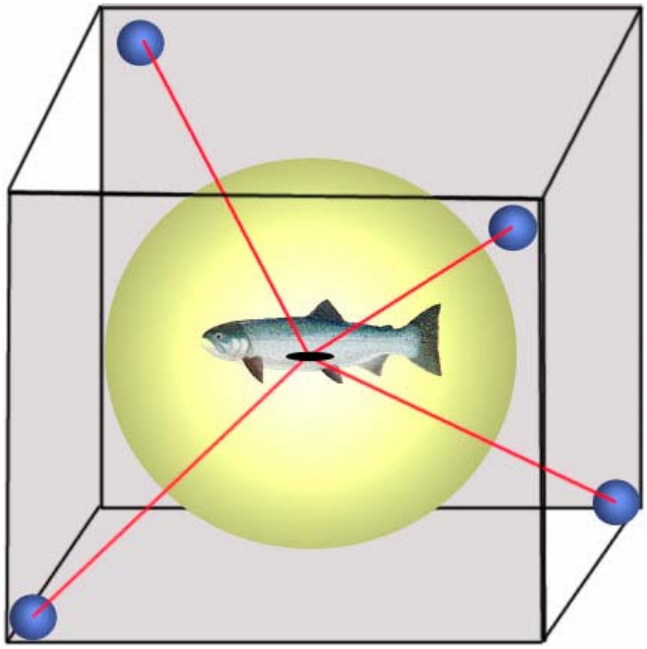

Figure 9. Positioning of an acoustic tag in three dimensions with a four-hydrophone array.

Then the travel time from the tagged fish to the ith hydrophone, t_i is given by

$$t_i = \frac{1}{c}\sqrt{(h_{ix} - F_x)^2 + (h_{iy} - F_y)^2 + (h_{iz} - F_z)^2}$$

where c is the velocity of sound. Unfortunately the absolute travel time cannot be directly measured. However the differences between the arrival times of the signal at the various hydrophones ($t_i - t_j$) can be measured as given by

$$t_i - t_j = \frac{1}{c}\left[\sqrt{(h_{ix} - F_x)^2 + (h_{iy} - F_y)^2 + (h_{iz} - F_z)^2} - \sqrt{(h_{jx} - F_x)^2 + (h_{jy} - F_y)^2 + (h_{jz} - F_z)^2}\right]$$

For four hydrophones, there are three such distinct signal arrival time difference equations. The system of nonlinear equations is determined by solving the tagged fish coordinates, F_x, F_y, F_z such that the mean squared difference between the measured (left side of the equation above) and calculated time differences (right side of the equation above) are minimized.

3.3 Monitoring Equipment Deployment and Hydrophone Array Design

The installation of the 34 node array of hydrophones at the GSNPB site was completed by March 5, 2012 (Figure 10). Hydrophones within the array that sampled at the GSNPB were located both up and downstream of the Georgiana Slough divergence. Hydrophones were positioned to assure optimal coverage as fish passed through the vicinity of the GSNPB.

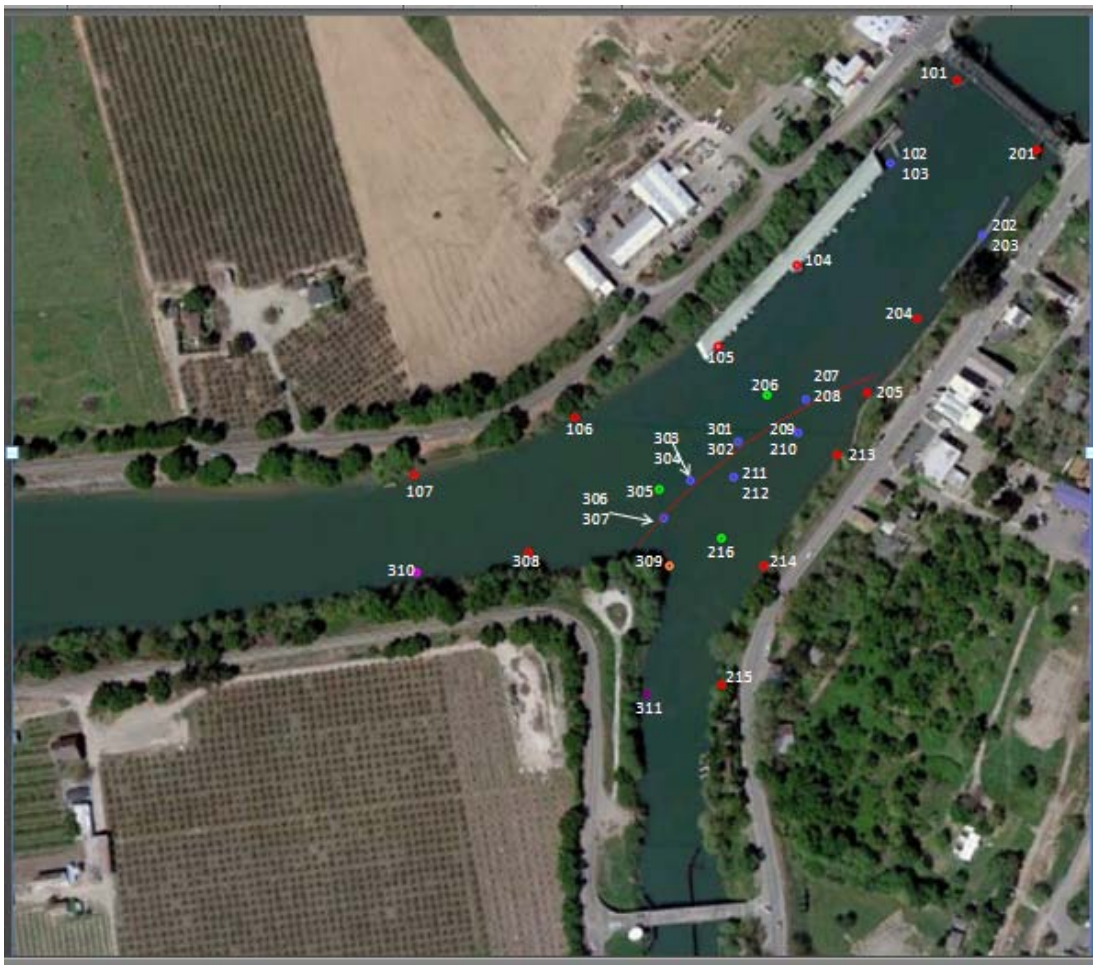

Figure 10. Location of the 34 hydrophones as deployed at Georgiana Slough NPB 2012.

Deployment Overview

DWR, USGS, USBR, and Normandeau Associates Environmental Consultants (NAEC) completed deployment of the hydrophone array in February and March 2012. Pre-season testing and establishment of the data collection parameters of the acoustic systems (HTI) was completed on March 5, 2012. All equipment was bench tested and calibrated prior to installation. Hydrophones were deployed and cables were routed to the electronic equipment housed in secure, climate-controlled structures supplied with 110 VAC power located on either shore of the Sacramento River near the divergence of Georgiana Slough.

The *Model 590 Hydrophones* were positioned to detect tagged fish passing through the region of the Sacramento River surrounding the GSNPB. A total of thirty-four hydrophones were installed, fifteen hydrophones positioned on the Sacramento River side of the GSNPB, fourteen hydrophones positioned downstream of the GSNPB on the Georgiana Slough side of the GSNPB, and five hydrophones installed on the GSNPB. Individual hydrophone cables were paired with tensioned aircraft cable to increase cable stiffness and strength.

3.4 Data Collection/Back-up Procedures

Data collection for the acoustic tag tracking system at the GSNPB began March 5, 2012 at 0900 h, and the acoustic monitoring system was maintained throughout the duration of the study. A summary of dates and times for each release is presented in Appendix A.

The tag coding and activation procedure was developed and maintained throughout the study for all Chinook, steelhead, and predatory species. Tags were activated and programmed at the the staging area temporary office near the GSNPB. Tag activation and programming was conducted using the HTI *Model 490-LP* Acoustic Tag Programmer. Tags were delivered within 8 hours of activation to the fish release barge. An experienced technician verifed tag codes and operation prior to fish release.

Experienced technicians were on-site 24h/d throughout the duration of the study. Additionally, at least one HTI staff scientist was on-site for a minimum of 18h/d monitoring data acquisition and analysis activitites. These staff scientists were in direct communication and worked under the supervision of a senior-level HTI scientist throughout the duration of the monitoring activities. The supervising senior-level HTI scientists were on-site no less than 8 hours in a 48-hour period during the field data collection period to review and participate in the ongoing data collction and processing efforts.

In addition to monitoring the acoustic tag tracking system at the GSNPB, HTI helped to maintain and troubleshoot the remotely operated peripheral hydrophone/data logger sites. Additional recording of the GSNPB operational parameters were completed each day it was operating.

Daily data acquisition activities included merging data files from the three acoustic tag receiver systems. A primary check through each merged hourly file to isolate and identify tag codes and subcodes and auto-track tags was completed. During the study period, preliminary fish track reduction was completed on 100% of the fish tracks. The entire dataset was backed up daily to a pair of identical external hard drives on alternating days.

3.5 System Testing Procedures

Each sampling site has its own unique characteristics that affect underwater sound propagation. These characteristics include acoustic noise interference, underwater structures, floating debris, water density differences and bathymetry, among others. This section describes the testing procedures including ambient noise measurements, hydrophone placement and positioning using the “ping-around” and *in-situ* tag testing (the “tag drag”). Tests conducted to measure the precise location of hydrophones in the array were completed throughout the monitoring period at the GSNPB. In addition, “tag drag” tests to measure the effective range of detection and overlap of hydrophones in the array were also completed. Both the “ping-around” and the “tag drag” results will be reported with the analyzed tag tracking data in the Final Data Collection Report.

Ambient Noise Measurement

Quantifying the acoustic noise interference provides the basis for setting the individual hydrophone receiver gains to maximize detection ranges without impacting individual fish detectability. This is an iterative process, involving recording and evaluating the amplitude of background noise levels under a series of amplification steps. The objective of this evaluation was to set the receiver gain to the lowest value that achieved total coverage over the sampling array, yet minimized echoes from background noise. At the conclusion of these measurements, the acoustic tag receiver gains were set to the appropriate levels.

Periodic evaluations of background noise and system gain settings continued throughout the study period, based on ongoing review of the data files. If the environmental conditions at the site changed,

system gain adjustments were made to optimize sampling coverage and resolution. Other acoustic monitoring devices located in the immediate vicinity, such as Acoustic Doppler Current Profilers (ADCP's) and the operation of other systems can create underwater noise.

Hydrophone Location Geometry and Positioning

The accuracy of each tagged fish position depends on accurate estimation of the location of the hydrophones in the array. To describe the hydrophone locations in two-dimensional space a Cartesian coordinate system (X, Y) with equivalent units of distance in each plane is used. Latitude and longitude measurements are based on a polar coordinate system and the units of distance are not equivalent in the X and Y planes (except at the equator). The most convenient coordinate system to use for acoustic tag monitoring applications is the UTM grid system (Universal Transverse Mercator), which expresses the X and Y coordinates in meters. The UTM grid system is also supported and used in most GIS systems. For these reasons, all hydrophone locations are referenced using UTM coordinates. Determining hydrophone locations is a two step process that begins with measuring hydrophone GPS coordinates and then using hydrophone generated signal delays to improve the accuracy of those original measurements.

A high-quality GPS supplied by DWR was used to measure the UTM coordinates for each hydrophone in the array. The X, Y coordinates were expressed in meters and located on a standardized UTM grid. Several measurements were made for each hydrophone deployment and the mean value defined the location during the initial installation. The absolute UTM coordinate positions for each hydrophone were verified and further refined using the "ping-around" technique.

The "ping-around" procedure was used to measure absolute hydrophone locations at the GSNPB. During the ping-around test, the calibration circuit in one hydrophone is enabled to transmit a series of "pings" in the same way that an acoustic tag "pings". While one hydrophone "pings" or transmits, all other hydrophones are receiving (Figure 11). The time difference between the transmit signal on one hydrophone and the signal arrival at each of the other hydrophones is a measure of the signal time delay between the transmitting and receiving pair of hydrophones. This procedure is repeated in an iterative process for all hydrophones in the array, providing multiple signal time delay measurements between each pair of hydrophones under the same environmental conditions.

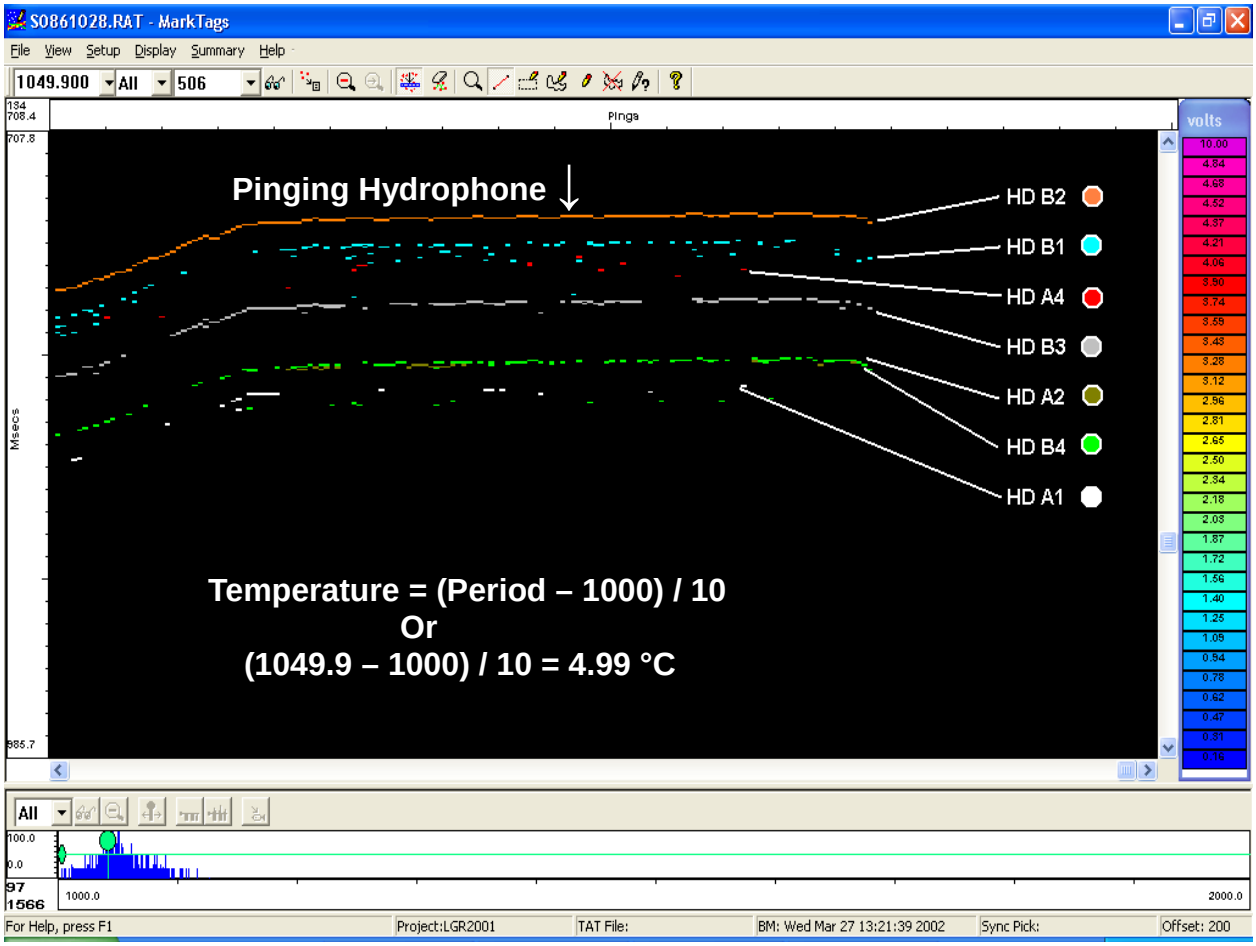

Figure 11. Results of a "ping-around" test in *MarkTags* program.

The *AcousticTag* program collected ping-around data automatically each week for the GSNPB array. The raw acoustic data files (*.RAT) were manually marked using the *MarkTags* program. Data from each hydrophone was analyzed to measure the water temperature and the signal time delays. For each pinging hydrophone, only the set of linear returns indicating constant temperature are marked and included for analysis (Figure 12).

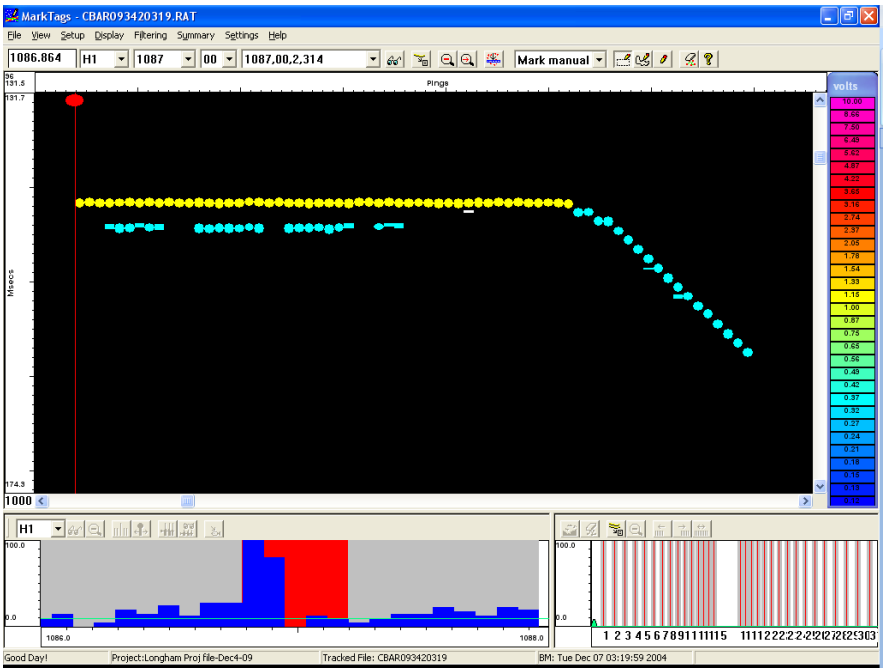

Figure 12. *MarkTags* marked signals (yellow) received from a transmitting hydrophone, included in the ping around analysis.

The location of each hydrophone is calculated by minimizing the mean squared differences between the GPS measurements and the temperature-corrected signal delays. Comparison of hydrophone positions measured by GPS and modified by the "ping-around" position adjustments will be completed and presented with the analyzed tag data by USGS in the final report.

In-Situ Tag Testing

The size and shape of the overall detection area is affected by the interaction of the hydrophone directivity, tag signal characteristics, and the surrounding environment. Factors affecting hydrophone signal detection include hydrophone receiver gain, directivity pattern, spacing, and array geometry (spatial relationship of hydrophones). Factors affecting the energy transmitted by the tags include the programmed tag pulse width and the source level. Environmental factors that can affect tag detection range and resolution include ambient background acoustic noise levels, large amounts of entrained air, and bathymetric variability that blocks line of sight signal transmission between hydrophones. Determination of the optimum acoustic tag sampling parameters for a given site is an iterative process that considers all of these factors.

The extent of the hydrophone array detection area, and the ability to accurately position tagged fish within it, were examined using *in-situ* test tags collected during sampling. This process involved transiting the sample area with a deployed transmitting tag, called the "tag drag" procedure. As the name implies, one or more active acoustic tags were located and moved within and beyond the hydrophone array. A GPS

unit on the boat was used to log vessel position over time. The acoustic tag system data files were reviewed to verify the ability to obtain consistent tag returns on three or more hydrophones over the areas surrounding the GSNPB, verifying the desired overlap of individual hydrophone detection areas and overall system performance before the study period.

4.0 REFERENCES

Adams N. S., D. W. Rondorf, S. D. Evans, and J. E. Kelly. 1998a. Effects of surgically and gastrically implanted radio transmitters on growth and feeding behavior of juvenile Chinook salmon. *Trans. Am. Fish. Soc.* 127:128-136.

Bowen, M.D. and R. Bark. 2010. 2010 Effectiveness of a Non-Physical Fish Barrier at the Divergence of the Old and San Joaquin Rivers (CA). Technical Memorandum 86-68290-10-07. U.S. Bureau of Reclamation, Denver, CO.

Bowen, M. D., Hiebert, S., Hueth, C., and V. Maisonneuve. 2009. *2009 Effectiveness of a Non-Physical Fish Barrier at the Divergence of the Old and San Joaquin Rivers (CA)*. Technical Memorandum 86-68290-09-05. U.S. Bureau of Reclamation, Denver, CO.

California Department of Water Resources. 2012. 2011 Georgiana Slough Non-Physical Barrier Performance Evaluation Project Report. Final Report. Prepared by California Department of Water Resources pp. 228.

Ehrenberg, J.E. and T.W. Steig. 2003. Improved techniques for studying the temporal and spatial behavior of fish in a fixed location. ICES J of Mar. Sci, 60: 700-706.

National Marine Fisheries Service (NMFS). 2009. *Biological Opinion and Conference Opinion on the Long-term Operations of the Central Valley Project and State Water Project*. NMFS, Southwest Region. June 4, 2009.

Perry, R. W. 2010. *Survival and Migration Dynamics of Juvenile Chinook Salmon* (Oncorhynchus tshawytscha) *in the Sacramento-San Joaquin River Delta*. A dissertation submitted in partial fulfillment of the requirements for the degree of Doctor of Philosophy, University of Washington.

Welton, J. S., W. R. C. Beaumont, and R. T. Clarke. 2002. The Efficacy of Air, Sound and Acoustic Bubble Screens in Deflecting Atlantic Salmon, *Salmo salar* L., Smolts in the River Frome, UK. *Fisheries Management and Ecology* 9:11–18

APPENDIX A-1

SUMMARY OF RELEASE NUMBER, TAG PROGRAMMING DATE, RELEASE DATE AND TIME AND NUMBER OF TAGS RELEASED FOR EACH RELEASE DURING THE GSNPB STUDY, 2012.

Release	Program Date	Release Date	Release Hour	# tags released
GC001	4-Mar	6-Mar	15:00	5
GC002	4-Mar	6-Mar	18:00	4
GC003	4-Mar	6-Mar	21:00	4
GC004	4-Mar	7-Mar	0:00	4
GC005	4-Mar	7-Mar	3:00	4
GC006	4-Mar	7-Mar	6:00	4
GC007	5-Mar	7-Mar	9:00	4
GC008	5-Mar	7-Mar	12:00	4
GC009	5-Mar	7-Mar	9:00	5
GC010	5-Mar	7-Mar	18:00	5
GC011	5-Mar	7-Mar	15:00	3
GC012	5-Mar	7-Mar	15:00	3
GC013	5-Mar	7-Mar	21:00	3
GC014	5-Mar	7-Mar	21:00	3
GC015	9-Mar	11-Mar	9:00	5
GC016	9-Mar	11-Mar	12:00	5
GC017	9-Mar	11-Mar	15:00	4
GC018	9-Mar	11-Mar	18:00	4
GC019	9-Mar	11-Mar	21:00	4
GC020	9-Mar	12-Mar	0:00	5
GC021	9-Mar	12-Mar	3:00	5
GC022	9-Mar	12-Mar	6:00	5
GC023	10-Mar	12-Mar	9:00	4
GC024	10-Mar	12-Mar	12:00	5
GC025	10-Mar	12-Mar	15:00	4
GC026	10-Mar	12-Mar	18:00	4
GC027	10-Mar	12-Mar	21:00	4
GC028	10-Mar	13-Mar	0:00	5
GC029	10-Mar	13-Mar	3:00	5
GC030	10-Mar	13-Mar	6:00	5
GC032	11-Mar	13-Mar	12:00	5
GC034	11-Mar	13-Mar	15:00	4
GC036	11-Mar	14-Mar	3:00	4
GC037	11-Mar	14-Mar	3:00	5
GC038	11-Mar	14-Mar	6:00	5
GC039	12-Mar	14-Mar	9:00	4
GC040	12-Mar	14-Mar	12:00	4
GC041	12-Mar	14-Mar	18:00	4
GC042	12-Mar	14-Mar	21:00	4
GC043	12-Mar	15-Mar	0:00	4
GC044	12-Mar	15-Mar	6:00	4
GC045	13-Mar	15-Mar	9:00	4
GC046	13-Mar	15-Mar	12:00	4
GC047	13-Mar	15-Mar	15:00	5

Release	Program Date	Release Date	Release Hour	# tags released
GC048	13-Mar	15-Mar	18:00	5
GC049	13-Mar	15-Mar	21:00	4
GC050	13-Mar	16-Mar	0:00	5
GC051	13-Mar	16-Mar	3:00	5
GC052	13-Mar	16-Mar	6:00	5
GC053	14-Mar	16-Mar	9:00	5
GC054	14-Mar	16-Mar	12:00	5
GC055	14-Mar	16-Mar	15:00	5
GC056	14-Mar	16-Mar	18:00	4
GC057	14-Mar	16-Mar	21:00	4
GC058	14-Mar	17-Mar	0:00	4
GC059	14-Mar	17-Mar	3:00	4
GC060	14-Mar	17-Mar	6:00	5
GC061	15-Mar	17-Mar	9:00	4
GC062	15-Mar	17-Mar	12:00	5
GC063	15-Mar	17-Mar	15:00	5
GC064	15-Mar	17-Mar	18:00	4
GC065	15-Mar	17-Mar	21:00	5
GC066	15-Mar	18-Mar	0:00	5
GC067	15-Mar	18-Mar	3:00	4
GC068	15-Mar	18-Mar	6:00	5
GC069	16-Mar	18-Mar	9:00	5
GC070	16-Mar	18-Mar	12:00	4
GC071	16-Mar	18-Mar	15:00	4
GC072	16-Mar	18-Mar	18:00	4
GC073	16-Mar	18-Mar	21:00	5
GC074	16-Mar	18-Mar	0:00	5
GC075	16-Mar	19-Mar	3:00	4
GC076	16-Mar	19-Mar	6:00	5
GC077	17-Mar	19-Mar	9:00	5
GC078	17-Mar	19-Mar	12:00	3
GC079	17-Mar	19-Mar	15:00	4
GC080	17-Mar	19-Mar	18:00	3
GC081	17-Mar	19-Mar	21:00	5
GC082	17-Mar	20-Mar	0:00	5
GC083	17-Mar	20-Mar	3:00	4
GC084	17-Mar	20-Mar	6:00	5
GC085	18-Mar	20-Mar	9:00	4
GC086	18-Mar	20-Mar	12:00	4
GC087	18-Mar	20-Mar	15:00	4
GC088	18-Mar	20-Mar	18:00	4
GC089	18-Mar	20-Mar	21:00	5
GC090	18-Mar	21-Mar	0:00	5
GC091	18-Mar	21-Mar	3:00	4
GC092	18-Mar	21-Mar	6:00	5
GC093	19-Mar	21-Mar	9:00	4
GC094	19-Mar	21-Mar	12:00	4

Release	Program Date	Release Date	Release Hour	# tags released
GC095	19-Mar	21-Mar	15:00	4
GC096	19-Mar	21-Mar	18:00	4
GC097	19-Mar	21-Mar	21:00	5
GC098	19-Mar	22-Mar	0:00	5
GC099	19-Mar	22-Mar	3:00	4
GC100	19-Mar	22-Mar	6:00	5
GC101	20-Mar	22-Mar	9:00	4
GC102	20-Mar	22-Mar	12:00	4
GC103	20-Mar	22-Mar	15:00	4
GC104	20-Mar	22-Mar	18:00	4
GC105	20-Mar	22-Mar	21:00	5
GC106	20-Mar	23-Mar	0:00	5
GC107	20-Mar	23-Mar	3:00	4
GC108	20-Mar	23-Mar	6:00	5
GC109	21-Mar	23-Mar	9:00	4
GC110	21-Mar	23-Mar	12:00	4
GC111	21-Mar	23-Mar	15:00	4
GC112	21-Mar	23-Mar	18:00	4
GC113	21-Mar	23-Mar	21:00	5
GC114	21-Mar	24-Mar	0:00	5
GC115	21-Mar	24-Mar	3:00	4
GC116	21-Mar	24-Mar	6:00	5
GC117	22-Mar	24-Mar	9:00	4
GC118	22-Mar	24-Mar	12:00	4
GC119	22-Mar	24-Mar	15:00	4
GC120	22-Mar	24-Mar	18:00	4
GC121	22-Mar	24-Mar	21:00	5
GC122	22-Mar	25-Mar	0:00	5
GC123	22-Mar	25-Mar	3:00	4
GC124	22-Mar	25-Mar	6:00	5
GC125	23-Mar	25-Mar	9:00	4
GC126	23-Mar	25-Mar	12:00	4
GC127	23-Mar	25-Mar	15:00	4
GC128	23-Mar	25-Mar	18:00	4
GC129	23-Mar	25-Mar	21:00	5
GC130	23-Mar	26-Mar	0:00	5
GC131	23-Mar	26-Mar	3:00	4
GC132	23-Mar	26-Mar	6:00	5
GC133	24-Mar	26-Mar	9:00	5
GC134	24-Mar	26-Mar	12:00	5
GC135	24-Mar	26-Mar	15:00	4
GC136	24-Mar	26-Mar	18:00	4
GC137	24-Mar	26-Mar	21:00	4
GC138	24-Mar	27-Mar	0:00	4
GC139	24-Mar	27-Mar	3:00	4
GC140	24-Mar	27-Mar	6:00	4
GC141	25-Mar	27-Mar	9:00	5

Release	Program Date	Release Date	Release Hour	# tags released
GC142	25-Mar	27-Mar	12:00	5
GC143	25-Mar	27-Mar	15:00	4
GC144	25-Mar	27-Mar	18:00	4
GC146	25-Mar	28-Mar	0:00	5
GC147	25-Mar	28-Mar	3:00	4
GC148	25-Mar	28-Mar	6:00	4
GC149	26-Mar	28-Mar	9:00	4
GC150	26-Mar	28-Mar	12:00	4
GC151	26-Mar	28-Mar	15:00	4
GC152	26-Mar	28-Mar	18:00	4
GC153	26-Mar	29-Mar	0:00	3
GC154	26-Mar	29-Mar	0:00	4
GC155	26-Mar	29-Mar	3:00	5
GC156	26-Mar	29-Mar	6:00	5
GC157	27-Mar	29-Mar	9:00	4
GC158	27-Mar	29-Mar	12:00	4
GC159	27-Mar	29-Mar	15:00	5
GC160	27-Mar	29-Mar	18:00	4
GC161	27-Mar	29-Mar	21:00	4
GC162	27-Mar	30-Mar	0:00	5
GC163	27-Mar	30-Mar	3:00	4
GC164	27-Mar	30-Mar	6:00	4
GC165	28-Mar	30-Mar	9:00	4
GC166	28-Mar	30-Mar	12:00	4
GC167	28-Mar	30-Mar	15:00	4
GC168	28-Mar	30-Mar	18:00	4
GC169	28-Mar	30-Mar	21:00	4
GC170	28-Mar	31-Mar	0:00	4
GC171	28-Mar	31-Mar	3:00	5
GC172	28-Mar	31-Mar	6:00	4
GC173	29-Mar	31-Mar	9:00	4
GC174	29-Mar	31-Mar	12:00	4
GC175	29-Mar	31-Mar	15:00	4
GC176	29-Mar	31-Mar	18:00	4
GC177	29-Mar	31-Mar	21:00	4
GC178	29-Mar	1-Apr	0:00	5
GC179	29-Mar	1-Apr	3:00	4
GC180	29-Mar	1-Apr	6:00	4
GC181	30-Mar	1-Apr	9:00	4
GC182	30-Mar	1-Apr	12:00	4
GC183	30-Mar	1-Apr	15:00	4
GC184	30-Mar	1-Apr	18:00	5
GC185	30-Mar	1-Apr	21:00	5
GC186	30-Mar	2-Apr	0:00	4
GC187	30-Mar	2-Apr	3:00	4
GC188	30-Mar	2-Apr	6:00	4
GC189	31-Mar	2-Apr	9:00	4

Release	Program Date	Release Date	Release Hour	# tags released
GC190	31-Mar	2-Apr	12:00	4
GC191	31-Mar	2-Apr	15:00	4
GC192	31-Mar	2-Apr	18:00	4
GC193	31-Mar	2-Apr	21:00	4
GC194	31-Mar	3-Apr	0:00	5
GC195	31-Mar	3-Apr	3:00	5
GC196	31-Mar	3-Apr	6:00	4
GC197	1-Apr	3-Apr	9:00	4
GC198	1-Apr	3-Apr	12:00	4
GC199	1-Apr	3-Apr	15:00	4
GC200	1-Apr	3-Apr	18:00	5
GC201	1-Apr	3-Apr	21:00	4
GC202	1-Apr	4-Apr	0:00	4
GC203	1-Apr	4-Apr	3:00	4
GC204	1-Apr	4-Apr	6:00	4
GC205	2-Apr	4-Apr	9:00	4
GC206	2-Apr	4-Apr	12:00	4
GC207	2-Apr	4-Apr	15:00	4
GC208	2-Apr	4-Apr	18:00	4
GC209	2-Apr	4-Apr	21:00	4
GC210	2-Apr	5-Apr	0:00	4
GC211	2-Apr	5-Apr	3:00	4
GC212	2-Apr	5-Apr	6:00	4
GC213	3-Apr	5-Apr	9:00	4
GC214	3-Apr	5-Apr	12:00	4
GC215	3-Apr	5-Apr	15:00	4
GC216	3-Apr	5-Apr	18:00	4
GC217	3-Apr	5-Apr	21:00	6
GC218	3-Apr	6-Apr	0:00	4
GC219	3-Apr	6-Apr	3:00	4
GC220	3-Apr	6-Apr	6:00	4
GC221	4-Apr	6-Apr	9:00	4
GC222	4-Apr	6-Apr	12:00	4
GC223	4-Apr	6-Apr	15:00	4
GC224	4-Apr	6-Apr	18:00	4
GC225	4-Apr	6-Apr	21:00	6
GC226	4-Apr	7-Apr	0:00	4
GC227	4-Apr	7-Apr	3:00	4
GC228	4-Apr	7-Apr	6:00	4
GC229	5-Apr	7-Apr	9:00	4
GC230	5-Apr	7-Apr	12:00	4
GC231	5-Apr	7-Apr	15:00	4
GC232	5-Apr	7-Apr	18:00	6
GC233	5-Apr	7-Apr	21:00	4
GC234	5-Apr	8-Apr	0:00	4
GC235	5-Apr	8-Apr	3:00	4
GC236	5-Apr	8-Apr	6:00	4

Release	Program Date	Release Date	Release Hour	# tags released
GC237	6-Apr	8-Apr	9:00	4
GC238	6-Apr	8-Apr	12:00	4
GC239	6-Apr	8-Apr	15:00	4
GC240	6-Apr	8-Apr	18:00	6
GC241	6-Apr	8-Apr	21:00	4
GC242	6-Apr	9-Apr	0:00	4
GC243	6-Apr	9-Apr	3:00	4
GC244	6-Apr	9-Apr	6:00	4
GC245	7-Apr	9-Apr	9:00	4
GC246	7-Apr	9-Apr	12:00	4
GC247	7-Apr	9-Apr	15:00	4
GC248	7-Apr	9-Apr	18:00	4
GC249	7-Apr	9-Apr	21:00	4
GC250	7-Apr	10-Apr	0:00	4
GC251	7-Apr	10-Apr	3:00	5
GC252	7-Apr	10-Apr	6:00	4
GC253	8-Apr	10-Apr	9:00	4
GC254	8-Apr	10-Apr	12:00	4
GC255	8-Apr	10-Apr	15:00	4
GC256	8-Apr	10-Apr	18:00	4
GC257	8-Apr	10-Apr	21:00	4
GC258	8-Apr	11-Apr	0:00	4
GC259	8-Apr	11-Apr	3:00	5
GC260	8-Apr	11-Apr	6:00	4
GC261	9-Apr	11-Apr	9:00	4
GC262	9-Apr	11-Apr	12:00	4
GC263	9-Apr	11-Apr	15:00	4
GC264	9-Apr	11-Apr	18:00	4
GC265	9-Apr	11-Apr	21:00	4
GC266	9-Apr	12-Apr	0:00	4
GC267	9-Apr	12-Apr	3:00	5
GC268	9-Apr	12-Apr	6:00	4
GC269	10-Apr	12-Apr	9:00	3
GC270	10-Apr	12-Apr	12:00	4
GC271	10-Apr	12-Apr	15:00	4
GC272	10-Apr	12-Apr	18:00	4
GC273	10-Apr	12-Apr	21:00	4
GC274	10-Apr	13-Apr	0:00	4
GC275	10-Apr	13-Apr	3:00	4
GC276	10-Apr	13-Apr	6:00	3
GC277	11-Apr	13-Apr	9:00	4
GC278	11-Apr	13-Apr	12:00	4
GC279	11-Apr	13-Apr	15:00	4
GC280	11-Apr	13-Apr	18:00	4
GC281	11-Apr	13-Apr	21:00	4
GC282	11-Apr	14-Apr	0:00	4
GC283	11-Apr	14-Apr	3:00	4

Release	Program Date	Release Date	Release Hour	# tags released
GC284	11-Apr	14-Apr	6:00	4
GC285	12-Apr	14-Apr	9:00	4
GC286	12-Apr	14-Apr	12:00	4
GC287	12-Apr	14-Apr	15:00	4
GC288	12-Apr	14-Apr	18:00	4
GC289	12-Apr	14-Apr	21:00	4
GC290	12-Apr	15-Apr	0:00	4
GC291	12-Apr	15-Apr	3:00	4
GC292	12-Apr	15-Apr	6:00	4
GC293	13-Apr	15-Apr	9:00	4
GC294	13-Apr	15-Apr	12:00	4
GC295	13-Apr	15-Apr	15:00	4
GC296	13-Apr	15-Apr	18:00	4
GC297	13-Apr	15-Apr	21:00	4
GC298	13-Apr	16-Apr	0:00	4
GC299	13-Apr	16-Apr	3:00	4
GC300	13-Apr	16-Apr	6:00	4
GC301	14-Apr	16-Apr	9:00	5
GC302	14-Apr	16-Apr	12:00	4
GC303	14-Apr	16-Apr	15:00	4
GC304	14-Apr	16-Apr	18:00	4
GC305	14-Apr	16-Apr	21:00	4
GC306	14-Apr	17-Apr	0:00	4
GC307	14-Apr	17-Apr	3:00	4
GC308	14-Apr	17-Apr	6:00	4
GC309	15-Apr	17-Apr	9:00	5
GC310	15-Apr	17-Apr	12:00	4
GC311	15-Apr	17-Apr	15:00	4
GC312	15-Apr	17-Apr	18:00	4
GC313	15-Apr	17-Apr	21:00	3
GC314	15-Apr	18-Apr	0:00	3
GC315	15-Apr	18-Apr	3:00	4
GC316	15-Apr	18-Apr	6:00	4
GC317	16-Apr	18-Apr	9:00	4
GC318	16-Apr	18-Apr	12:00	4
GC319	16-Apr	18-Apr	15:00	4
GC320	16-Apr	18-Apr	18:00	4
GC321	16-Apr	18-Apr	21:00	4
GC322	16-Apr	19-Apr	0:00	4
GC323	16-Apr	19-Apr	3:00	3
GC324	16-Apr	19-Apr	6:00	4
GC325	17-Apr	19-Apr	9:00	4
GC326	17-Apr	19-Apr	12:00	4
GC327	17-Apr	19-Apr	15:00	3
GC328	17-Apr	19-Apr	18:00	4
GC329	17-Apr	19-Apr	21:00	4
GC330	17-Apr	20-Apr	0:00	4

Release	Program Date	Release Date	Release Hour	# tags released
GC331	17-Apr	20-Apr	3:00	4
GC332	17-Apr	20-Apr	6:00	4
GC333	18-Apr	20-Apr	9:00	4
GC334	18-Apr	20-Apr	12:00	4
GC335	18-Apr	20-Apr	15:00	4
GC336	18-Apr	20-Apr	18:00	4
GC337	18-Apr	20-Apr	21:00	4
GC338	18-Apr	21-Apr	0:00	4
GC339	18-Apr	21-Apr	3:00	4
GC340	18-Apr	21-Apr	6:00	4
GC341	19-Apr	21-Apr	9:00	4
GC342	19-Apr	21-Apr	12:00	5
GC343	19-Apr	21-Apr	15:00	4
GC344	19-Apr	21-Apr	18:00	4
GC345	19-Apr	21-Apr	21:00	5
GC346	19-Apr	22-Apr	0:00	3
GC347	19-Apr	22-Apr	3:00	4
GC348	19-Apr	22-Apr	6:00	4
GC349	20-Apr	22-Apr	9:00	4
GC350	20-Apr	22-Apr	12:00	4
GC351	20-Apr	22-Apr	15:00	5
GC352	20-Apr	22-Apr	18:00	3
GC353	20-Apr	22-Apr	21:00	4
GC354	20-Apr	23-Apr	0:00	4
GC355	20-Apr	23-Apr	3:00	5
GC357	21-Apr	23-Apr	9:00	5
GC358	21-Apr	23-Apr	12:00	5
GC359	21-Apr	23-Apr	15:00	5
GC360	21-Apr	23-Apr	18:00	5
GC361	21-Apr	23-Apr	21:00	4
GM001	16-Mar	18-Mar	12:00	6
GM002	16-Mar	18-Mar	15:00	7
GM003	16-Mar	18-Mar	18:00	6
GM004	16-Mar	18-Mar	21:00	6
GM005	16-Mar	19-Mar	0:00	6
GM006	16-Mar	19-Mar	3:00	7
GM007	16-Mar	19-Mar	6:00	6
GM008	17-Mar	19-Mar	9:00	7
GM009	17-Mar	19-Mar	12:00	6
GM010	17-Mar	19-Mar	15:00	7
GM011	17-Mar	19-Mar	18:00	6
GM012	17-Mar	19-Mar	21:00	7
GM013	17-Mar	20-Mar	0:00	6
GM014	17-Mar	20-Mar	3:00	7
GM015	9-Apr	11-Apr	6:00	6
GM016	9-Apr	11-Apr	9:00	6
GM017	9-Apr	11-Apr	12:00	6

Release	Program Date	Release Date	Release Hour	# tags released
GM018	9-Apr	11-Apr	15:00	7
GM019	9-Apr	11-Apr	18:00	6
GM020	9-Apr	11-Apr	21:00	8
GM021	9-Apr	12-Apr	0:00	6
GM022	9-Apr	12-Apr	3:00	7
GM023	9-Apr	12-Apr	6:00	6
GM024	10-Apr	12-Apr	9:00	7
GM025	10-Apr	12-Apr	12:00	6
GM026	10-Apr	12-Apr	15:00	7
GM027	10-Apr	12-Apr	18:00	6
GM028	10-Apr	12-Apr	21:00	7
GM029	10-Apr	13-Apr	0:00	6
GM030	10-Apr	13-Apr	3:00	7
GM031	10-Apr	13-Apr	6:00	6
GM032	11-Apr	13-Apr	9:00	8
GM033	11-Apr	13-Apr	12:00	6
GM034	11-Apr	13-Apr	15:00	7
GM035	11-Apr	13-Apr	18:00	6
GM036	11-Apr	13-Apr	21:00	7
GM037	11-Apr	14-Apr	0:00	6
GM038	11-Apr	14-Apr	3:00	7
GM039	11-Apr	14-Apr	6:00	6
GM040	12-Apr	14-Apr	9:00	7
GM041	12-Apr	14-Apr	12:00	6
GM042	12-Apr	14-Apr	15:00	7
GM043	12-Apr	14-Apr	18:00	6
GM044	12-Apr	15-Apr	21:00	7
GM045	12-Apr	15-Apr	0:00	6
GM046	12-Apr	15-Apr	3:00	7
GP001	24-Feb	Various	Various	5
GP002	24-Feb	Various	Various	5
GP003	15-Mar	Various	Various	5
GP004	15-Mar	Various	Various	5
GP005	20-Mar	Various	Various	5
GP006	20-Mar	Various	Various	5
GP007	13-Apr	Various	Various	5
GP008	13-Apr	Various	Various	5
GP009	6-May	Various	Various	5
GP010	6-May	Various	Various	5

APPENDIX B

2012 GEORGIANA SLOUGH NON-PHYSICAL BARRIER STUDY
STUDY FISH SUMMARY STATISTICS

Appendix B – GSNPB 2012 Study Fish Summary Statistics

Table B-1. Mean and range fork length (mm) and weight (g) of juvenile Chinook salmon released by date.

		Fork length (mm)		Weight (g)	
Date	**N**	**Mean**	**Range**	**Mean**	**Range**
6-Mar	13	135	109 – 170	26.4	14.4 – 48.5
7-Mar	42	132	104 – 185	25.0	13.0 – 62.2
11-Mar	22	128	116 – 151	21.9	16.3 – 32.7
12-Mar	36	135	110 – 167	25.6	13.8 – 45.6
13-Mar	24	149	109 – 193	35.2	13.0 – 66.2
14-Mar	30	147	108 – 193	33.7	12.9 – 68.9
15-Mar	30	140	107 – 185	29.4	13.3 – 71.4
16-Mar	38	138	108 – 198	28.8	13.0 – 80.4
17-Mar	37	137	109 – 187	27.3	13.0 – 66.3
18-Mar	36	143	109 – 208	32.3	13.8 – 95.4
19-Mar	36	144	106 – 188	32.0	13.7 – 73.9
20-Mar	35	133	104 – 190	26.3	14.2 – 63.8
21-Mar	35	145	106 – 188	33.7	13.1 – 73.2
22-Mar	35	138	105 - 185	29.5	13.1 – 63.7
23-Mar	35	145	115 – 205	33.3	16.3 – 84.3
24-Mar	35	144	112 – 202	33.2	15.0 – 74.8
25-Mar	35	136	111 – 180	27.9	13.9 – 63.5
26-Mar	36	140	107 – 188	30.6	13.7 – 73.0
27-Mar	30	148	114 – 194	37.7	16.0 – 85.6
28-Mar	29	138	108 – 186	28.8	13.3 – 72.3
29-Mar	38	144	110 – 191	33.5	14.4 – 76.8
30-Mar	33	145	113 – 188	34.3	14.4 – 74.0
31-Mar	34	144	116 – 187	32.7	14.8 – 71.6
1-Apr	35	145	111 – 186	34.1	14.1 – 78.9
2-Apr	32	145	122 – 209	33.4	19.4 – 106.8
3-Apr	35	146	116 – 190	34.5	16.0 – 74.5
4-Apr	32	149	108 – 198	36.9	13.5 – 83.6
5-Apr	34	142	113 – 188	32.7	15.0 – 73.5
6-Apr	34	153	113 – 201	40.0	15.1 – 92.3
7-Apr	34	146	115 – 215	35.4	15.1 – 106.3
8-Apr	34	136	110 – 175	28.2	14.2 – 60.2
9-Apr	32	140	115 – 169	30.5	16.1 – 56.8
10-Apr	33	138	112 – 172	29.6	15.0 – 59.4
11-Apr	33	131	112 – 169	24.0	13.1 – 53.4
12-Apr	33	130	115 – 148	23.6	15.1 – 34.4
13-Apr	32	126	108 – 164	21.7	13.8 – 45.1
14-Apr	32	133	111 – 169	26.2	14.2 – 53.0
15-Apr	32	136	115 – 156	27.9	16.8 – 40.4
16-Apr	33	133	113 – 169	26.4	15.5 – 48.2
17-Apr	32	126	107 – 154	23.4	13.0 – 64.0
18-Apr	32	126	112 – 150	22.3	14.4 – 36.9
19-Apr	32	126	107 – 194	22.3	13.1 – 75.2
20-Apr	32	132	108 – 158	25.2	13.9 – 43.1
21-Apr	35	129	108 – 161	23.3	13.0 – 44.6
22-Apr	33	131	115 – 168	23.7	14.5 – 48.4
23-Apr	33	131	110 – 160	23.9	14.0 – 45.2
Overall	1513	138	104 – 215	29.4	12.9 – 106.8

Table B-2. Mean and range fork length (mm) and weight (g) of juvenile steelhead released by date.

		Fork length (mm)		Weight (g)	
Date	**N**	**Mean**	**Range**	**Mean**	**Range**
18-Mar	26	214	182 – 237	97.7	62.1 – 131.4
19-Mar	52	210	180 – 238	92.3	58.4 – 136.8
20-Mar	13	206	184 – 225	89.4	63.4 – 122.6
11-Apr	40	213	119 – 258	103.9	75.2 – 164.5
12-Apr	52	218	183 – 241	106.3	62.5 – 145.6
13-Apr	53	217	185 – 243	106.5	63.3 – 145.3
14-Apr	52	218	176 – 245	103.9	54.3 – 140.4
15-Apr	13	216	191 – 249	100.3	59.7 – 149.7
Overall	301	215	119 – 258	101.5	54.3 – 164.5

APPENDIX C

2012 GEORGIANA SLOUGH NON-PHYSICAL BARRIER STUDY
SUMMARY OF STANDARD OPERATING PROCEDURES

QUALITY ASSURANCE/QUALITY CONTROL PLAN

2012 Georgiana Slough Non-Physical Barrier Performance Evaluation

Focus Area: Effectiveness of a non-physical barrier at deterring juvenile fish from entering Georgiana Slough on the Sacramento River

Prepared for:
California Department of Water Resources
Jacob McQuirk and Ryan Reeves
1416 9th Street
Sacramento, CA, 94236-001
Phone: 916-653-6868
Email: jacobmc@water.ca.gov/ rreeves@water.ca.gov

Prepared by:
US Geological Survey
Noah Adams
Columbia River Research Laboratory
5501A Cook-Underwood Road
Cook, WA, 98650
Phone: 509-538-2299
Email: nadams@usgs.gov

The purpose of the Quality Assurance/Quality Control (QA\QC) plan for the 2012 Georgiana Slough Non-Physical Barrier Performance Evaluation was to ensure that the data were collected, analyzed, and reported in a standardized manner in close accordance with good laboratory practices procedures. Many investigators from multiple federal, state, and local agencies as well as the private sector were involved in this project. Each of these organizations has their own procedures and guidelines for ensuring QA/QC. This plan attempted to take the information from different organizations and present it in a standardized format.

Due to the length of the final project report, DWR decided not to include the QA/QC plan in its entirety in the report. Instead, the table of content for the QA/QC plan as well as a list of the Standard Operating Procedures (SOPs) included in the plan are provided below. The QA/QC plan in its entirety is on file with DWR and is available upon request.

Table of Contents for QA/QC Plan

Project Management
- A1. Purpose
- A2. Distribution List
- A3. Project/Task Organization
- A4. Problem Definition/Background
- A5. Project/Task Description
- A6. Quality Objectives and Criteria
- A7. Special Training/Certification
- A8. Documents and Records

Measurement Data Acquisition
- B1. Sampling Process Design
- B2. Sampling Methods
- B3. Sample Handling and Custody
- B4. Analytical Methods
- B5. Quality Control
- B6. Instrument/Equipment Testing, Inspection, and Maintenance
- B7. Instrument/Equipment Calibration and Frequency
- B8. Inspection/Acceptance of Supplies and Consumables
- B9. Data Management

Assessment and Oversight
- C1. Assessment and Response Actions
- C2. Reports to Management

Data Validation and Usability
- D1. Data Review, Verification, and Validation
- D2. Verification and Validation Methods
- D3. Reconciliation with User Requirements

APPENDIX:
- The Standard Operating Procedures and completed in-season compliance and monitoring evaluation sheets

The Standard Operating Procedures appended to QA/QC plan

Standard Operating Procedure (SOP)

Pre-Deployment Testing of Cables and Hydrophones for 3D Acoustic Array
Tag-Drag Tests of the 3D Acoustic Array
Remote Access for Georgiana 3D Array
Raw Data Transfer
General Operation of the Bio-Acoustic Fish Fence
Obtaining Underwater Light Level Data
Obtaining Underwater Sound Measurements
Estimating Deterrence, Protection, and Overall Efficiency Metrics - Bio-Acoustic Fish Fence
Obtaining Climate and Weather Data
Obtaining Water Quality Data
Equipment Cleaning, Inspection and Treatment for Invasive Aquatic Organisms
Tag Coding of Acoustic Transmitters
Tag Programming of Acoustic Transmitters
Incorporating Tags into Drifter Releases
Keeping Instrument Logs
Completing Field Over Site Checklist
Recording Data in Laboratory Notebooks
Daily QA/QC Checks on Remote Acoustic Nodes
Daily On-Site-Checks of the 3D Acoustic Array
Daily QA/Q Checks on ATR at 3D Acoustic Array
Fish Transport Procedures
Surgical Tag Implantation
Tag Assistant and Curator
Installation and Maintenance of Fixed Hydroacoustic Monitoring Equipment
Drifter Study Plan
Hydrodynamic Monitor

APPENDIX D

2012 GEORGIANA SLOUGH NON-PHYSICAL BARRIER
FISH TAGGING EFFECTS STUDY

Survival, wound healing, transmitter loss, and growth in juvenile Chinook salmon and steelhead surgically implanted with acoustic transmitters.

T. L. Liedtke
U.S. Geological Survey
Western Fisheries Research Center
5501A Cook-Underwood Road
Cook, WA 98505
Theresa_Liedtke@usgs.gov

Introduction

In support of the 2012 Georgiana Slough Non-Physical Barrier (GSNPB) Study, a controlled laboratory study was completed to evaluate the condition of juvenile Chinook salmon and steelhead surgically implanted with acoustic telemetry transmitters and to document the risk of transmitter loss. The objectives of the study were to evaluate: 1) risk of mortality due to tagging, 2) the healing of the surgical wounds through time, 3) the risk of transmitter loss, and 4) differences between taggers.

Telemetry studies make the assumption that fish equipped with transmitters will behave and perform comparably to untagged fish. More explicitly stated, the assumption is that the collection, handling, and tagging of the fish, combined with the act of carrying the transmitter, will have minimal impact on the fish. When transmitters are implanted using invasive procedures such as surgery there is more likely to be a "transmitter effect". Testing this assumption by measuring potential transmitter effects is critical to making valid inferences to the untagged population. Evaluating transmitter effects can be difficult in field settings due to the limited opportunity to recapture and examine tagged fish and the often limited information available on the "normal" behavior of untagged fish with which comparisons could be made. For the 2012 GSNPB study, the assumption was evaluated under controlled laboratory conditions where tagged fish could be closely monitored and there was opportunity to examine fish following tagging. This study (hereafter referred to as "the tag effects study") was conducted at the U.S. Fish and Wildlife Service's California and Nevada Fish Health Center in Anderson, California (co-located with the Coleman National Fish Hatchery) with the assistance of Scott Foott (Center Director) and his staff.

Methods

Study Design

The ideal study design for an evaluation of transmitter effects is to exactly replicate the conditions used in the primary telemetry study. For example, the ideal study design for this tag effects study would involve the same fish, the same tagging procedures, the same personnel, and the same water source and temperatures as the GSNPB study, which it was designed to support. Logistical considerations unfortunately prevented us from meeting that ideal. Nonetheless every effort was made to match the GSNPB study whenever possible. As will be outlined in the methods, the tag effects study procedures matched the GSNPB study on several details including: fish source and transport, tagging procedures, taggers, and post-tagging recovery and holding (Figure 1). Differences between the two studies included: an additional transport for the tag effects study fish when GSNPB fish were released into the Sacramento River, and different water sources and thermal regimes during the holding period (Figure 1). Although the tag effects study design was less than ideal, any evaluation of transmitter effects is a worthwhile effort considering the value of the data generated for the GSNPB study. In

addition, the tag effects study was rigorous enough to support the inferences that could be made with the findings of from the GSNPB study.

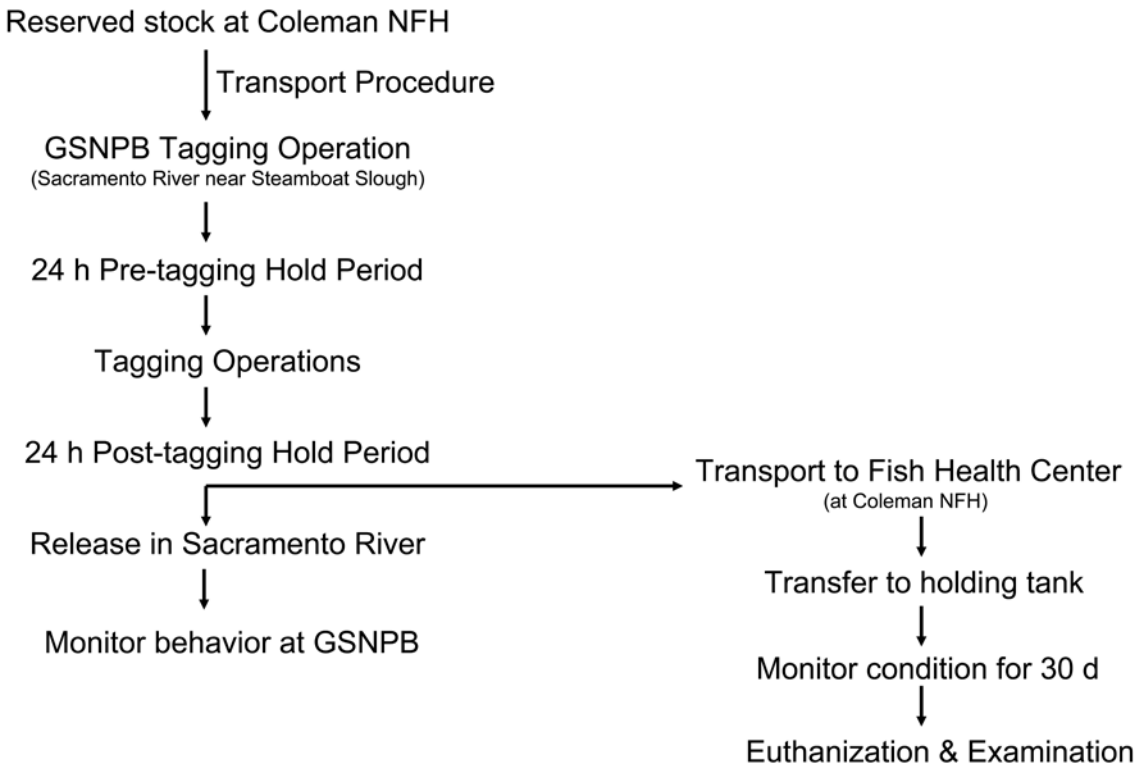

Figure 1. — Flow chart showing the procedures used for the GSNPB study (left column) and the tag effects study conducted at the Fish Health Center (right column).

A 30 d monitoring period was used for the tag effects study based on the anticipated life of the transmitters used for the GSNPB study. Dummy transmitters (with no working components) that simulated the transmitters used for the GSNPB study were surgically implanted into the abdominal cavity of the fish, along with a 12.5 mm passive integrated transponder (PIT) tag. The PIT tags were required to individually identify fish in the study. The GSNPB study did not use PIT tags as study fish were identified by the unique signal from the acoustic transmitter. The dummy acoustic transmitters used for Chinook salmon had a mean weight of 0.62 g. The dummy transmitters used for steelhead had a mean weight of 0.89 g. The PIT tag mean weight was 0.09 g. The combined transmitter weights were 0.71 g for Chinook salmon and 0.98 g for steelhead.

Similar to the GSNPB study, Chinook salmon were the primary species of interest for the tag effects study, and juvenile steelhead were included, but at a lower level of effort, reflecting the pilot level of evaluation for this species. Three experiments were conducted for Chinook salmon to represent the early season, mid-season, and late season influences of the taggers and fish condition. Two experiments were conducted for steelhead. Two taggers were used for the GSNPB study and their potential influence was evaluated in the tag effects

study. Three dates were selected (one early in the GSNPB study period, one near the middle, and one near the end) when both taggers were present. On these dates, each tagger tagged 10 - 15 fish with dummy tags and PIT tags to be used in an experiment. On each of the dates each tagger also handled 4-8 control fish which were minimally handled and held using the same procedures as the tagged groups of fish. The control fish were included to allow detection of large-scale effects such as poor conditions during transport or a disease outbreak that could have influenced the tagged fish and confounded our interpretation of the survival or condition of the experimental groups. A summary of the tagging dates, and sample sizes by tagger and species is presented in Table 1.

Table 1. — Summary of the tag date, the numbers of fish tagged, the number of control fish, the species, and the tagger for the three experiments that comprised the tag effects study, 2012.

Experiment	Tag date	Species	Tagger	Number of fish tagged	Number of controls
1	3/19	Chinook	1	15	8
	3/19	Chinook	2	15	7
	3/19	steelhead	1	10	4
	3/29	steelhead	2	10	7
2	4/15	Chinook	1	10	5
	4/15	Chinook	2	10	5
	4/15	steelhead	1	10	5
	4/15	steelhead	2	10	5
3	4/21	Chinook	1	10	5
	4/21	Chinook	2	10	5
TOTAL		Chinook		70	35
		Steelhead		40	21

The California and Nevada Fish Health Center was selected as the study site based both on logistical ease and on the capability of staff. The logistical consideration involved executing the transport of fish. A transport crew (from Professional Aquaculture Services) was established for the GSNPB study and it moved fish daily from Coleman National Fish Hatchery to the tagging location. This system was used, in reverse, for the tag effects study. The study fish were tagged at the tagging location on the Sacramento River near Steamboat Slough, and then transported to the Fish Health Center at Coleman. The fish transport protocols put in place for the GSNPB study were used when dummy-tagged fish were transported. The second rationale for using the Fish Health Center as the study site was based on the availability and capability of Center staff. Following delivery, fish were put into tanks at the Fish Health Center. Center staff have experience in fish culture and monitoring, and their assistance was requested to feed the fish and regularly monitor the tank for dead, dying, or sick fish and for any transmitters that might have been shed. They were prepared to do diagnostic testing for disease on fish that died or became sick during the experiment. This regular care and

monitoring was critical to the full evaluation of transmitter effects and would not have been possible without the support of Scott Foott and his staff at the Fish Health Center.

Fish Source

Juvenile late fall-run Chinook salmon and steelhead used for the tag effects study were from the same source as those used for the GSNPB study and were treated identically. Fish were removed from a dedicated holding tank at the Coleman National Fish Hatchery and transported in an insulated container to the GSNPB tagging operation on the Sacramento River near Steamboat Slough. Fish for the tag effects study were transported concurrently, separated by species, with GSNPB study fish on selected dates.

Tagging and Recovery Procedures

The standard operating procedures (SOP) and taggers used for the GSNPB study were used for the tag effects study. As part of the SOP, fish fork length (FL) and weight information were collected. These data were used as the initial size for the growth calculations. On dates when an experiment was started, one tagger was randomly selected to start tagging. That tagger continued until they completed tagging their study fish and then the second tagger completed their allotted fish.

Following the SOP for the GSNPB study, tagged fish were held in perforated 76 L containers in the Sacramento River for 24 h after tagging to recover from handling and tagging. Fish were always held separately by species. Following this holding period the containers were removed from the river and transferred to an insulated tote for transport to the Fish Health Center.

Fish Holding and Monitoring at the Fish Health Center

Dummy-tagged fish arrived at the Fish Health Center approximately 3 h after their departure from the tagging operation near Steamboat Slough. Upon arrival fish were removed from the 76 L containers and each species was placed into a single tank (approximate volume 1700 L) for the 30 d monitoring period. Fish were fed commercial pellets based on a maintenance ration. The tank was monitored daily for dead or compromised fish and for shed PIT or acoustic tags. Temperature monitors were placed into the tank and recorded water temperature approximately every 10 min for the duration of the holding period.

Evaluation Procedures

At the completion of each experiment fish were euthanized, weighed, measured, photographed, and necropsied using the unique PIT tag to individually identify fish. Photographs were taken to show both the internal and external view of the incision. Wound healing and fish condition were assessed using a rubric developed by USGS to

establish criteria for consistent grading of fish. During the necropsy procedure scores were assigned for seven categorical variables from the USGS rubric which were designed to document the condition of the fish, the progress of wound healing, and the potential for transmitter loss. Three variables were binomial, using presence and absence as the two possible states. The binomial variables included suture retention, fungus, and internal organ damage. The four additional variables were categorical with 3-5 possible states (Table 2) and included suture effectiveness, incision apposition, incision healing, and signs of tag expulsion. In all cases, the best outcome for a variable was zero so that low scores predict better fish condition or wound healing.

Table 2. — Variables from the USGS rubric that were used to assess fish condition and wound healing and the definitions of their categorical scores. The best outcome for all variables is a score of zero, with condition decreasing with higher scores.

Variable	Score 0	Score 1	Score 2	Score 3	Score 4
Suture effectiveness	Intact	Not fully intact	Not intact		
Incision apposition	0% open	25% open	50% open	75% open	100% open
Incision healing	100% Healed	75% healed	50% healed	25% healed	Not healed
Tag expulsion	No signs of expulsion	Some pressure or bulging	Expulsion process active		

Analysis

Mean initial and final (30 d) fish size data and summaries of the wound healing variables are presented. The percentage weight increase was calculated as (final weight-initial weight)/initial weight *100. Findings for each tagger are presented, along with a combined total.

Results

Three 30 d experiments for Chinook salmon and two 30 d experiments for juvenile steelhead were initiated during the GSNPB tagging operation to represent the early, middle, and late season potential changes in tagger proficiency and fish condition (Table 3). Mean water temperature in the holding tanks at the Fish Health Center ranged from 10.7 to 13.8 °C during the three experiments (Table 3). A total of 110 tagged fish and 56 control fish were used for the experiments (166 total fish). There were no mortalities for any of the experimental groups or control groups, in any of the experiments. During the second experiment one tagged steelhead was removed from the tank after 15 d of holding because Fish Health Center staff observed significant amounts of fungus on the fish's caudal peduncle. The fish was euthanized and preserved in the freezer for examination with the remainder of the fish from the experiment. Based on

observations of fish in the tanks, Fish Health Center staff did not observe any gross signs of disease or distress during any of the experiments.

The mean initial FL of Chinook salmon (all experiments combined) was 133.9 mm, and the initial mean weight was 25.8 g (Table 4). The mean initial FL of steelhead (both experiments combined) was 212.5 mm, and the initial mean weight was 96.6 g (Table 5). Using the combined mass of the dummy acoustic transmitter and the PIT tag, the tag burden (tag weight to body weight ratio) range was 1.1% - 5.2% for Chinook salmon and 0.6% - 1.6% for steelhead at the time fish were tagged. The mean tag burden was 2.8% for Chinook salmon (Table 4) and 1.1% for steelhead (Table 5). The initial size (FL and weight) of both Chinook salmon and steelhead were very similar for both taggers. The control fish were minimally handled, so weight and length measurements were not taken for those groups. Considering that all the treatment and control fish were removed from the same cohort of hatchery fish that was used for the GSNPB study, it is reasonable to assume that the size distribution of the control fish was similar to the treatment fish for the same species.

Both Chinook salmon and steelhead showed positive weight increase over the 30 d holding periods. The Chinook salmon had a mean weight increase of 8.2% for all the fish combined (Table 4), and the steelhead had an overall mean weight increase of 2.3% (Table 5). Steelhead tagged by tagger 2 had a higher mean percent weight increase compared to steelhead tagged by tagger 1 (Table 5).

Table 3. — Tagging date, sampling date, and mean water temperatures for the three experiments conducted at the Fish Health Center in 2012.

	Experiment 1	**Experiment 2**	**Experiment 3**
Tagging date	March 19	April 15	April 21
Sampling date	April 19	May 15	May 22
Mean Water Temperature (°C)	10.7	13.8	13.7

Table 4. — Mean initial and final fork length (FL; mm) and weight (g), mean tag burden (%), and mean percent weight increase for Chinook salmon used in the tag effects study, 2012, by tagger and overall.

	N	Initial Mean FL	Initial Mean Weight	Mean Tag Burden	Final Mean FL	Final Mean Weight	Mean % Weight Increase
Tagger 1	35	133.9	26.2	2.7%	135.8	28.2	9.1%
Tagger 2	35	133.8	25.4	2.8%	135.0	26.9	7.4%
Total	**70**	**133.9**	**25.8**	**2.8%**	**135.4**	**27.5**	**8.2%**

Table 5. — Mean initial and final fork length (FL; mm) and weight (g), mean tag burden (%), and mean percent weight increase for steelhead used in the tag effects study, 2012, by tagger and overall.

	N	Initial Mean FL	Initial Mean Weight	Mean Tag Burden	Final Mean FL	Final Mean Weight	Mean % Weight Increase
Tagger 1	20	210.3	94.9	1.1%	206.8	95.9	0.6%
Tagger 2	20	214.7	98.3	1.0%	215.4	102.3	4.0%
Total	**40**	**212.5**	**96.6**	**1.1%**	**211.1**	**98.5**	**2.3%**

Necropsies conducted 30 d after tagging revealed that fish were in good general condition. There were no gross external or internal signs of disease, and none of the fish showed any signs of internal organ damage from the tagging procedure or the presence of the tags. Over half of fish examined did however have some fungal growth on or near the incision or sutures (51.8% overall). There was no difference between the taggers related to the presence of fungus: each tagger handled 50% of the fish that had fungus present.

One acoustic tag was lost from a tagged steelhead during the first experiment. The tag burden for this fish was 1.1% at the time of tagging, well within the SOP maximum of 5% tag burden. No tags were lost from any of the tagged Chinook salmon. Necropsies revealed that two Chinook salmon (2.8%) and 13 steelhead (32.5%) showed some signs of lateral pressure on the incision that could have, through time, led to some transmitter loss. The remaining 95 tagged fish (86.4%) had a tag expulsion score of zero, meaning that there were no signs of transmitter expulsion. The risk of tag expulsion did not appear to be related to differences in taggers as eight of the 15 fish were handled by tagger 1 and seven were handled by tagger 2. Both of the Chinook salmon that showed some signs of tag expulsion had scores of 1 using the USGS rubric, meaning that the tag was putting some pressure on the incision or the lateral body wall. The steelhead showed more significant signs of transmitter loss: of the 13 fish with non-zero scores, 10 fish had an expulsion score of 1 showing some signs of lateral pressure, and 3 of them had expulsion scores of 2, suggesting an active expulsion process. The mean tag expulsion scores were 0.03 for Chinook salmon and 0.40 for steelhead.

Most (76.4%) of the sutures used to close the incisions in Chinook salmon were in place at 30 d post-tagging, with slightly higher suture retention for tagger 2 (78.6%) compared to tagger 1 (74.3%; Table 6). For steelhead 88.7% of the original sutures were retained at 30 d, with slightly higher retention for tagger 1 (90.0%) compared to tagger 2 (87.5%; Table 7).

The sutures that were still in place at the time of necropsy were scored for effectiveness. Most Chinook salmon (91.1%) had a suture effectiveness score of zero, indicating that the suture pattern was intact and effective. The overall mean suture effectiveness score for Chinook salmon was 0.13 (Table 6), which was very close to zero which represents perfectly effective suture patterns in all fish. Both taggers had very similar suture effectiveness scores for Chinook salmon (Table 6). The majority (83.8%) of steelhead had a suture effectiveness score of zero, indicating that the suture pattern was fully intact and effective. The overall mean suture effectiveness score for steelhead

was 0.26 (Table 7). Tagger 1 had a higher incidence of partially effective sutures (mean score of 0.33) compared to tagger 2 (mean score of 0.17; Table 7).

The incisions made to insert transmitters were completely healed or significantly advanced in the healing process at 30 d post-tagging. The overall mean incision apposition score for Chinook salmon (0.07) and incision healing score (0.24) reflected a high proportion of fish that showed good apposition of the edges of the incision and incision healing (Table 6). Tagger 1 had a higher proportion of scores above zero for these variables (Table 6). The overall mean scores for steelhead were 0.40 for incision apposition and 0.48 for incision healing (Table 7). Apposition and healing scores for steelhead were similar between the two taggers (Table 7).

Table 6. — Mean suture retention (%) and wound healing scores for Chinook salmon used in the tag effects study, 2012 by tagger and overall. Wound healing scores of zero represent the most advanced wound healing.

	N	% suture retention	Suture Effectiveness Score	Incision Apposition Score	Incision Healing Score
Tagger 1	35	74.3%	0.11	0.14	0.34
Tagger 2	35	78.6%	0.14	0.00	0.14
Total	**70**	**76.4%**	**0.13**	**0.07**	**0.24**

Table 7. — Mean suture retention (%) and wound healing scores for steelhead used in the tag effects study, 2012 by tagger and overall. Wound healing scores of zero represent the most advanced wound healing.

	N	% suture retention	Suture Effectiveness Score	Incision Apposition Score	Incision Healing Score
Tagger 1	20	90.0%	0.33	0.35	0.40
Tagger 2	20	87.5%	0.17	0.45	0.55
Total	**40**	**88.7%**	**0.26**	**0.40**	**0.48**

The tag effects study was designed with multiple experiments so that fish condition and tagger competency could be evaluated throughout the study period. There were some differences in fish size and healing between the experiments. Chinook salmon were largest at the time of tagging for the first experiment and smallest for the second experiment (Table 8). The percent weight increase for Chinook salmon was largest for experiment 1 and smallest for experiment 3. Steelhead were largest at the time of tagging for the second experiment and smallest during the first (Table 9). Similar to Chinook salmon, the percent weight increase for steelhead was largest for experiment 1 (Table 9). During the second experiment the steelhead showed a net weight loss (Table 9). The temporal trends in suture effectiveness and wound healing were similar for Chinook salmon and steelhead. The scores for suture effectiveness were consistently low across all experiments (Tables 8 and 9). Considering the scale for suture effectiveness scores

ranged from 0 (sutures fully intact and functional) to 2 (suture pattern not intact), the mean scores for each experiment show consistently effective sutures. The healing scores were lowest for the first experiment and then showed a slight increase. Again, considering the scale used for healing where zero represents complete healing and four represents less than 25% of the length of the incision being healed, the mean scores show that the average condition in all experiments was significantly healed incisions (75-100% of the incision length on average). The small increase in healing scores (reduction in healing) through time was likely due to the increase in water temperature for the second and third experiments. The higher water temperature likely fostered greater fungal growth, which can delay incision healing.

Table 8. — Mean initial weight (g), weight increase (%), suture effectiveness score, and incision healing score for the three Chinook salmon experiments used in the tag effects study 2012.

	Experiment 1	**Experiment 2**	**Experiment 3**
Initial Weight (g)	28.2	22.0	26.1
% Weight Increase	14.6%	5.3%	1.6%
Suture Effectiveness	0.10	0.18	0.11
Incision Healing	0.04	0.60	0.20

Table 9. — Mean initial weight (g), weight increase or loss (%), suture effectiveness score, and incision healing score for the two steelhead experiments used in the tag effects study 2012.

	Experiment 1	**Experiment 2**
Initial Weight (g)	89.0	104.3
% Weight Increase/Loss	7.3%	-3.0%
Suture Effectiveness	0.18	0.35
Incision Healing	0.40	0.60

Discussion

The objectives of the study were to evaluate: 1) risk of mortality due to tagging, 2) the healing of the surgical wounds through time, 3) the risk of transmitter loss, and 4) differences between taggers.

There were no mortalities among the 166 experimental and control fish for the Chinook salmon and steelhead experiments, so the risk of mortality due to tagging was minimal. Fish implanted with acoustic transmitters and PIT tags performed well during the 30 d holding period following tagging, feeding and showing positive weight gain. There were so signs of gross disease or distress while the fish were held for 30 d in tanks,

and there was no evidence of disease processes when fish were euthanized and necropsied following 30 d of holding. The most significant finding, from the perspective of observations of fish in the holding tanks, was the presence of fungus on some individuals. One fish was removed from the experiment after 15 d due to a significant fungal load. Review of the tagging record for this fish showed that the fish had several areas of fungus on the caudal peduncle at the time of tagging rendering it more vulnerable to the effects of handling and continued fungal growth. The presence of fungus on fish is not surprising considering that fish were held in tanks where water velocities were nominal and the presence of residual commercial fish food can encourage fungal growth. Future evaluations could potentially limit fungal growth with increased flow in tanks, increased rigor in tank cleaning, and reduced water temperatures.

The surgical wounds for both Chinook salmon and steelhead showed significant healing through time, with the mean condition showing that incisions were 75-100% healed 30 d after tagging. There are several related drivers that lead to incision healing such as effective sutures and incision apposition. The USGS rubric used to score tagged fish evaluated seven variables to capture the influence of these drivers. Each of the variables had positive outcomes. We found that suture effectiveness was high, meaning that the suture patterns were well executed initially, and were effective at creating enough tension across the incision to maintain the edges of the incision in contact (apposition) to enable healing. The apposition scores support this finding, showing that the incision edges were well approximated 30 d after tagging. There were no instances of internal organ damage due to the tagging procedure of the presence of the tags. There was a high proportion (51.8%) of fungus for experimental fish, and the fungus was most commonly noted to be on or near the incision area of the fish. Although the fungal load may have delayed healing in individual fish, leading to increased variability in healing scores, it did not have a significant effect on overall healing, as evidenced by the low mean scores for wound healing.

No acoustic transmitters were lost from Chinook salmon during the experiments, and one transmitter (2.5%) was lost from steelhead. In Chinook salmon the risk of transmitter loss was very low as evidenced by the low mean tag expulsion score of 0.03. With the USGS rubric, a score of zero represents no sign of transmitter loss and the Chinook mean score is very close to zero. Two tagged Chinook (2.8%) showed some signs of lateral pressure during the 30 d exams, and all remaining fish (97.2%) had scores of zero. Alternately, there was some evidence of tag loss risk in steelhead. One transmitter was shed from a tagged fish during the 30 d holding period. The tag was not recovered in the tank, so the timing of the tag loss could not be determined. At the time of tagging the tag burden for this fish was 1.1%, well below the SOP maximum of 5% tag burden. The weight of the tag, relative to the weight of the fish was not likely, therefore, to be the strongest driver of the tag loss. In addition to the one documented tag loss in steelhead, there were 33% of the steelhead that had tag expulsions scores that were above zero: 25% with a score of 1, and 8% with a score of 2. The rubric score of 1 suggests that the tag is exerting some pressure on the incision or lateral body wall, but does not imply that the tag is likely to be shed. The rubric score of 2, however, is evidence that the pressure is significant and the tissue (incision or lateral body wall) is affected enough that

the tag will likely eventually be lost. If we assume that the 8% of steelhead (three individuals) with scores of 2 would eventually lose their transmitters, and combine those fish with the one steelhead that lost a transmitter during the experiments, the total transmitter loss for steelhead would be four individuals or 10%. Clearly, loss of 10% of the tagged population could have a large effect on the outcome of a telemetry study. During the necropsies for the steelhead we were concerned with the scores for tag expulsion and we examined each fish and its corresponding transmitter closely. We noted that the dummy acoustic transmitters used for steelhead were more variable in weight and shape than the active transmitters used for the steelhead in the GSNPB study. The dummy tags had especially large batteries relative to the active transmitters and some very abrupt changes in shape that resulted in severe edges in the dummy transmitters. Specifically, the edges did not have the ability to damage fish tissue (that is, they were not rough), but they were exaggerated and appeared to cause irritation in the tissues surrounding the implanted transmitter. We believe that this difference in shape was the cause of the lateral pressure and elevated risk of transmitter loss that we noted in steelhead.

There were few differences between the two taggers. Both taggers had equivalent mortality, risk of transmitter loss, and incidence of fungus on tagged fish. There were some minor differences in the scores for the variables in the USGS rubric, for example tagger 1 had a higher mean suture effectiveness score and healing score for Chinook salmon compared to tagger 2. Alternately, tagger 2 had a higher healing score than tagger 1 for steelhead. Overall the differences between the scores for the taggers were small, and there were no clear trends that one tagger had greater proficiency than the other tagger. Some differences noted in the rubric scores for the two taggers could be the result of variability in scoring using the USGS rubric. We have found in other studies that it takes a considerate amount of effort and training to standardize the scoring of fish. Although the scoring done for this study is reliable for distinguishing major surgical or healing outcomes such as poorly healed incisions or gross inflammation or infection, the minor differences noted between taggers could be attributed to the subjective nature of the scoring system and lack of rigorous standardization. Several different project personnel were used to necropsy and score the fish from these experiments, and although training was provided, it was brief. The trends in fish survival and tag retention, which are less subjective, suggest that the two taggers had very similar outcomes for both species examined. The largest difference noted between the taggers was for the percent weight increase in steelhead over the 30 d holding period. The mean growth for tagger 1 was 0.6% compared to 4.0% for tagger 2 (Table 5). As tagger 2 had larger fish initially, these fish may have established feeding dominance in the tank, limiting access to food for the smaller fish tagged by tagger 1. Generally, fish implanted with transmitters that show growth over time are considered to have a positive surgical outcome, and both taggers met this criterion.

In conclusion, the results of the tag effects study suggest that juvenile Chinook salmon and steelhead surgically implanted with acoustic transmitters for the GSNPB study were not likely to lose their transmitters or suffer negative effects from the tagging process or the presence of the transmitter. The risk of transmitter loss was a concern for

the dummy tags used in the tag effects study but likely did not impact the steelhead that were tagged with active transmitters for the GSNPB evaluation. Additionally, the two taggers that contributed to the GSNPB study demonstrated equivalent competency during the tag effects study and should therefore not introduce any bias into the evaluation of the GSNPB.

APPENDIX E

2012 GEORGIANA SLOUGH NON-PHYSICAL BARRIER STUDY
FISH TRACK PROCESSING AND DEVELOPMENT COMPARISON

FISH TRACK PROCESSING AND DEVELOPMENT COMPARISON

Introduction

Evaluating the effect of the NPB at Georgiana Slough on fish behavior required generating and analyzing multidimensional tracks of the acoustically-tagged fish as they moved through the study area. The multidimensional tracks are the product of a complex combination of hardware that filters and records underwater acoustic signals, advanced signal processing software that separates tag echoes from acoustic noise, and tag tracking software that uses applied numerical methods to estimate the location of the acoustic tags that produce these signals. The process of turning acoustic signals into multidimensional fish tracks is not a simple pre-processing step in the research process, but rather, an integral part of the experiment with many steps that require parameterization and design decisions that significantly affect the end product. In the past it has been difficult to ascertain how much influence these decisions have on the overall study analysis, because investing the amount of time required to completely reprocess the data from a large tracking study with multiple parameter sets has not been possible. The 2012 GSB study presented a unique opportunity to explore the effects of different echo-selection and tag-positioning methodologies in the context of a multi-dimensional fish passage analysis. This study allowed us to use the USGS FishCount and GeneticFish algorithms to provide an independent technology for evaluating how different methodology can be used to generate and analyze multidimensional tracks of the acoustically-tagged fish.

To explore the performance of different echo selection and acoustic tag positioning algorithms, a subset of tag codes were processed multiple times using different technology combinations. This resulted in three sets of tag tracks that were used for the tag comparison analysis:

- **Group 1 Tracks**: a set of tracks produced using HTI MarkTags software for echo selection, and AcousticTag software for tag positioning
- **Group 2 Tracks**: a set of tracks produced using the USGS FishCount algorithm for echo selection and the HTI AcousticTag software for tag positioning
- **Group 3 Tracks**: a set of tracks produced using the USGS FishCount algorithm for echo selection, and the USGS GeneticFish algorithm for tag positioning

This combination of echo selection and tag positioning approaches allowed us to examine the effects of echo selection on tracking (Group 1 Tracks compared to Group 2 Tracks), and allowed us to examine the effects of different tracking methodologies using the same echo selection (Group 2 tracks vs Group 3 tracks).

The subset of tags used for this comparison included 291 uniquely coded tags that had been surgically implanted in Chinook salmon and steelhead or attached to drifters that were allowed to float through the study area. Four additional tags were suspended underneath a small floating platform outfitted with an RTK antenna and pulled behind a boat through the study area. These tags are hereafter referred to as RTK tags and the other 291 tags are hereafter referred to as fish tags. Quantitative comparisons were made between the three different groups of

tracks for each of the 291 fish tags, and the overall distribution of differences between the tracks for each of these groups was examined for each metric used to evaluate the different technologies. The tracks for the RTK tags were analyzed separately by comparing the tracks of the RTK tags to the tracks generated by the GPS signal collected by the RTK antenna, the results of this analysis are contained in Attachment E-1.

Methods

Group 1 Track Set Echo Selection and Tag Positioning Methodology

Echo selection for Group 1 tags was accomplished using MarkTags (Figure i). The procedure for isolating the signals using MarkTags the same method used for displaying the signal in real time as the fish moved through the study area. Each vertical depiction of the signal in the plot shows the detected arrivals of the signal in the time window for those signals that are equal to the pulse-rate encoding of a particular tag (Ehrenberg and Steig 2003). In this example, only signals from the (double pulse) tag programmed with a 3078 ms period fall along the two curved lines. The MarkTags program includes an automated signal selection option which utilizes user selectable parameter to control a time-windowing tracking algorithm. In addition, manual editing and marking of tag signals was used to reject multipath and other sources of noise, or to select signals that were filtered out by the automated process. The results of the tag signal selection process using MarkTags was written to tracked acoustic tag files (*.TAT). These files contained the individual raw acoustic signals which had been assigned a Tag ID but no spatial position. AcousticTag was then used to perform triangulation calculations and provided a database of point locations for each tag.

Figure i

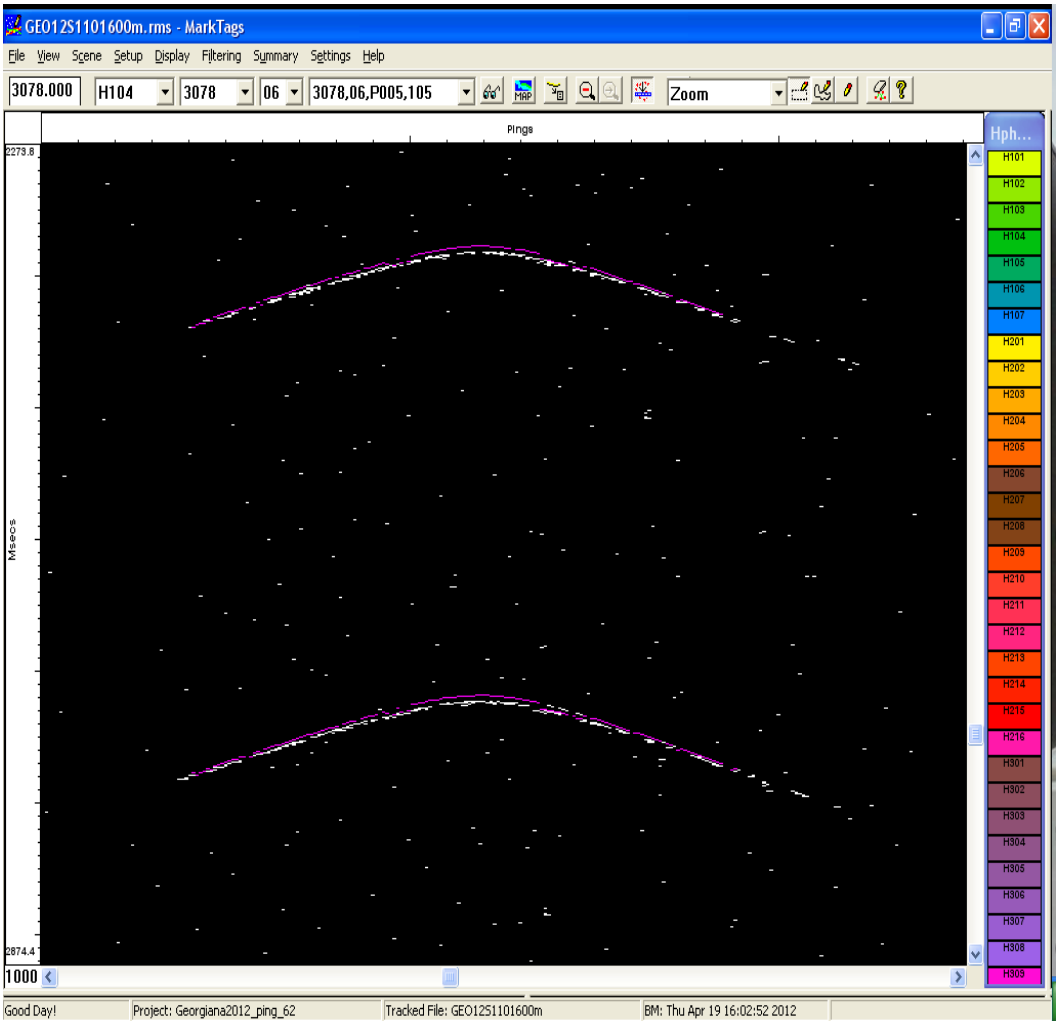

Figure i: MarkTags (zoomed) view of tag signals from Tag 3078.06, showing selected signals (magenta), and multipath and noise signals (white).

Group 2 Track Set Echo Selection and Tag Positioning Methodology

Echo selection for the Group 2 track set was performed with USGS FishCount algorithm which was executed autonomously on the Amazon EC2 platform supported by the USGS DistributedFish software package. After echo selection was completed a data processing utility was used to convert the binary instrument files created by FishCount into *.TAT files that could be read by the HTI AcousticTag software. The USGS CRRL laboratory used the HTI AcousticTag software to create multidimensional fish tracks from the *.TAT files using the same input parameters and hydrophone positions as those used for the Group 1 track set.

Group 3 Track Set Echo Selection and Tag Positioning Methodology

The Group 3 track set and the Group 2 track set use the same FishCount echo selection data, but rely on different methodologies to convert the marked echoes into multidimensional fish tracks. For the Group 3 track set, the instrument files created by FishCount were processed into multidimensional tracks using the USGS GeneticFish algorithm. The GeneticFish algorithm estimates the position of a tag echo using a genetic algorithm, rather than the standard multi-lateralization approach used by AcousticTag and other positioning software. The GeneticFish tracking was performed autonomously on the Amazon EC2 platform supported by the USGS DistributedFish software package. The hydrophone positions, water temperatures, and input parameters used by GeneticFish are documented in Attachment E-4.

RTK Tag Drags

RTK GPS ground truth data was collected at the start of the 2012 NPB study in order to evaluate the absolute error of the acoustic tag tracking. The ground truth data was collected by suspending 4 acoustic tags underneath a small floating platform outfitted with an RTK antenna and pulling this platform through the study area with a boat. As shown in Table 1, the tags were suspended at depth intervals of 0.5 m beginning 1 m below the water surface on a weighted linel. During the course of the ground truth data collection nine transects were completed in the study area while the BAFF, the ADCPs, and the active acoustic transducers were turned on or off to evaluate ambient acoustic noise in the study area. During analysis of the RTK data, the RTK track and the tag tracks were divided into four segments, with each segment made up of data from one or more transects that shared the same ambient noise conditions. Table 2 summarizes the ambient noise conditions and transacts for each of these four segments. The ground truth data collection was designed so that tracking accuracy could be compared for high ambient noise conditions versus low ambient noise conditions and as a result, segments one (high noise) and two (low noise) are made up of more transect data than segments three and four. As a result, tracking accuracy should not be compared between segments one or two, and segments three or four.

Table 1 - Tag Codes And Depths For Tag Drag Study

Tag #	Tag Code	Depth (m)
1	1020.06	1
2	2007.06	1.5
3	3078.06	2
4	4086.06	2.5

Table 2 - Study Area Conditions For Each Tag Drag Replicate

Segment	State	Transect
1	BAFF ON, Active Acoustics ON, ADCP's ON	Transects 2,7,8,9
2	BAFF OFF, Active Acoustics OFF, ADCP's OFF	Transects 4,5
3	BAFF OFF, Active Acoustics ON, ADCP's ON	Transect 3
4	BAFF ON, Active Acoustics OFF, ADCP's OFF	Transect 6

Results: Quantitative Comparisons of Echo Quantity

Number of Positions and Position Density

The first metric used to compare each Group of tracks is simply the number of points that make up each track. Because the same tracking software and settings were used to track the Group 1 and Group 2 data sets, differences in the number of points in each track should be due to differences in the echo selection process, so this metric provides a rough evaluation of how each technology identifies echos within a raw acoustic tag (.rat) file.

For the 291 fish tags, the mean difference between the number of points found for each tag in the Group 1 tracks versus the Group 2 tracks was -296, indicating that on average, the Group 2 tracks contained 296 more points than the Group 1tracks. However, as seen below in Figure 1, this average is skewed by a handful of large outliers.

Figure 1

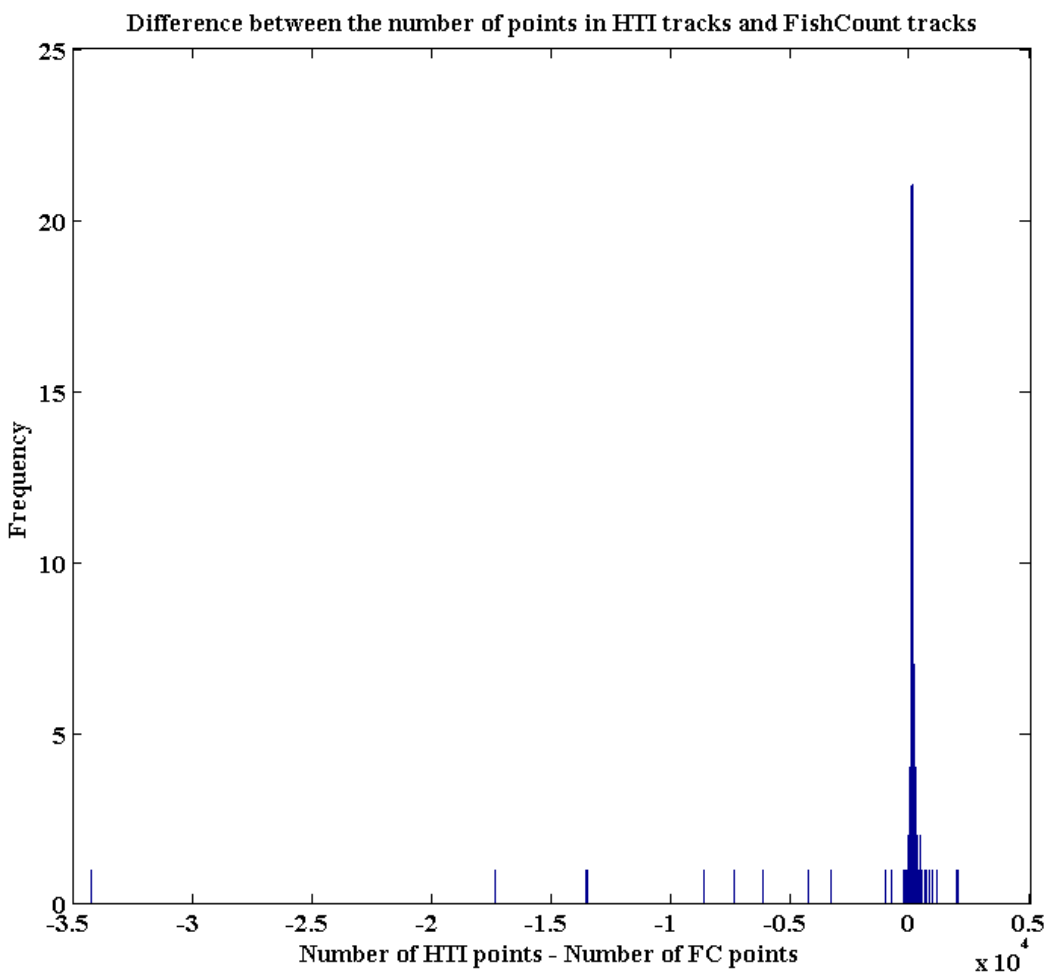

When these outliers are removed by limiting the range of differences to +/- 500 points, the average difference in the number of points between the Group 1 and Group 2 is 36, which indicates that for most of the tracks, the echo selection used by MarkTags, including the manual selection of signals that were initially removed by the automated process, detected slightly more echos than the fully automated FishCount process. However, the mean length for these tracks without the outliers included was a little over 1000 points, so a 36 point difference only represents about a 3% change in the length of each track. The distribution of differences with outliers removed is shown in Figure 2; negative differences indicate that the Group 2 track contains more points, positive differences indicate that the Group1 track contains more points.

Figure 2

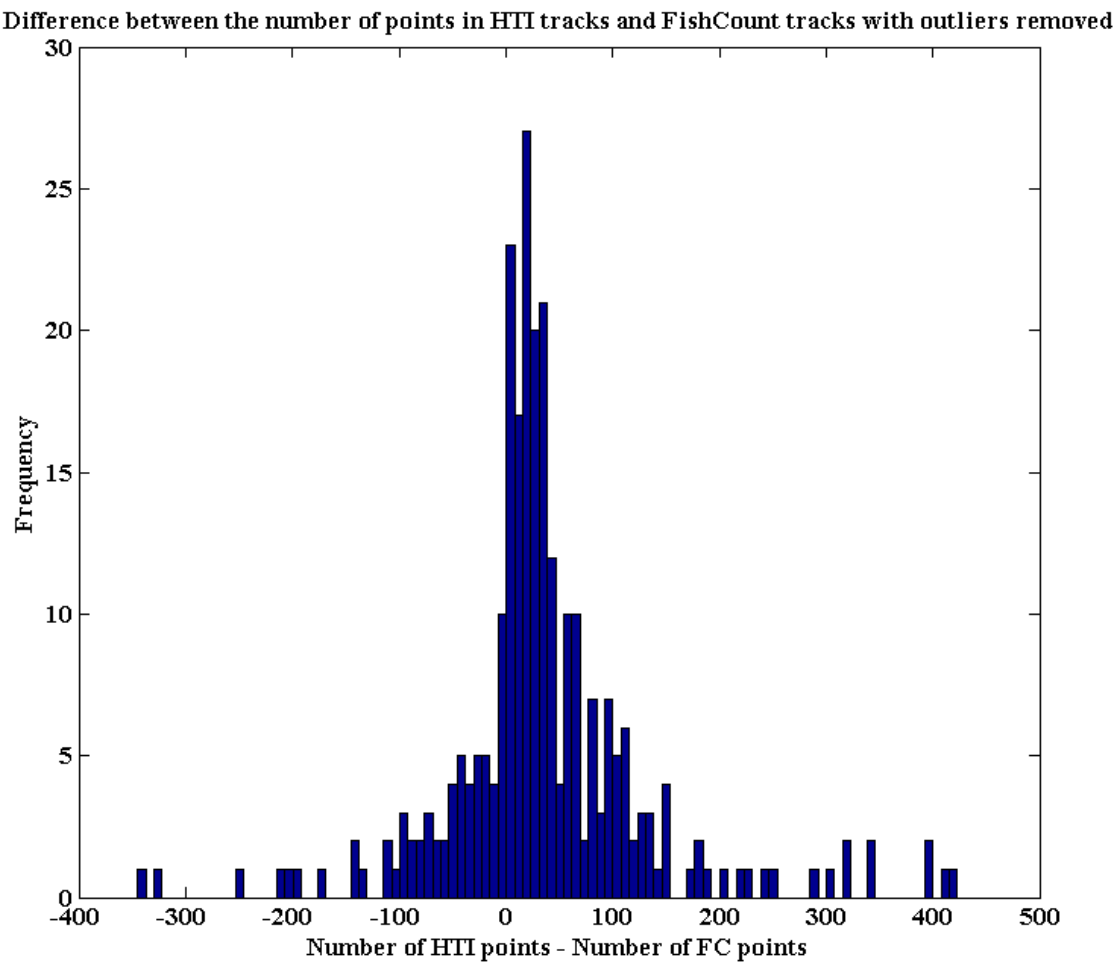

While the number of points in each track reflects each marking techniques overall ability to detect tag echos, the position density of each track indicates the percentage of echos emitted by each tag that were marked during the time that elapsed between the first and last point in each track. It is important to note that all of the echos emitted by a tag might not be recorded in a .rat file, so even if 100% of a tags echos are marked in a .rat file the track might not contain

100% of the theoretically possible echos; given the large amount of acoustic noise present in the study area during the 2012 study it is unlikely that many .rat files contained 100% of a tags possible echos.

The mean position density values for the Group 1 and Group 2 tracks are given in Table 3, and the distribution of position density differences between Group 1 and Group 2 tracks are shown in Figure 3. While there is a mean difference of +8.4% between the position densities of tracks generated by MarkTags vs FishCount, the distribution of individual track differences shown in Figure 3 indicates that this mean difference is mostly driven by a few tracks with large positive differences. This observation is supported by computing other measures of central tendency for the difference in position density across all 291 fish tracks, as the population of differences has a median of +1.3, and a mode of -1.5. Ultimately, it appears that the MarkTags marking technique is likely to produce tracks that have higher position densities, but the difference is likely to be much lower than the population averages would indicate.

Table 3

Group 1 Average Position Density (fish tracks)	83.5% of possible echos
Group 2 Average Position Density (fish tracks)	75% of possible echos

Figure 3

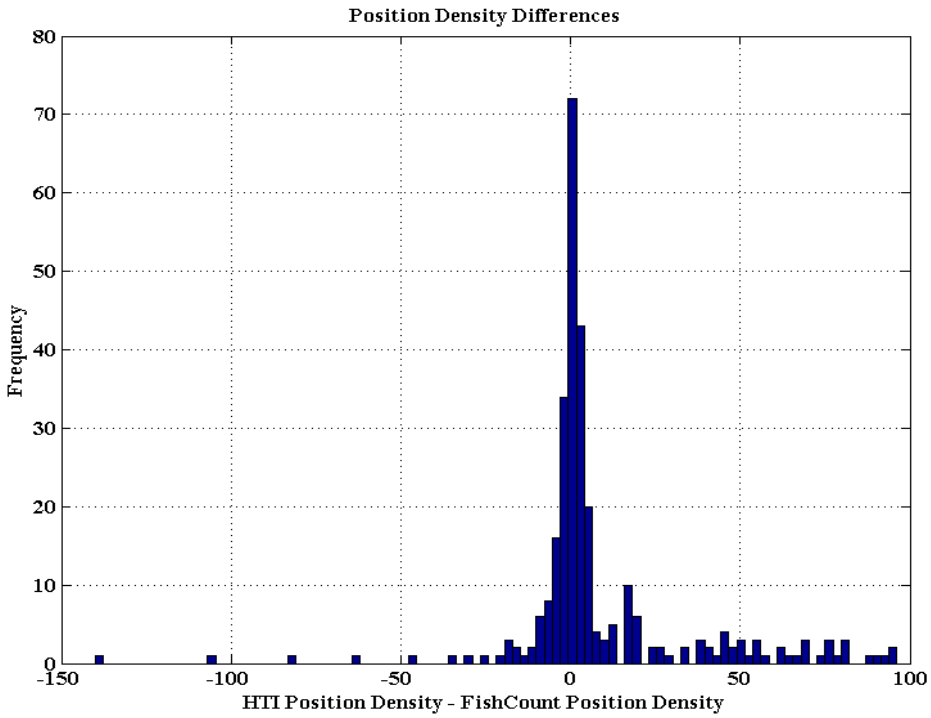

Figures 4 and 5 show the differences in the number of track points and track position densities between the Group 1 and Group 3 tracks. On average, GeneticFish produced 96 fewer positions per track, and Group 3 tracks had a lower position density by about 8 percent detections. However, these differences are to be expect, as the MarkTags acoustic tag tracking parameters were configured to produce two-dimensional tracks and calculated a position for pings recorded on three or more hydrophones, while GeneticFish was configured to produce full three-dimensional solutions. As a result, GeneticFish was constrained to tracking pings recorded on four or more hydrophones. While this means that echo quantity comparisons are not particularly useful for evaluating GeneticFish, it is worth noting that including pings recorded on only 3 hydrophones (two-dimensional positions only) resulted in about a 10% increase in the amount of usable track data for the 2012 study; although this number will certainly vary with array geometries, it might be a useful starting point for evaluating trade offs in future study designs.

Figure 4

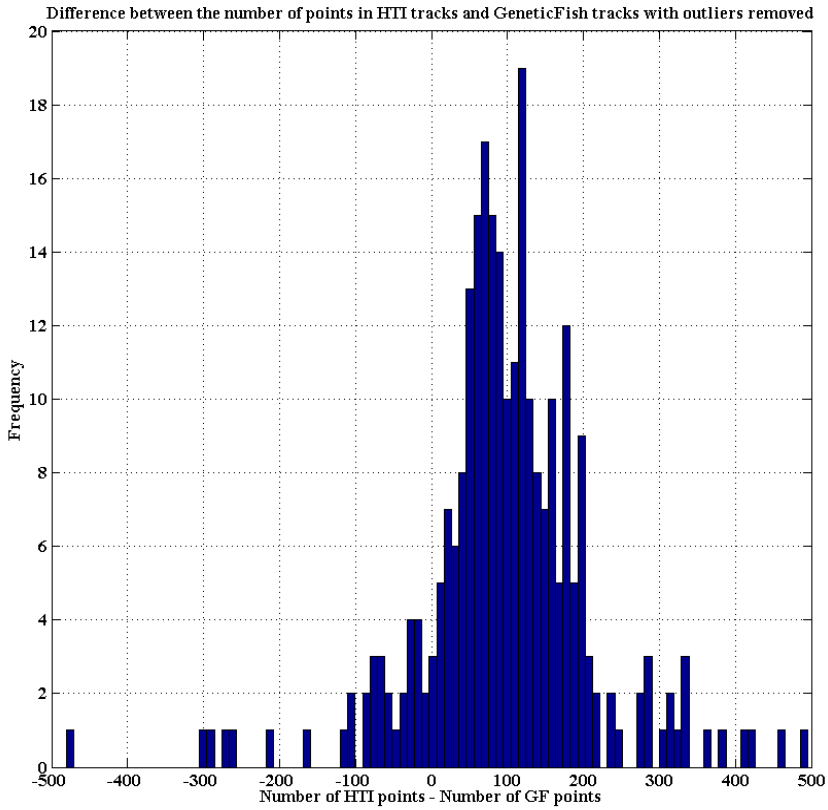

Figure 5

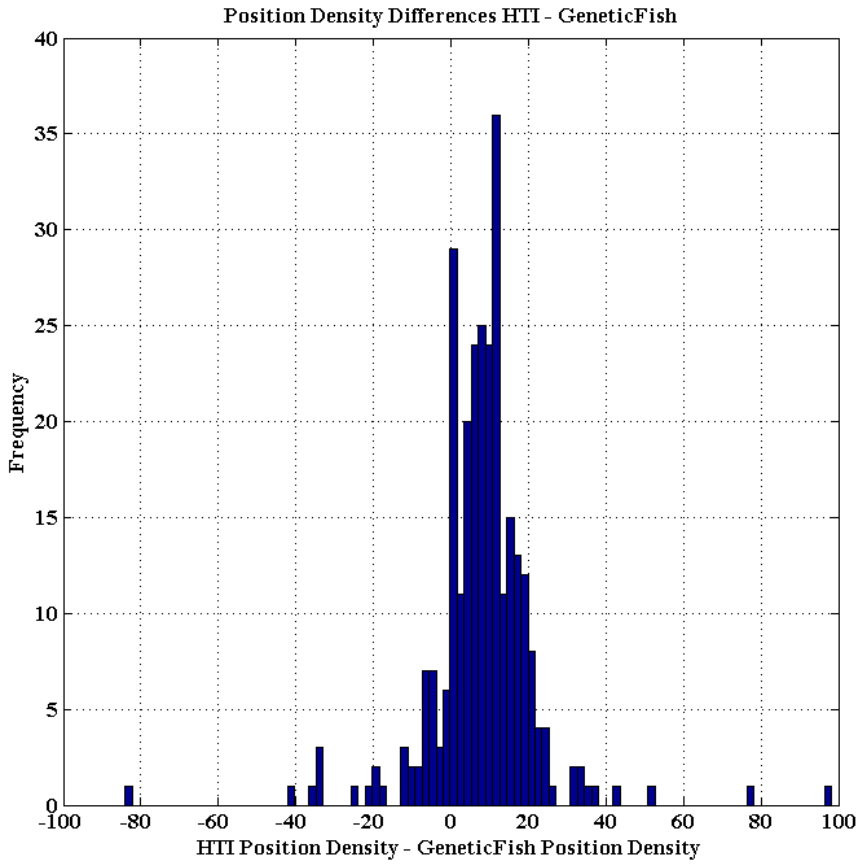
Position Density Differences HTI - GeneticFish
Frequency
HTI Position Density - GeneticFish Position Density
40
35
30
25
20
15
10
5
0
-100
-80
-60
-40
-20
0
20
40
60
80
100

Results: Comparison of Echo Quality

Sinuosity

The number of tracked points and position density provide an indication of how effective an echo marking technique is at detecting tag signals in a .rat file. However, in environments where multipath is a possibility it is important for echo marking techniques to be able to select the first echo (often called the primary echo) for tracking and at the same time reject echos created by multipath. If multipath is marked, either instead of the primary echo or in the absence of a primary echo, then the position estimate for that echo is likely to have an increased level of error. This type of error often results in increasing the total integrated length of the track while resulting in a negligible increase in the overall displacement of the track. As a result, the difference between the sinuosity of Group 1 and Group 2 track can be indicative of differences in the number of multipath echos selected by MarkTag and FishCount.

Figure 6 shows the distribution of differences between the sinuosity of Group 1 tracks and Group 2 tracks for the 291 fish tags. The negative distribution mean of -0.085 m/m represents a +4.6% increase in the sinuosity of Group 2 tracks versus Group 1 tracks, which suggests that on average, the Group 1 marking process did a slightly better job of rejecting multipath echos than the Group 2 marking process.

Figure 6

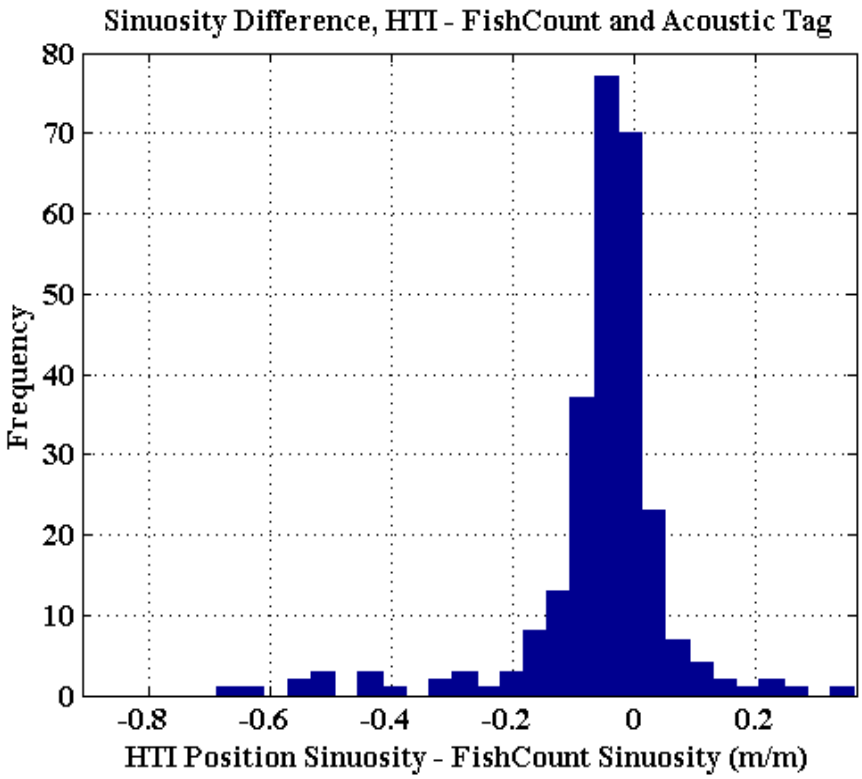

The fish tracks produced by Geneticfish had significantly higher sinuosity than either set of tracks produced by AcousticTag. Figure 7 shows the distribution of differences between the sinuosity of Group 1 tracks and the sinuosity of Group 3 tracks with outliers removed; the mean difference of -1.6 m/m represents a 116% increase in sinuosity for Group 3 tracks, but the distributions negative skew indicates that many Group 3 tracks were 200%-300% more sinuous than the Group 1 tracks. Given the significant differences in the tracking process used to create these two sets of tracks it is likely the sinuosity differences are almost entirely due to the tracking processes and not indicative of differences in echo selection efficacy.

Figure 7

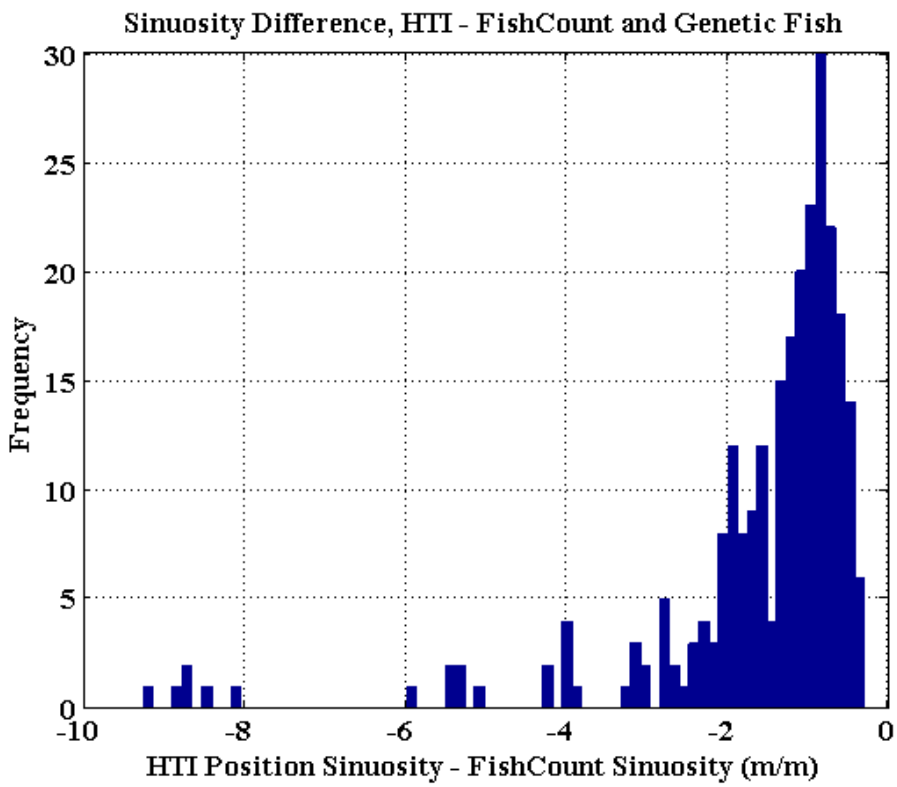

Location and Velocity at Phenomenon Time

While measures of echo quantity and track sinuosity provide broad quantifications of marking performance between the two methodologies, they do not assess differences in the tracks that could have influenced the evaluation of the NPB. In order to evaluate whether differences between the echo selection technologies might result in different interpretations of the data, the location of each fish at the phenomenon time provided in the fates spreadsheet was interpolated using each set of tracks, and the resulting phenomenon locations were compared. Additionally, the net advection vector for each tag was calculated for the 10 sec leading up to the phenomenon time (approach vector) and for the 10 sec after the phenomenon time (exit vector), and these vectors were compared by computing the angle, in degrees, between the Group 1

entrance and exit vectors, and the corresponding vectors computed for the Group 2 and Group 3 tracks.

The distribution of distances between the phenomenon location computed using Group 1 and Group 2 tracks is shown in Figure 8. Although the mean distance difference was 2.5 m, the distribution had a significant positive skew, and in reality, the majority of the Group 2 tracks were within 2 m of the Group 1 acoustic tag tracks at the phenomenon time.

Figure 8

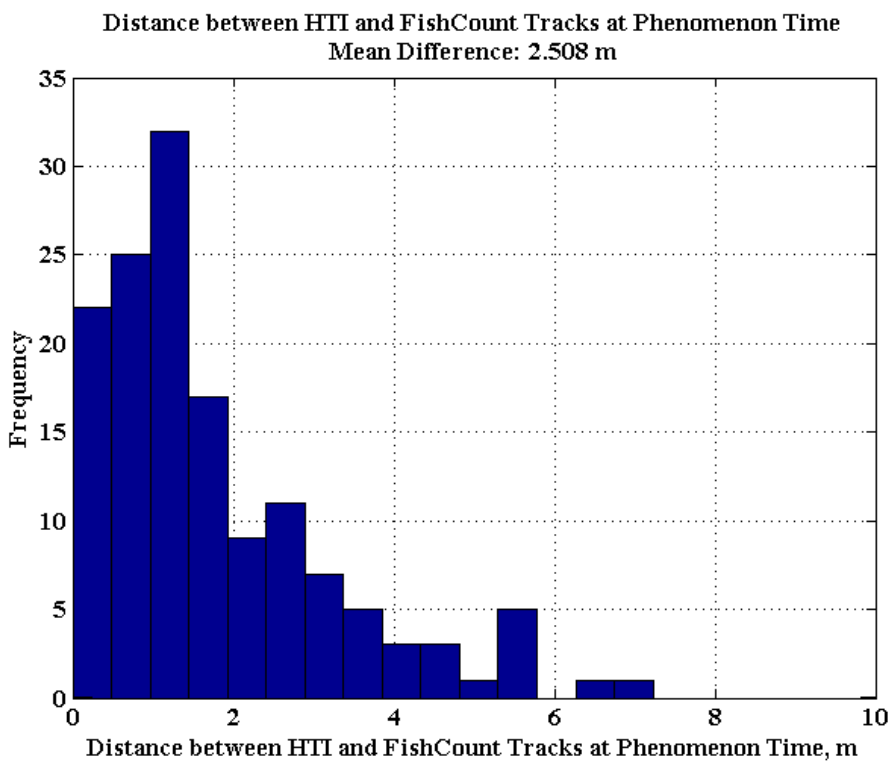

Distributions of angle differences between entrance and exit vectors computed from Group 1 tracks and Group 2 tracks are shown in Figure 9 and Figure 10. The magnitude of the differences in the entrance and exit vectors is larger than one would expect given the relatively small differences in the other comparison metrics. However, when tracks for individual tag codes were analyzed in detail we found that the Group 1 and Group 2 tracks were more similar than the angular differences would suggest. In these cases, the disagreement in the entrance and exit angles was not due to radically different track shapes, but rather, timing discrepancies between the two sets of tracks.

Figure 11 illustrates how timing differences can lead to discrepancies in entrance and exit vectors. For the tag show in Figure 11, the Group 1 track appears to be about 1 minute behind the Group 2 and Group 3 tracks. Because the Group 1 track is delayed relative to the Group 2 and Group 3 tracks, computing entrance and exit vectors based on the phenomenon time

means that the entrance and exit vectors will be calculated for different points in space for each track. Given the rapid directional change of this track in the area around the phenomenon point, even a small discrepancy in timing will result in radically different vector angles between the Group 1 and Group 2 tracks. We were unable to examine every track with significant differences between the Group 1 and Group 2 vectors, but examination of a small subset of tracks with large discrepancies indicated that the majority of the errors was due to discrepancies in timing rather than major spatial differences in tag positioning.

Figure 9

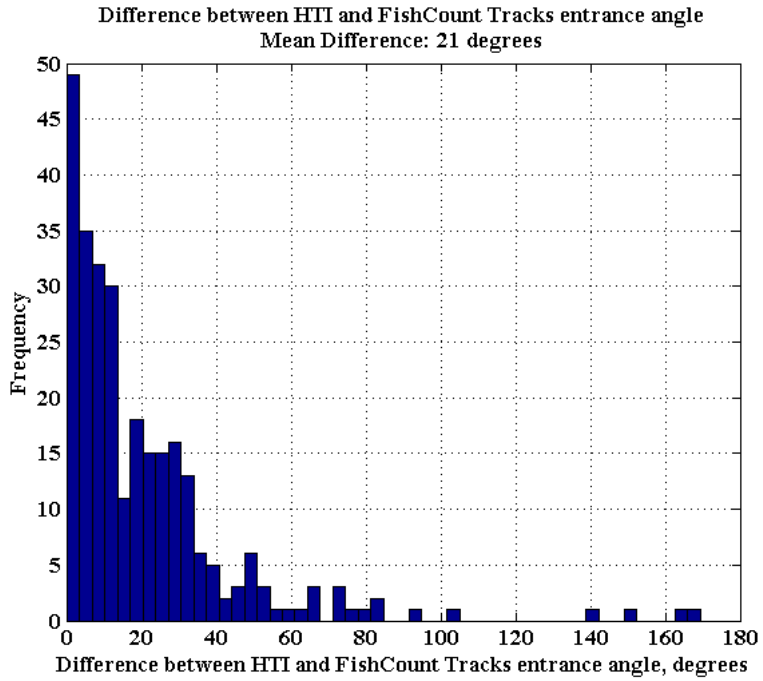

Figure 10

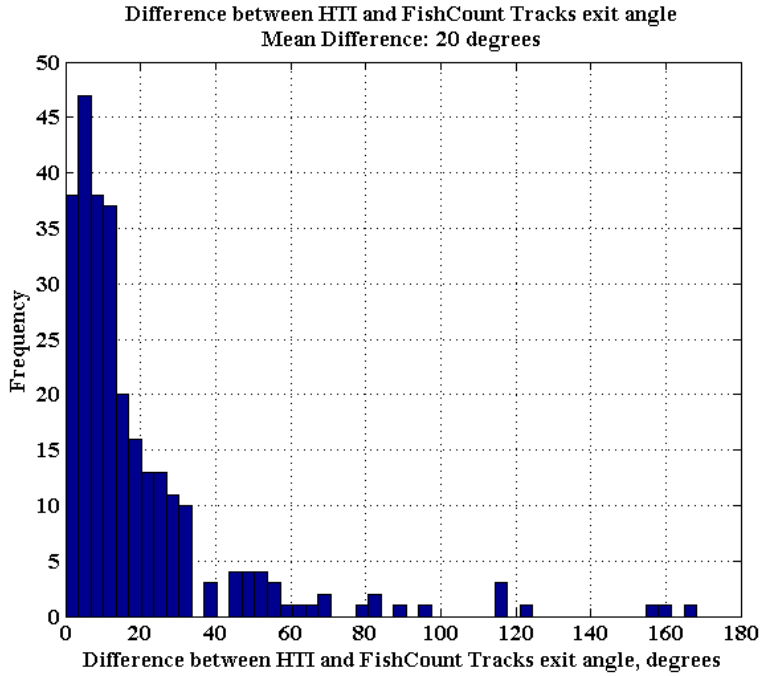

Figure 11

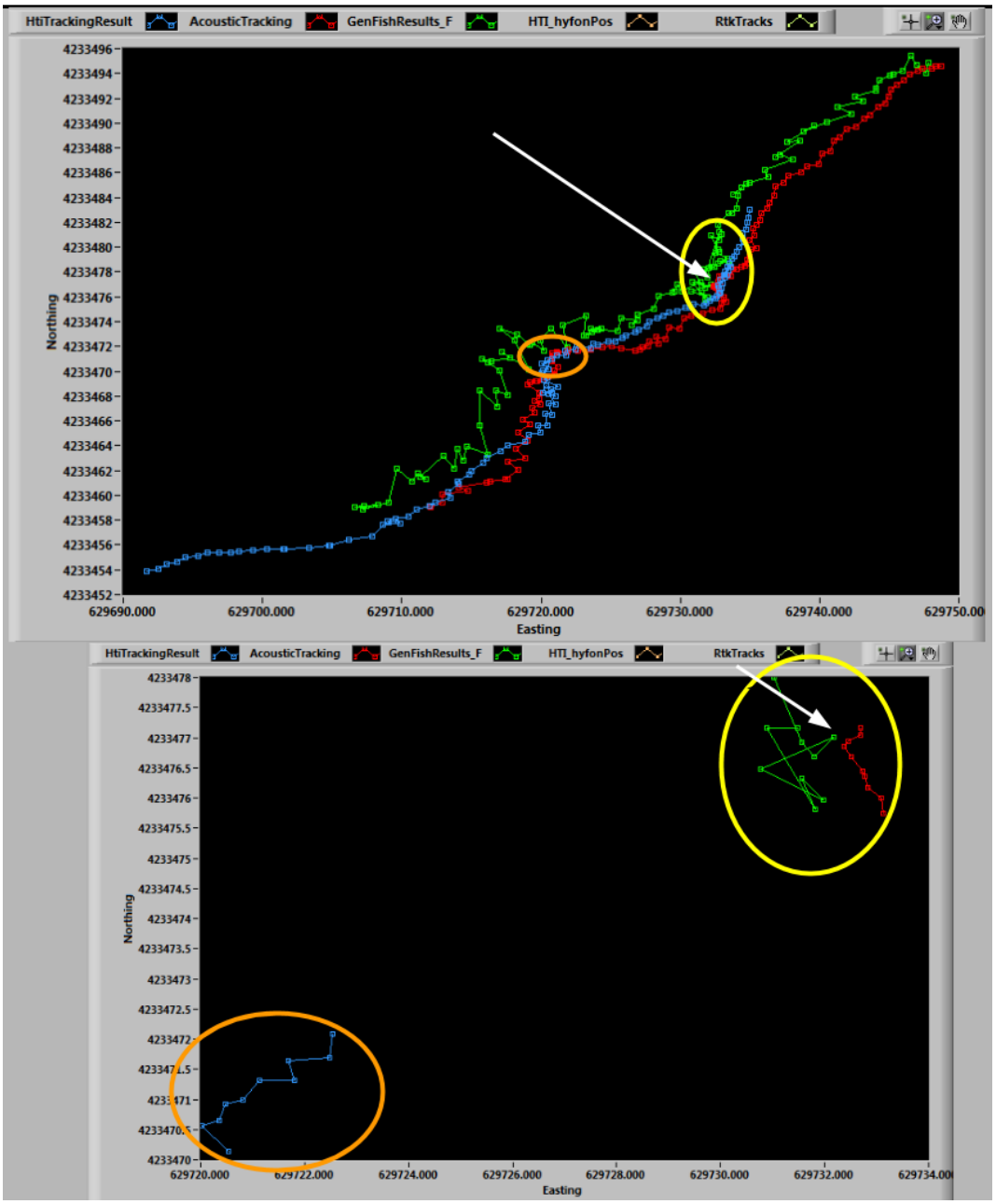

Figure 11 - Illustration of the effects of timing discrepancies on computed entranced vectors. The tracks shown in each pane have been clipped spatially to have the same start and end times: the Group 1 AcousticTag track is shown in blue, the Group 2 track is shown in red, and the Group 3 GeneticFish track is shown in green. The yellow oval highlights the 10 second period leading up to the phenomenon time for the Group 2 and Group 3 tracks, and the orange oval highlights the 10 seconds leading up to the phenomenon time for the Group 1 track. The location of the phenomenon point given in the fates spreadsheet is shown by the white arrow. The lower pane shows only the 10 seconds leading up to the phenomenon time for all tracks.

The distribution of differences between the phenomenon point locations between Group 1 and Group 3 is shown in Figure 12, and the distribution of differences between the approach vector and exit vectors for these sets of tracks are shown in Figure 13 and 14. Overall, the distributions of these metrics are very similar to those comparing Group 1 and Group 2 tracks. One noticeable difference is that the distribution of phenomenon point location differences for the Group 3 tracks appears to be very similar to that for the Group 2 tracks, but shifted to the right by slightly less than 1 m. This is likely due to the fact that the Group 3 tracks are not smoothed, and appear to have slightly less than 1 m of random error in the positioning. Thus, it is likely that the Group 3 tracks have the same systematic timing errors as the Group 2 tracks, with an additional random error with a mean amplitude of about 0.7 m. As discussed above, the Group 2 and Group 3 tracks appear to be closely synchronized, so differences between the Group 1 track and Group 3 track entrance and exit vectors are likely due to timing discrepancies as well.

Figure 12

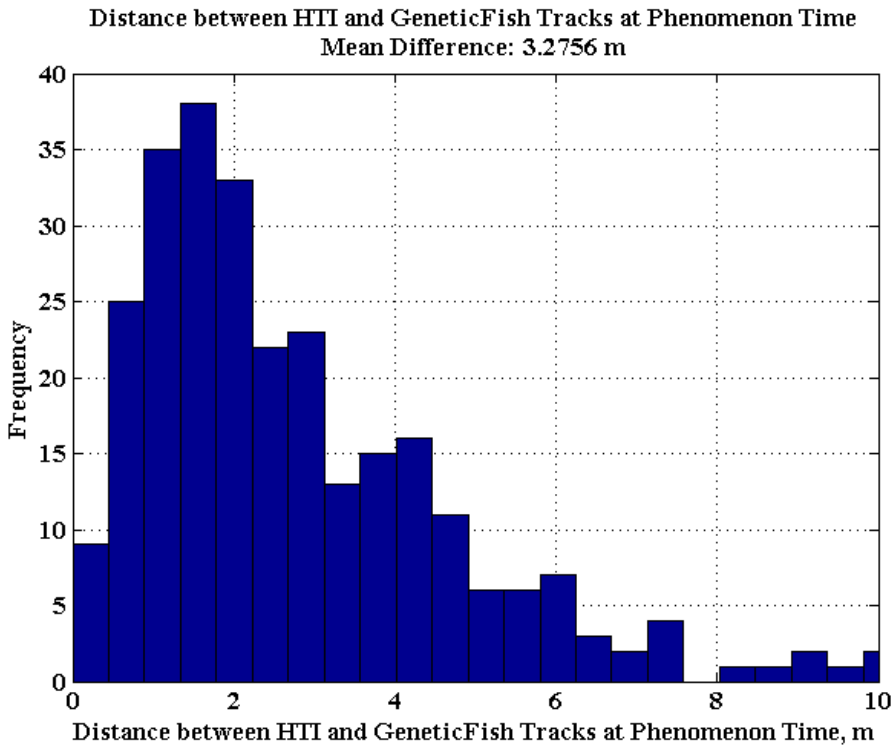

Figure 13

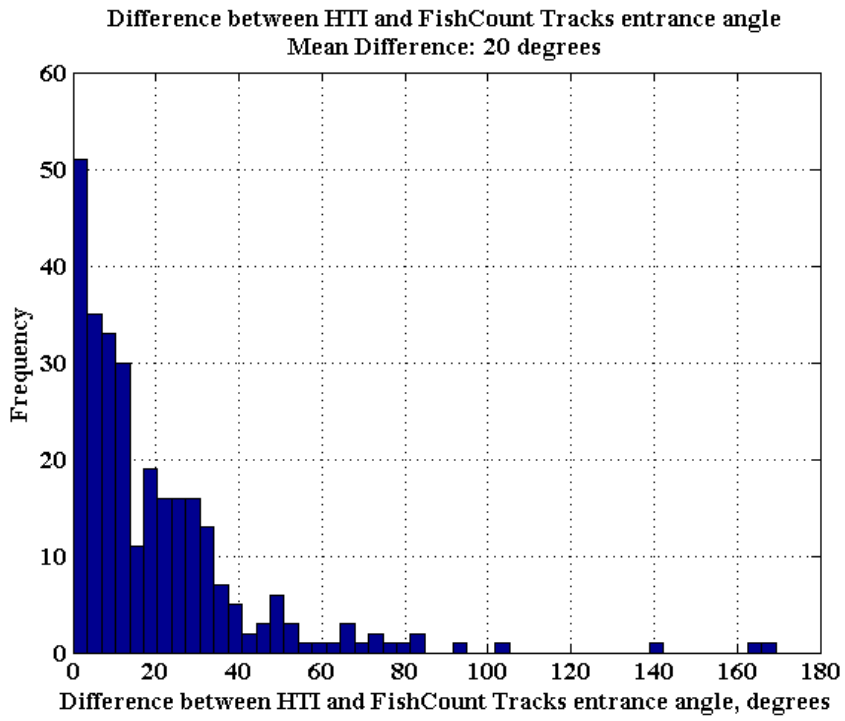

Figure 14

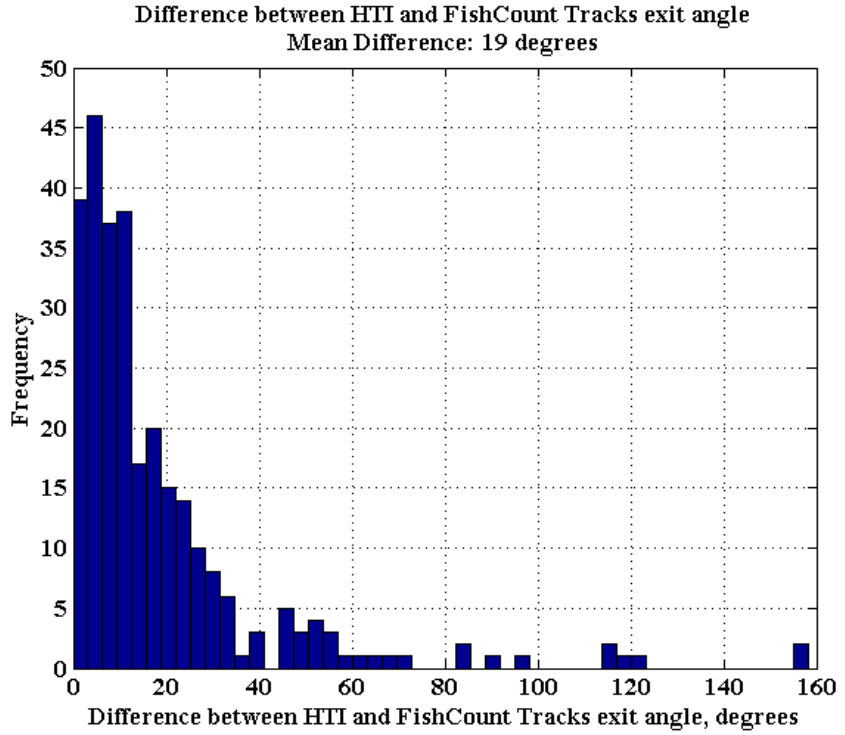

Discussion and Recommendations

Choice of echo selection technology

A primary goal of the track comparison study was to determine whether the FishCount automatic echo selection algorithm can be used to produce multidimensional fish tracks of the same quality as those produced with echos selected manually using the HTI MarkTags software. The echo quality and quantity metrics analyzed for the 291 fish tag tacks suggest that performing echo selection with FishCount will result in a slight degradation in track quality, with quantitative measures of track quality decreasing on the order of a few percentage points. If reductions in data processing cost and data turnaround time can be achieved using FishCount to automate echo selection on cloud platforms, then these benefits should be weighed against the risk of a slight decrease in track quality when designing future studies.

Recommended development to support future studies

Whenever time series data is combined, the time reference used to collect that data is crucial to being able to link observed events to each other. Fisheries studies are increasingly able to take advantage of systems that measure such variables as the location of an individual fish at any given time, or the current local environmental conditions at any given time, to ever increasing levels of accuracy and precision. This allows new insights into fish behavioral responses and greater understanding of migration patterns on very small scales. When these measurements are combined, their basic time reference must be the same and must be comparable in accuracy and precision in order for causal inferences to be meaningful.

1. Use a recognized, universal time source for all timestamps in data files. A variety of instruments collected data in 2012 that was linked to time, and was combined with other data to enhance the interpretation of fish behavior. For data sources to be useful, they should all have a common (or derivable) universal time source linked to a recognized standard. GPS receivers all produce very accurate timing signals, and are probably the only readily available sources of time signals that are both accurate and precise. For instruments that do not have a direct link to GPS receivers, the time stamps should be in a form that can be converted to the agreed upon offset from UTC (the time reference output by GPS receivers when a multi-satellite fix is achieved), and should be as accurate and precise as possible, given the nature of the data collected and its intended use.

2. Prior to the start of data collection, all data collection systems should be reviewed to ensure that the times that are to be stored in the data files will allow merging with other data sets, to the level of accuracy required for the fulfillment of project objectives. If it is possible to represent time in a standardized way for all systems, this should be done, or time should at least be represented so that appropriate conversions can be accomplished after data is recorded.

3. Allow time prior to the start of data collection to collect and process at least some ‘ground truth’ GPS data to ensure that project objectives will be met by the observed level of tagged fish position accuracy.

4. Allow time prior to the start of data collection to merge a small subset of data from all data sources expected to be used, in order to ensure that the time references for all data sets are properly aligned.

5. Continue to improve marking and tracking software, in simplicity of use, in accuracy and repeatability of fish positions, and in turnaround time of results.

Attachment E-1: Evaluation of Absolute Accuracy

Analytical approach

The tracks created during the GPS ground truth exercise were analyzed separately from the rest of the fish tracks because the GPS record makes it possible to measure the absolute accuracy of each set of tracks, rather than making relative comparisons between the Groups of tracks.

The first step in the analysis of all of the track sets was to develop a correction factor to account for timing differences between the tag tracks and the GPS track. These timing differences are due to the fact that the tag tracks are referenced to timestamps generated using the Windows operating system time on each acquisition computer, while the GPS track has true sub second timing accuracy. An individual offset was calculated empirically for each tag code in each of the Group 2 and Group 3 tracks as follows;

1. For every point in a tag track, the closest GPS point in space was found and the difference between the track point time and that GPS point time was calculated.
2. The population of resulting time differences was examined and thresholds were determined manually for rejecting outliers.
3. After outliers were rejected the mean of the resulting population of time differences was used as a fixed offset to correct the timestamp of every point in that tag track.

This process was not followed to correct the Group 1 tracks because they included a 12 Khz clock value that was synchronized to GPS timing chips attached to the ATRs. The Group 1 tracks for the GPS tags were reprocessed using Labview software that replaced the standard Group 1 date-time string for each track point with a decimal Day of Year (DOY) time stamp with sub millisecond precision computed using the 12Khz clock value associated with each position. Although the accuracy of this technique has not been verified, it is thought to be sub-second.

After the timestamps for each set of tracks were corrected, the GPS tracks were interpolated to produce a GPS position estimate for the time stamp associated with each tag track position estimate. The interpolated GPS positions were then used to evaluate the absolute accuracy of each set of tag tracks. Absolute accuracy was quantified for each point in terms of total error, along-track error and cross-track error, and easting and northing error. Along track error was estimated using a second-order central difference derivative to estimate easting and northing velocity components, normalizing the resulting velocity vector to estimate along track direction, and taking the dot product between this direction vector and the point's error vector.

The along track vector was rotated 90° to estimate the cross track vector, and the normalized cross track vector was dotted with the error vector for each point to calculate the cross track error. For the purpose of this analysis, cross track error is a better predictor of the ability to estimate tag positions with each tracking technology because small errors in timing synchronization can result in a systematic errors along the length of the track. These systematic errors are unlikely to bias statistical measurements of cross track error. Measures of cross track error are presented in two forms: 1) true cross track error, which is greater than

zero for errors to the left of the path of the and less than zero for errors to the right of the path of the tag, and 2) cross track error magnitude, which is the absolute value of the true cross track error.

All of the point error metrics were compiled into error populations for each tag code and track segment. In order to focus the error analysis on the normal tracking performance for each segment, absolute error or cross track error values greater than 10 m were treated in a special manner: 1) when compiling the distributions of the error, values greater than 10 m were given a fixed value of 10.0 m, 2) when calculating means for each track segment, values greater than 10 m were removed from the sample, and 3) when plotting error scatter plots, values greater than 10 m were colored black. This approach was taken to prevent a few large outliers from biasing distributions, colormaps, or estimates of central tendency.

Group 1 Track Set Accuracy

Group 1 track segment points for each of the GPS test tags colored by total error are shown in Figure 15, while the total error distributions for each of these track segments is shown in Figure 16. Each row in these figures represents tracks with the same acoustic conditions, and each column represents tracks from the same tag. Tag depth is constant in each column, with tag depth increasing as the panels in the figure are viewed from left to right. There are several important attributes of the accuracy of Group 1 track that are illustrated by these plots. First, by examining a single row at a time one can see that both the magnitude and the variance of the absolute error in the tracks increases moving from left to right for all rows, indicating an increase in total error from tag1 to tag 4. This is most likely due to the fact that the AcousticTag settings used to produce this data assumed a fixed, near-surface depth for each tag, and as a result, any difference between the assumed tag depth and the actual tag depth could be translated into increased horizontal error. This explanation is consistent with our understanding of the AcousticTag algorithms, but due to the fact that the tag code also increased with tag depth, it is possible that there is some positive relationship between tag code and total error that is contributing to the pattern.

The second important attribute of the accuracy of the Group 1 tracks can be seen by comparing the error histograms or scatter plots in row one to those in row two, and by comparing the plots in row three to those in row four. The mean and variance of the absolute error distributions in Figure 16, row two, are greater than the mean and variance of the distributions in row 1. This means that the transects conducted with all noise sources turned off (second row, labeled “segment 2”) had lower tracking accuracy than the transects conducted with all noise sources turned on (first row, labeled “segment 1”). This is counterintuitive because decreasing the amount of ambient noise usually results in increased tracking accuracy. That said, both the Group 2 and Group 3 track sets showed the same trend, so there is some physical process leading to the inverse relationship between ambient noise and tracking accuracy.

The relationship between the error distributions shown in row 3 and row 4 of Figure 16 is more intuitive; for tags passing near the barrier, tracking accuracy is higher with the barrier on, but all

active acoustic sources turned off, then for tags that pass through this area with the barrier off and the active acoustics turned on. This result is not surprising, given that past studies have shown that side-looking ADCPs and active acoustic transducers can have a significant effect on tracking accuracy.

One aspect of the Group 1 GPS track set that is consistent for all tags and noise levels is that many points have total error values that are greater than pre-study accuracy predictions. Given these unexpectedly high error levels, a variety of analysis were conducted to look for sources of systematic error in either the tracking process or the grountruthing process. The total error was divided into cartesian components for each tag segment to look for an array positioning error, but the easting and northing error distributions for each tag segment showed no consistent coordinate errors. When the total error was broken into along track and cross track components the cross track error magnitude showed similar relationships between noise, depth, and accuracy as the total error, but the cross track error magnitude was consistent with pre-study accuracy predictions (Figure 17 and Figure 18). Unexpectedly, the along track error was significantly greater than the cross track error, and was the cause of the high total error values. Ordinarily, elevated along track error values in this type of ground truth data would indicate a systematic error in synchronizing the tag tracks with the GPS tracks. However, given the expected accuracy of the timing process applied to the Group 1 track set this type of error is unlikely, and temporal offset distributions computed using the method employed for synchronizing the Group 3 and Group 2 track sets showed no systematic timing error between the GPS record and the Group 1 track set. Instead, the spatial distribution of the along track and cross track errors in the Group 1 tracks suggest that much of this error is the result of a smoothing process internal to the AcousticTag positioning algorithm.

Figures 19 through 22 illustrate the spatial distribution of total error and cross track error in the Group 1 track for Tag 4, Segment 1, and provide a good example of the unique error structure of the Group 1 track set. When comparing the color maps of total error against the color maps of cross track error in Figures 19 and 20, it becomes clear that the cross track error is often the lowest when the total error is large. The reason for this discrepancy is more clear when tracks are viewed at high magnification, as illustrated in Figure 21. By drawing a line connecting each tag track point to its corresponding interpolated point from the GPS track (Figure 21, frame 1) it appears that the Group 1 tracking algorithm closely matched the tag track to the GPS path in the cartesian plane, but the tag track is out of sync with the GPS path. The tag track appears to consists of points that are uniformly spaced along a smoothed approximation of the GPS path in both time and space, so the resulting track points are longer and temporally synchronized with the GPS path. Because the track points are no longer temporarly synchronized with the GPS path, the track of the tag contains erroneous velocity and acceleration information. Although we lack the ground truth data to determine if these errors are present in the 291 fish tracks analyzed in the quantitative analysis section, this type of along track error would explain the systemic timing discrepancies that were discovered while analyzing the entrance and exit vector angles at phenomenon point . The temporal discrepancy illustrated in Figure 12 appears similar to the timing errors found in the ground truth data, and could be explained by a systemic along track error in the estimate of the position of the tag. Another consequence of the apparent

smoothing in the Group 1 tracks is that the angular accelerations are dampened. This is well illustrated in Figure 22, where the Group 1 track smooths out the tight corners in the GPS path. Although the exact nature of the smoothing applied to the Group 1 tracks is unclear, this behavior is consistent with other applications of a low-pass filter being applied to spatial data.

Figure 15

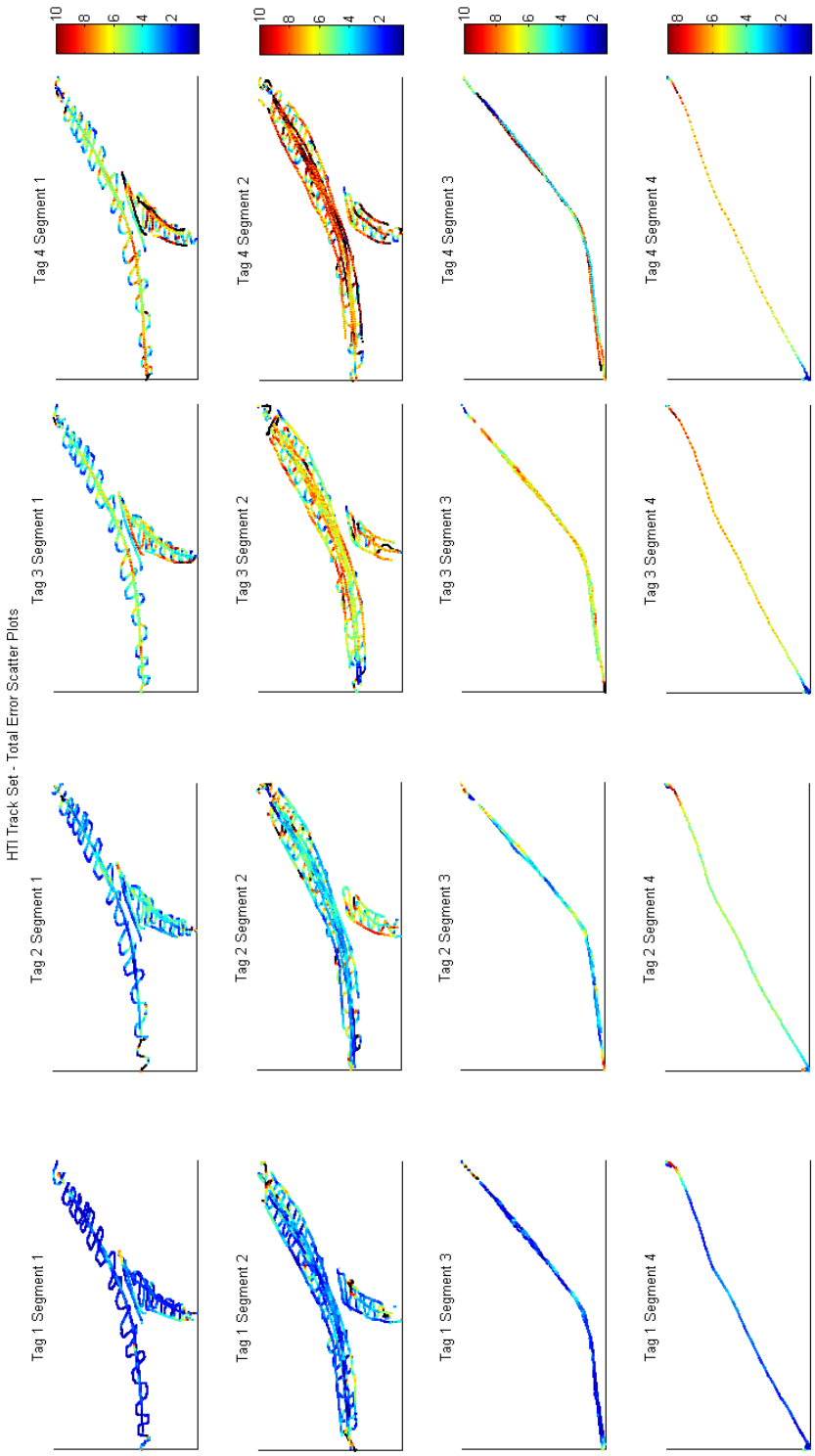

Figure 15 - Group 1 GPS tag track positions colored by total error, in meters. The color gradient is the same for all frames, indicated by the color bars to the right. Hotter colors represent increasing error.

Figure 16

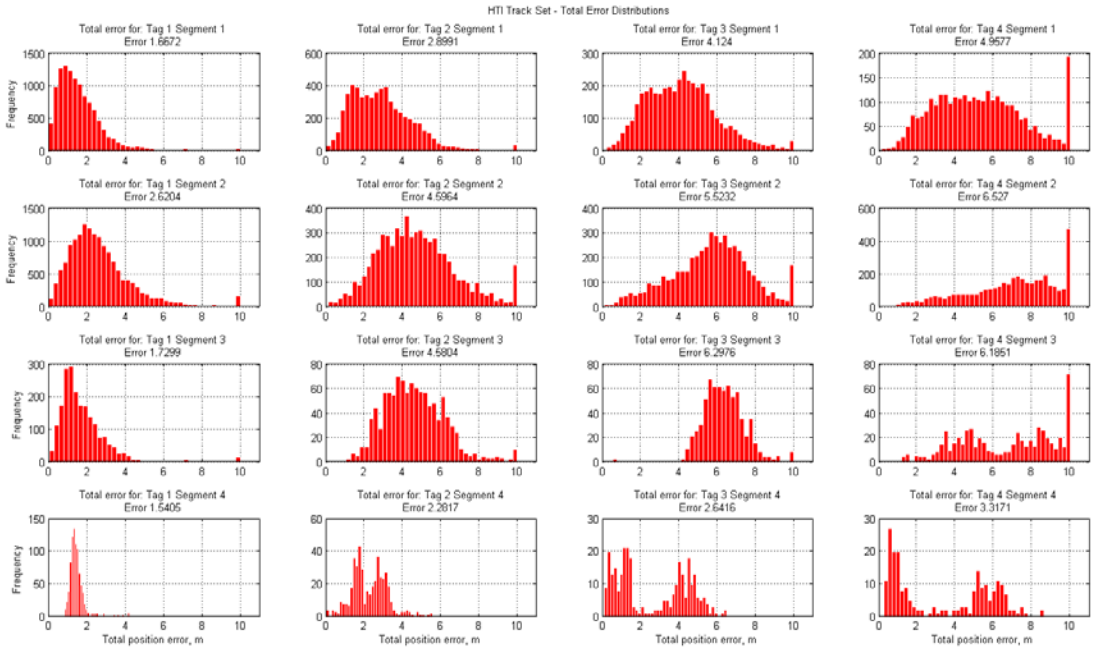

Figure 16 - Group 1 GPS tag track total error distributions for each tag segment. For display purposes, all error values greater than 10 meters are shown in the 10 meter bin on the histograms. Total error values greater than or equal to 10 meters were discarded before the distribution means were calculated; as a result the distribution means indicated may underestimate central tendency.

Figure 17

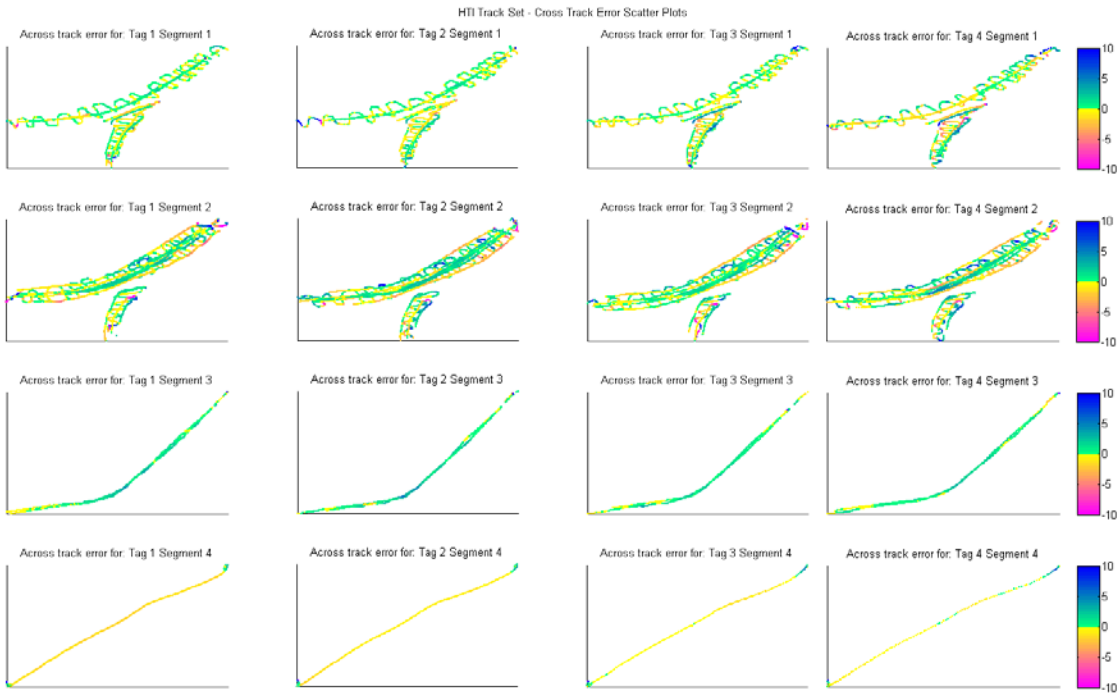

Figure 17 - Group 1 GPS tag track positions colored by cross track error, in meters. The color gradient is the same for all frames, indicated by the color bars to the right.

Figure 18

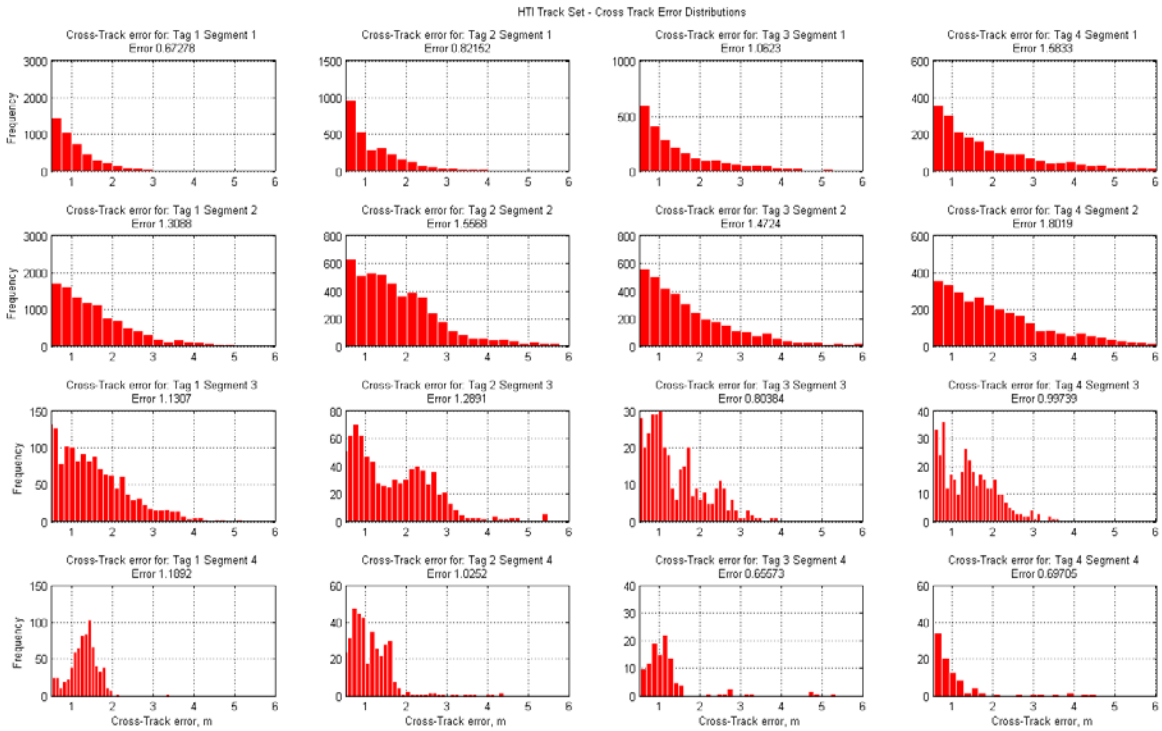

Figure 18 - Group 1 GPS tag track cross track error magnitude distributions for each tag segment. For display purposes, all error values greater than 6 meters are shown in the 6 meter bin on the histograms. Total error values greater than or equal to 10 meters were discarded before the distribution means were calculated; as a result the distribution means indicated may not be an accurate representation of central tendency.

Figure 19

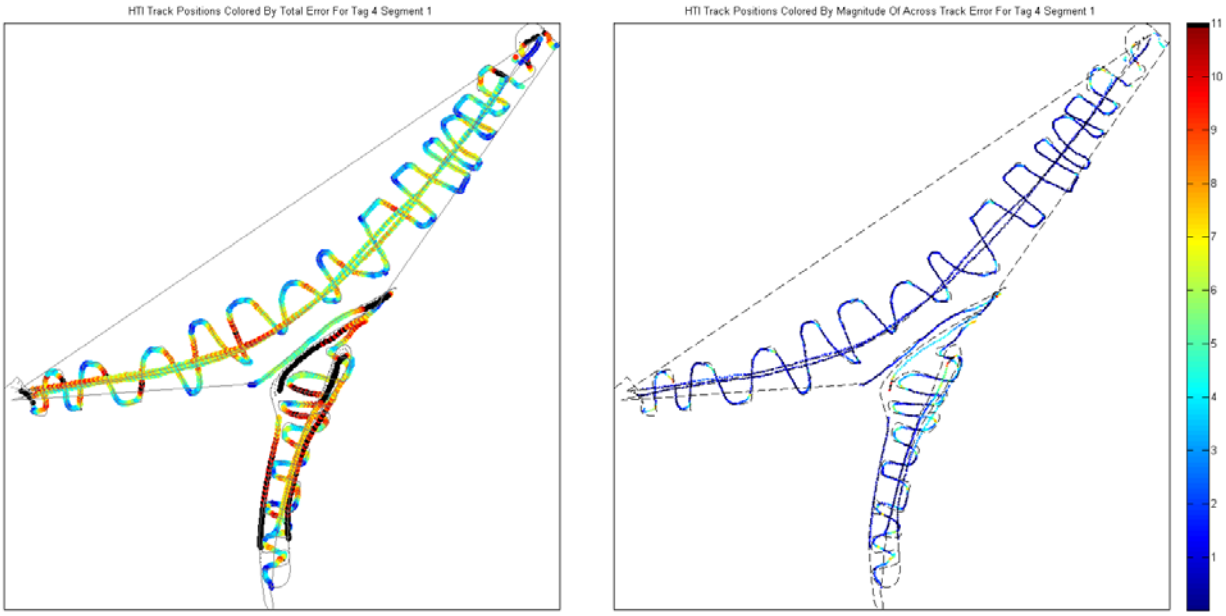

Figure 19 - Group 1 GPS tag track positions for Tag 4 Segment 1 colored by total error, in meters, in frame 1, and colored by magnitude of cross track error, in meters in frame 2. The color gradient is the same for both frames, indicated by the color bar to the right. Hotter colors represent increasing error, black indicates an error value greater than 10 meters. In the first (left) frame the gps path is shown as a solid grey line, with dotted black lines connecting each tag position to the corresponding interpolated gps track position. In the second (right) frame the gps track is shown as a dotted black line.

Figure 20

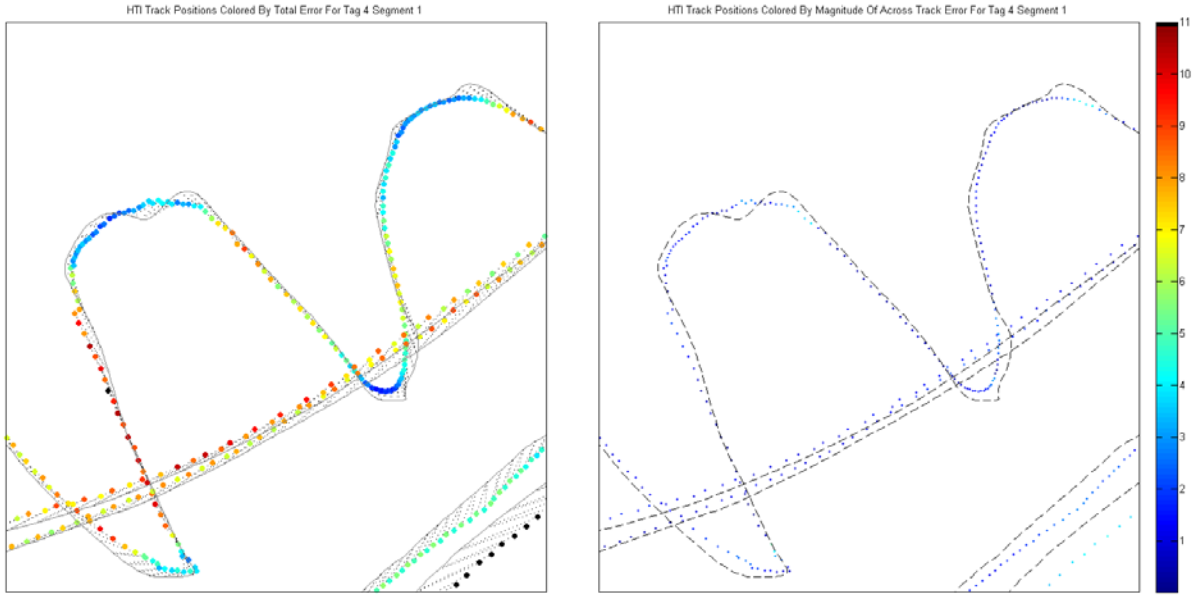

Figure 20 - Group 1 GPS tag track positions for Tag 4 Segment 1 colored by total error, in meters, in frame 1, and colored by magnitude of cross track error, in meters in frame 2. The color gradient is the same for both frames, indicated by the color bar to the right. Hotter colors represent increasing error, black indicates an error value greater than 10 meters. In the first (left) frame the gps path is shown as a solid grey line, with dotted black lines connecting each tag position to the corresponding interpolated gps track position. In the second (right) frame the gps track is shown as a dotted black line.

Figure 21

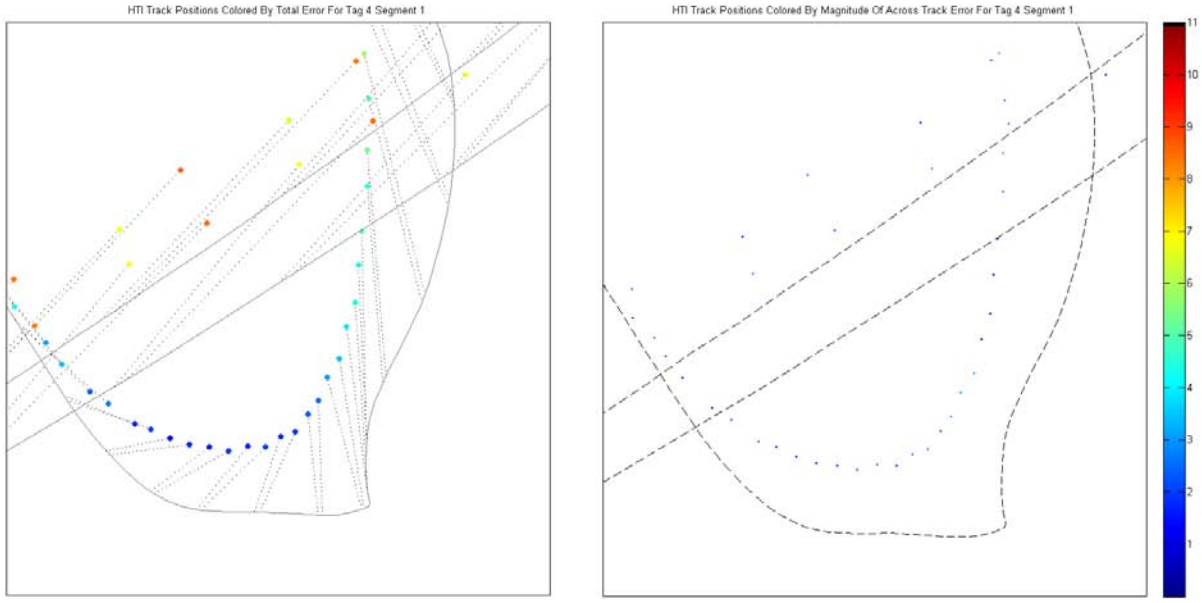

Figure 21 - Group 1 GPS tag track positions for Tag 4 Segment 1 colored by total error, in meters, in frame 1, and colored by magnitude of cross track error, in meters in frame 2. The color gradient is the same for both frames, indicated by the color bar to the right. Hotter colors represent increasing error, black indicates an error value greater than 10 meters. In the first (left) frame the gps path is shown as a solid grey line, with dotted black lines connecting each tag position to the corresponding interpolated gps track position. In the second (right) frame the gps track is shown as a dotted black line.

Figure 22

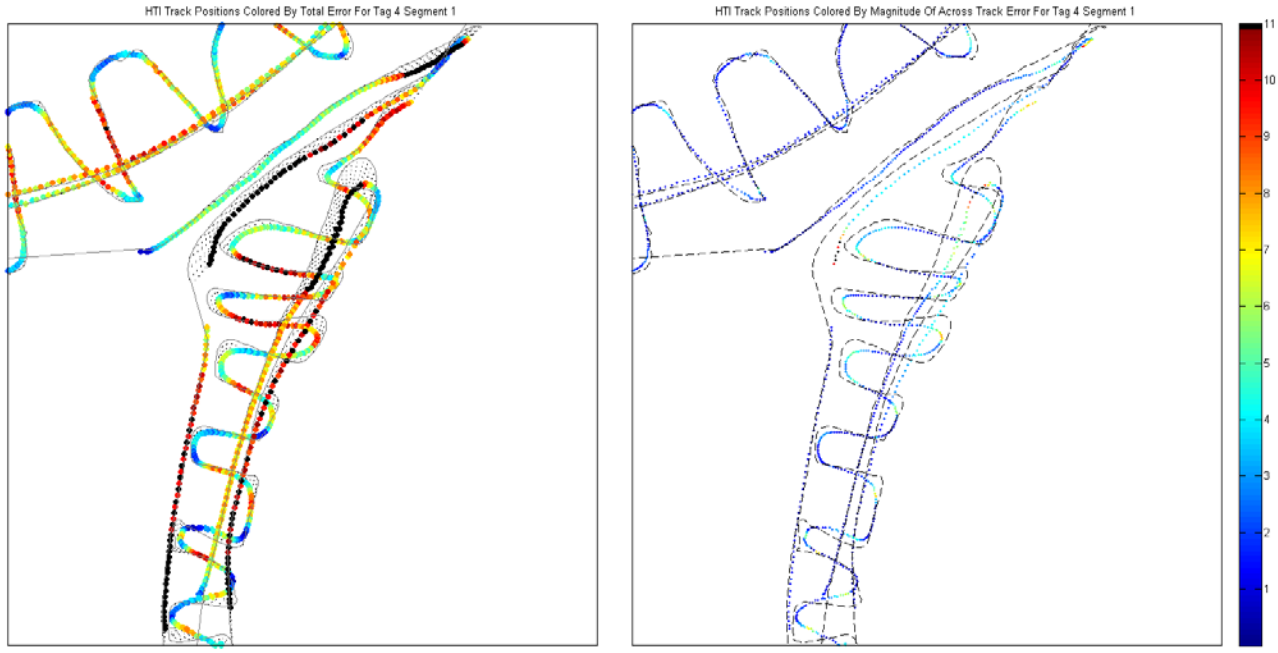

Figure 22 - Group 1 GPS tag track positions for Tag 4 Segment 1 colored by total error, in meters, in frame 1, and colored by magnitude of cross track error, in meters in frame 2. The color gradient is the same for both frames, indicated by the color bar to the right. Hotter colors represent increasing error, black indicates an error value greater than 10 meters. In the first (left) frame the gps path is shown as a solid grey line, with dotted black lines connecting each tag position to the corresponding interpolated gps track position. In the second (right) frame the gps track is shown as a dotted black line.

Group 2 Track Set Accuracy

The Group 2 track set showed similar relationships between tag depth, ambient noise conditions, and total accuracy as the Group 1 track set, but the spatial distribution and structure of the error in the Group 2 track set was significantly different from that of the Group track set. As was the case with the Group 1 tracks, the total error in the plots shown in Figure 24 and Figure 25 increases along each row, and increases for each tag from row one to row two, and from row three to row four. These trends suggest that tracking error increases with depth for the Group 2 track set, and corroborates the relationships between ambient noise and tracking accuracy found in the Group 1 track set. However, degradation in tracking accuracy for the Group 1 track set tended to result in increased along track error throughout the array, while degradation in tracking accuracy for the Group 2 track set tended to result in missing track segments and areas of increased cross track error. This behavior is well illustrated by the scatter plots shown in Figure 23, which show tracks for segment 2, tags 2,3, and 4 that have significant gaps in the area around Georgiana Slough and on the edges of the Sacramento River. In addition, there are no tracks for segment 3, tas 1 and 2, or for segment 4, tag 4. It is unclear why the Group 2 track set has these gaps; based on the Group 3 tracks we know that FishCount marked a significant number of echos when the tags were in these areas, but AcousticTag was unable to generate position estimates with the echos that FishCount selected.

The error in the positions that AcousticTag was able to create with FishCount echoes for track segments with poor accuracy tended to be highest in a few trouble areas, particularly downstream of the barrier in the Sacramento River, and along the edges of the Sacramento River. This is especially evident when looking at the total error scatter plots for the Group 2 track set (Figure 23) and the total error scatter plots for the Group 1 track set (Figure 15), particularly in the first two rows of plots (tag segments 1 and 2). These plots show the tendency of Group 2 tracks to include erroneous segments outside of the hydrophone array. These erroneous track segments are particularly noticeable in the second row of plots in Figure 23, in the vicinity of Georgiana Slough. As was the case with the missing track segments, the Group 3 track set does not contain these erroneous tracks, so it is unclear why they are present in the Group 2 track set and not the Group 1 track set. The heterogeneous spatial distribution of error in the Group 2 track set is reflected in the frequency distributions shown in Figure 24; the concentration of tracking error in a few locations results in distributions with lower central tendencies but more skew than the Group 1 error distributions, and the erroneous segments in the Group 2 tracks create a large number of outliers as indicated by the number of points in the 10 m and greater error bin.

While the total error frequency distributions for the Group 2 tracks have a significantly lower central tendency than the frequency distributions of total error for the Group 1 tracks, a greater portion of the Group 2 tracks' total error was due to cross track positioning errors. As a result, the Group 2 tracks' total error and cross track error tended to be positively correlated indicating

the spatial distribution of cross track error (Figure 25) in the Group 2 tracks is similar to the spatial distribution of total error (Figure 23).

The frequency distributions of cross track error for the Group 2 tag segments are similar to those for the Group 1 tag segments, though the distributions for Group 2 tracks have slightly higher means and greater variance (Figure 26). The similarities between the cross track error frequency distributions for these two Groups is likely due to the fact that the Group 2 tracks show the same systematic error in areas of rapid angular acceleration evident in the Group 1 tracks. For long track segments this behavior becomes the dominant source of cross track error, so the frequency of cross track errors is largely determined by the amount of angular acceleration in the tag's path.

The high-resolution scatter plots of the Group 2 tracks for tag 4 segment 1 shown in Figures 27 through 30 illustrate the effects of the Group 2 track set's unique error structure on the position estimates for a single tag segment. While there are some localized areas where the tracks exhibit significant along track error similar to that seen the Group 1 tracks, the majority of the error in these plots is either cross track error on the peripheries of the array, or systematic cross track error in areas of rapid angular acceleration.

The location of the Group 2 position estimates for this tag segment in the Cartesian plane are very similar to those produced by Group 1 (Figures 19 through 22). The major differences between the Group 1 and Group 2 position estimates for this tag segment are in the temporal synchronization of these position estimates to the GPS path. It is unlikely that the larger synchronization errors in the Group 1 track set are due to differences in echo selection performance between AcousticTag and FishCount, because both echo selection technologies produced the same timestamps for marked echoes. Time stamp agreement was verified manually by checking to ensure that FishCount and AcousticTag output files recorded the same 1200 kHz clock tick value for coincident echoes. Spatial evidence of the apparent agreement between echo selection timestamps can be seen in frame 1 of Figures 21 and 29. The dotted lines connecting each position estimate to the location of the GPS at the timestamp for each estimate indicate that the Group 1 position estimates and the Group 2 position estimates had very similar timestamps. For this reason, it is unclear why the Group 1 tracks have greater synchronization error that the Group 2 tracks.

Figure 23

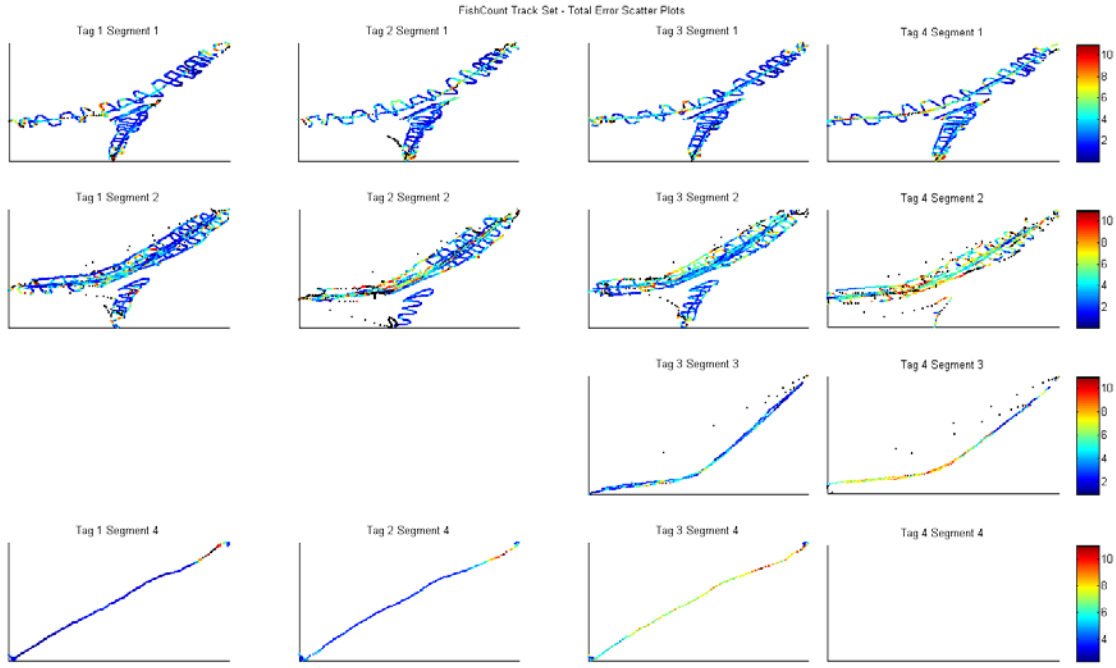

Figure 23 - Group 2 GPS tag track positions colored by total error, in meters. The color gradient is the same for all frames, indicated by the color bars to the right. Hotter colors represent increasing error. No plots are shown for segment 3, tags 1 and 2, because there were no position estimates for these tag segments.

Figure 24

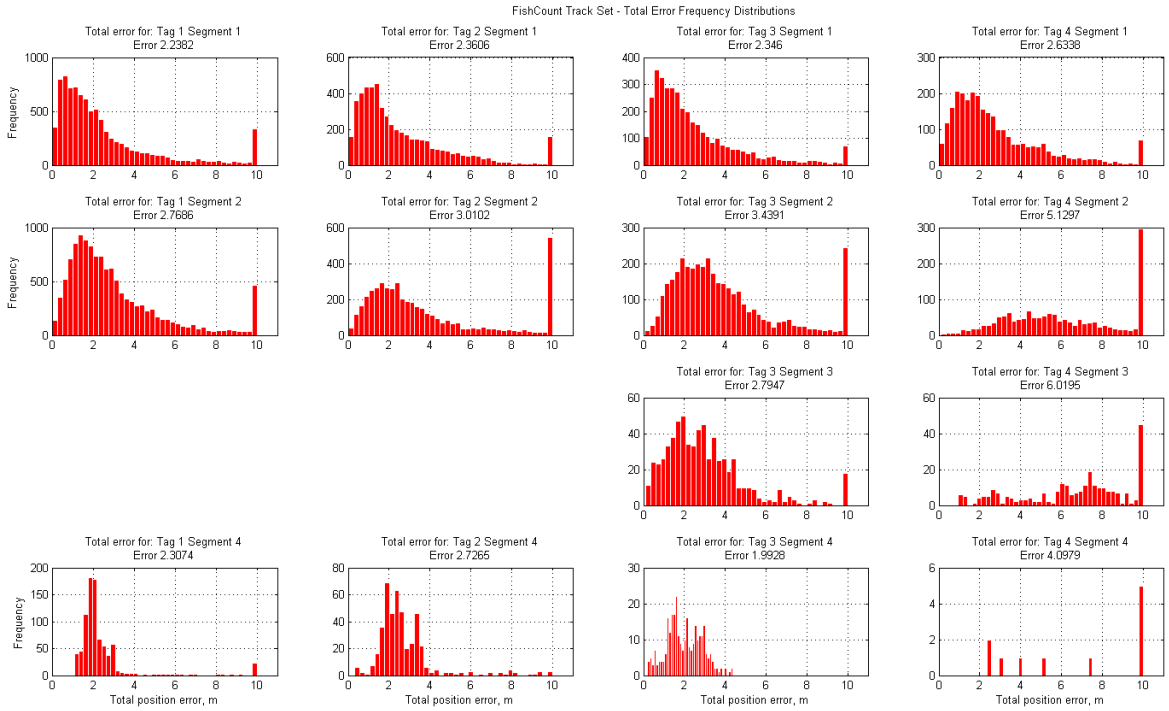

Figure 24 - Group 2 GPS tag track total error distributions for each tag segment. For display purposes, all error values greater than 10 meters are shown in the 10 meter bin on the histograms. Total error values greater than or equal to 10 meters were discarded before the distribution means were calculated; as a result the distribution means indicated may underestimate central tendency. No distributions are shown for Segment 3, tags 1 and 2, because there were no position estimates for these tag segments.

Figure 25

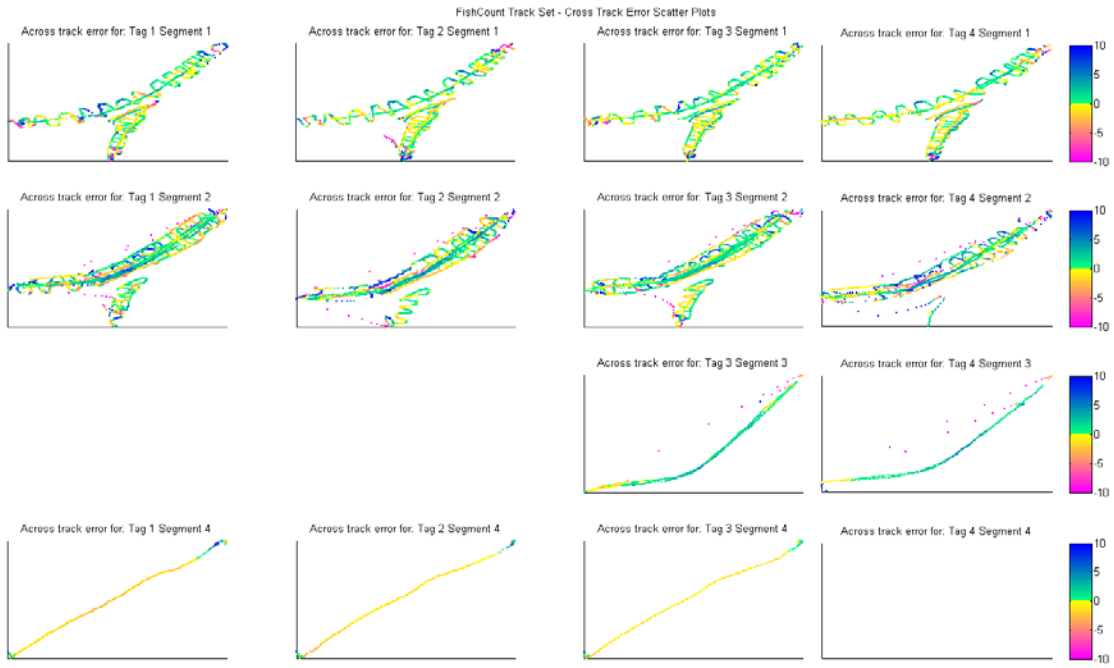

Figure 25 - Group 2 GPS tag track positions colored by cross track error, in meters. The color gradient is the same for all frames, indicated by the color bars to the right. No plots are shown for segment 3, tags 1 and 2, because there were no position estimates for these tag segments.

Figure 26

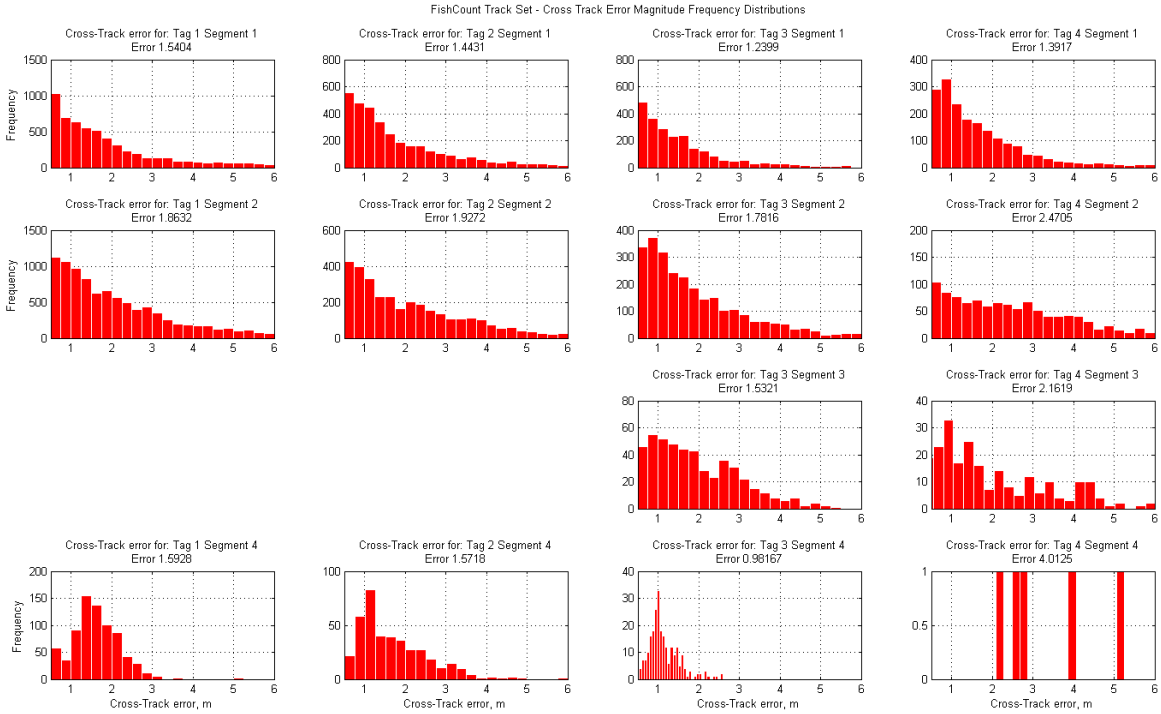

Figure 26 - Group 2 GPS tag track cross track error magnitude distributions for each tag segment. For display purposes, all error values greater than 6 meters are shown in the 6 meter bin on the histograms. Total error values greater than or equal to 10 meters were discarded before the distribution means were calculated; as a result the distribution means indicated may not be an accurate representation of central tendency. No distributions are shown for Segment 3, tags 1 and 2, because there were no position estimates for these tag segments.

Figure 27

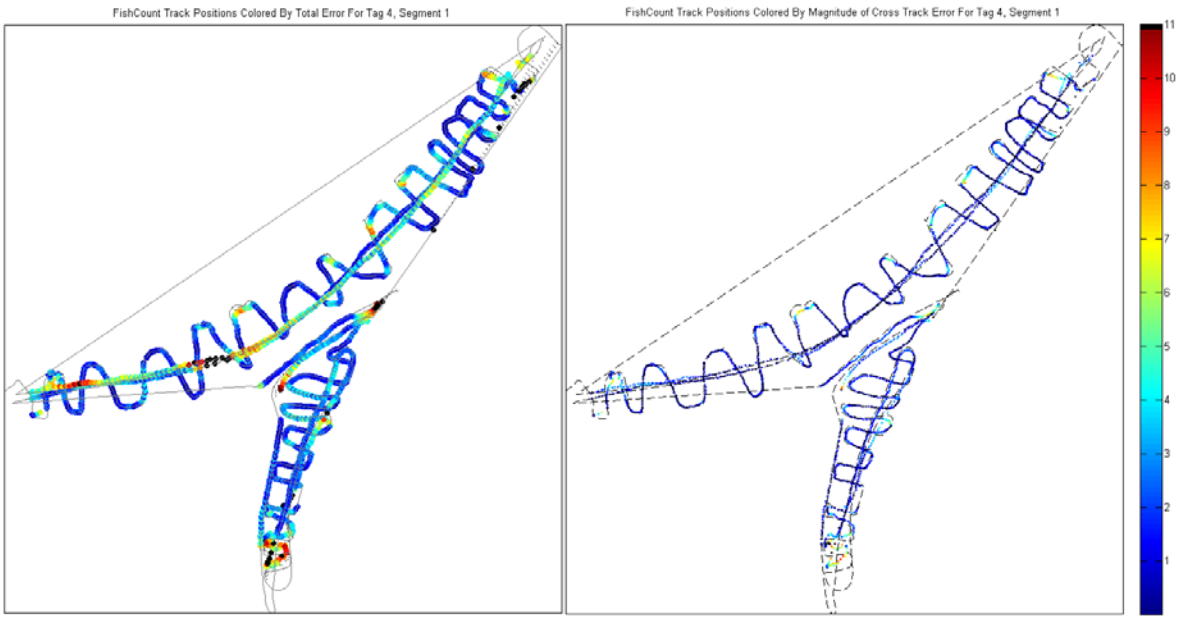

Figure 27 - Group 2 GPS tag track positions for Tag 4 Segment 1 colored by total error, in meters, in frame 1, and colored by magnitude of cross track error, in meters in frame 2. The color gradient is the same for both frames, indicated by the color bar to the right. Hotter colors represent increasing error, black indicates an error value greater than 10 meters. In the first (left) frame the gps path is shown as a solid grey line, with dotted black lines connecting each tag position to the corresponding interpolated gps track position. In the second (right) frame the gps track is shown as a dotted black line.

Figure 28

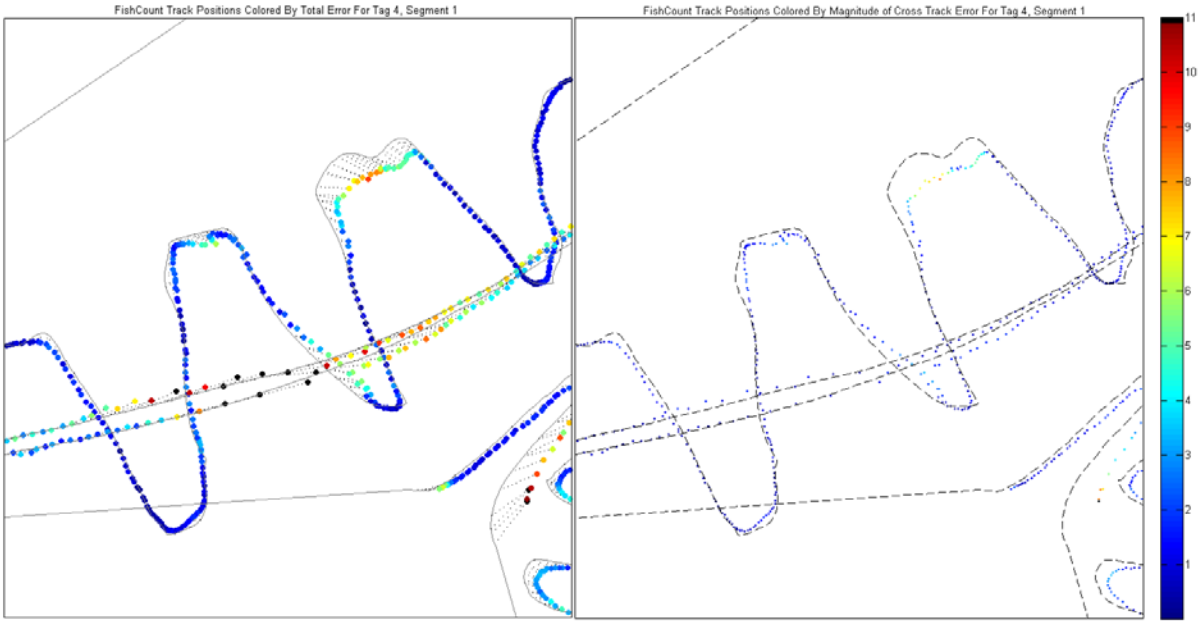

Figure 28 - Group 2 GPS tag track positions for Tag 4 Segment 1 colored by total error, in meters, in frame 1, and colored by magnitude of cross track error, in meters in frame 2. The color gradient is the same for both frames, indicated by the color bar to the right. Hotter colors represent increasing error, black indicates an error value greater than 10 meters. In the first (left) frame the gps path is shown as a solid grey line, with dotted black lines connecting each tag position to the corresponding interpolated gps track position. In the second (right) frame the gps track is shown as a dotted black line.

Figure 29

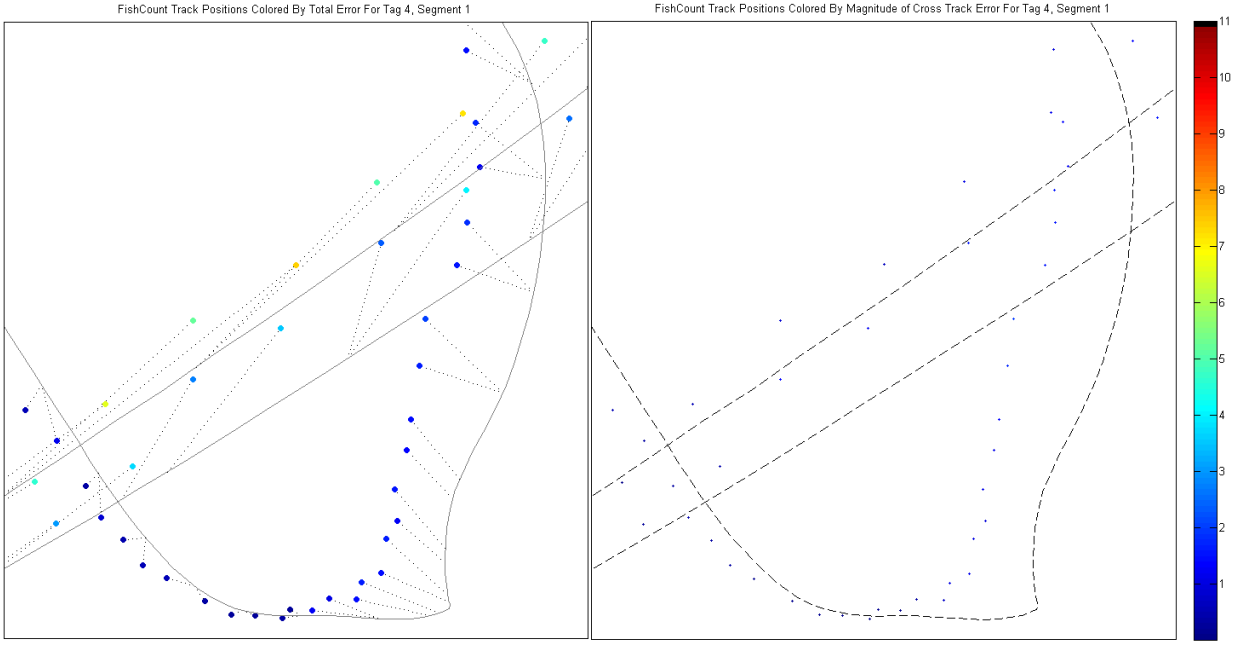

Figure 29 - Group 2 GPS tag track positions for Tag 4 Segment 1 colored by total error, in meters, in frame 1, and colored by magnitude of cross track error, in meters in frame 2. The color gradient is the same for both frames, indicated by the color bar to the right. Hotter colors represent increasing error, black indicates an error value greater than 10 meters. In the first (left) frame the gps path is shown as a solid grey line, with dotted black lines connecting each tag position to the corresponding interpolated gps track position. In the second (right) frame the gps track is shown as a dotted black line.

Figure 30

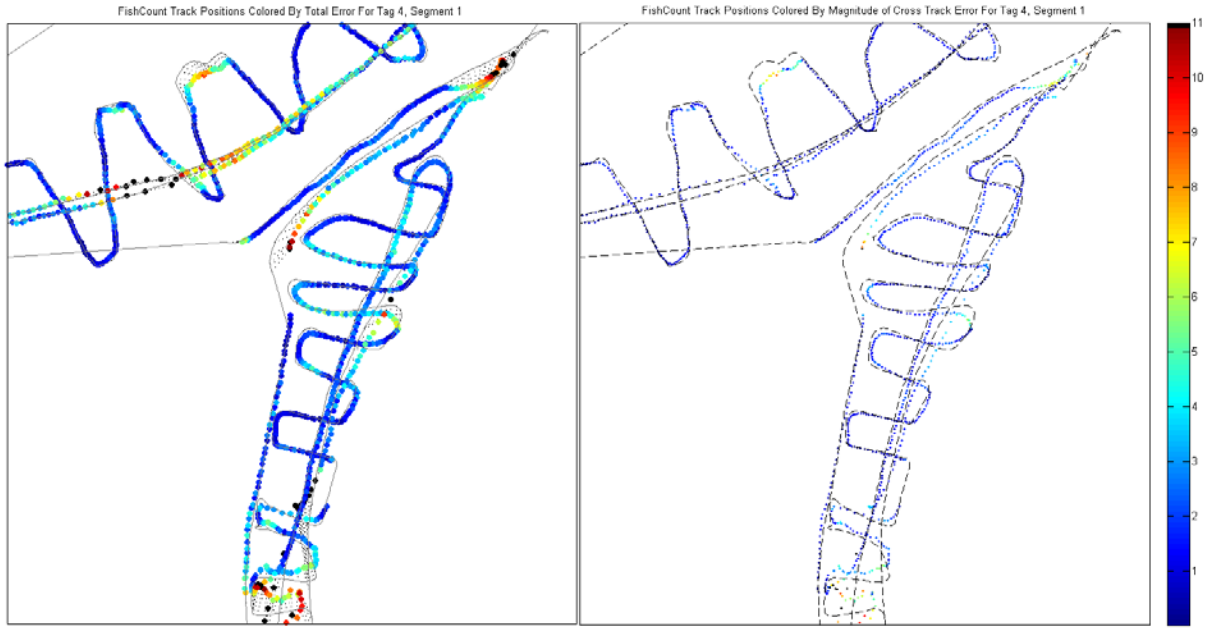

Figure 30 - Group 2 GPS tag track positions for Tag 4 Segment 1 colored by total error, in meters, in frame 1, and colored by magnitude of cross track error, in meters in frame 2. The color gradient is the same for both frames, indicated by the color bar to the right. Hotter colors represent increasing error, black indicates an error value greater than 10 meters. In the first (left) frame the gps path is shown as a solid grey line, with dotted black lines connecting each tag position to the corresponding interpolated gps track position. In the second (right) frame the gps track is shown as a dotted black line.

Group 3 Track Set Accuracy

The Group 3 tracking algorithm estimates each position in a tag's track independently from all other position estimates and does not utilize any type of interpolation, smoothing, or spatial filtering during the tracking process. As a result, the GPS tag tracks produced by the Group 3 algorithm contain more random point-to-point movement than the Group 1 and Group 2 tracks, but the Group 3 tracks do not exhibit the same systematic cross track errors observed in the Group 1 and Group 2 tracks. The net result is that the Group 3 tracks for the GPS tags appear to be less precise but have lower aggregate error metrics than the other GPS tag tracks. This can be seen when comparing the total error scatter plots in Figure 15, Figure 23 and Figure 30; because of the increased random positioning error in the Group 3 tag segment tracks shown in Figure 30, these tracks appear to be "blurry" and "less crisp" than the corresponding Group 1 and Group 2 tracks, but the track colors indicate that that the Group 3 positions have lower total error.

The total error frequency distributions for the Group 3 tracks shown in Figure 31 have lower central tendencies and lower variances than the total error frequency distributions for the Group 1 tracks (Figure 16) and the Group 2 tracks (Figure 24). Additionally, the total error frequency distributions for the Group 3 tracks are unimodal, while the total error frequency distributions for many Group 1 and Group 2 tag segments are multimodal. This observation is consistent with the hypothesis that the total error in the Group 1 and Group 2 tracks is the combination of a systematic along track error source, systematic cross track error due to smoothing, and random positioning error, while the error in the Group 3 tracks can be attributed to random positioning error. The idea that the total error in the Group 3 tracks can be attributed to a single mechanism is supported by the fact that the cross track error in the Group 3 tracks (Figure 32) has the same spatial distribution as the total error, but is about half the vector magnitude of the total error, suggesting that the distribution of total error into along track and cross track components is random and not affected by the motion of the tag.

The mean magnitude of the error for each Group 3 tag increased between segment one tracks and segment two tracks, and decreased between segment three tracks and segment four tracks. These trends agree with the ambient noise related error trends observed in the Group 1 and Group 2 tag tracks. However, the Group 3 track error did not show the same relationship between increasing tag number/depth and increasing track error seen in the Group 1 Group 2 tracks. Because GeneticFish was configured to produce full three-dimensional position estimates for each point, this observation supports the hypothesis that the increase in error with tag depth for the Group 1 and Group 2 tracks was a result of the AcousticTag settings that relied on a single apriori estimate of tag depth. The trade-off of the increased accuracy of GeneticFish for deeper tags can be seen by comparing the scatter plots in Figure 15, Figure 23 and Figure 30. Because the AcousticTag settings allowed positions to be calculated with only three hydrophones, the Group 1 and Group 2 tag tracks have more points on the periphery of the array and in the lower Sacramento River than the Group 3 tracks, which only include positions for tags heard by four or more hydrophones.

The high-resolution scatter plots shown in Figures 34 through 38 illustrate the effects of the GeneticFish algorithms error structure on the resulting track position estimates, as well as providing an example of the trade-offs between precision and accuracy that result from a lack of smoothing. The Group 3 track for this tag segment follows the GPS path more closely than the tracks produced using AcousticTag in areas of rapid angular acceleration, but the track has significant random error at the peripheries of the array, especially in nearshore areas. Additionally, the small random along track error present in most portions of the Group 3 tracks makes it difficult to understand the temporal sequencing of points without the aid of the GPS path when these tracks are viewed at higher magnification (Figure 36). Finally, while the majority of points appear to have random position error, there are some locations in the array where the Group 3 tracking error appears to be due to a systematic physical process. This mostly occurred in the downstream end of the Georgiana Slough portion of the array, and resulted in parallel position estimates spaced 5 m apart (Figure 38). In the absence of GPS data it would be difficult to determine which of the two sets of points was correct.

Because the GeneticFish algorithm produced vertical position estimates as well as a variety of error metrics for each track point, analyses were carried out on the Group 3 tracks to determine the accuracy of these additional data components. The results of these analyses showed that the GeneticFish error metrics could be used to remove extreme outliers, but for the majority of the Group 3 track points, these error metrics were poor predictors of point accuracy. In addition, the frequency distribution of vertical position estimates for each tag appeared identical, and appeared to be uniformly distributed throughout the possible range of vertical position values. This indicates that for the GPS tags, the vertical component of the GeneticFish positioning solution simply provided an additional degree of freedom for optimizing the horizontal position estimate. Analysis of a small number of GeneticFish tracks produced for fish tag codes suggests that the Group 3 error metrics and vertical position estimates for some fish tag tracks are more accurate than those produced for the GPS tags, but validating these observations requires analytical rigor beyond the scope of this study.

Figure 30

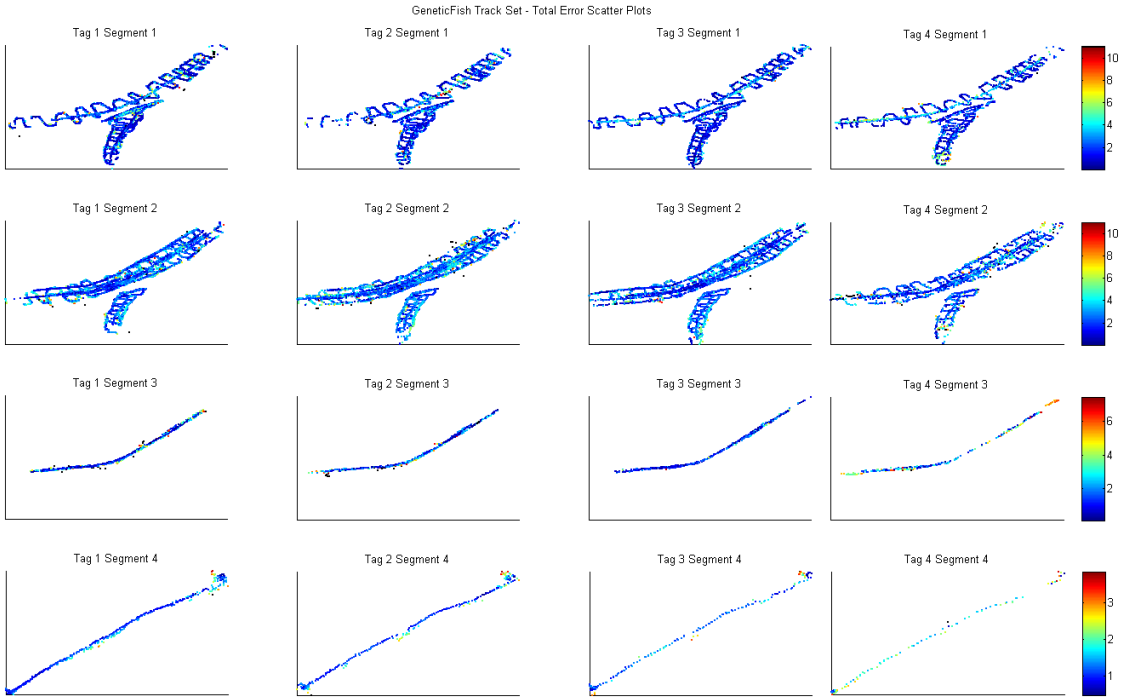

Figure 30 - Group 3 GPS tag track positions colored by total error, in meters. The color gradient is the same for all frames, indicated by the color bars to the right. Hotter colors represent increasing error. No plots are shown for segment 3, tags 1 and 2, because there were no position estimates for these tag segments.

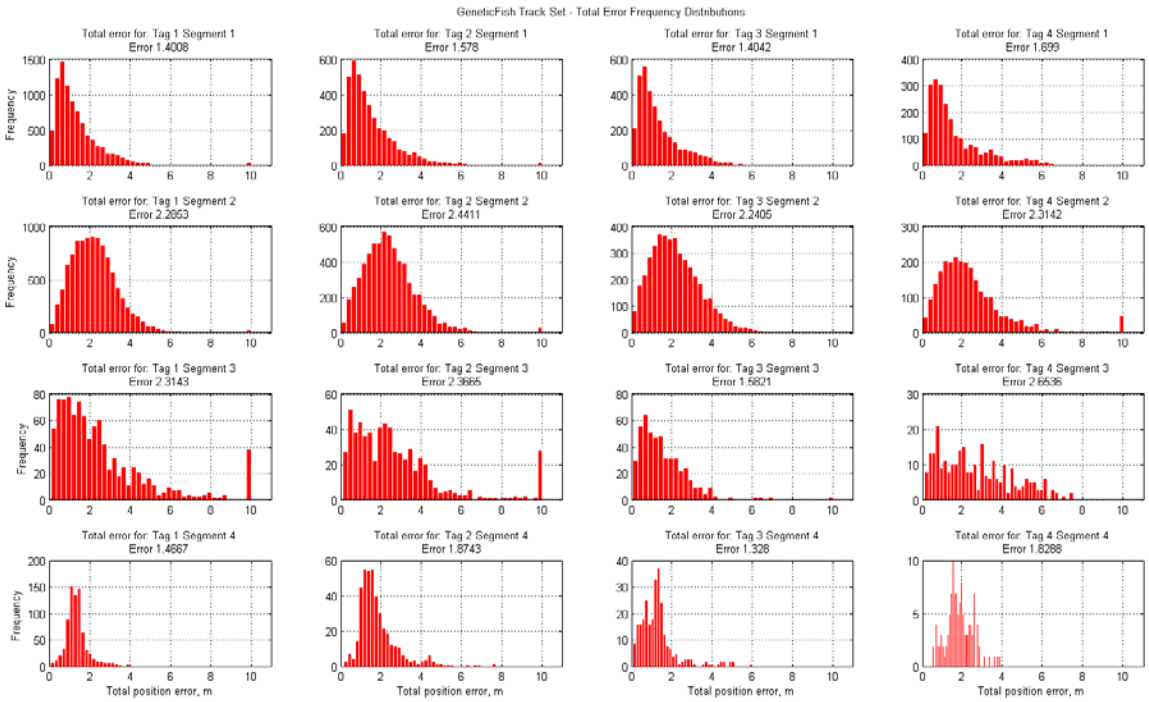

Figure 31 - Group 3 GPS tag track total error distributions for each tag segment. For display purposes, all error values greater than 10 meters are shown in the 10 meter bin on the histograms. Total error values greater than or equal to 10 meters were discarded before the distribution means were calculated; as a result the distribution means indicated may underestimate central tendency. No distributions are shown for Segment 3, tags 1 and 2, because there were no position estimates for these tag segments.

Figure 32

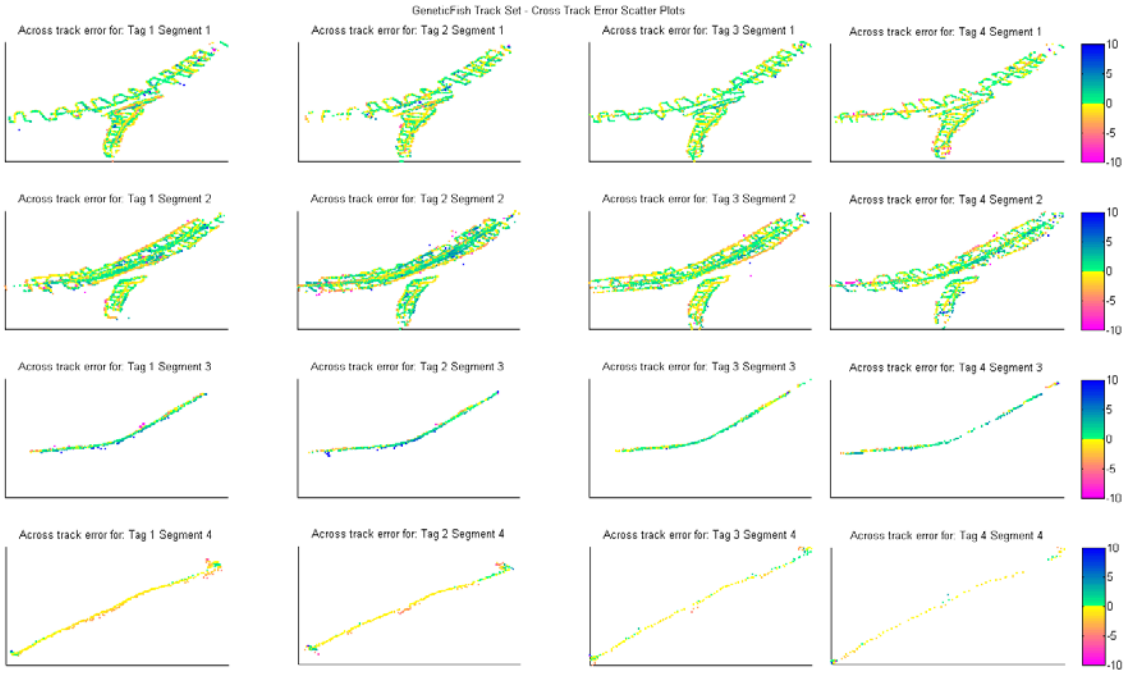

Figure 32 - Group 3 GPS tag track positions colored by cross track error, in meters. The color gradient is the same for all frames, indicated by the color bars to the right. No plots are shown for segment 3, tags 1 and 2, because there were no position estimates for these tag segments.

Figure 33

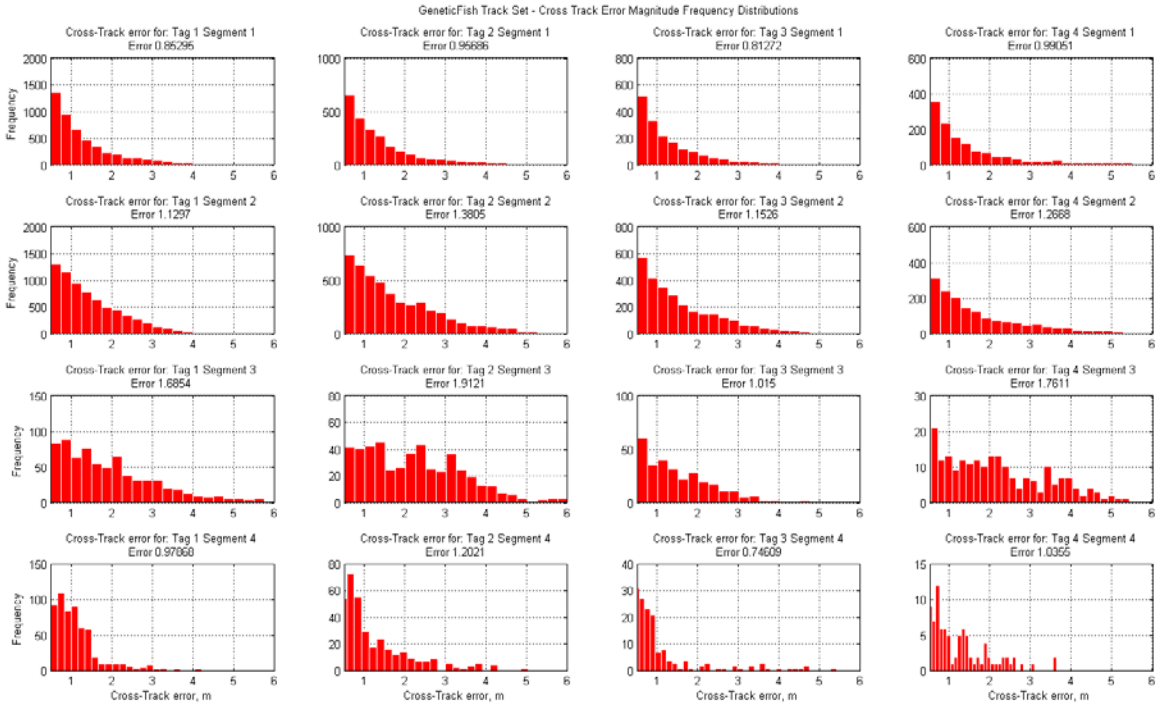

Figure 33 - Group 3 GPS tag track cross track error magnitude distributions for each tag segment. For display purposes, all error values greater than 6 meters are shown in the 6 meter bin on the histograms. Total error values greater than or equal to 10 meters were discarded before the distribution means were calculated; as a result the distribution means indicated may not be an accurate representation of central tendency. No distributions are shown for Segment 3, tags 1 and 2, because there were no position estimates for these tag segments.

Figure 34

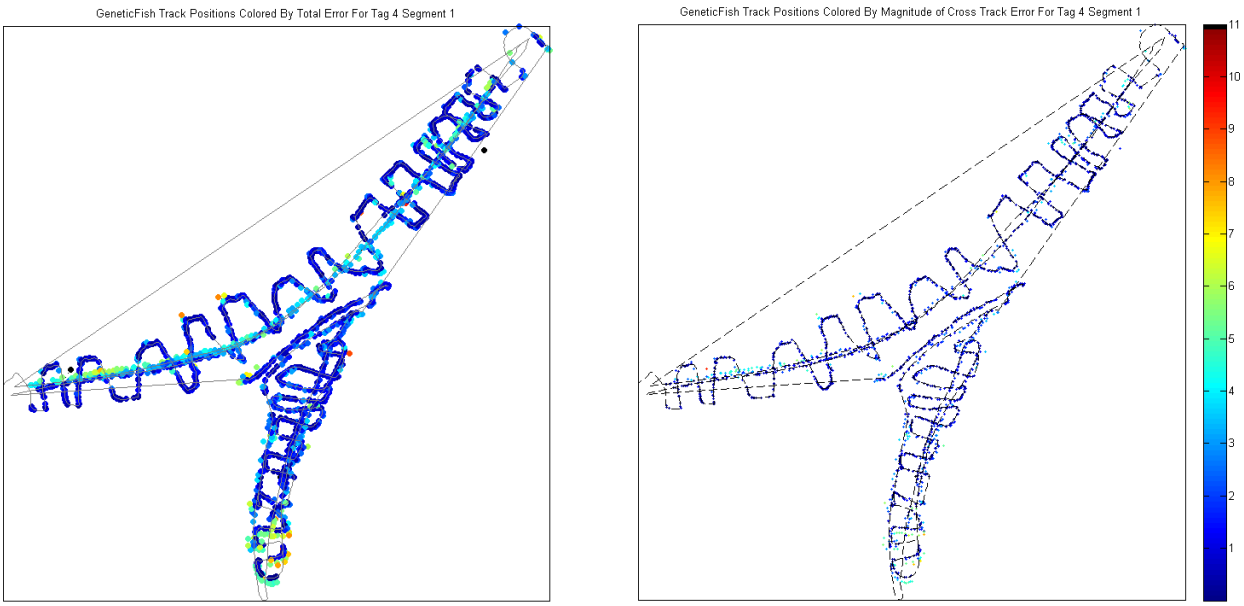

Figure 34 - Group 3 GPS tag track positions for Tag 4 Segment 1 colored by total error, in meters, in frame 1, and colored by magnitude of cross track error, in meters in frame 2. The color gradient is the same for both frames, indicated by the color bar to the right. Hotter colors represent increasing error, black indicates an error value greater than 10 meters. In the first (left) frame the gps path is shown as a solid grey line, with dotted black lines connecting each tag position to the corresponding interpolated gps track position. In the second (right) frame the gps track is shown as a dotted black line.

Figure 35

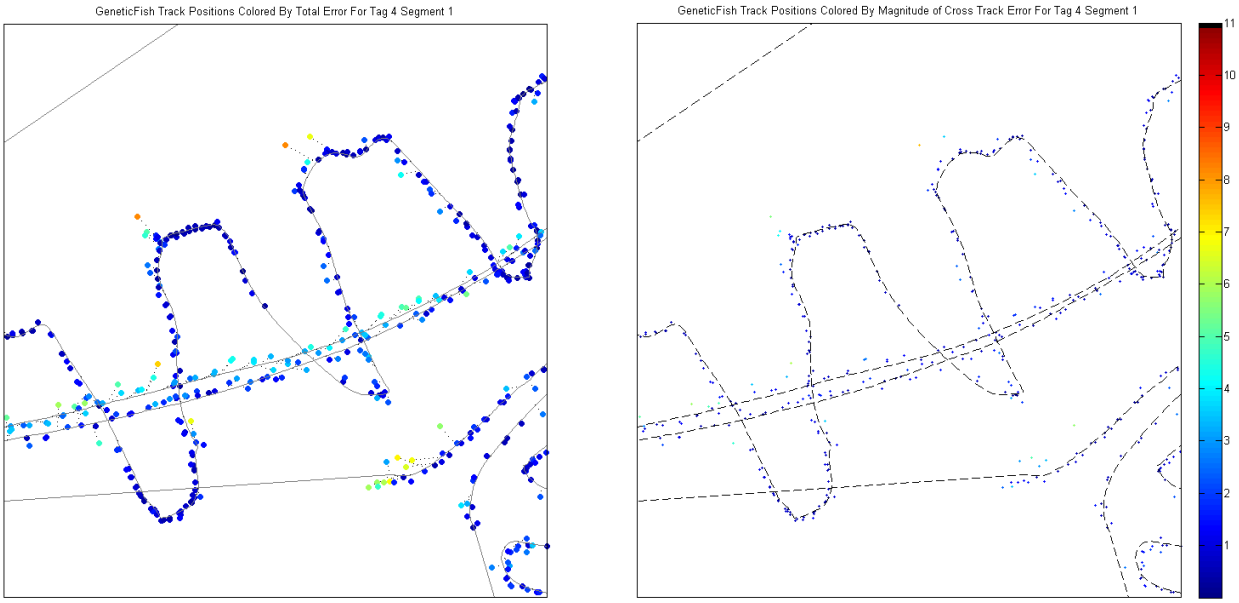

Figure 35 - Group 3 GPS tag track positions for Tag 4 Segment 1 colored by total error, in meters, in frame 1, and colored by magnitude of cross track error, in meters in frame 2. The color gradient is the same for both frames, indicated by the color bar to the right. Hotter colors represent increasing error, black indicates an error value greater than 10 meters. In the first (left) frame the gps path is shown as a solid grey line, with dotted black lines connecting each tag position to the corresponding interpolated gps track position. In the second (right) frame the gps track is shown as a dotted black line.

Figure 36

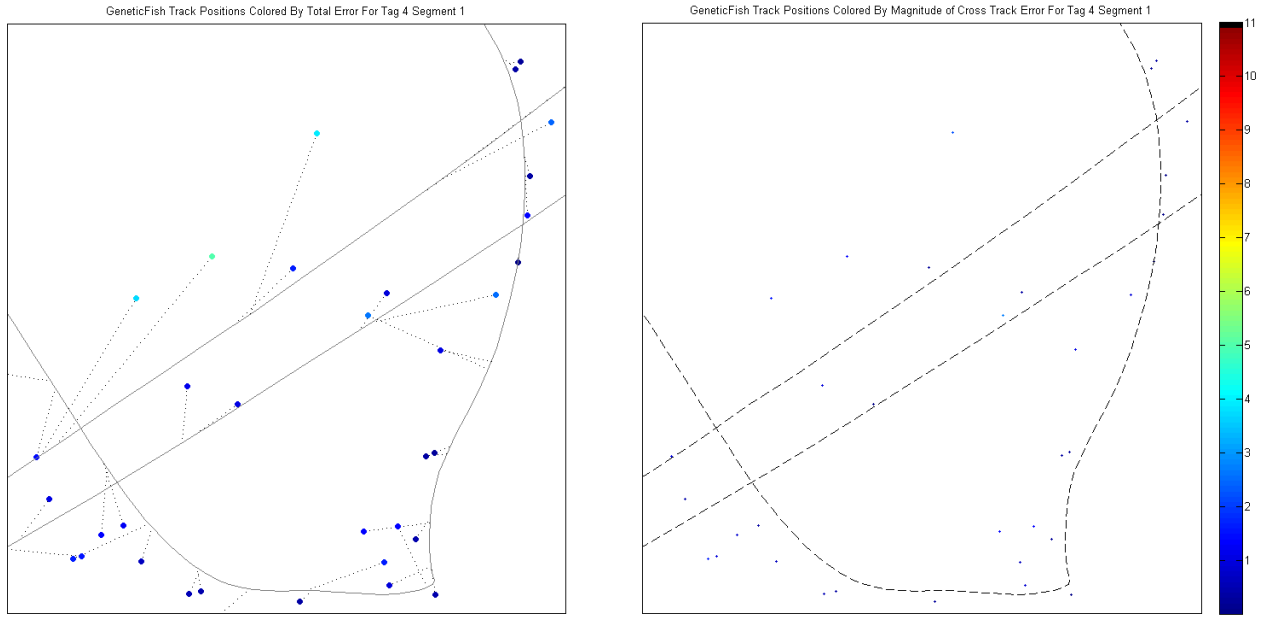

Figure 36 - Group 3 GPS tag track positions for Tag 4 Segment 1 colored by total error, in meters, in frame 1, and colored by magnitude of cross track error, in meters in frame 2. The color gradient is the same for both frames, indicated by the color bar to the right. Hotter colors represent increasing error, black indicates an error value greater than 10 meters. In the first (left) frame the gps path is shown as a solid grey line, with dotted black lines connecting each tag position to the corresponding interpolated gps track position. In the second (right) frame the gps track is shown as a dotted black line.

Figure 37

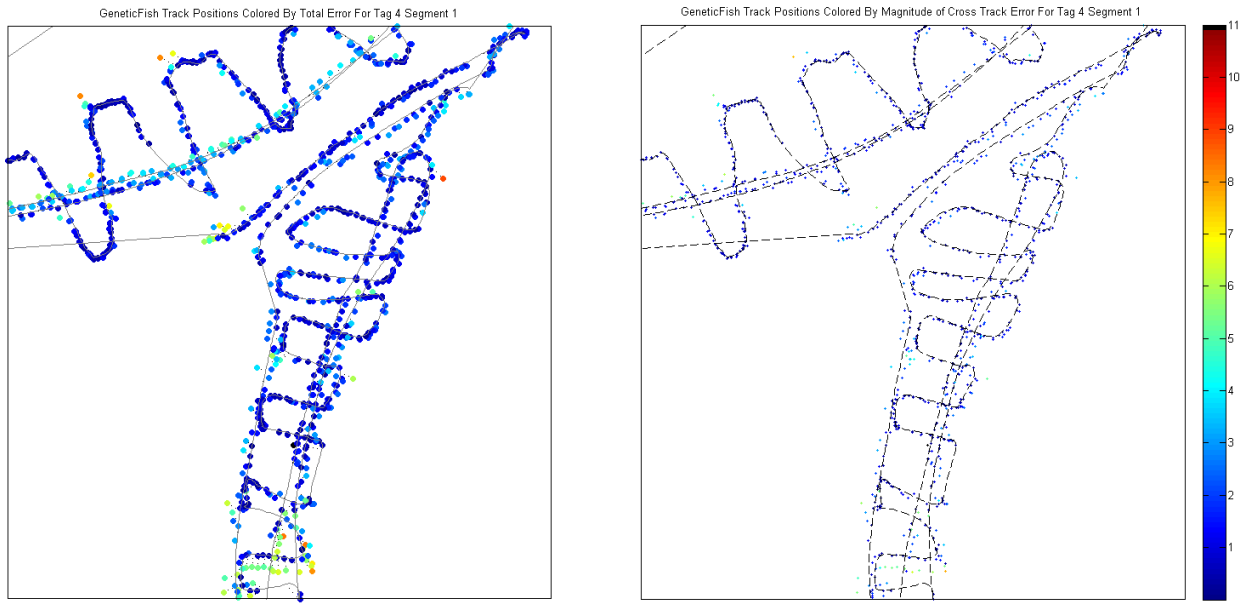

Figure 37 - Group 3 GPS tag track positions for Tag 4 Segment 1 colored by total error, in meters, in frame 1, and colored by magnitude of cross track error, in meters in frame 2. The color gradient is the same for both frames, indicated by the color bar to the right. Hotter colors represent increasing error, black indicates an error value greater than 10 meters. In the first (left) frame the gps path is shown as a solid grey line, with dotted black lines connecting each tag position to the corresponding interpolated gps track position. In the second (right) frame the gps track is shown as a dotted black line.

Figure 38

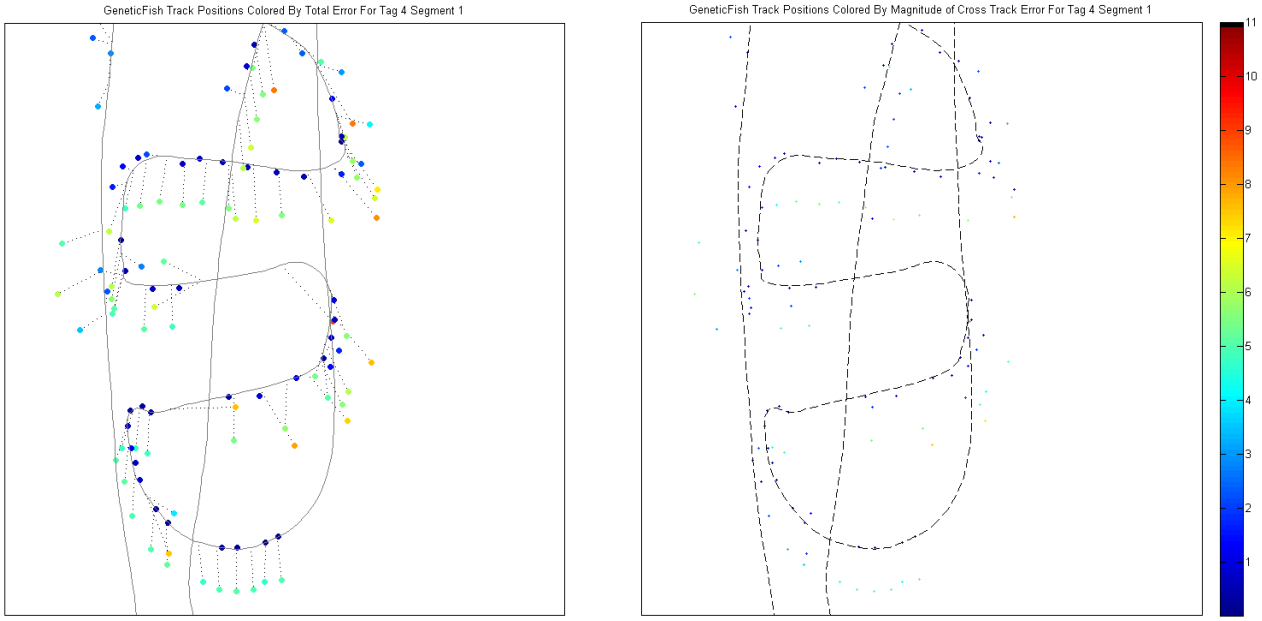

Figure 38 - Group 3 GPS tag track positions for Tag 4 Segment 1 colored by total error, in meters, in frame 1, and colored by magnitude of cross track error, in meters in frame 2. The color gradient is the same for both frames, indicated by the color bar to the right. Hotter colors represent increasing error, black indicates an error value greater than 10 meters. In the first (left) frame the gps path is shown as a solid grey line, with dotted black lines connecting each tag position to the corresponding interpolated gps track position. In the second (right) frame the gps track is shown as a dotted black line.

Discussion of RTK Analysis

Tracking accuracy, tracking precision, and smoothing

The GPS tag accuracy analysis showed that quantifying tracking accuracy can be more complicated than computing a single number to represent positioning confidence or tracking resolution. If researchers do not collect a significant amount of ground truth data and invest in analyzing this data they're likely to remain ignorant of the magnitude and structure of positioning errors in the tracks they use to make inferences about fish behavior. For this reason, smoothing tracks during data processing can create a situation in which researchers will tend to mistake the apparent precision of smoothed tracks as an indicator of the positioning accuracy of these tracks. Such a mistake could lead to erroneous interpretation of fish behavior in situations where researchers make inferences based on quantitative or qualitative observations of a track's motion at temporal or spatial scales affected by the smoothing. This is a particular risk if the type of smoothing used changes the information on velocity, acceleration, or angular acceleration of the tagged fish that was contained in the raw track. For this reason, researchers should strongly consider using non-smoothed tracks as the starting point for all study analyses, and if smoothing is required for an analysis, researchers should take care to consider the low-pass filter effects that result from many smoothing techniques. Additionally, future studies should incorporate a significant ground truth data collection effort at the beginning of the study, and if possible, leverage the rapid turnaround provided by cloud-based automated processing to conduct preliminary analysis of this data before any inferences are made about fish behavior.

Observed relationship between ambient noise and tracking accuracy

The GPS tag accuracy analysis showed that for all combinations of echo selection and tag positioning technology, tracking accuracy was greatest for transects conducted when there was the largest amount of ambient noise in the study area. This finding is not consistent with our understanding of acoustic tag positioning technology, or with data collected in past studies. The GPS tag transect metadata, and the field notebooks of the personnel performing the transecting are in agreement with Table 2, and suggest that the observed relationship between ambient noise and tracking accuracy was a real phenomenon, and not a result of clerical error. There are a variety of hypotheses that could explain this relationship, ranging from multipath caused by the hull of the transacting vessel, to synchronization errors between ATR's. Without further experimentation is impossible to validate any of these hypotheses, but this situation highlights the value of ground truth data, because analysis of this data may surface problems that might otherwise have gone undetected. Given the possibility that boat hull effects altered the accuracy of the GPS tag tracks, researchers should consider this possibility in the design of future studies, and consider minimizing the use of full-size vessels during ground truth data collection. In addition, it would be ideal to design future studies with the goal of collecting and evaluating ground truth data before beginning fish releases, so that ground truth data could be used to improve array operations.

Tag positioning technology

The USGS GeneticFish algorithm used to estimate tag positions for the Group 3 track set is a new technology that was developed by the USGS to support cloud-based automated processing of FishCount echo selection data for large hydrophone arrays. Unlike FishCount, GeneticFish is still a nascent technology, and this analysis is the first evaluation of the algorithm's efficacy. Based on the results of the GPS tag accuracy analysis it appears that GeneticFish is capable of producing tracks that are as accurate as those produced by AcousticTag. However, due to the differences in smoothing and vertical positioning between the Group 1 and Group 3 GPS tag tracks, it is difficult to thoroughly compare the tracking performance of these two technologies. In order to adequately understand the trade-offs between GeneticFish and AcousticTag more ground truth data collection is required; any GPS tag transect data that can be collected in hydrophone arrays used for future studies would truly valuable for evaluating tracking technologies for future barrier studies.

Attachment E-2 - documentation of input parameters used to create Group 1 track set

Attachment E-3 - documentation of input parameters used to create FishCount track set

Attachment E-4 - documentation input parameters used to create GeneticFish track set

APPENDIX F

ON THE HYDRODYNAMICS OF ENTRAINMENT OF JUVENILE SALMON IN TIDALLY FORCED JUNCTIONS
GEORGIANA SLOUGH: A CASE STUDY

On the hydrodynamics of entrainment of juvenile salmon in tidally forced junctions Georgiana Slough: A case study.

DRAFT 3 - DO NOT SITE

J.R. Burau, P. R. Stumpner and A.R. Blake
9/20/2013

1 Introduction

Entrainment of fish in junctions is controlled by their entrance distribution and the interaction between hydrodynamics and fish behavior that occurs within the junction as is shown schematically in figure 1.1. The entrance distribution is, in turn, controlled by the interaction between behavior and water moving past up-current geomorphology and man-made structures such as docks, bridge piers, and marinas. The scope of this analysis is limited to investigating the interaction between hydrodynamics and fish behavior in the immediate vicinity of the Georgiana Slough junction, but it is important to recognize that understanding juvenile salmon entrance distributions could lead to management actions that would increase overall survival.

2 Background and introduction – Why Hydrodynamics?

In this chapter we focus strictly on the hydrodynamics of fish entrainment, admittedly ignoring the behavioral aspect entirely for clarity. The interaction between hydrodynamics and behavior is discussed in sections 3.5 and 3.6 – see chapters by Perry, Blake, and others). Nevertheless, based on scaling arguments (see below) and previous studies (Blake and Horn, in press (a,b)), hydrodynamics alone can play a commanding role in controlling entrainment rates during periods of high Sacramento River inflows, the period in which salmon typically out-migrate, or during peak ebb and flood tides that occur during low Sacramento River inflows.

Scaling Analysis - Hydrodynamics VS behavior

The interaction between hydrodynamics and behavior govern entrainment rates in junctions. But, which is more important? Or, said another way: are there periods, or conditions, where one dominates over the other?

Firstly, the time spent in junctions in the north delta varies considerably depending on the Sacramento River inflows but, in general, the time spent in junctions is short. Thus, if fish are to change their fate within a junction they must do so by reacting quickly and decisively as they enter the junction. For example, when the Sacramento River is running above 56k

cfs at Freeport, typical of a middling winter high flow condition, the currents in the Sacramento River downstream of Georgiana Slough can exceed 3.5 ft/s (January 2010). Under these conditions, the time spent in the Georgiana Slough Junction is <5 minutes (assuming the spatial scale of the junction is 1000 m (e.g. the length of the acoustic telemetry array as is shown in figure 3.20). And, during low Sacramento River flows (>10k cfs), ebb current speeds can exceed 1.5 ft/s (fish will be in junction for 10 min), and for flood tides 1.0 ft/s (fish will be in junction for 15 min).

So are there behavioral cues that would trigger a rapid and decisive response within junctions in the delta? Work by Goodwin and Nestler (2006) suggests that juvenile salmon cue behavioral changes in response to hydrodynamic features such as localized lateral and vertical shears and local increases in turbulence intensity. In the prismatic channels typical of the delta there are few physical or bathymetric features that would generate localized lateral and vertical shears or localized increases that would initiate a behavioral response, in particular a response that would change a fish's fate (Figure 3.10). The exception is in near shore areas or near man-made structures such a bridge piers, docks, etc.

In very broad terms, the answer to the question of whether hydrodynamics or behavior controls entrainment in junctions depends on the strength of the current speeds relative to the swimming capabilities of fish in question or, based on a simple scaling analysis, the fish swim number (Blake and Horn, in press (a,b))

S = fish swim speed/current speed.

Typically, juvenile Chinook salmon can sustain ~ 2 body lengths per second (Nelson and others, 1994), so the fish swim number is

$$S = (2bl/s)/U \qquad (2.1)$$

where U is the local current speed. So if S ~ 1, the fish's sustained swimming ability just matches the water velocity. However, when S >> 1, behavior is likely to have a first order influence on fish movements within junctions and hydrodynamics will play a secondary role depending, of course, on whether fish choose to swim at this rate in the first place. On the other hand if S << 1 we expect hydrodynamics to dominate fish movements over behavior within junctions.

In the north delta, during high Sacramento River flows typical of most winters and coincident with the peak in salmon outmigration, the currents in the mainstem Sacramento River at Freeport are strong (~5 ft/s) throughout the tidal day and S is low - suggesting physical processes dominate. During periods when river inputs are low the flows reverse tidally in virtually every junction in the delta. Tidal forcing creates periods of downstream

flow (ebb tide periods), upstream flow (flood tide periods) and a roughly hour-long periods where the currents are extremely weak to non-existent. Periods where the velocities are weak, so-called "slack water", are times when we expect fish behavior to dominate their movements within junctions because swim numbers during these periods are greater than one. During peaks in the ebb and flood tidal currents in the Walnut Grove area, water velocities can approach 1.5 ft/s (S~ 0.43), suggesting that both hydrodynamics and behavior are important for entrainment at these times.

Table 2.1 provides a summary of the "fish number" scaling for a 100 mm (~4") juvenile salmon and for 0.75m (~2.75') striped bass. For comparison we use the mean surface current speeds that occur in junctions throughout the north delta. This simple scaling suggests that a 0.75m fish (bass) can freely move about, even against currents during peaks in Sacramento River inflow. It also suggests that the movements of juvenile salmon in junctions are strongly influenced by the currents during the tidal current peaks. Still, this scaling also suggests that juvenile salmon can move about in the vertical under almost any conditions in the delta, even under extremely high Sacramento River flows.

	Horizontal Tidal Currents 0.6m/s (2ft/s)	Horizontal high Sac flows 1.2m/s (4 ft/s)	Vertical currents 0.1m/s (0.3 ft/s)
100mm juvenile salmon	0.32	0.16	2.0
0.75m Striped Bass	2.5	1.25	15

Table 2.1. Swim number, S, scaling for a 100 mm juvenile salmon and a 0.75 m predator under a variety of typical current speeds in the Walnut Grove area.

Thus, hydrodynamics, specifically horizontal velocity distributions, can play a central role in controlling entrainment of juvenile salmon in junctions in the North Delta. For this reason, a comprehensive hydrodynamic measurement program was included in the 2012 Georgiana Slough Non-physical barrier (GSNPB) study.

In this section we discuss the hydrodynamic measurements made during the 2012 GSNPB study, including a description of the sampling design and the rationale behind it. We then discuss various analytical approaches aimed at characterizing the physical processes that contribute to the entrainment of juvenile salmon in junctions. The focus of the analysis section is aimed at developing approaches for documenting the flow fields in strongly tidally forced junctions typical of the delta. At the highest level of complexity, we interpolate the complete flow field based measurements from an array of Sideward-Looking Acoustic

Doppler Current Profilers (SL-ADCP's). Then, we collapse the flow field complexity to a few simple metrics based on the entrainment zone and critical streakline concepts (more on this later).

3 Methods – Field Deployments

During the 2012 Georgiana Slough field investigation, two types of complementary hydrodynamic measurements were made to document the temporal evolution of the velocity field on the Sacramento River side of the Bio-Acoustic Fish Fence (BAFF). Measurements of the velocity fields within the Georgiana Slough/Sacramento River junction were made using both (1) Eulerian (fixed position) Sideward-Looking Acoustic Doppler Current Profilers (SL-ADCP's) and (2) Lagrangian measurements (e.g. drifters). The SL-ADCP measurements were made by the USGS, while the drifter measurements were carried out by the USGS and DWR.

3.1 Eulerian Measurements

Six (6) 600 kHz SL-ADCP'S (Figure 3.1) were deployed along the BAFF face (figure 3.2). The piling location and mounting orientation for each SL-ADCP was chosen so that the SL-ADCP array would provide maximum coverage under a variety of flow conditions (figures 3.2-7).

All of the SL-ADCP's were mounted on buoys attached to pilings (Figure 3.1, 3.8-3.9) so that the SL-ADCP's (and hydrophones) remained at a fixed depth below the water surface. Placing the SL-ADCP's on buoys allowed us to continually monitor the *surface* currents under a broad range of Sacramento River flows and water levels. The ability to focus on surface currents was an important component of the study design, because past research in the area suggest that salmon outmigrants typically reside within 3 meters of the surface (Blake and Horn, in press (a,b)).

We chose not to deploy upward looking ADCP's (UL-ADCP's) to capture the 3D velocity field because log-law approximations of barotropic velocity profiles (Chow, 1959) adequately predict the vertical variation in the velocity field. In the prismatic, canal-like channels in the delta there is actually very little vertical variation in velocity field except very near the bed and very near the surface (See figure 3.10). Finally, measurements made along the BAFF face using UL-ADCP's in 2011 confirm a near constant velocity profile in the upper third of the water column were salmon outmigrants are concentrated in the vertical and our data collection in 2012 was focused.

Acoustic telemetry hydrophones were also mounted to the ADCP buoys (figure 3.9) to improve the vertical resolution of estimated tag positions by allowing for the maximum vertical separation between the surface and bottom mounted hydrophones. This approach ensured that tagged fish would pass below the "surface" hydrophones even if flows increased after installation, preventing the extrapolation errors that occurred during the 2011 GSNPB study when fish passed over the "surface" hydrophones mounted at a fixed elevation.

During high flows these buoys periodically got stuck, although neither the SL-ADCP nor telemetry hydrophones were ever out of the water. Because the buoys didn't precisely follow water surface variations, time series data measuring the depth below the water surface from the "up beam" on the SL-ADCP's were used to calculate the vertical position of these instruments.

All of the SL-ADCP's were powered by small solar panels attached to the top of pilings (figure 3.3) and the data were telemetered via a cell phone modem, obviating the need for communication cables on the river bed. Thus, the only cables on the river bed in 2012 were associated with the HTI acoustic telemetry gear, significantly reducing the risk of cable tangling reducing the effort of deploying and recovering equipment. By transferring data wirelessly, we had fewer scheduling conflicts with the other aspects of the study (BAFF construction/testing, HTI deployment/maintenance, etc.) and we were able to repair equipment immediately after a problem was detected.

3.1.1 Measurements at the study boundaries

Pilings at locations 1 and 5 (Figure 3.2) were placed sufficiently downstream and upstream of the junction, respectively, such that the velocity streamlines at these locations were parallel to the prevailing bathymetry. They were placed as close to the river bank as possible while ensuring the buoy/SL-ADCP remained floating at lower low water. At these locations the SL-ADCP's were aimed directly cross channel (e.g. perpendicular to the flow). The data from these locations were used to: (1) profile the cross section at the junction's entrance sections, and (2) provide interpolated velocity fields (section 3.2.2), and (3) estimate the critical streakline position following equations 3.17, 3.18 in section 3.3.

3.1.2 Measurements along the BAFF face

The three pilings deployed along the BAFF face (locations 2, 3, 4 and 6 in figure 3.2) were driven roughly 1-2 meters off the BAFF face toward center channel to ensure the SL-ADCP's and HTI hydrophones deployed on them were not enveloped by bubbles emanating from the BAFF and rendered useless under any tidal conditions.

3.1.3 Challenges associated with measuring currents with SL-ADCP's

SL-ADCP's measure the along-beam velocity distribution using two distinct ensonified cones (2 degree beam width) separated by 20 degrees off-axis as is shown in figure 3.11. The velocity distribution is measured in a sequence of discrete volumes of water known as "bins" by time-gating the sound reflected off small particles in the water. Because the SL-ADCP differences the Doppler shift between adjacent bins along each ensonified cone to determine the measured velocity, the instrument assumes that the velocity is perpendicular to the centerline of the two cones (beams) (Figure 3.11B). In other words, the water that flows through bin 5 in one beam is assumed to flow through bin 5 on the adjacent beam. However, if the velocity distribution is not perpendicular to the SL-ADCP orientation (Figure 3.11C), then errors occur in proportion to how far the actual real velocity is off-axis. Completely erroneous velocities are measured when the velocity is directed at or away from the SL-ADCP. SL-ADCP's are typically used to measure the cross sectional velocity distribution in straight reaches and thus the assumption of perpendicular flow is generally valid. However, in a junction like Georgiana Slough, where the velocity distribution changes with the tide, maintaining the beam orientation perpendicular to the principal flow direction can be problematic.

One solution to this problem is to place the SL-ADCP's on rotators and change the orientation of each SL-ADCP based on maximizing the correlation between bins. This did not happen during 2012 the experiment due to time constraints. The next best option is to orient SL-ADCP's on fixed mounts in such a way as to measure the three flow state "bookends" shown schematically in figure 3.3 for downstream flow, figure 3.5 for converging flow and figure 3.7 for upstream flow. The yellow triangles indicate which SL-ADCP's would be used to measure a given velocity distribution, and the black triangles indicate which ADCPs would be disregarded for that velocity distribution. In the case of downstream flow shown in figure 3.3, all of the SL-ADCP's that point perpendicular to the BAFF face would be used and the data from the two ADCP's parallel to the BAFF face would not. Figures 3.3-7 show which SL-ADCP's would be used to deduce the velocity field under a full range of flow conditions. However, during the 2012 study the velocity distribution shown in figure 3.3 occurred throughout the majority of the study period, except for a few days at the beginning of the experiment.

Velocity data from all of the SL-ADCP were collected and recorded on a 15 minute interval throughout the study period, the ping rate was set at 3 seconds/ping to avoid adversely affecting the acoustic telemetry equipment.

3.2 Discussion of the trade-offs between Eulerian/Lagrangian data

The principal advantage to using SL-ADCPs to collect Eulerian measurements is that they yield a high resolution continuous record of the water velocity in the cross section they are measuring. A major disadvantage is that SL-ADCP's measure a relatively small portion of

the total velocity field within the junction, (a cross-stream profile) and thus, the complete velocity distribution must be generating using some form of interpolation. Mass and momentum conserving interpolation techniques are under development (David, L., A. Esnault, et al., 2002; Tsubaki, R., Y. Kawahara, et al., 2012); however, for flow structures that are complex and that change drastically over time, interpolation to a relatively few SL-ADCP profiles may be problematic. Interpolated velocity fields based on the proposed SL-ADCP deployment were quite good under downstream conditions (Figures 3.3 and 3.4), the conditions we saw in 2012, and were sub-optimal under converging (Figure 3.5) and upstream conditions (Figure 3.6,7) because of the complexity and temporal evolution of the flow fields during these periods. Therefore, we also conducted a series of Lagrangian measurements using surface current following drifters (Figure 3.12), which allowed us to capture snapshots of the complete surface velocity structure in the junction. The downside of drifter studies is they are extraordinarily man-power intensive and thus cannot be carried out continuously over the several month study period. We therefore conducted drifter studies at the beginning of the experiment, after major changes in Sacramento River flow, and at the end of the experiment. Thus, the Eulerian and Lagrangian measurements were complementary in that the Eulerian measurements provide continuous temporal coverage at a few locations in space and the Lagrangian measurements provide excellent spatial coverage at a few, although key, snapshots in time. We discuss the Lagrangian measurements next.

3.3 Lagrangian Measurements

In collaboration with DWR, the USGS documented the surface velocity field using surface following drifters (Figure 3.12). These measurements were used to: (1) produce snapshots of surface current maps by interpolating velocities inferred from the drifter paths and (2) calculate estimates of the location and shape of the critical streakline at the junction.

When the flows were downstream and strongly uni-directional, as is shown in Figure 3.13, only a handful of drifter releases were made. However, during conditions where the flow field was demonstrably affected by the tides, drifters were deployed over a 12 hour flood/ebb cycle to document a specific hydrologic condition (Sacramento River flow).

For downstream conditions, a number of drifters were placed across the upstream section, as is shown in figure 3.13, as quickly as this could be accomplished (say over a 5-10 minute period). Putting out the drifters rapidly is important because the velocity fields in junctions can change rapidly with the tides and we would like all of the drifters to experience, as near as possible, the same conditions (the drifters used in this experiment are small so they could be rapidly deployed). We decreased the cross-sectional spacing between drifters near the critical streakline so we could determine the position and shape of the critical streakline as accurately as possible.

For converging conditions, we deployed drifters in the Sacramento River both upstream and downstream of the Georgiana Slough junction (Figure 3.14). And finally, for upstream conditions, drifters were released downstream of the junction as is shown in figure 3.15.

Given the number of drifters in the water and the desire to release and recovery drifters rapidly, two boats, with two people each for safety, were needed to do this work.

3.3.1 Time-shifting drifter data

It would have been ideal to release all the drifters in the river cross-section at the same time, but this is was not feasible in practice. However, given that the velocity distribution in the junction principally responds to variations on a 12 hour cycle, small differences in drifter release times do not affect the results long as the drifters are released within 15 minutes of each other. In other words, we assume the velocity field in the junction is temporally static over the drifter release period AND over the period the drifters are in the study area (usually less than ½ hour). If we assume the flow field changes little over the period the drifters are in the study area then we can ignore the time-history of each drifter and set the complete path to a single period of time - the mean time between when the first drifter passed an arbitrary entrance (white) line and the last drifter passed an exit (white) line shown in figure 3.16.

3.3.2 Deducing velocity fields from drifter data

Again, if we ignore unsteadiness of the velocity field over the period the drifters are in the study area, particle streakiness = velocity streamlines, and thus, we can generate a velocity field registered to the mean time drifters were in the study area. As a first cut, the velocity field, V_i at each $(X_i Y_i)$, can be computed as (see figure 3.17)

$$V_i = \frac{\Delta S_i}{\Delta t} \qquad (3.1)$$

where,

$$\Delta S_i = \sqrt{(x_{i+1} - x_i)^2 + (y_{i+1} - y_i)^2} \qquad (3.2)$$

where each velocity vector is placed at

$$(X_i Y_i) = \left(\frac{x_i + x_{i+1}}{2}, \frac{y_i + y_{i+1}}{2}\right) \qquad (3.3)$$

for each pair of data points collected on each drifter.

3.3.3 Drifter data, examples

Drifter data were collected on six separate days. There were 12 drifters used for each daily study and they were each programmed to store GPS coordinates approximately every 7 seconds. During each study day between 3 and 24 drifts were made, during each drift the twelve drifters were released at intervals from a boat traversing the upstream cross-section. The drifters were allowed to drift past the flow split at the Sacramento River and Georgiana Slough confluence and were retrieved after they had committed to either the Sacramento River or Georgiana Slough. Start and stop times for each drift were recorded on paper logs by the field crew. Data were recorded continuously within each drifter during the entire day. After the final transect of the day, data were downloaded from each drifter. An example of drifter tracks recorded during converging flow is given in figure 3.18, and an example of drifter tracks recorded during downstream flow conditions is given in figure 3.19.

3.2.2 Surface Velocity Interpolations

3.2.1 Introduction

This section describes the data processing and methods used for two-dimensional (2D) water velocity interpolation of hydrodynamic data collected at the junction of the Sacramento River and Georgiana Slough (SR-GS) for the 2012 Georgiana Slough Non-Physical Barrier (GSNPB) experiment. Six side-looking acoustic Doppler current profilers (SL-ADCP's) where deployed from March 5 – April 30, 2012 to provide near surface velocity data, close to the SR-GS junction (see Figure 3.2). Bathymetry data and data from three USGS gage stations: 11447890 - Sacramento River above Delta Cross Channel (WGA), 11447905 - Sacramento River below Georgiana Slough (WGB) and 11447903 - Georgina Slough near Sacramento River (GEO) (available at http://waterdata.usgs.gov/ca/nwis) were used to define boundary conditions used for the time-series of 2D water velocity interpolation. Water velocities calculated from GPS drifter tracks are used for qualitative comparison with the 2D interpolated velocity fields.

To be specific, this section describes: (1) the processing steps taken to ready the data for interpolation, (2) the 2D interpolation algorithms, (3) the results of the 2D interpolation, and, (4) recommendations for future projects.

In field investigations there is always a necessary feedback between the analysis of the data, the configuration of the instruments and the deployment of equipment in the field. To our knowledge, a time-series of 2D interpolated velocity fields from SL-ADCP's data has not been attempted before. Thus, our recommendations apply to future data collection efforts aimed at similar desired outcomes.

3.2.2 DATA PROCESSING AND QA/QC

Data processing constituted merging the SL-ADCP data into a single file, geo-referencing the measurement locations, QA/QC data quality, and estimating velocity values to fill in data gaps. The processed data was then used to perform a 2D velocity interpolation. The following steps were performed during the data processing and interpolation:

Convert raw data files

The raw data was transmitted and averaged on a CR1000 data logger. The raw data from the SL-ADCP's consists of 300 samples time averaged over a 15 minute period. For each SL-ADCP, 27 horizontal bins were collected. The 27 time averaged data samples for each timestamp from the CR1000 were converted into MATLAB format for processing and interpolation.

Geo-Reference SL-ADCP Data

Each bin collected by the SL-ADCP's was geo-reference using field notes of deployment location and programming parameters for each SL-ADCP (outlined in Table 3.1). The location (*R*) of the velocity magnitude at each bin is defined as the midpoint between the bin location within each beam and is defined by the following equation:

$$R = blank\ dist. + [\cos(beam\ angle) * bin\ number * binsize] \quad (3.4)$$

The resultant bin location (*R*) is added to the UTM coordinates, along the heading of each SL-ADCP location. The *blank distance* is a user specified distance away from the instrument head along the acoustic beam where velocity calculations begin. The *beam angle* of each acoustic beam on the SL-ADCP is +/- 20° from the heading of each instrument. A *bin* is a

velocity estimate for a specified location along the acoustic path; *bin number* is a monotonically increasing number along the acoustic beam; and *bin size* is the horizontal distance of the bin (m).

Table 3.1 Site Parameters for each SL-ADCP location and estimated velocity distribution at GEO

Site	1	2	3	4	5	6	GEO
Piling #	22	21	19	17	16	N/A	N/A
Easting (m)	629892	629820	629776	629744	629640	629717	629727
Northing (m)	4233575	4233521	4233493	4233467	4233420	4233425	4233173
Instrument Heading (°)	313	330	330	12	335	26; 30 on 3/16	86
Blank (m)	1.00	1.00	1.00	1.00	1.00	1.00	1.00
Bin Size (m)	3.00	3.00	2.25	2.70	2.00	2.10	2
Num Bins	27	27	27	27	27	27	24

Velocity Vector Rotation – Sites 1, 2, 3 and 5

Sites 1-3 and 5 had one component of velocity recorded (velocity magnitude), therefore velocity direction from these sites was not known, and had to be estimated. At each geo-referenced bin location the direction of the velocity magnitude vector was initially assumed to be normal to the orientation of the SL-ADCP. This is a reasonable assumption for Site 1 since the SL-ADCP at this location is oriented perpendicular to the channel and the channel geometry is roughly prismatic. At Sites 2 & 3 this assumption is less valid since angle of SL-ADCP's are not oriented perpendicular to the channel, and the flow field is presumed to diverge closer to the junction. At Site 5, the SL-ADCP is oriented perpendicular to the channel, but since the location is on a river bend it is likely the orientation of the velocity vectors varied in space and time and thus we could not assume the velocities were either perpendicular to the beam orientation nor parallel to the bank. The correction of the velocity vector orientation is accomplished within the 2D interpolation algorithm, but the initial direction is assumed to be perpendicular to the SL-ADCP orientation (see Figure 3.23).

Velocity Vector Rotation – Sites 4 and 6

At Sites 4 and 6 the SL-ADCP's water velocity was recorded in beam coordinates. The orientation of the SL-ADCP's is into the predominant flow direction during the downstream flow condition (~93% of data collected during the study period). The transformation of beam coordinates into U and V velocity components required bin-mapping solutions for SL-ADCP's that can accommodate an orientation different from normal to the predominant flow direction. The bin-mapping solution requires that the predominant flow vector travels through bins on both acoustic beams of the SL-ADCP (RDI; pers. comm.). This requirement is violated at sites 4 and 6 when the follow is strictly downstream (non-reversing) and thus valid solutions exist for reversing flow conditions (~5 % of the data collected during the study period). This was known at the time of the deployment and thus sites 4 & 6 were deployed to cover conditions of reversing flows.

The bin-mapping solutions at Sites 4 and 6 were determined to be a 20° and 0° angle offset from the perpendicular to the instrument head, respectively. These angle offsets were held constant through time, since no other information could be used to determine a time-variable solution. Velocity profiles were generated from bin-mapping solutions for the entire dataset, but only a subset of conditions was used in the final velocity interpolation. It should be noted that changing the angle offset by +/- 20° did little to the final bin-mapping solution.

Missing or Erroneous Data – Small Data Gaps

Since the data was used for interpolation was a 15 minute average of a large number of samples a minimal amount of data was considered bad data. Missing or obviously bad data was rejected and interpolated temporally, using linear interpolation, for small data gaps (< 1hr.).

Missing or Erroneous Data – Large Data Gaps

One time period from March 10 – March 12, 2012 had erroneous data at Site 5. An estimated mean cross-section velocity for this time period was made based on the 2nd order polynomial regression of measured velocity at Site 5 and measured velocity data at WGB, located 425 m downstream from site 5 (Figure 3.22a). The data gap at Site 5 occurred during flow conditions from -150 m^3/s to 250 m^3/s. Velocity data from Site 5 during similar flow conditions were used to develop a mean velocity profile for upstream and downstream flow conditions. The two mean velocity profiles were then fitted to the mean cross-section velocity magnitude; thereby generating an estimate of the velocity distribution at Site 5 for the data gap period (Figure 3.22b).

Extrapolate Velocity Profiles to Banks

Cross-sectional velocity profiles were extrapolated to the banks at Sites 1-3 & 5 (see Figure 3.23), for the final processing step. This extrapolation assumes turbulent, shear flow and a logarithmic boundary layer from the last measurement point to the bank (Kundu and Cohen, 1990). Velocity components were extrapolated at increments equivalent to the bin spacing of the measured values for each cross-section (Figure 3.23).

3.2.3 BOUNDARY CONDITIONS

A Lagrangian Particle Tracking Algorithm (LPTA) was used to generate particle pathlines within the study domain and to rotate the velocity magnitudes at Sites 2 & 3. To implement the (LPTA) three boundary conditions are needed. A downstream velocity boundary condition in Georgina Slough was estimated based discharge measured at the GEO gaging station (located approximately 225 meters downstream of the junction), and the index velocity rating curve to determine the mean cross-sectional velocity. A cross-sectional velocity distribution was estimated once again assuming a logarithmic boundary layer to the river banks.

A second boundary condition is needed to keep particles within the domain as they move through the flow field. The banks of the river were determined from the bathymetry data. At the river banks velocity vectors were defined in a direction tangent to the bank direction. The magnitude of the velocity vector is set to the minimum measured value for the entire domain at each timestamp. A third boundary condition is water surface elevation (WSE) for each timestamp. This data is available at each of the USGS gaging stations. The offset from GEO to the SR-GS junction is 0.04 m (Jim DeRose pers. comm.). Because this is within the range of uncertainty of the bathymetric data this correction was not applied. The WSE for the domain was set to the elevation measured at the GEO gage station (in NAVD 88). At each timestamp the 10 x 10 m interpolation grid is adjusted to account for changing WSE.

3.2.4 TWO-DIMENSIONAL VELOCITY INTERPOLATION

A 2D velocity interpolation algorithm was developed to interpolate velocity magnitude and direction along particle pathlines within the domain. A Lagrangian Particle Tracking Algorithm (LPTA) was used to rotate velocity vectors at Site 2 and 3, due to the fact that the SL-ADCP's were not oriented normal to the predominant flow direction, and the likelihood that velocity vectors diverge as they approach the SR-GS junction. The initial pathlines generated from the particle paths were then used to interpolate velocity magnitude and direction using inverse path length weighting between each velocity cross-section (measured or extrapolated values). The resultant velocity vectors provided a data rich velocity field throughout most of the domain, but sparse in some areas and was time dependent. Therefore at each timestamp the velocity field was updated on uniform 10 x 10 m grid using a linear grid interpolation.

Lagrangian Particle Tracking Algorithm

The LPTA released particles at each bin in the cross-section at Site 1. The particles were distributed across the river as a function of the estimated flow (Q_E) at Site 1 (Figure 3.25a) so that particles were released in each segment of the cross section in proportion to the amount of flow passing through each segment in the river cross section. For example, fewer particles are released at the edge of the river than at the center of the river. The Q_E at Site 1 is determined by the product of the integrated cross-sectional area and the measured velocity. The Q_E is well correlated with measured flow (Q_A) at WGA (Figure 3.24b) and the summation of flow at WGB (Q_{SR}) and GEO (Q_{GS}) agrees with Q_A (not shown). The particles were moved through the domain at each time step using the closest measured velocity vector in the domain. The velocity vectors at Site 2 and 3 were iteratively rotated until the ratio of particles (R_P) in each junction (Sacramento River and Georgiana Slough) was within 5 % of the discharge ratio (R_Q) of each junction.

During the iterative process used to correct the velocity vectors at sites 2 and 3, the velocity vectors from each site were rotated in different directions depending on their location in the river cross section. This process was accomplished as follows: First, a critical streakline (C_{SL}) was estimated based on the distance from the left bank where $Q_E = Q_{GS}$. The estimated C_{SL} was then projected downstream along a trajectory in the direction of the right bank of the river. Second, the point where the estimated C_{SL} crossed the cross-section at Site 2 and 3 was picked as the 'critical point' where velocity vectors diverged. Finally, velocity vectors on the right side of the critical point were rotated to a direction parallel to the right river bank, and velocity vectors on the left side are rotated in a direction parallel to the left bank (Figure 3.25b illustrates the routine logic).

Anecdotal evidence from the Langranian drifters suggests the mean flow direction at these locations is parallel to the river banks, under a varying range of flow conditions, thereby justifying the logic used for velocity vector rotation. The algorithm iteratively moves the C_{SL} left or right depending on the whether R_P is greater than or less than R_Q. The algorithm converges and moves to the next timestamp if one of three conditions is meet: (1) the percent difference in R_P and R_Q is less than 5%, or (2) the percent difference at iteration $i+1$ is greater than the solution at iteration i, or (3) 20 iterations; this criteria is conservatively high and no solutions met this criteria.

Pathline Interpolation Algorithm

An along-pathline interpolation algorithm was implemented, as it was presumed to have increased accuracy over traditional methods used in 2D grid interpolations such as kriging or inverse distance weighting. Inverse distance weighting (IDW) has shown good results in

previous 2D grid velocity interpolations, for high density data fields (Dinehart and Burau 2005a, David et al. 2002). For sparse density data field, IDW shows comparable results to more sophisticated methods, although there is a dependence on data density (Tsubaki et al. 2012). The measured SL-ADCP has high spatial resolution in the cross-stream direction, but sparse spatial resolution in the along stream direction. Moreover, IDW interpolations can create discontinuities (or sharp bends), which can be smoothed with different weighting parameters but this smoothing then creates little cross-stream variation. To overcome the confounding difficulties of varying data resolution (in two dimensions) and choosing appropriate weighting parameters (to minimize along stream variation and to accurately estimate cross stream variation) a method for along pathline interpolation was developed. The main difficulty in implementing along pathline interpolation of velocity vectors is determining the actual pathline. The particle pathlines generated in the LPTA were used as an approximation of the actual pathlines. Implicit in the mass balance approach used to generate pathlines, is the assumption that these pathlines give an accurate representation of the mean flow direction. For the initial flow field generation an IDW function was used to move particles through the domain. At each iteration of the algorithm, the flow field was updated with the solution from the along-pathline interpolation.

The interpolation along the pathline is an inverse path-length weighting (IPLW) function:

$$U(x) = \frac{\sum_{i=0}^{N} w_i(x) u_i}{\sum_{i=0}^{N} w_i(x)} \qquad (3.6)$$

$$w_i(x) = \frac{1}{d(x,x_i)^P} \qquad (3.7)$$

Where $U(x)$ is the interpolated velocity at point x, u_i is a known velocity at point i, at a distance d from the interpolated point x. The number of points (N) used in the interpolation are weighted by the inverse distance from the interpolated point, by the weighting parameter (w_i), which is adjusted by the power parameter (P). For this data set P and N were set to 4 and 2, respectively. The velocity field generated by IPLW is then interpolated onto a 10 X 10 m uniform grid using linear interpolation (Figure 3.26).

Complex Flow Conditions

For converging flow conditions, defined as Q at WGB < 30 m^3/sec and Q at WGA > 0 m^3/sec, or reversing flow conditions, defined as Q at WGB < 0 m^3/sec, the LPTA and IPLW algorithms could not be implemented in the final 2D interpolation. Particle pathlines generated for these conditions did not produce a realistic flow field, due to only one

component of velocity being recorded. The flow fields during these time periods become more two-dimensional and too many degrees of freedom exist to reasonably constrain the velocity vector corrections using the techniques developed for the downstream flow conditions. For converging and reversing flow conditions an inverse distance weighting (IDW) function was used to produce 2D velocity interpolations, this has been shown to be an effective method in previous studies (Dinehart and Burau 2005, David et al. 2002).

The bin-mapping solutions for Site 6 were included in the 2D interpolation for a subset of the complex flow conditions. Site 6 had some periods of obvious erroneous or missing data and these time periods could not be estimated; these time periods were removed and not included in the 2D interpolation. Site 4 was not included in the 2D interpolation because it was concluded that the flow conditions at this Site were too complex to determine viable bin-mapping solutions. This was determined based on visual inspection of all measured cross-sections in the domain. The velocity recorded at Site 4 was much different than the velocities that were recorded at other cross-sections for much of these time period. This is mostly likely due to the high spatial variability in velocity vectors for these flow conditions at this site. The velocities recorded at Site 3 were removed for converging flow conditions for the same reason.

The final 2D interpolation for converging and reversing flow conditions was a result of two interpolation iterations. The first iteration used the IDW function. The IDW was the same as the IPLW function (See Equations 3.6 and 3.7), except instead of using neighbors along a pathline the IDW used neighbors on a 2D grid. The first iteration was on a coarser grid (20 x 20 m) with the power parameter (P) set to 4 and the amount of nearest neighbors (N) set to 50. This was done in order to produce a more realistic along stream flow field, but this resulted in minimal cross-stream variation. For the second iteration a boundary condition of near zero velocity at the banks was incorporated into the solution. The 10 x 10 m grid used for the downstream flow conditions was used and a linear grid interpolation was performed. This allowed the velocities to decrease as they got closer to the river banks. The final 2D interpolation for the converging flow conditions was then merged with the 2D interpolation for downstream flow conditions.

3.2.4 ALGORITHM PERFORMANCE

The LPTA and IPLW interpolations were run on 92.4% of the data that represents downstream flow conditions (Q at WGB > 30 m^3/sec). The percent difference in the particle ratio (R_P) to the discharge ratio (R_Q) was less than 10% (Figure 3.27a) for 93.5% of the data. For 94% of the data, zero particle paths moved outside of the domain. The particle paths that did move outside of the domain were less than 1% of the total particle paths (Figure 3.27b). Based on these two metrics the particle pathlines give an accurate representation of the flow field for the large majority of the dataset. These algorithms

converged on a solution fairly quickly, the majority converging after 5 iterations and nearly all of them converging after 10 iterations (Figure 3.27c).

A qualitative assessment of the 2D interpolation to calculated water velocities from the GPS drifter data was performed. The GPS drifter data was not included in the original scope of the project, therefore only a subset of the data has been analyzed up to this point. As can be seen in Figure 3.28, general features of the flow field are well represented in the interpolated velocity field: (1) the generated pathlines accurately predict which junction branch the drifters will enter, and (2) the velocity magnitudes are fairly accurately represented (for this instance). The velocity direction is in good agreement with the drifter data at locations away from the SR-GS junction, but less so closer to the junction. All the drifter data (n=23) for March 21, 2012 was analyzed in this fashion and exhibited similar trends, except for time periods when the barrier (GSNPB) was on (this was also noted by the field crew).

3.3 Methods - Analytical

In this section we discuss several analytical approaches to address, from a physical perspective, the question: **Do fish "go with the flow" in junctions?**

There are several layers to this question that involve the interaction between fish behavior and physical processes. From a physical point of view, the answer to the question of "Do fish go with the flow" depends on how one defines "flow" - at what spatial and temporal scales. In space, the answer depends on whether one is talking about the scale of the fish (fractions of a meter), the scale of the junction or the scale of the delta. In time, the answer depends on whether one is focused on the fish decision-making process – timescales of seconds – or discussing entrainment at tidal, tidally averaged or seasonal timescales. Often flow (bulk discharge, in say, cfs) is used synonymously with velocity and velocity distributions. This lack of linguistic precision often leads to confusion and arguments where none exist. In this paper we seek clarity by clearly defining the temporal and spatial scales of interest.

The question of whether "fish go with the flow" is ultimately about understanding entrainment rates and what controls them.

3.2.1 Entrainment in Junctions – Fish fluxes – Oh my!

We therefore begin the entrainment discussion starting with first principles. First we conceptually divide the problem of entrainment in junctions into two regions: (1) those things that control/create the fish entrance spatial distributions – things such as the interaction between hydrodynamics (influenced by geometry, structures (dock, bridge piers, etc.) and behavior that occur up-current of the junction and (2) hydrodynamic and

behavioral interactions that occur within the junction. The entrainment rate, E(t), or fish flux (# of fish/time) into the junction at any given time t, through the up-current cross section is simply the spatial integral of the product of the fish concentration, C(x,z,t), (# fish/m^3) with the velocity distribution, V(x,z,t) (m/s) as

$$E(t) = \int_0^w \int_{-h(x)}^0 V(x,z,t)C(x,z,t)dzdx \qquad (3.5)$$

Where x is the cross channel direction (in meters), z is the vertical direction (meters) measured from the water surface, w is the width of the channel and h(x) is the depth of the channel at location x, as is shown in figure 3.10.

Example real world distributions of V(x,z,t) and C(x,z,t) are shown in figure 3.10, 3.20 and 3.21 respectively, where in the case of figure 3.10, C(x,z,t) are acoustic backscatter amplitude, which provides a measure of the suspended sediment concentration. In the case of figures 3.20 and 3.21, the horizontal spatial distribution of tagged fish is given.

Forgetting the problem of understanding and predicting fish distributions for the purposes of this section, we begin with the easy part of the problem, the hydraulics of entrainment.

In this section we assume that, to be precise, fish "go" with the instantaneous (e.g. 15 minute averaged) velocity distribution. Under many circumstances, when the swim number is low (periods of peak tidal currents and high river flows) fish movements within junctions are "mostly" due to advection by the local velocities, with behavior providing a relatively small perturbation to a strong advective signal. This assumption allows us to study the hydrodynamics of junctions without muddying the water with non-uniform junction entrance fish distributions or behavior that occurs within the junction. Indeed, the assumption that fish "go with the flow" based on the total discharge at tidal timescales assumes that C = constant and that fish movement approximates that of a non-behaving particle within the junction. Assuming C= constant allows us to focus on understanding entrainment from a purely hydrodynamic perspective which, in turn, allows us to make useful simplifications of the complex velocity fields that occur in junctions when they are strongly tidally forced.

We begin with our first simplification of the full velocity field; for the next section we assume that the flow is two-dimensional in the horizontal plane. This simplification is reasonable, because even though the flow is clearly three dimensional (figure 3.10), the vertical velocity gradients can be predicted using log and power laws (Chow, 1959).

3.3 The Critical Streakline

In the last section we simplified the full three dimensional velocity fields to include only the two dimensional surface currents. In this section we simplify further using the entrainment zone concept to motivate critical streakline calculations. Particles (or drifters) that enter the junction of the Sacramento River with Georgiana Slough are either transported into Georgiana Slough or bypass it, as is shown in figure 1.1 for downstream flow conditions. We call areas in the junction where a large percentage of particles share the same fate entrainment zones. We define the critical streakline as the spatial divide between the entrainment zones; in figure 1.1 the critical streakline separates the entrainment zone for particles that enter the side channel (red) and the entrainment zone for particles that bypass it (green) (figure 1.1). This concept is further illustrated by the tracks of surface drifters released by DWR during the 2011 BAFF experiment; drifter tracks for downstream flow conditions (Figure 3.18) and for reversing conditions (figure 3.19) show drifter paths diverging in the region around the critical streakline.

The critical streakline concept is a way of collapsing a complex flow field into its essence with regard to fish fates. The critical streakline provides a simple metric for comparing the potential for entrainment under a variety of conditions within a junction and between junctions. For example, at any instant in time the critical streakline reduces the complexity of the entire flow field down to a single Lagrangian trajectory that can be well represented by the distance from the shore, Xu, to the trajectory's location in the river cross section (figure 1.1).

This can be seen mathematically by spatially separating the entrance entrainment rate in equation (1) into two integrals based on the lateral position of the critical streakline, Xu. If we assume no behavior within the junction, and V(x,z,t) = V(t) and C(x,z,t) = C(x,t) as discussed above, we have

$$E(t) = \int_0^{Xu} V(t)C(x,t)dx + \int_{Xu}^{W} V(t)C(x,t)dx \qquad (3.8)$$

where the first term represents the entrainment rate into the side channel, Georgiana Slough in this case, and the second term represents the entrainment rate in the main channel, the Sacramento River in this case.

In this section we derive relations for estimating the critical streakline location based on (1) SL-ADCP measurements and (2) the bulk discharges in the channels that make up the junction (e.g. the discharge measured at a standard flow station). In both cases, the appropriate relations are developed through simplifications of relations based on first principles (e.g. equation 3.4).

We begin with the general formula for calculating the discharge, Q(t), in a channel following the schematic in figure 3.29A (e.g. C(x,z,t) = C), for a natural channel.

$$Q(t) = \int_0^W \int_0^{h(x)} V(x,z,t)dzdx \qquad (3.9)$$

Unlike the previous sections which focused on interpolating the surface current velocity field, here we focus on simplifications of the flow field in the up-current, or entrance sections that bound a junction. Equation 3.4 assumes we take into account variations in bathymetry and the complete vertical velocity distribution as is shown in figure 3.10 to calculate the discharge. In practice, equation 3.4 is not particularly useful since measuring the full flow field is often prohibitively expensive, so we simplify the process by assuming that velocity is not a function of depth and that the surface velocity is a reasonable proxy for the entire water column $V(x,z,t) \sim V(x,t)$. We also assume that the discharge is time invariant over the 15 minute samples we typically take with SL-ADCP's (e.g. we model discharge as a series of steady state conditions), or, $V(x,t) \sim V(x)$. Applying these assumptions we are left with

$$Q = \int_0^W V(x)h(x)dx \qquad (3.10)$$

consistent with the variability in bottom depth and (horizontal) velocity structure shown in figure 3.29B.

With these simplifications, the discharge upstream of the junction is

$$Q_u = \int_0^{W_u} V_u(x)h_u(x)dx \qquad (3.11)$$

Where the cross stream surface velocity profile, $V_u(x)$, is measured using a SL-ADCP shown schematically in figure 3.29B, figure 3.2 (SL-ADCP 1) and $h_u(x)$ is based on a bathymetric survey, including the banks. Now, the total discharge in a typical cross section is

$$Q_g = \int_0^{X_g} V_g(x)h_g(x)dx \qquad (3.12)$$

and the discharge in the Sacramento River downstream (Figure 3.2 – SL-ADCP 6) is

$$Q_d = \int_0^{X_d} V_d(x)h_d(x)dx \qquad (3.13)$$

Finally, by conservation of mass, the discharges in the junction are related through

$$Q_u = Q_g + Q_d \qquad (3.14)$$

Since, from an entrainment perspective, we aren't really interested in where the water comes from once it is in Georgiana, X_g is not all that interesting except as a simple indicator of when flows are converging into Georgiana. Nonetheless, we can compute X_g based on equation (3.14) without having to compute a detailed integration (we didn't instrument behind the BAFF anyway).

Critical Streakline estimates based on SL-ADCP and bathymetry data

We are most interested in calculating the location of the critical streakline in the Sacramento River at both the upstream and downstream entrances to the junction (e.g. where it intersects the acoustic telemetry array). For this we use the discrete forms of equation (3.11) and equation (3.13) where we obtain velocity data from SL-ADCP's and bathymetry data at locations 1 and 6 in figure 3.2.

In discrete form (3.11) becomes,

$$Q_u = \sum_{i=0}^{i=imx} V_u(x_i) h_u(x_i)\, \Delta x \qquad (3.15)$$

And (3.13) becomes,

$$Q_d = \sum_{i=0}^{i=imx} V_d(x_i) h_d(x_i)\, \Delta x \qquad (3.16)$$

To find the location of the upstream critical streakline, X_u, for conditions where the flow is downstream in the junction (Q_u>0 and Q_d>0), we use (from equation (3.15))

$$Q_g = \sum_{i=0}^{i=iu} V_u(x_i) h_u(x_i)\, \Delta x \qquad (3.17)$$ **(Calculation of Xu based on SL-ADCP data)**

We compute iu and thus X_u (figure 3.29B) by summing the product of the velocity and depth in the upstream entrance section on the Sacramento River (e.g. equation (3.17)), beginning on the left bank, by incrementing the counter "i" until Q_g is reached.

Similarly, we compute id and thus X_d (figure 3.29B) by integrating the product of the velocity and depth in the downstream entrance section on the Sacramento River beginning

on the left bank during upstream flows (Q_u<0 and Q_d <0) by incrementing the counter "i" until Q_g is reached using equation (3.18) below (from equation (3.16)),

$$Q_g = \sum_{i=0}^{i=id} V_d(x_i) h_d(x_i)\, \Delta x \qquad (3.18)$$ **(Calculation of Xd based on SL-ADCP data)**

Critical Streakline estimates based on flow station data

In most cases we will not be able to afford to collect downward-looking ADCP data at the entrance sections to the junction so we further simplify equation 3.9 by assuming a rectangular channel (figure 3.29C) with vertical sidewalls (e.g. the water line and cross section width does not vary in space as discharge changes) and no sidewall boundary layers (which are shown in figure 3.29B)(e.g. no cross channel variation in velocity).

If we make these assumptions (V≠ f(x,z), h≠f(x) and W = constant), we can estimate the critical Streakline distances X_u, X_d, X_g based on the simple proportions given in figure 3.30.

Based on figure 3.30A we know that, for downstream flow (Q_u>0 and Q_d >0)

$$\frac{X_u}{W_u} = \frac{Q_g}{Q_u} \qquad (3.19)$$

Or,

$$\boldsymbol{X_u = \left(\frac{Q_g}{Q_g + Q_d}\right) W_u} \qquad \textbf{(3.20)}$$ **(Estimate of Xu based on flow station data)**

Similarly for converging flow (figure 3.30B) (Q_u>0 and Q_d <0),

$$\frac{X_g}{W_g} = -\frac{Q_d}{Q_g} \qquad (3.21)$$

Or,

$$\boldsymbol{X_u = -\left(\frac{Q_d}{Q_g}\right) W_g} \qquad \textbf{(3.22)}$$ **(Estimate of Xg based on flow station data)**

Finally for upstream flow, (figure 3.30C) (Q_u<0 and Q_d <0)

$$\frac{X_d}{W_d} = \frac{Q_g}{Q_d} \qquad (3.23)$$

Or,

$$\boldsymbol{X_d = -(\frac{Q_g}{Q_d})W_d} \qquad \textbf{(3.24) (Estimate of Xd based on flow station data)}$$

3.4 The Discharge Ratio

The streakline positions are extremely useful in understanding entrainment by comparing streakline positions with observed tagged fish spatial distributions. However, streakline positions are site specific and depend on the local bathymetry. But, if we assume that V≠ f(x,z), h≠f(x) and W = constant in time, we note that the relations for the streakline positions are nothing more than the discharge ratio scaled by the width of the channel. Thus, if we define the discharge ratio R_U as the proportion of the flow that enters the side channel from the main channel from upstream and R_D as the proportion of the flow that enters the side channel from downstream we can reformulate equations 3.20 and 3.21 as

$$X_u = W_u\left(\frac{Q_s}{Q_u}\right) = W_u R_u \qquad (3.25)$$

and

$$X_d = -W_d\left(\frac{Q_s}{Q_d}\right) = W_d R_d \qquad (3.26)$$

When the flow is converging into the side channel from the main channel we define the discharge ratio under these conditions as R_C, which is identically 1 (or 100%) (e.g. all of the water from the main channel is flowing into the side channel from both up and downstream). Defining the discharge ratios in this way suggests a series of six states shown in figures 3.31 and 3.32 that represent all of the conditions that must be considered to correctly compute the discharge ratio (and streakline positions based on the bulk channel discharges) in junctions where the tidal currents are reversing. Since each of the states shown in figures 3.31 and 3.32 are mutually exclusive we define the total discharge ratio as

$$R_Q = R_U + R_C + R_D \qquad (3.27)$$

which varies from zero to unity and encompasses all possible flow conditions. By mutually exclusive we mean only one of the component R's (R_U, R_C, R_D) is non-zero at any time. By convention, the R's are all strictly positive for water entering a side channel (figure 3.31), and negative for water exiting a side channel into the main channel (figure 3.32). In this way, we account for conditions in which fish may be entrained in a side channel but return when the flows reverse in the side channel into the main channel (more on this later). In addition, when the flows and R's are negative - out of a side channel - the entrainment into the side channel during this time is likely zero based on purely advective arguments.

By maintaining all three of these variables separate from the total discharge ratio we can independently quantify how each of the conditions in figures 3.31 and 3.32 varies throughout the tidal cycle which is important in understanding what types of fish guidance technologies may work in a given junction and under what conditions (more on this later). In addition, the total discharge ratio will tell us how each of the flow conditions contribute to the tidally averaged discharge ratio under a variety of hydrologic conditions, especially when the flows from the side channel are reversing (more on this later).

The R's may be more appropriate for understanding the influence of the tidal dynamics (the purpose of this paper) and for statistical purposes than the streakline calculations, mostly because the assumptions outlined above are pretty good. Moreover, since the R's are non-dimensional, they are the metric of choice in understanding the influence of the tidal dynamics between channels in a junction, on tidally averaged entrainment (more on this later) and for use in comparing the tidal dynamics between junctions. Since the streakline calculation using the bulk discharge formulation (equations 3.25 and 3.26) is merely the discharge ratio scaled by the channel width, the discharge ratio can be thought of as the percentage of the main channel width (0 to 1) that is engaged in entrainment into the side channel. This thinking only works because the channels in the delta are canals with prismatic channels. Still, for the design of barriers and other on-the-ground physical features the SL-ADCP data combined with an accurate cross sections (equations 3.17 and 3.18) should be used to accurately place the streakline in space.

4 Results

4.1 Tidal timescale dynamics in junctions – Sacramento River/Georgiana Slough Junction

Before we discuss results from the discharge ratios and streakline positions we begin with time series plots that examine the tidal timescale variability in the bulk flows that occur within the junction of the Sacramento River and Georgiana Slough. We need to understand how the flow distributions evolve in junctions over a complete tidal cycle, because this is the

temporal scale where fish entrainment is determined mechanistically – fish don't move through junctions, nor respond behaviorally, at tidally averaged or longer timescales, such as the 14-day average flow of Old and Middle River (OMR) used in the regulatory environment. Analysis of data collected at widely differing timescales is common in the delta, with predictably bad results.

Except for the fact that Georgina Slough rarely reverses, the Sacramento River/Georgiana Slough junction is typical of most junctions in the delta. In figure 4.1 we plot 5 days of the discharge in the Sacramento River at Freeport and the discharge in the Sacramento River/Georgiana Slough junction. We chose this period because it transitions from a net Freeport flow of ~8.5k cfs (a very low discharge even by typical low-flow conditions in the late summer/fall) to ~30k cfs (Figure 4.1A) which provides the opportunity for us to examine how the dynamics in Georgiana Slough change from bi-directional flow to fully uni-directional (all downstream) flow. In this figure, the flow at Freeport nearly reverses at Julian Day 73.25, which can happen when the tidally averaged flows (dashed line in figure 4.1A) are less than ~8.7k cfs. Reverse flows only usually happen at Freeport during drought years, and then only rarely. In figure 4.1B, the discharge in Georgiana is plotted in red, the flows just upstream of the junction are blue and the flows downstream of the junction are green.

First off, the flows entering Georgiana are nearly always positive (except at extremely low Sac River flows) and are a fraction (roughly 30%) of the flows that exchange into and through the junction during low Sacramento River flows. From figure 4.1B we note that: Sacramento River upstream of Georgiana Slough varies from -3 to 12 k cfs, Sacramento river flows downstream of Georgiana Slough varies from -6 to 10k cfs and Georgiana Slough varies from 1 to 3.6k cfs.

In terms of timing, the flows in Georgiana are generally in quadrature with the mainstem Sacramento River flows – that is, 90 deg out of phase. This means the peak Georgiana tidal discharge roughly occurs near the transition from ebb to flood on the Sacramento River (see "(II) Georgiana max" in figure 4.1B) and the flow minimums into Georgiana roughly occurs during the transition from flood to ebb (see "(I) Georgiana min" in figure 4.1). This phase relation between the Sacramento River and Georgiana Slough, where peak flows in Georgiana Slough occur when the Sacramento River is changing between flood and ebb tides is somewhat unique. Generally side channels are phase-locked with the main channel, that is peak flows in the side channel occur at the same time as the main channel. The fact the discharge in Georgiana Slough is in quadrature with the mainstem Sacramento River makes it absolutely critical we rigorously define how we compute the discharge ratio in this junction because the bypass flow in the Sacramento River is out of phase with the discharge entering Georgiana Slough.

Once the net Freeport flows exceed approximately 15k cfs, around Julian Day 75.5 (Figure 4.1A), the flows become unidirectional in the Sacramento River/Georgiana Slough junction and the tidal signal into Georgiana becomes progressively less pronounced. Finally, *the proportion* of Sacramento River water that enters Georgiana decreases with increasing Sacramento River flows because the conveyance in the Sacramento River increases at a faster rate than Georgiana Slough as the net Sacramento River flow rates increase (more on this later). Tidal dynamics and entrance fish distributions aside, we expect the entrainment rate into Georgiana Slough to go down as the Sacramento River net flows increase because of this conveyance relation between the Sacramento River and Georgiana Slough.

4.1 Variation in the discharge ratios at the tidal timescale

In figure 4.2C we plot the three component discharge ratios where it is readily apparent which of the three flow conditions, shown as diagrams at the top of the figure, exist at any given time. We've shaded the periods that correspond to each of the three flow states shown in the diagrams at the top of the figure: Light blue – periods that are indicative of downstream flow; white (no shading) - periods of converging flow; and, yellow – periods of upstream flow. Clearly, at low Sacramento River flows, downstream flow conditions occur most often in Georgiana Slough. Next periods of upstream flow, followed lastly by converging flow conditions.

Tidal periods that encompass converging flows have two basic modes indicated by the I and II in figure 4.2D. Periods of extended converging flow occur when the flow reverses into Georgiana but the tides don't have the momentum to reverse the flow upstream in the Sacramento River above Georgiana Slough, as is indicated by I. Periods of converging flow are extremely important for overall entrainment of fish in a side channel because these periods represent periods of weak to no bypass flows in the main channel - during these periods all of the water, and presumably all of the fish from the main channel enter the side channel, unless they seek refuge along the bank opposite the side channel. This condition often happens during spring tides when a substantial diurnal inequality exists – essentially occurring every other flood tide, as is shown. During the maximum flood tide, the periods of converging flow are short lived, indicated by the II's in figure 4.2B, occurring for short periods of time immediately before and after the flood tidal flows on the Sacramento River bypass Georgiana Slough.

During the downstream and upstream flow periods the discharge ratio varies, significantly in the case of the downstream flow condition. In a prismatic channel, the discharge ratio can be thought of as the percentage of the width of the channel that is used to convey water into the side channel. Therefore, the progression for the upstream and downstream conditions both start with $R_Q = 1$ during converging flow conditions which is a condition where the full

width of the main channel is engaged in providing water to the side channel. However, as either condition progresses, less of the channel width is involved in providing water to the side channel, the remainder of the water and the fish in it bypasses the side channel. In the case of the prolonged downstream condition, the discharge ratio decreases from 100% to less than 25% of the channel width (see, for example, III in figure 4.2C) whereas during the peak upstream flow conditions, 50% to 60% of the channel width is involved (see, for example, II in figure 4.2C). At high flows, Julian Days 75.5-77, the percentage of the Sacramento River channel involved in providing water to Georgiana Slough is still relatively low, 25 – 50%, at Sac River discharges of 15-30k cfs, because the Georgiana cross section is considerably smaller than the Sacramento River at this location so most of the flow continues seaward in the mainstem.

Figure 4.5 shows that both the converging and upstream flow conditions occur on the descending limb of the flows that enter Georgiana Slough, but begin near the peak discharge into Georgiana. Therefore, both converging and upstream conditions occur when significant volumes of water, and potentially fish, are entering Georgiana. It is therefore likely that both of these conditions significantly contribute to the tidally averaged entrainment of fish into Georgiana Slough (more on this later).

4.2 Implications of the streakline concept

The streakline concept can be used to evaluate the efficacy of placing up-current guidance structures to change the entrainment rate in side channels. In the case of Georgiana Slough, the purpose of the upstream guidance structure would be to move outmigrants across the streakline away from the side channel. A narrow and relatively stable entrainment zone (streakline position) into the side channel is optimal for a guidance structure because the distance that fish have to be moved to cross the streakline is short and has a consistent position in space. In figure 4.3 we see that the entrainment zone upstream of the Sacramento River/Georgiana Slough junction (e.g. R_U) varies considerably at low flows, but except for short-lived peaks, varies from 25 to 50% of the cross section. Peaks that exceed 50% of the width of the channel cease when Sacramento River Freeport flows exceed 12-14k cfs and flow in the Georgiana Slough junction becomes unidirectional (figure 4.4). As we have shown (figure 4.2), conveyance is less in Geo relative to the mainstem Sacramento river at higher Sacramento River flows, thus the entrainment zone gets smaller as the Sacramento River flows increase. The near shore, relatively narrow band of streakline positions shown in figure 4.2 suggests that the Sacramento River/Georgiana Slough junction is a good candidate for an upstream guidance structure aimed at reducing entrainment into the central delta, , especially during Sacramento River at Freeport flows that exceed 14k cfs.

Conversely, the position of the downstream streakline during DCC gates closed conditions suggests that a guidance structure downstream of Georgiana Slough would likely not work. For example, we can see in figure 4.5 that the entrainment zone for flows entering Georgiana Slough during low flow conditions from downstream varies from 70% to 100% of the river cross-section. In other words, reducing entrainment in Georgiana Slough when the flows are reversing would require a guidance structure to move fish across 70-100% of the river cross section. Given the fact that upstream flow conditions occur for a relatively short period of time during low Sacramento River flow rates, and given the fact that on a tidally averaged basis upstream flows only account for roughly 10% of the total tidally averaged discharge ratio (figure 4.6), a downstream guidance structure would likely be ineffective at reducing overall entrainment in Georgiana Slough. Finally, during the typical outmigration period the Sacramento River flow rates often exceed 12-14 k cfs, and thus reversing flow conditions are relatively rare during the outmigration season. For these reasons, a downstream guidance barrier is not recommended based on the entrainment zone concept.

5 Discussion

Unlike our understanding of fish distributions, velocity distributions in open channels are well behaved, predictable in time (conservation of mass and momentum) and have been well understood since the 1900's, especially in the canal-like, prismatic channels of the delta Chow, 1959). The hydraulics of open channel flow are well known, and, as we have shown, for the purpose of understanding bulk entrainment rates, simplification of the hydraulics is relatively straightforward . Thus, going back to first principles, V(x,z,t) in equation 3.4 is relatively easy. The real challenge in being able to understand, and then to modify entrainment rates in junctions is in understanding fish distributions - C(x,z,t) in equation 3.4 is tough. Understanding and predicting fish distributions, and how to modify them, therefore is the central challenge of this research. Ultimately the aim of fish guidance technologies is to alter entrainment rates in junctions by modifying the fish spatial distributions either within or upstream of junctions with the objective of increasing total survival through the delta without significantly changing the bulk flow of water moving through the junction (e.g. change C(x,z,t) in equation 3.4 while leaving V(x,z,t) relatively unchanged).

The streakline concept and its non-dimensional counterpart the discharge ratio, R_Q, are conceptually useful because they laser-focus our attention on only those hydrodynamic/behavioral interactions that are relevant to entrainment – greatly simplifying an extremely complex problem. In the final analysis, the only behaviors that lead to a change in fate at a junction are those that lead to a crossing of the critical streakline (figure 1.1). Behaviors that result in fish remaining within each entrainment zone do not ultimately

change the fish's fate. Therefore, the farther a fish is away from the critical streakline the more it is "committed" to one channel or the other and thus the greater the effort it would take for fish to change fates – or the harder it will be for a behavioral barrier to change a fishes fate. Entrainment of individual fish near the critical streakline is likely a stochastic process because of the large eddies typical of large river systems in the near-streakline region, while at a distance from the critical streakline the process becomes more deterministic. In addition, once the streaklines begin to bend as the flows split in the junction secondary circulation creates downwelling at the horizontal location of the critical streakline (Figure 5.4) which may make it more difficult to move fish across the critical streakline using a behavioral barrier because this downwelling may create a behavioral barrier. If this is the case, moving a behavioral barrier upstream of the junction before the streaklines begin to bend into separate channels may increase the efficacy of the barrier. The greater the curvature of the streaklines the greater the secondary circulation and downwelling at the critical streakline will be.

If fish do not cross the critical streakline through changes in behavior AND fish are evenly distributed in the water column (or evenly distributed across the section within the surface) as they enter the junction (figure 1.1a) then this entrainment zone/critical streakline concept collapses to "fish go with the flow" – in this case the ratio of bulk discharge, R_Q. In other words, if both of these conditions are true, then fish will be entrained in proportion to the discharge in each channel. If either of these conditions is false, then fish will not be entrained in proportion to the flow at a junction (figure 1.1b). Thus, the only way fish "go" with the bulk discharge in each channel in a junctions is if the fish are uniformly distributed within the water column (or, at least, within the surface waters) AND fish don't behave within the junction (figure 1.1a). But, the 2011 BAFF experiment showed a decidedly non-uniform entrance spatial distribution for both barrier "on" and "off" conditions (figures 3.20, 3.21). Our scaling arguments (e.g. equation 2.1 and table 2.1) and past studies have shown that in the absence of the BAFF, behaviors that occur within the junction are relatively unimportant in creating entrainment rates that differ from the superposition of the entrainment zone and upstream fish distribution (Blake et.al., in press). Thus, in the absence of a way to induce fish to cross the critical streakline, say with a BAFF, the entrance fish distributions may have a greater influence on deviations from the "fish go with the bulk flow" model of entrainment than within junction behaviors.

In the absence of behavior within the junction, equation 3 suggests that in order to change the entrainment rate in the side channel we can either change the streakline position (X_u), the velocity distribution (V(t)) within the region 0 to X_u (these two variables are interdependent and changing them would involve significant changes in geometry) or change the entrance distribution (C(x,t)). In the context of this discussion, BAFF operation was

specifically designed to change the spatial distribution within the junction – specifically encouraging fish to move away from Georgiana Slough (figure 5.1).

Therefore, if changes in fate due to behaviors that occur within the junction are small, even in the context of the BAFF, then management actions that control *where* in the cross section fish enter the junction may be more effective in controlling entrainment rates than actions taken within junctions. Actions such as controlling secondary currents (Dinehart and Burau 2005a,b) (which is routinely done on the Mississippi to help barges negotiate channel bends), making changes to upstream channel alignment and structures, or installing upstream surface barriers, may be more effective than a behavioral barrier placed within a channel junction. For this reason, these alternatives should be considered.

5.1 Tidal average

From a management perspective, the question of whether "fish go with the flow" is most useful if answered at the tidally-averaged time scale and at the spatial scale of the junction because the things we control operate at these scales (e.g. changes in Sacramento River flow rates, gate closures, exports, etc.). Our goal in these junction experiments has always been to study the interaction between the hydrodynamics and fish behavior at the time and space scales relevant to the fundamental mechanics of entrainment, while our ultimate objective is to relate this detailed understanding back to the timescales relevant to management actions associated with improving survival through the delta. In most cases the timescale most relevant to these management actions is the tidally averaged timescale. Thus, the central aim of these studies is to collapse an understanding of the fast-time and small spatial-scale mechanics of entrainment to the tidally averaged timescale and spatial scale useful to managers.

In this section we address the correct way to compute the tidally average discharge ratio. The tidal average of this ratio is important in understanding how entrainment varies at time scales longer than the tidal day such as with changes in river flows, gate operations, etc. Indeed, much of the dispute over whether "fish go with the flow" involves the incorrect computation of the tidally averaged discharge ratio. For instance, in tidally forced systems, how one computes the tidally averaged discharge ratio can give different answers, most of them incorrect. Order of operations is important. The correct way to make these calculations is to first compute the ratio at the tidal timescale (e.g. on the 15 minute data) , then compute the tidal average, instead of computing the tidal average of each of the components in the ratio then computing the quotient. Computing the tidal average of the component discharges before performing the quotient will lead to incorrect conclusions when the flows are reversing.

In mathematical terms, $R_Q = < Q_S / Q_U > \neq < Q_S >/< Q_U >$, computing $< Q_S >/< Q_U >$ completely ignores the tidal timescale dynamics show in figures 3.31, 3.32 in the tidal average.

If we assume fish "go with the NET or tidally averaged flow" at Georgiana Slough one can straightforwardly estimate how many fish are entrained in Georgiana Slough relative to how many continue down the mainstem Sacramento River by computing the ratio of the respective flow rates, say

$$< R_{NET} > = < Q_S >/< Q_U > \qquad (5.1)$$

where R_{NET} is the ratio of the tidally averaged discharge in the side channel (Georgiana Slough in this case) divided by the tidally averaged discharge entering the junction from upstream (the Sacramento River), Q is the discharge, subscript "net" denotes a net or tidally averaged flow, subscript s denotes a side channel, subscript u denotes the upstream section in the river junction as is shown in figures 4.1 and 4.2 and < > is a tidal average operator (not a 24-hr moving average or equivalent which can give spurious results. See Walters and Heston, 1982).

But not so fast! Conceptually we know this is incorrect because actual entrainment varies significantly with the tidal conditions in the junction – most, if not all of the action with regard to entrainment occurs at the tidal timescale, especially during low flow periods.

So how do we capture the tidal timescale dynamics in the tidal average?

In tidally forced systems, where the flows can reverse in junctions, Equation 5.1 will incorrectly estimate the proportion of water entering the side-channel because it ignores all but one of the possible tidal flow conditions shown in figures 3.31 and 3.32 that can occur in a tidally forced junction - there are 6 in all! Equation 5.1 ignores all but the flow pattern shown in the top panel of figure 3.31 and equation 5.1 only applies in situations where the flows are unidirectional within the entire junction – e.g. non-reversing.

The discharge in the *main channel* of all junctions in the delta reverse during periods where the river inputs are low, some more than others depending on the strength of the local tidal signal relative to the river inputs and, in some cases, pumping. Thus, the flow patterns in junctions shown in figures 3.31 and 3.32 are ubiquitous features that occur in junctions throughout the delta and in some junctions as often as twice daily during low river inputs. During periods of flow reversal equation 5 will, in most cases, underestimate the discharge ratio, which we have defined as R_Q (equation 3.27). In addition, the *side channels* in most junctions in the delta also reverse during periods of low river inputs (conditions shown in figure 3.32). In the north delta, side channels of the Sacramento River (Sutter, Steamboat,

DCC) reverse at low Sacramento River discharges and side channels in junctions off the San Joaquin River in the South and Central almost always reverse, sometimes significantly so, because the San Joaquin River flows (minus exports) are weaker than the Sacramento River flows, relative to the tidal flows which are generally stronger in the San Joaquin River.

Georgiana Slough, however, is the exception – it has only reversed for two tidal cycles, over the 10 years (Station GSS installed 9/25/2003) we have been measuring the flow there (flows reversed out of Georgiana on 11/2/2011). Thus, the correct method for calculating the discharge ratio, R_Q (equation 3.27 and figures 3.31, 3.32), is a first step to understanding entrainment of fishes in junctions.

Therefore, instead of using equation 5.1 to compute the tidally averaged discharge ratio we merely take the tidal average of R_Q as defined in figures 3.31 and 3.32 and shown in figure 4.3B, $< R_Q >$, which we plot in figure (5.1) against $< R_{NET} > = < Q_S >/< Q_U >$for a period 1/1/2012 to 6/30/2012, which includes the GSNPB experimental period.

In figure 5.2A we plot the tidal average Sacramento River discharge at Freeport, the discharges in the Sacramento River/Georgiana Slough junction 5.2B and $< R_Q >$ and $< Q_S >/< Q_U >$ in 5.2C. Firstly, it is clear, as expected, $< R_Q >$ is significantly greater when the Freeport flows are low and the flows in the Sacramento River at Georgiana Slough junction are bi-directional. When the flows are unidirectional, as in the top panel of figure 3.31, both ratios collapse to the same value, although this only happens rarely, when the Sac River at Freeport flows exceed 12-14k cfs. Also, as expected, periods of low Freeport flows and bi-directional flow in Georgiana Slough are periods where a greater percentage of the water from the Sacramento River is entering Georgiana Slough and thus represent periods of greater potential for entrainment of fishes in Georgiana. Again, in very general terms we can think of the discharge ratio $< R_Q >$ as the percentage of the channel width that provides water to Georgiana Slough. So, on average, roughly half the width of the river (e.g. $< R_Q >$ ~ 45-50%) is providing water to Georgiana during low flow, whereas during high flow it is somewhere between 30-35%, significantly less. As a result, during drought conditions, when the Sacramento River flows are low throughout the winter salmon outmigration period, we expect greater entrainment in Georgiana Slough and thus into the Central Delta.

Throughout figure 5.2 ($< R_Q >$) > ($< Q_S >/< Q_U >$) except for the period Julian Day 145 – 155, where the relationship is significantly reversed, which corresponds precisely to when the DCC gates where open. Except for these dates the DCC gates were closed, suggesting that opening the DCC gates dramatically increases the percentage of water that enters Georgiana Slough (from 30-35% to 50-55%). Note that ($< Q_{GEO} >/< Q_U >$) increases during this period, exactly the opposite response of $< R_Q >$ and <Qgeo>, suggesting a large change in the tidal timescale dynamics relative to the change in the net flows with the change in gate position, emphasizing the importance of what you average and when; it is very easy to

"throw out the baby with the bath water", in this case the tidal timescale dynamics. It also suggests that we need to carefully consider the increase in entrainment of salmonids in Georgiana that is likely to occur when the DCC is closed. Hopefully, the increase in entrainment in Georgiana is offset by the decrease in entrainment in the DCC (e.g. zero) when the gates are closed.

To understand what is happening when the DCC gate position is changed, we switch back to the tidal timescale by plotting R_Q, the discharges in the Georgiana Junction and the discharge in the DCC. In figure 5.3A we plot the discharge in the Delta Cross Channel, 5.3B the discharges in the Georgiana Slough junction, and 5.3C we plot R_Q as defined in figures 3.31 and 3.32. Firstly, we note the peak discharges in the DCC are roughly 5.2k cfs or slightly less than twice the discharge in Georgiana Slough, 2.7k cfs. The periods of downstream flow have been shaded in blue, upstream flow yellow and converging flow is white. The DCC gates virtually eliminate periods of converging flow into Georgiana Slough in favor of increasing upstream flow past Georgiana – flow that ultimately exchanges into the DCC from the Sacramento River downstream of the DCC. By opening the gate we create increased tidal prism in the Mokelumne system, so water in the Sacramento River that flows past Georgiana is advected back into and through the DCC on flood tides. Thus, with the gate open we see a decrease in converging flow and an increase in bypass flows heading upstream at Georgiana. The downstream bypass flows remain the same, or ,when we take tidal averages of the components of R_Q, R_U remains roughly the same but R_C drops and R_D increases, the combined affect increases R_Q as is shown in figure 4.6D.

More generally, figure 4.6 gives us a sense of which of the flow patterns contributes to the total discharge ratio, $< R_Q >$ on a tidally averaged basis. Except when the DCC gates are closed or at extremely high Sacramento River net flows, roughly 30% of the discharge goes into Georgiana from upstream, the green line, $< R_U >$. During low periods, the converging flow condition, $< R_C >$ (red curve), contributes significantly, on the order of 20%. Water entering from downstream, $< R_D >$, contributes roughly 10% to the total discharge, except when the DCC gates are open. Finally, we note that gate closers under higher flow conditions can have a different effect (see day 174 forward in figure 4.6) in that R_C, R_D, and R_U respond similarly, yet the response of R_C and R_D are muted by R_U so that the net effect on R_Q isn't quite as dramatic.

SUMMMARY AND CONCLUSIONS

In this section we've provided a brief discussion of the importance of hydrodynamics in governing entrainment in junctions relying on simple scaling arguments based on the swimming performance of juvenile Chinook salmon relative to the current speed – the swim number. The swim number suggests that during flood stage on the Sacramento River and

during peaks in the tidal currents hydrodynamics is the first order driver of entrainment. During weaker current periods near slack-water behavior becomes much more important.

The critical streakline provides a simple metric for comparing the potential for entrainment under a variety of conditions within a junction and between junctions. The streakline concept and its non-dimensional counterpart the discharge ratio, R_Q, are conceptually useful because they laser-focus our attention on only those hydrodynamic/behavioral interactions that are relevant to entrainment – greatly simplifying an extremely complex problem. In the final analysis, the only behaviors that lead to a change in fate at a junction are those that lead to a crossing of the critical streakline (figure 1.1). Thus, in the context of the critical streakline, the ultimate aim of fish guidance technologies is to alter entrainment rates in junctions without significantly changing the bulk flow of water moving through the junction. Guidance structures can reduce entrainment by modifying the fish spatial distributions either within or upstream of junctions so that fish cross the critical streakline. Thus, junctions that have up-current critical streaklines that are near the bank and relatively stable are good candidates for fish guidance technologies because (1) the fish don't have to be moved very far to change their fate and (2) a structure can be reliably positioned within the range of the critical streakline. Upstream of Georgiana Slough is shown to be a good candidate for fish guidance technologies based on these criteria (Figures 4.3-4.4) whereas downstream of Georgiana is not (Figure 4.5).

The critical streakline is the dividing line between particles that enter a side channel and those that continue on in the main channel. We present two simplifications for computing the critical streakline. The first simplification, based on the velocity distribution in the up-current cross section, uses detailed bathymetry information and the SL-ADCP to estimate the streakline position. The second simplification, that assumes the up-current cross section can be approximated by a rectangular channel, allows flow station data to be used to estimate the streakline position. Finally, we note that the flow station formulation contracts to the up-current discharge ratio scaled by the channel width which leads to a detailed discussion of how to calculate the discharge ratio to fully capture the tidal timescale dynamics. Three component discharge ratios are developed that describe (1) downstream flow in the main channel past the side channel (R_U), (2) upstream flow in the main channel past the side channel (R_D), and (3) converging flow (R_C). These are summed into a total discharge ratio, $R_Q = R_U + R_C + R_D$, which we use to explore the tidal and tidally averaged dynamics of entrainment. Since the R's are non-dimensional, they are the metric of choice for understanding the influence of tidal dynamics in a junction on tidally averaged entrainment, and for use in comparing tidal dynamics between junctions. Finally, the relative importance of the various flow patterns shown in figure 3.31-3.32 on entrainment in Georgiana Slough is explored, and the effects of DCC gate operations on Georgiana Slough are discussed. This analysis revealed that closing the DCC gate causes a large change in the

tidal timescale dynamics at Georgiana Slough, despite the fact that these closures only cuase a small change in the net flows at Georgiana Slough. This finding highlights the importance of calculating the individual discharge ratios for tidally forced junctions.

REFERENCES

Blake, A. and M.J. Horn. In Press(a), "Acoustic Tracking of Juvenile Chinook Salmon Movement in the Vicinity of the Delta Cross Channel, Sacramento River, California - 2001 Study Results". USGS SIR -XXXX

Blake, A, and M.J. Horn. In Press (b), "Acoustic Tracking of Juvenile Chinook Salmon Movement in the Vicinity of Georgiana Slough, Sacramento River, California - 2003 Study Results". USGS SIR-XXXX

Chow, V.T., 1959, Open-channel hydraulics, McGraw-Hill, New York, pg. 680.

David, L., A. Esnault, et al. (2002). Comparison of interpolation techniques for 2D and 3D velocimetry. Eleventh International Symposium on Application of Laser Techniques to Fluid Mechanics, Lisbon.

Dinehart R.L. and J.R. Burau. 2005a Repeated surveys by acoustic Doppler current profiler for flow and sediment dynamics in a tidal river, Journal of Hydrology 314 (2005) 1–21

Dinehart R.L. and J.R. Burau. 2005b. Averaged indicators of secondary flow in repeated acoustic Doppler current profiler crossing of bends. Water Resources Research, VOL. 41, W09405, doi:10.1029/2005WR004050

Goodwin, R. A., Nestler, J. M., Anderson, J. J., Weber, L. J., and Loucks, D. P. (2006). "Forecasting 3–D fish movement behavior using a Eulerian–Lagrangian–agent method (ELAM)." *Ecological Modelling*, **192**, 197–223.

Kundu, P. and I. Cohen (1990). Fluid Mechanics. 2004, Elsevier Academic Press.

Nelson, W.R., L.K. Freidenburg, and D.W. Rondorf. 1994. Swimming performance of subyearling chinook salmon. Pages 39-62 in D.W. Rondorf and W.H. Miller, (eds.).

Identification of the spawning, rearing, and migratory requirements of fall chinook salmon in the Columbia River basin. Bonneville Power Administration, Annual Report 1992, Portland, Oregon.

Tsubaki, R., Y. Kawahara, et al. (2012). "New 3-D flow interpolation method on moving ADCP data." Water Resources Research 48(5): W05539.

Walters R.A., and C. Heston (1982) Removing tidal-period variations from time-series data using low-pass digital filters. J. Phys. Oceanogr., 12, 112-115.

FIGURES

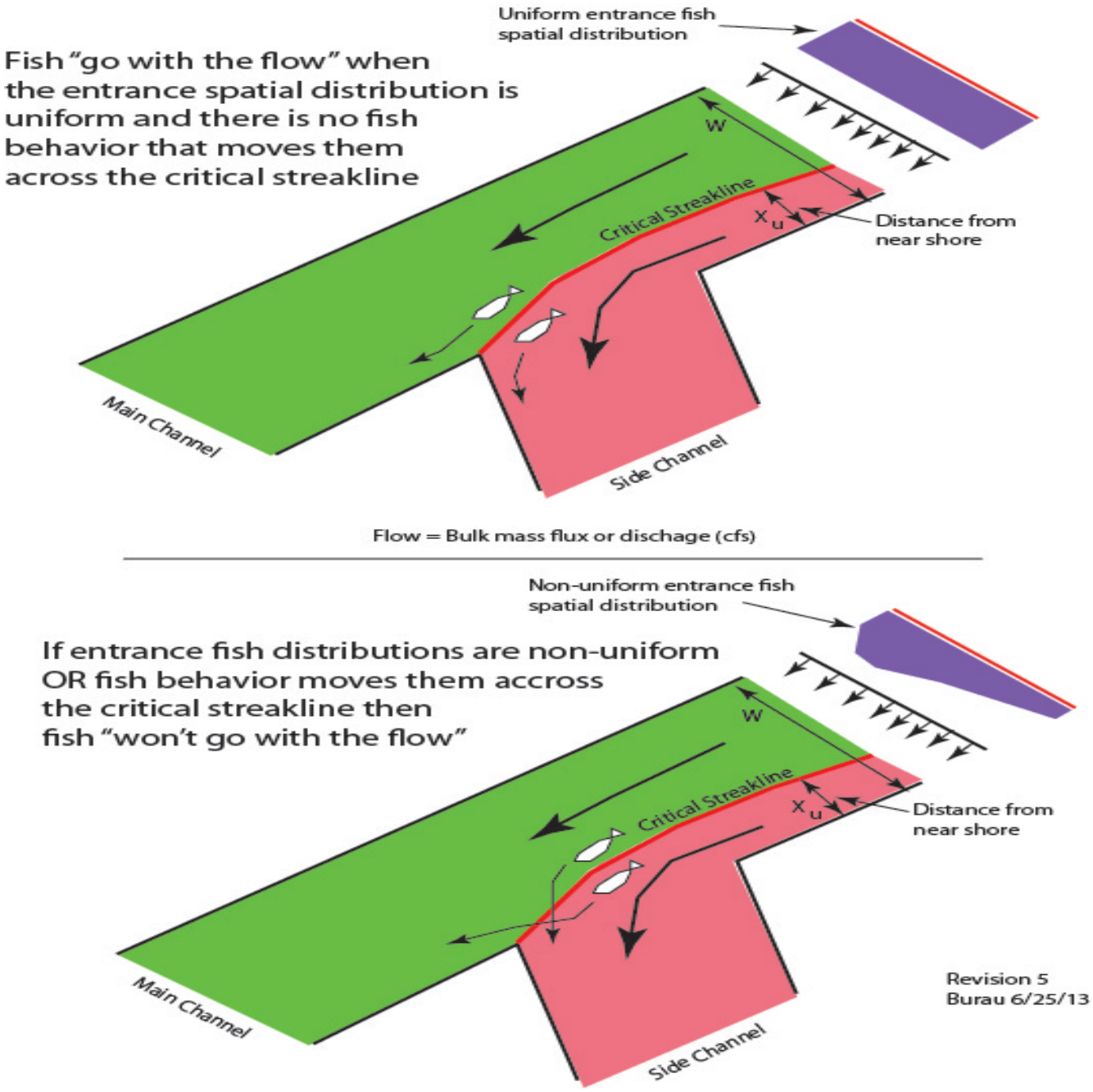

Figure 1.1 – Conceptual diagram of entrainment in a junction. Red regions denote the entrainment zone for the side channel whereas the green regions show the region where fish continue along the main channel. The red line between these regions is the critical streakline. Top panel shows the required conditions for fish to "go with the flow" – in this case the bulk discharge in each channel. These conditions include a uniform entrance fish spatial distribution AND behaviors that don't result in fish crossing the critical streakline. In

the bottom panel are indicated those conditions that create conditions where fish aren't distributed in proportion to the flows in each channel. These conditions include a non-uniform entrance fish distribution as is shown and behaviors that cause fish to transit the critical streakline.

Figure 3.1 – Photograph of Side-ward Looking Acoustic Doppler Current Profiler (SL-ADCP – it is the blue device with orange dot) attached to a buoy (black cylinder in this picture with vertical hinge) jointly developed by DWR and the USGS. Acoustic telemetry hydrophones, shown protruding from buoy toward the left of the picture, were also mounted on these buoys. By mounting these devices on buoys both the SL-ADCP and telemetry hydrophones remained on the surface, where salmon are typically located. The buoy allowed these instruments to follow the tidal fluctuations that occur at low Sacramento River discharges and to accommodate the large increase in stage that can occur during high Sacramento River discharge.

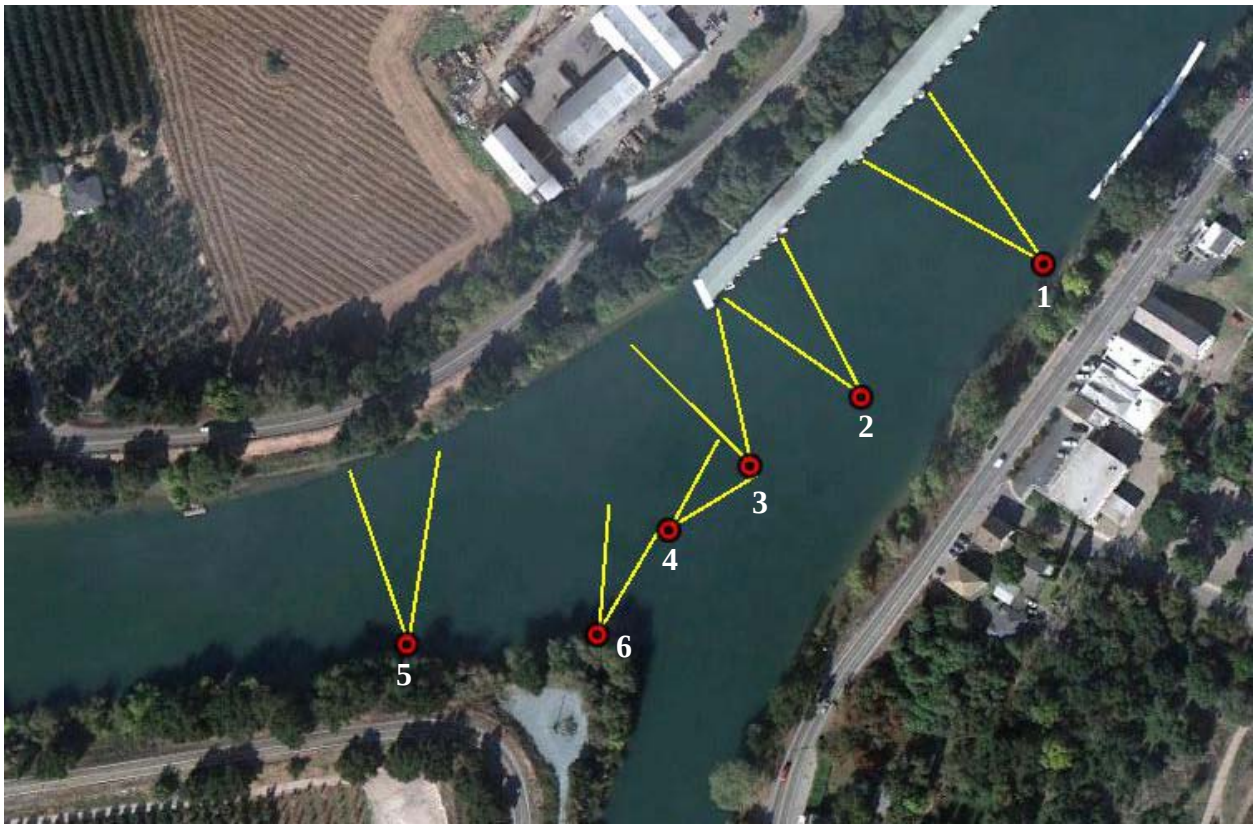

Figure 3.2 Location of six SL-ADCP's and approximate acoustic beam orientations (yellow lines); referred to in the text as Sites 1-6.

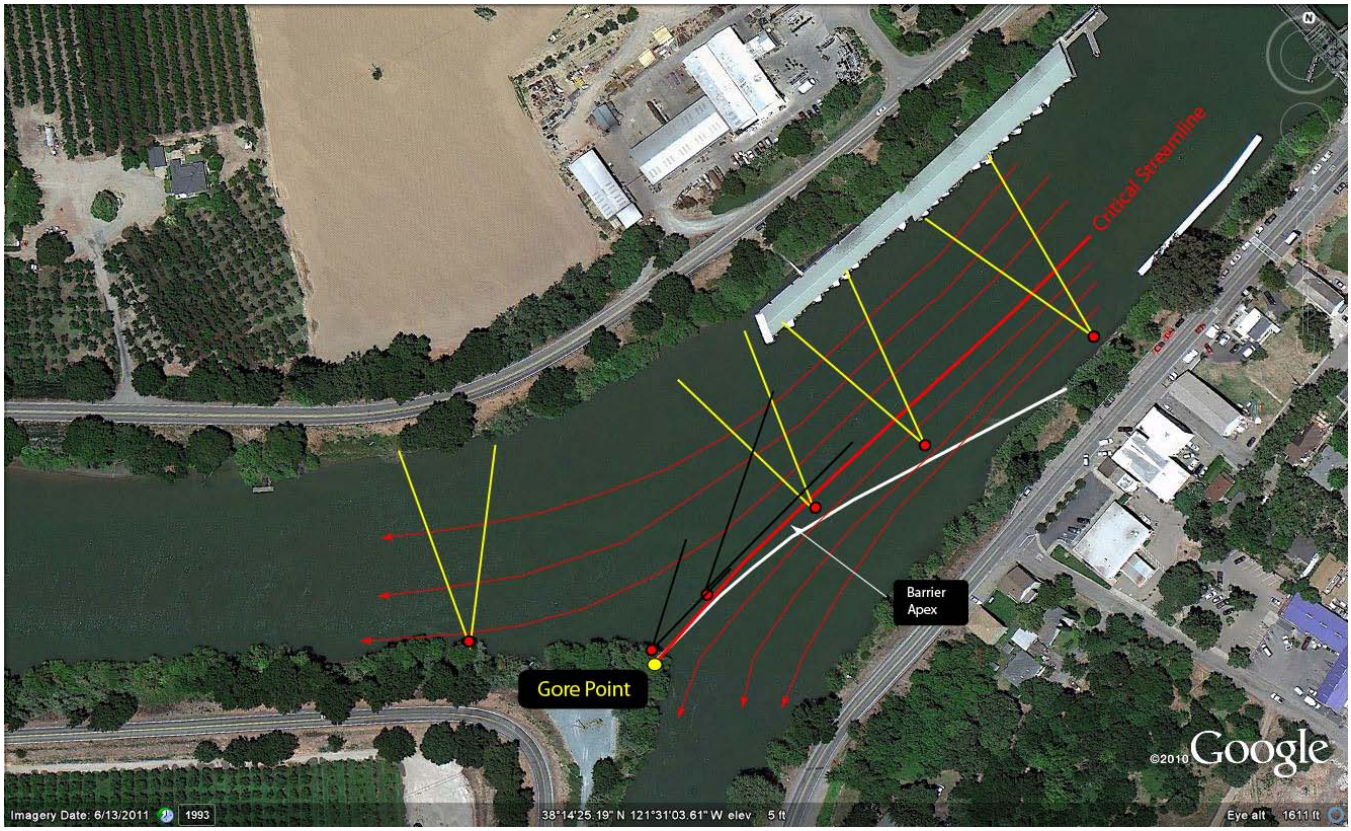

Figure 3.3 – Schematic of BAFF location (white line), SL-ADCP positions (red circles), SL-ADCP orientation (yellow cones if ADCP is "on" and back cones if ADCP is "off"). The location of the furthest point the BAFF projects into the Sacramento River is the barrier apex and the "gore point" is the location where all downstream critical streaklines converge. Streaklines indicate an ebb-tide (outgoing) tidal condition.

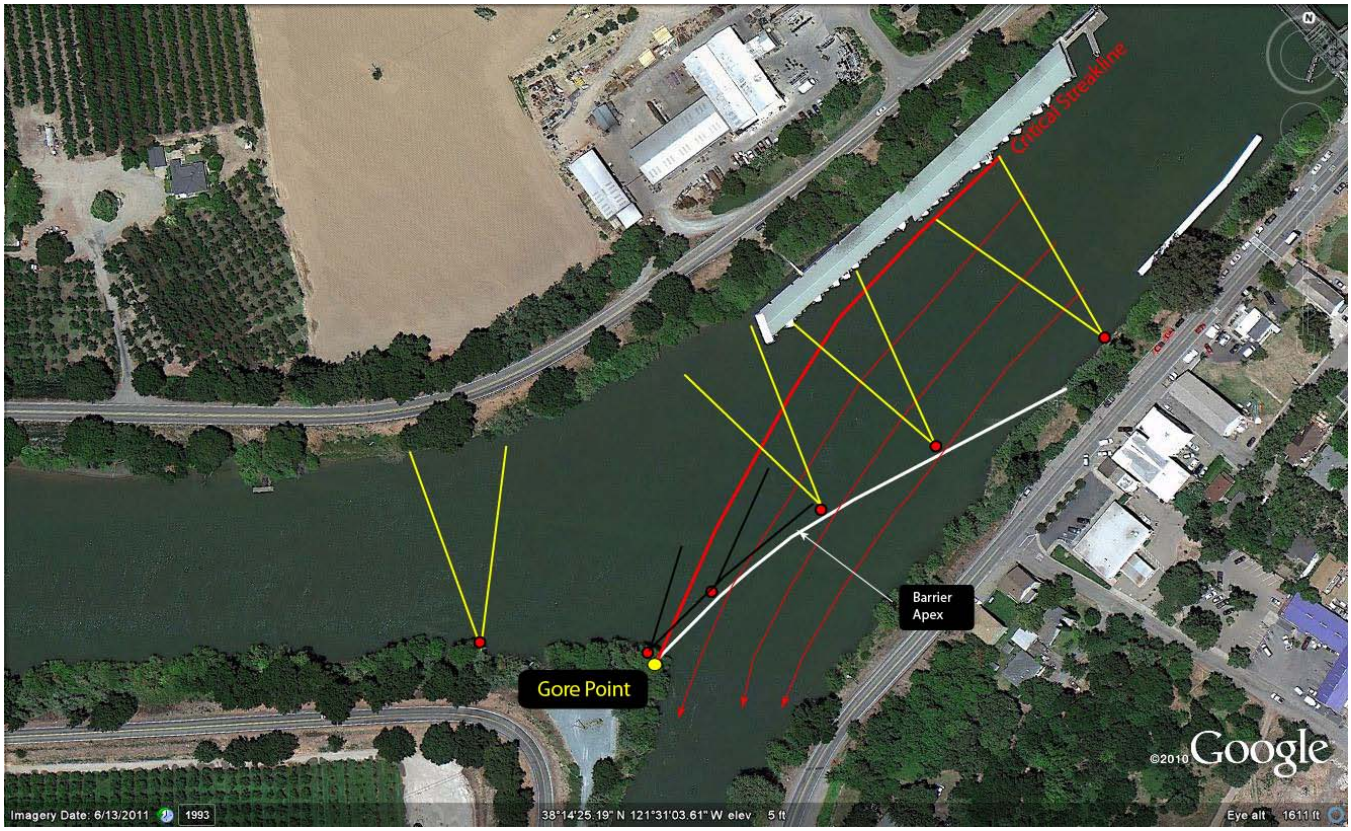

Figure 3.4 – Schematic of complete Sacramento River flow entering Georgiana Slough from upstream of the junction. Yellow triangles represent the measurement volume of SL-ADCP used to deduce the velocity distribution in the junction. Black triangles indicate SL-ADCP's that aren't used during this flow state.

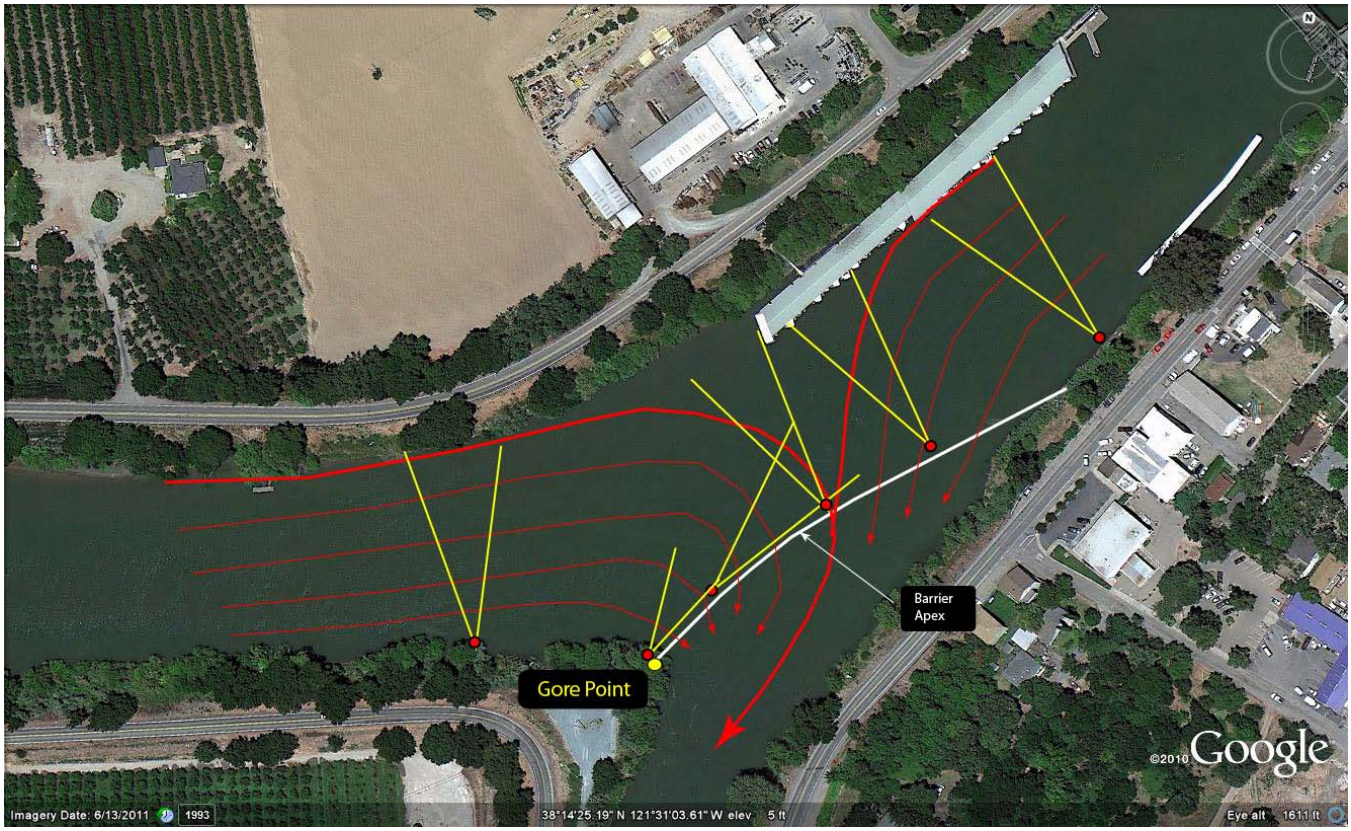

Figure 3.5 - Schematic of converging flow entering Georgiana Slough from both upstream and downstream of the junction. Yellow triangles represent the measurement volume of SL-ADCP used to deduce the velocity distribution in the junction. Black triangles indicate SL-ADCP's that aren't used during this flow state.

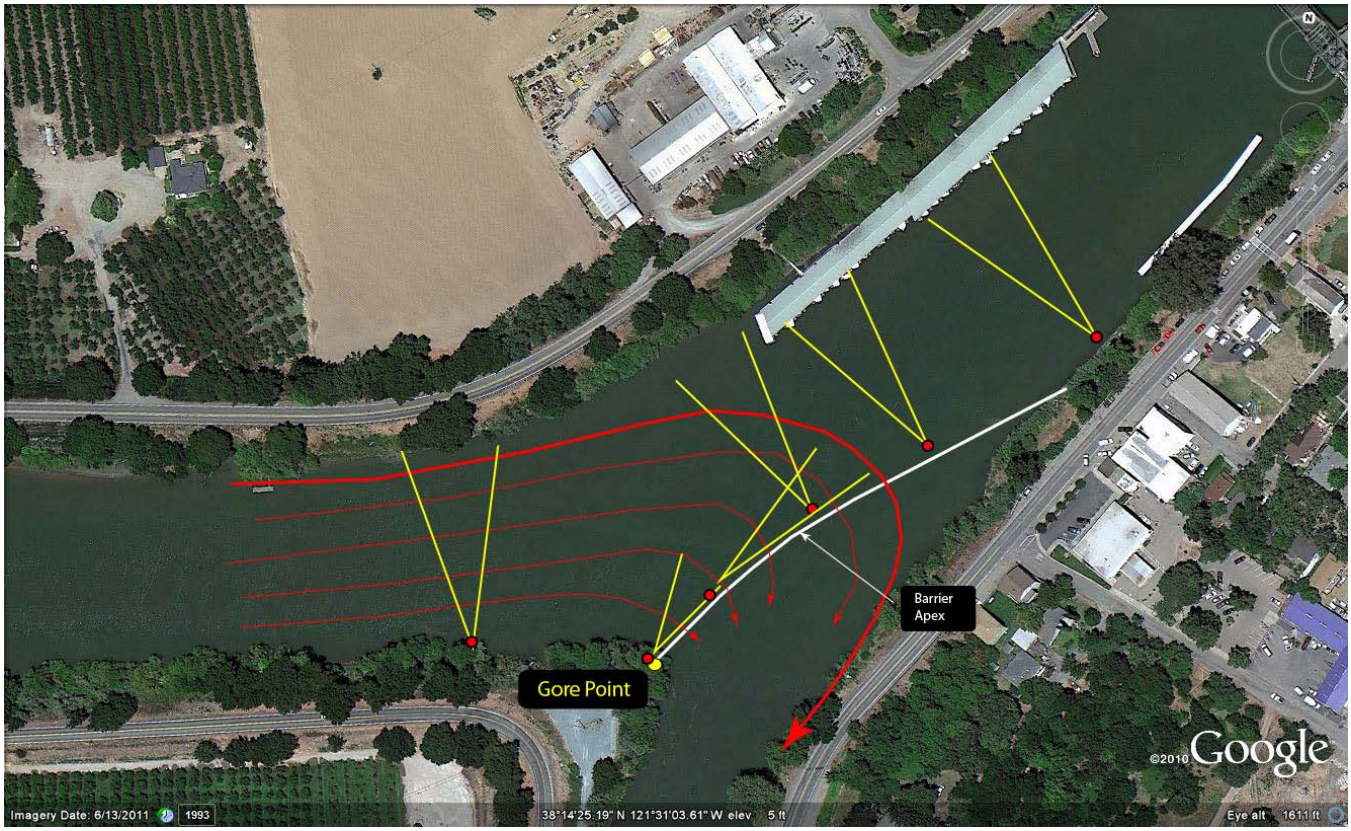

Figure 3.6 – Schematic of complete Sacramento River flow entering Georgiana Slough from below of the junction. Yellow triangles represent the measurement volume of SL-ADCP used to deduce the velocity distribution in the junction. Black triangles indicate SL-ADCP's that aren't used during this flow state.

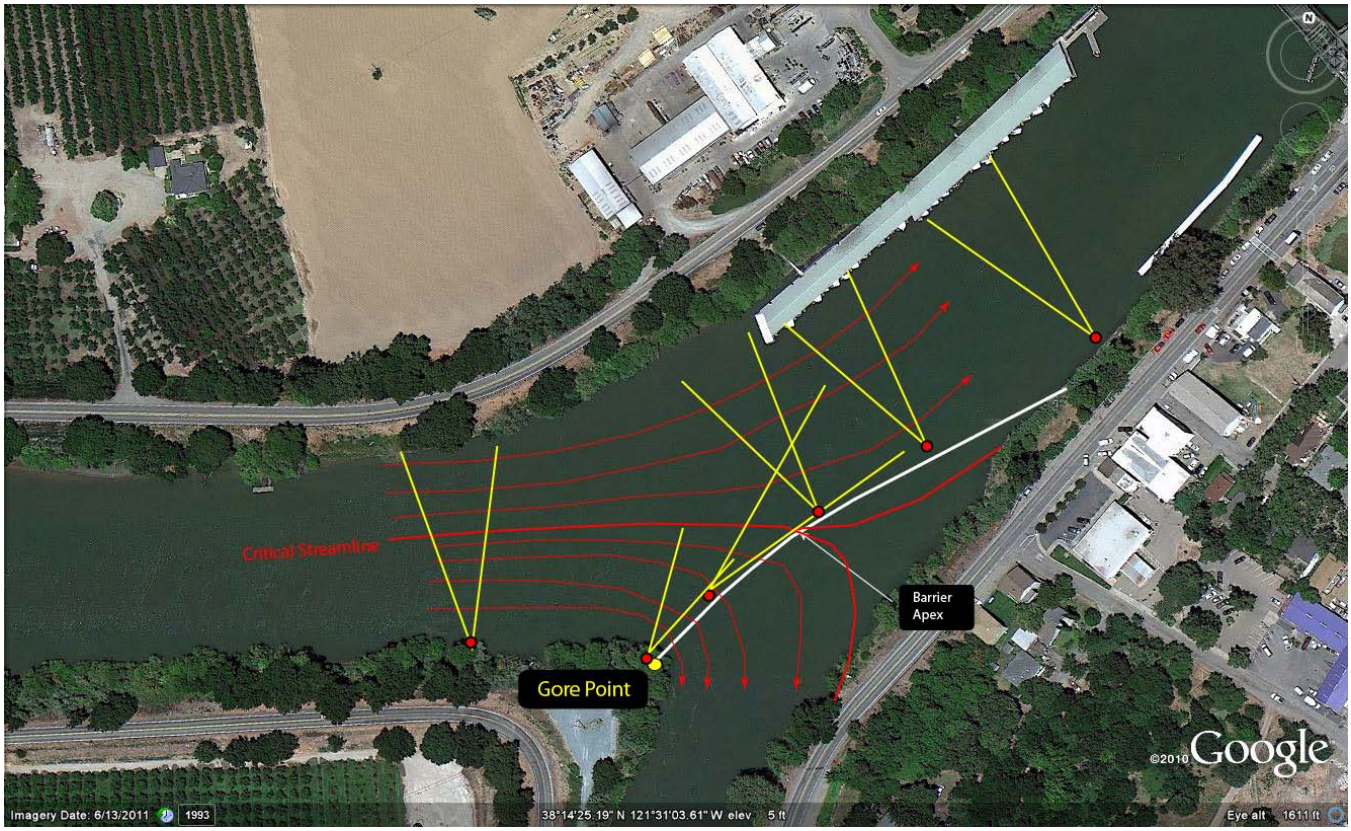

Figure 3.7 - Schematic of flow entering Georgiana Slough from downstream of the junction with a portion of the Sacramento River bypassing Georgiana Slough. Yellow triangles represent the measurement volume of SL-ADCP used to deduce the velocity distribution in the junction. Black triangles indicate SL-ADCP's that aren't used during this flow state.

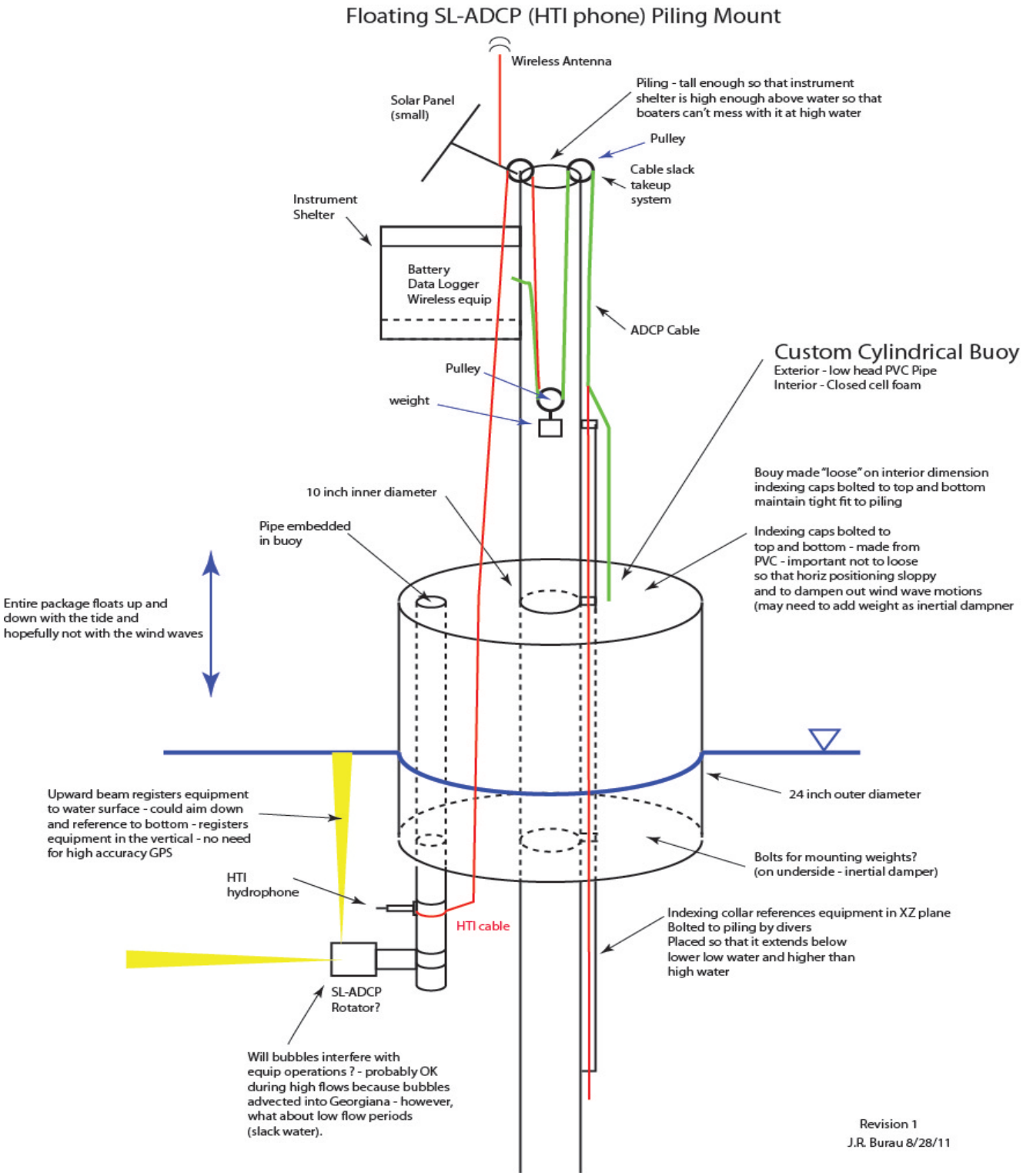

Figure 3.8 – Schematic of "piling-riding" buoy on which will be mounted SL-ADCP's and HTI hydrophones. The advantage of having these instruments attached to a piling is we will know there exact x-y (horizontal) position in space. Water level measurements will give us the z (or vertical) dimension through time. An indexing collar will be used to maintain SL-ADCP and hydrophone orientation.

Figure 3.9 – Instrument shelter, solar panel and take up wheel for SL-ADCP's deployed on pilings in the GSNPB study.

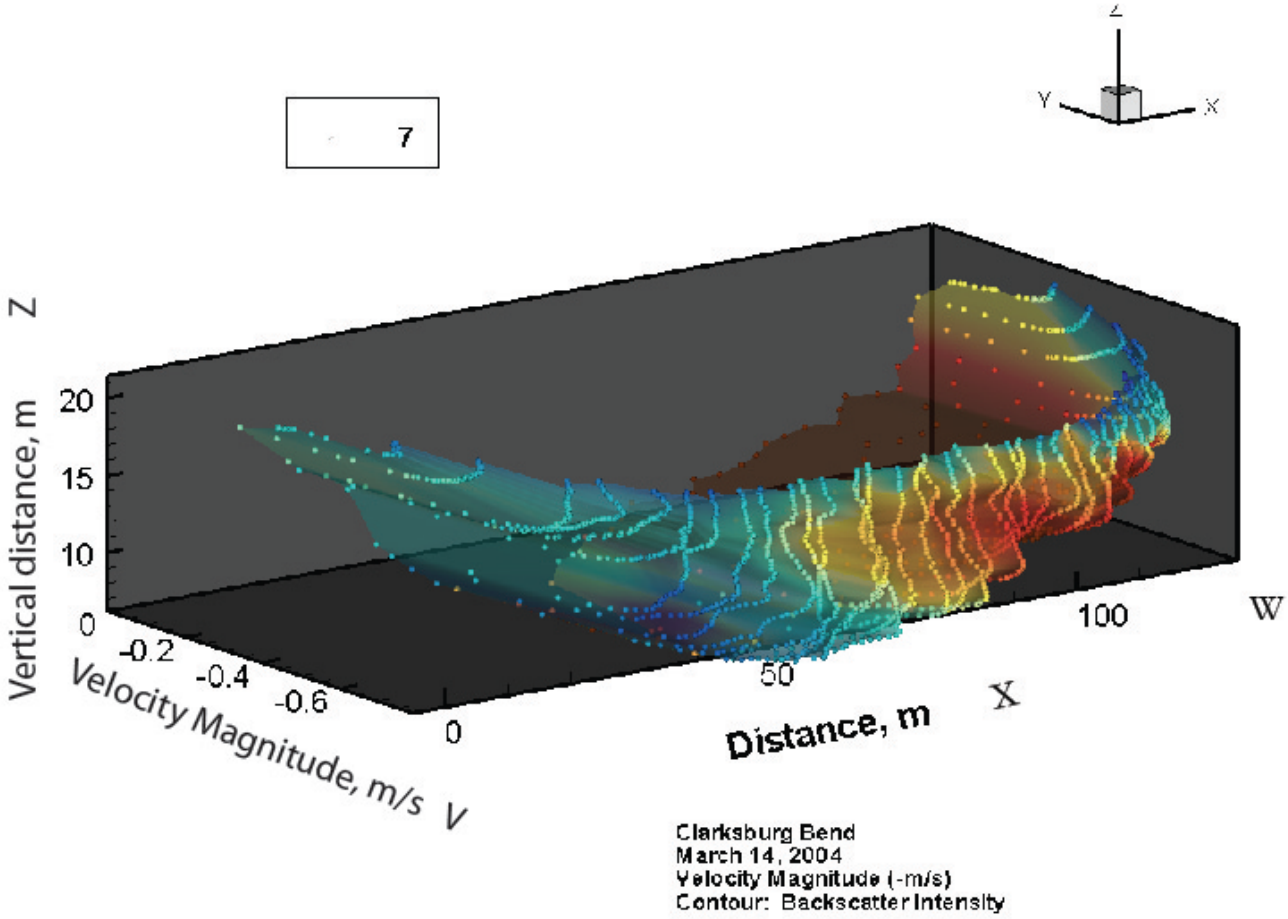

Figure 3.10 – Surface representing the horizontal velocity distribution in cross section of a typical open channel flow, in this case measured downstream of Clarkburg Bend (Courtesy of Randal Dinehart). As is typically the case, the velocity distribution across the section is relatively uniform in the center of the channel with strong shear near the bed and at the side of the channel. The color contour in this case represents the backscattered amplitude, a surrogate for sediment in the water. To determine the flux of anything, in this case suspended sediment in the water or, say fish, one integrates the product of the velocity distribution and the concentration of interest, say fish in numbers per square meter as is shown in equation 2 for fish.

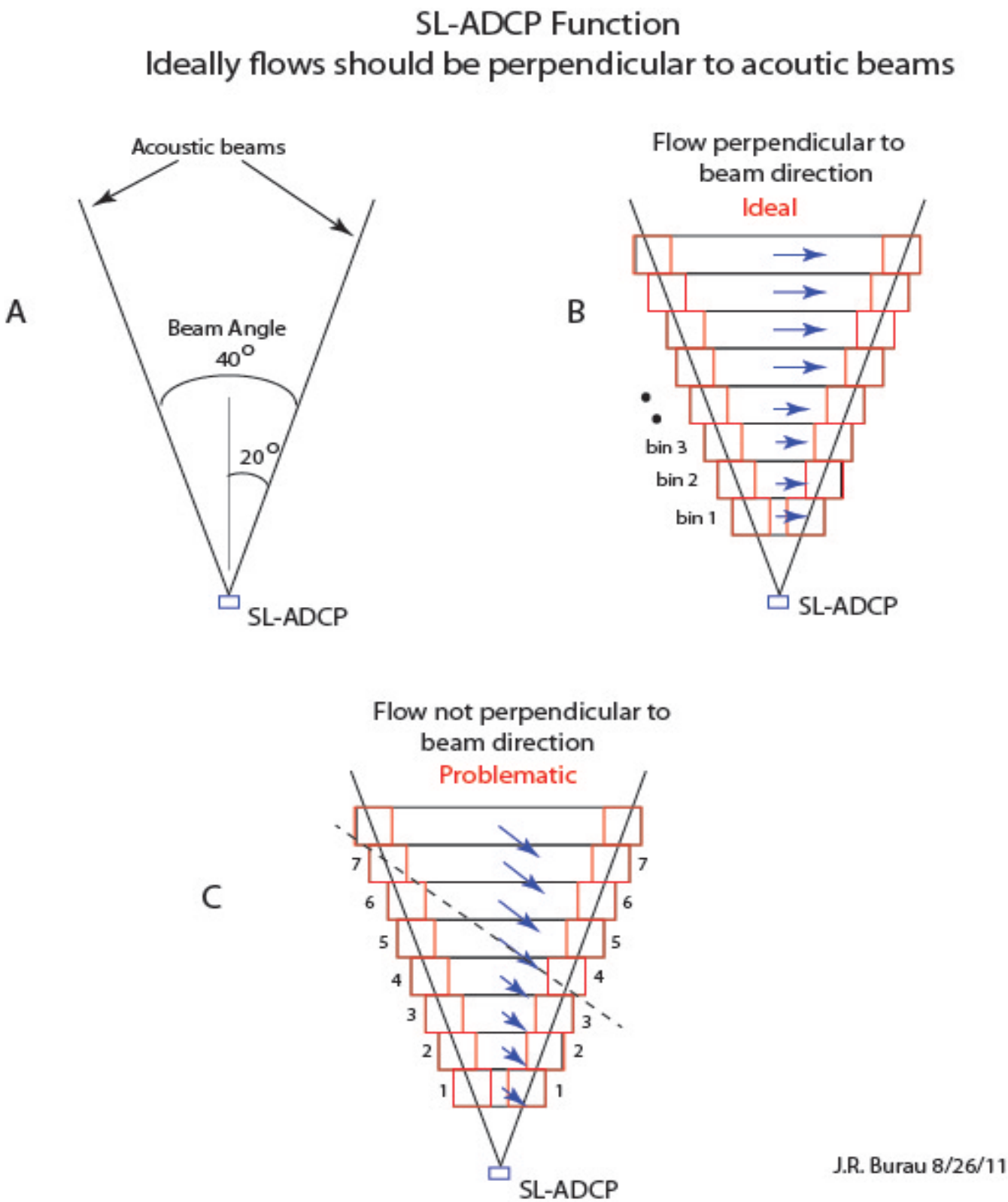

Figure 3.11 – Schematic of (A) SL-ADCP beam angles, (B) velocity discretization into user selectable bins (usually 0.5 m), (C) the problem of measuring the non-perpendicular velocity distribution using SL-ADCP's.

Figure 3.12 – Picture of small drifter designed to be used in tight spaces such as the Georgiana Slough junction where multiple drifters must be deployed quickly from a small boat. The drifter sail is collapsible and data are collected in a GPS in a watertight container at the surface. Typically drifter sails are much larger to avoid wind effects on drifter paths, however, wind drift is not so much an issue in the Walnut Grove area: (1) given the levee height in this region and (2) the current speed in the junction. The ability to quickly release and easily recover drifters for this experiment is the primary design consideration.

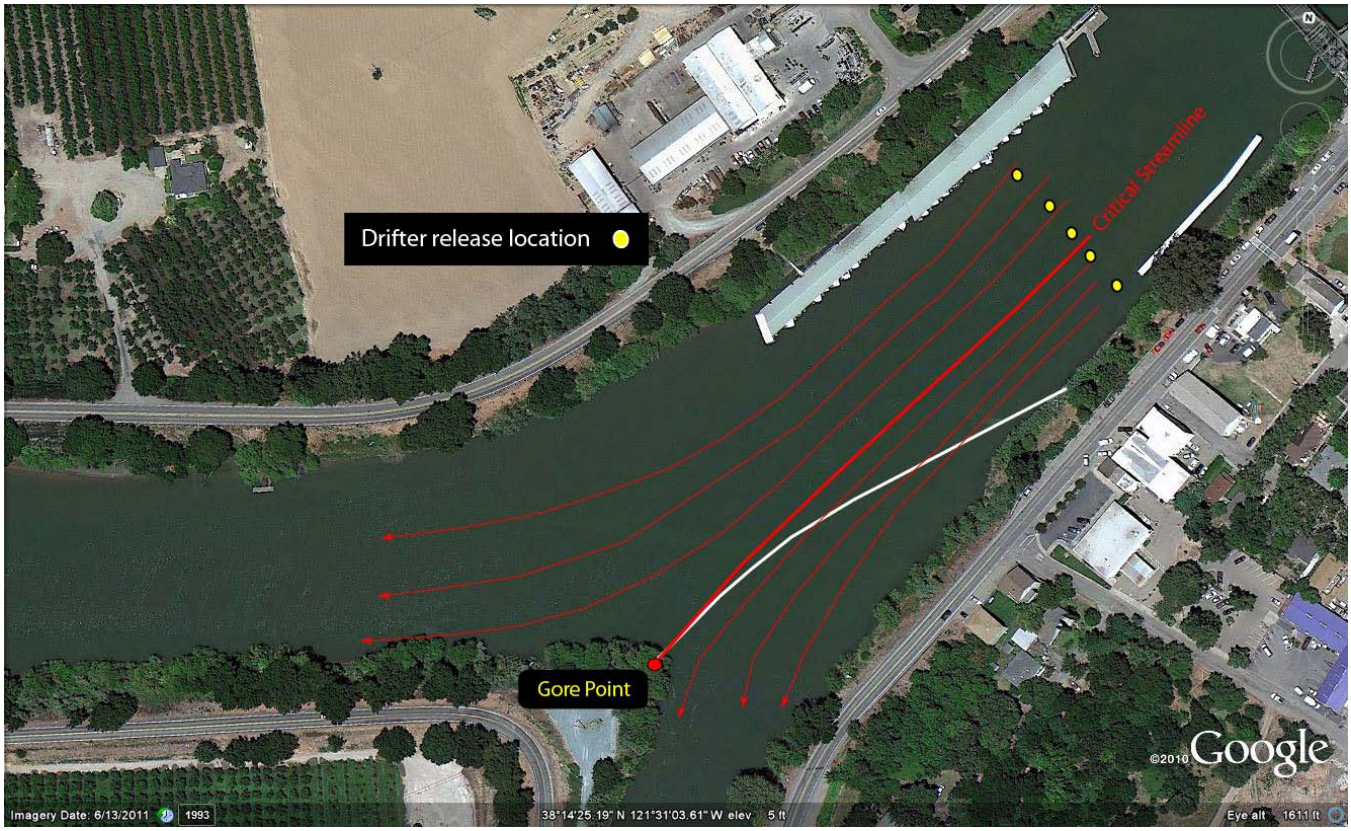

Figure 3.13 – Drifter release locations (yellow dots) during ebb tides. Drifters may be placed in greater densities near the critical streakline to increase the resolution of the location of the critical streakline.

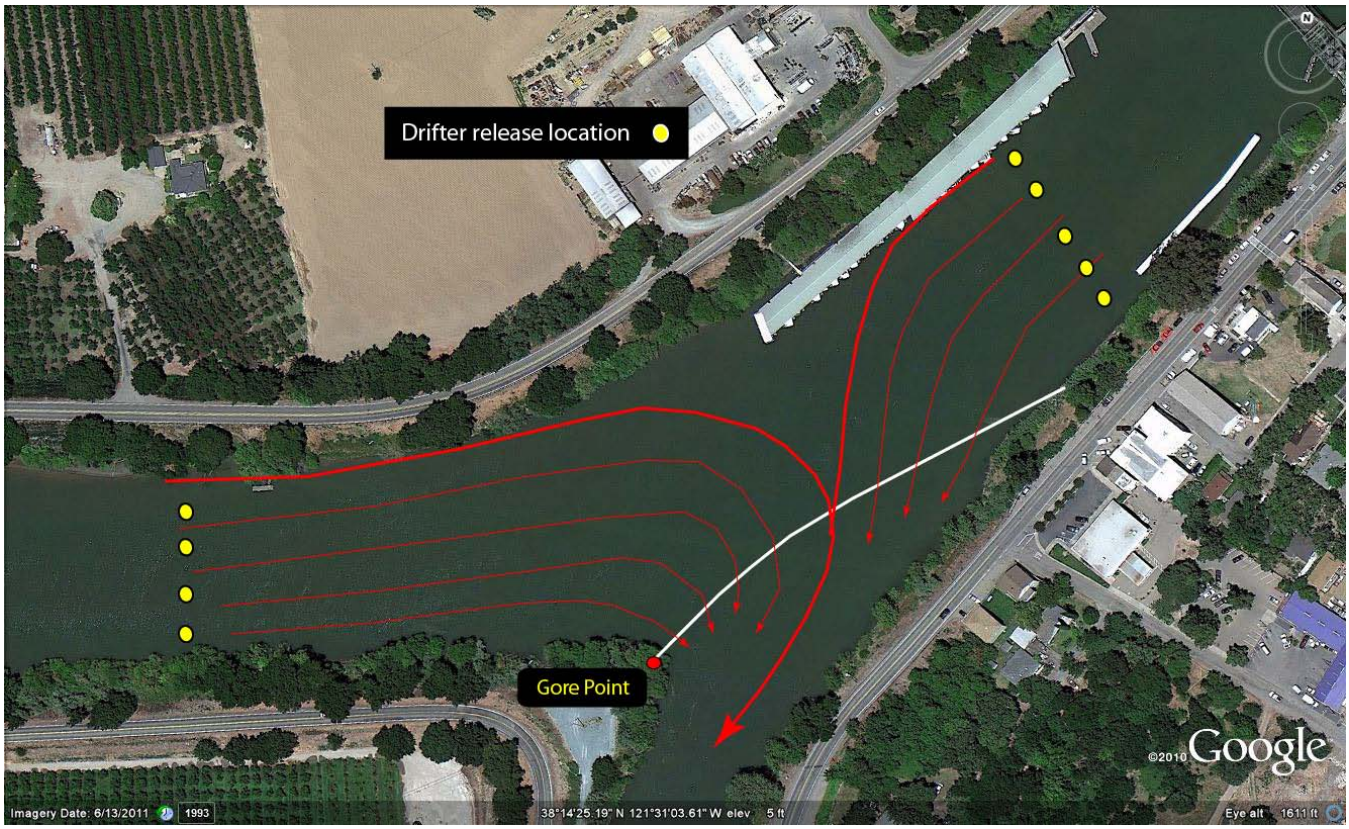

Figure 3.14 - Drifter release locations (yellow dots) during converging tides (two boats will be necessary. Drifters may be placed in greater densities near the critical streakline to increase the resolution of the location of the critical streakline.

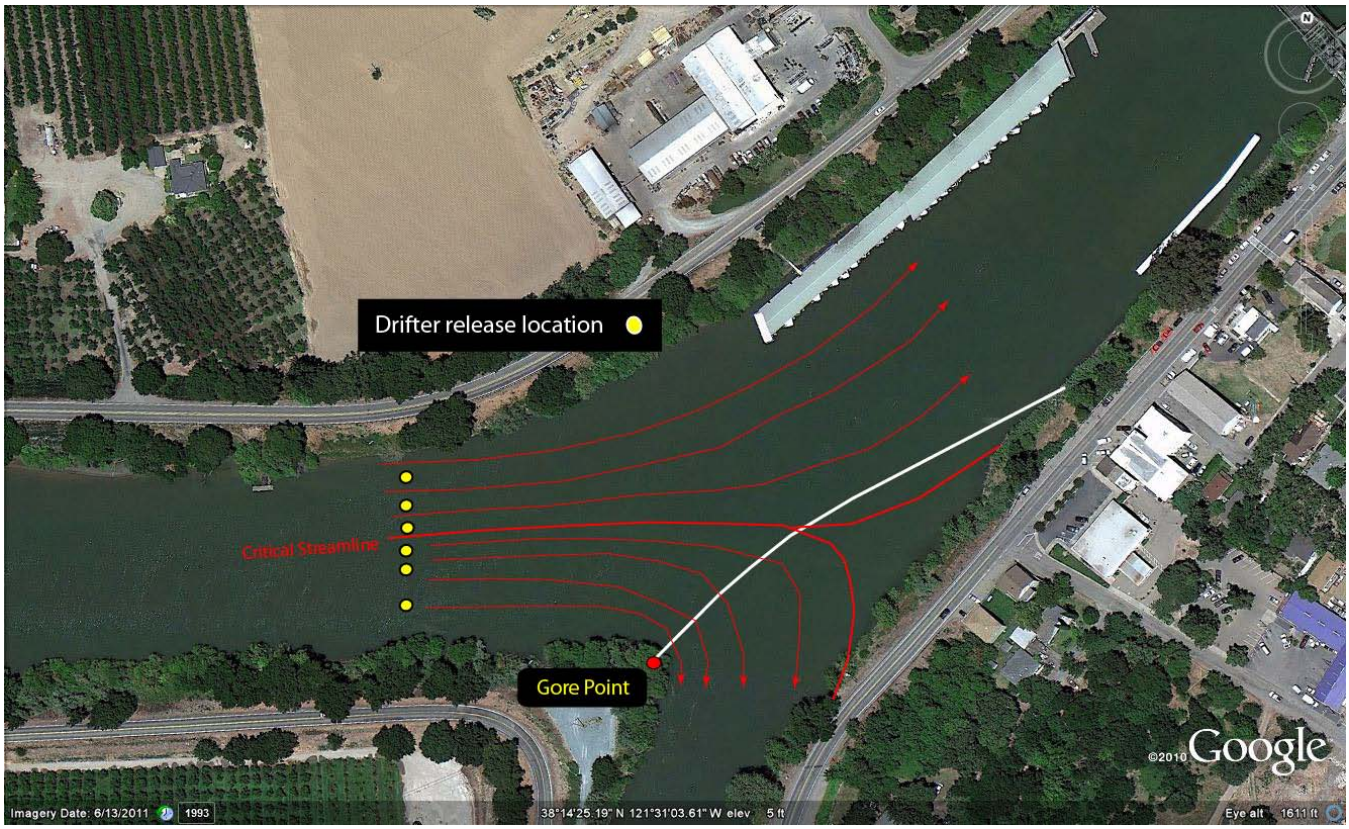

Figure 3.15 - Drifter release locations (yellow dots) during flood tides. Drifters may be placed in greater densities near the critical streakline to increase the resolution of the location of the critical streakline.

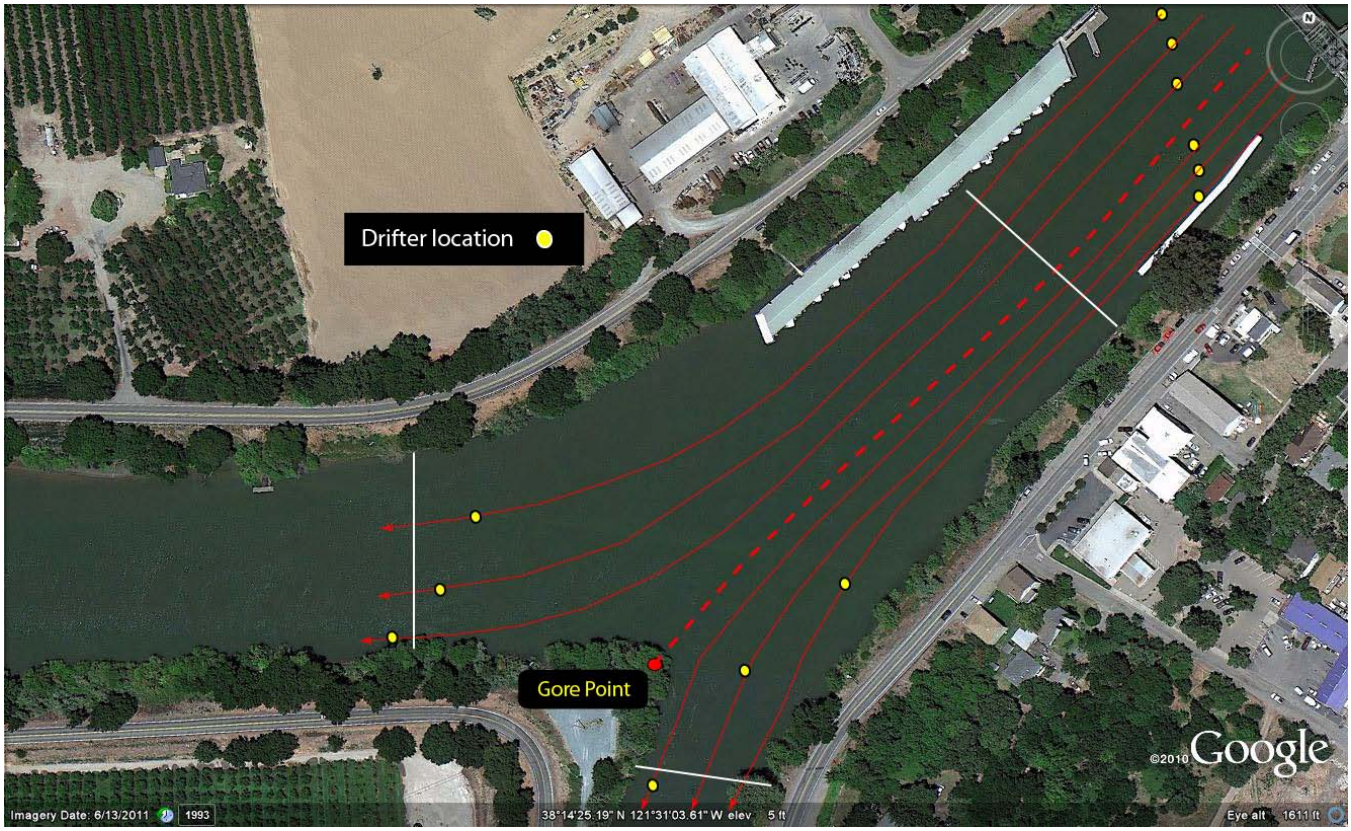

Figure 3.16 – Schematic of drifter positions (just after and near the end of release) and deduced streaklines (red lines). White lines show entrance and exit locations for drifter study.

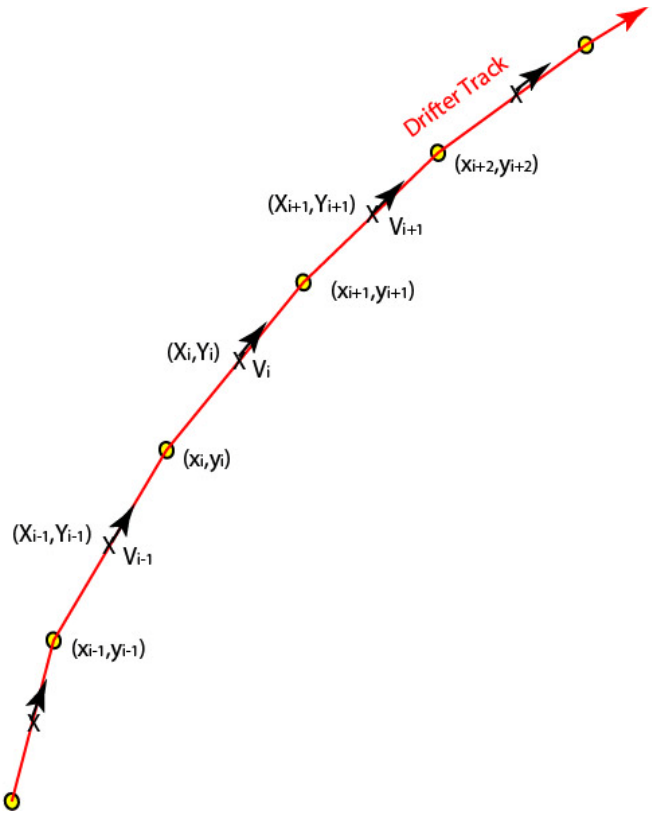

Figure 3.17 – Schematic of drifter track showing GPS positions (yellow dots) and inferred velocities at positions between GPS positions, at the X's. Some filtering of the velocities may be needed to reduce the standard deviation of velocity estimates; however, the same basic concepts will be applied.

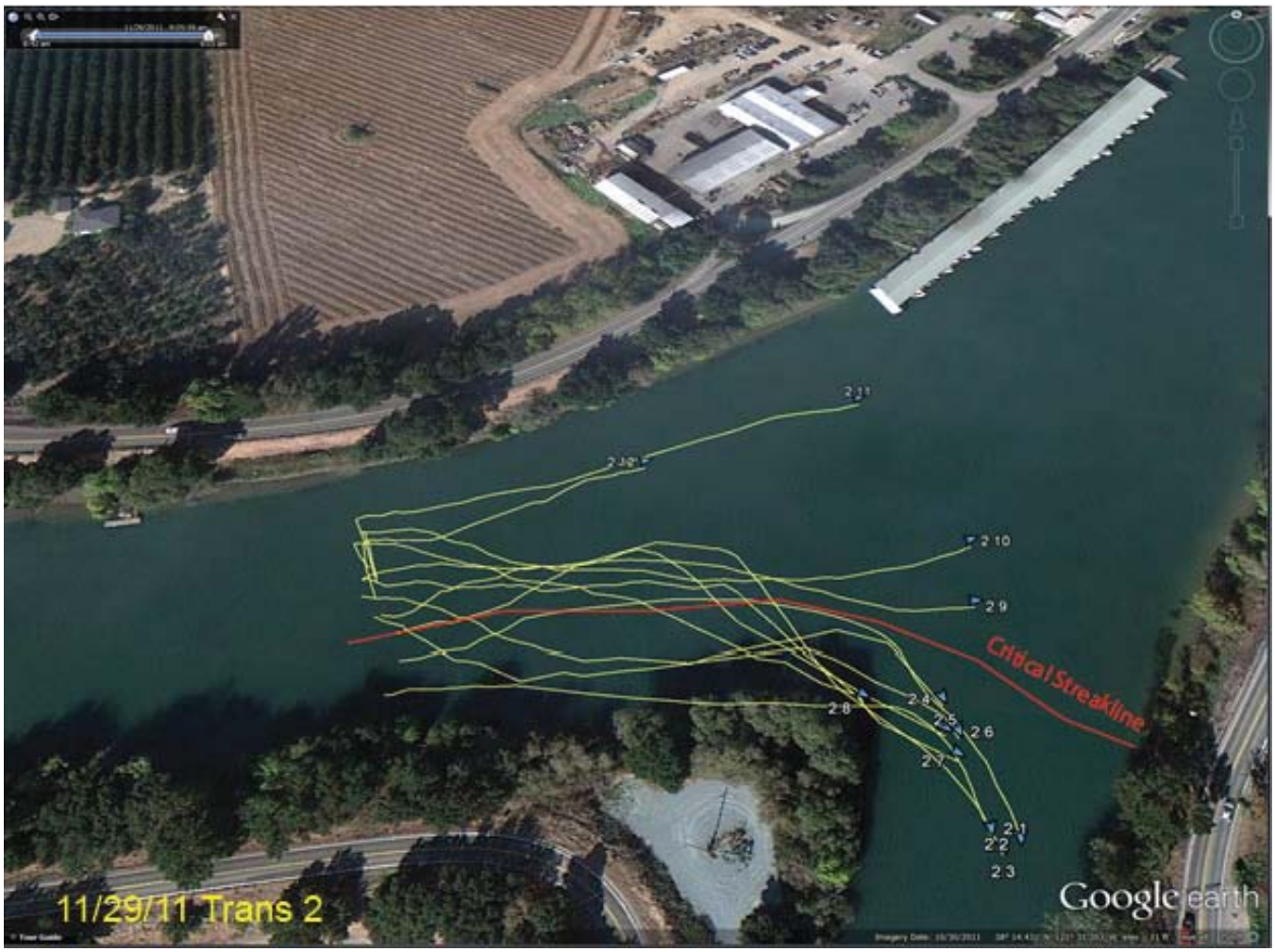

Figure 3.18 – The paths of taken by drifters (yellow lines) deployed during the 2011 BAFF experiment by the Department of Water Resources during converging flow conditions (Data courtesy of Dave Huston, DWR). The critical streakline is shown as a red line.

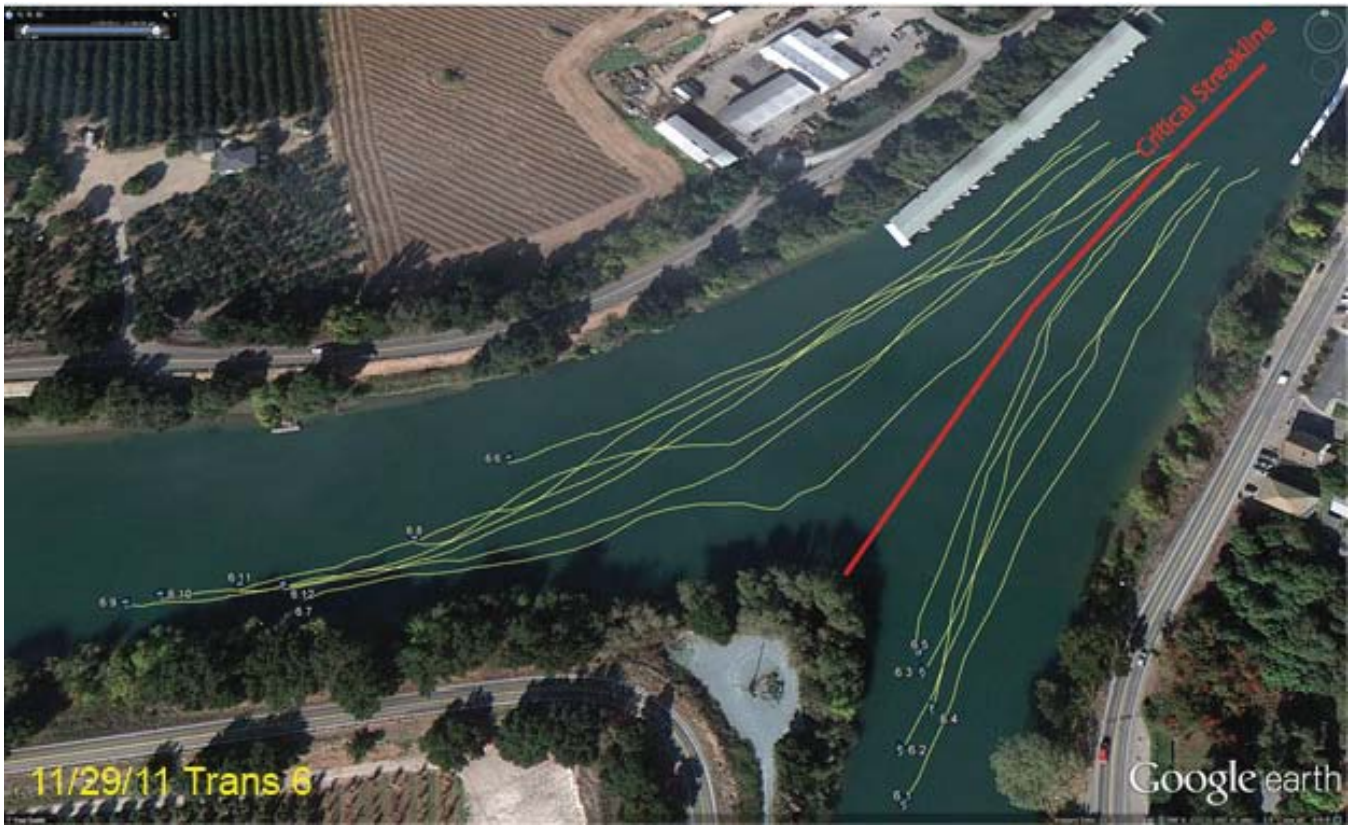

Figure 3.19 – The paths of taken by drifters (yellow lines) deployed during the 2011 BAFF experiment by the Department of Water Resources during downstream flow conditions (Data courtesy of Dave Huston, DWR). The critical streakline is shown as a red line.

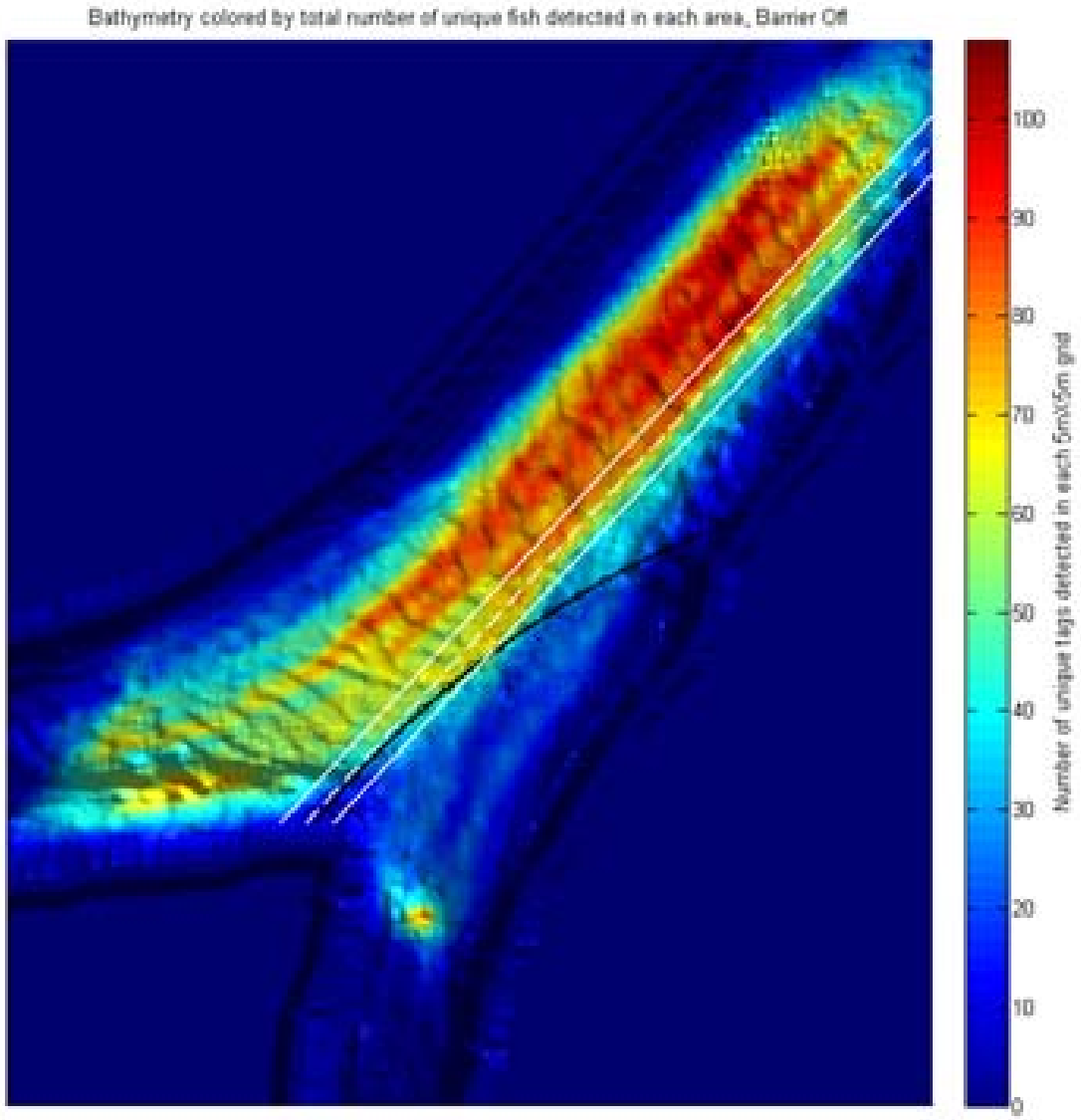

Figure 3.20 – Horizontal spatial distribution of tagged juvenile salmon from 2011 BAFF experiment – barrier OFF conditions. Warmer colors represent regions of greater fish concentrations.

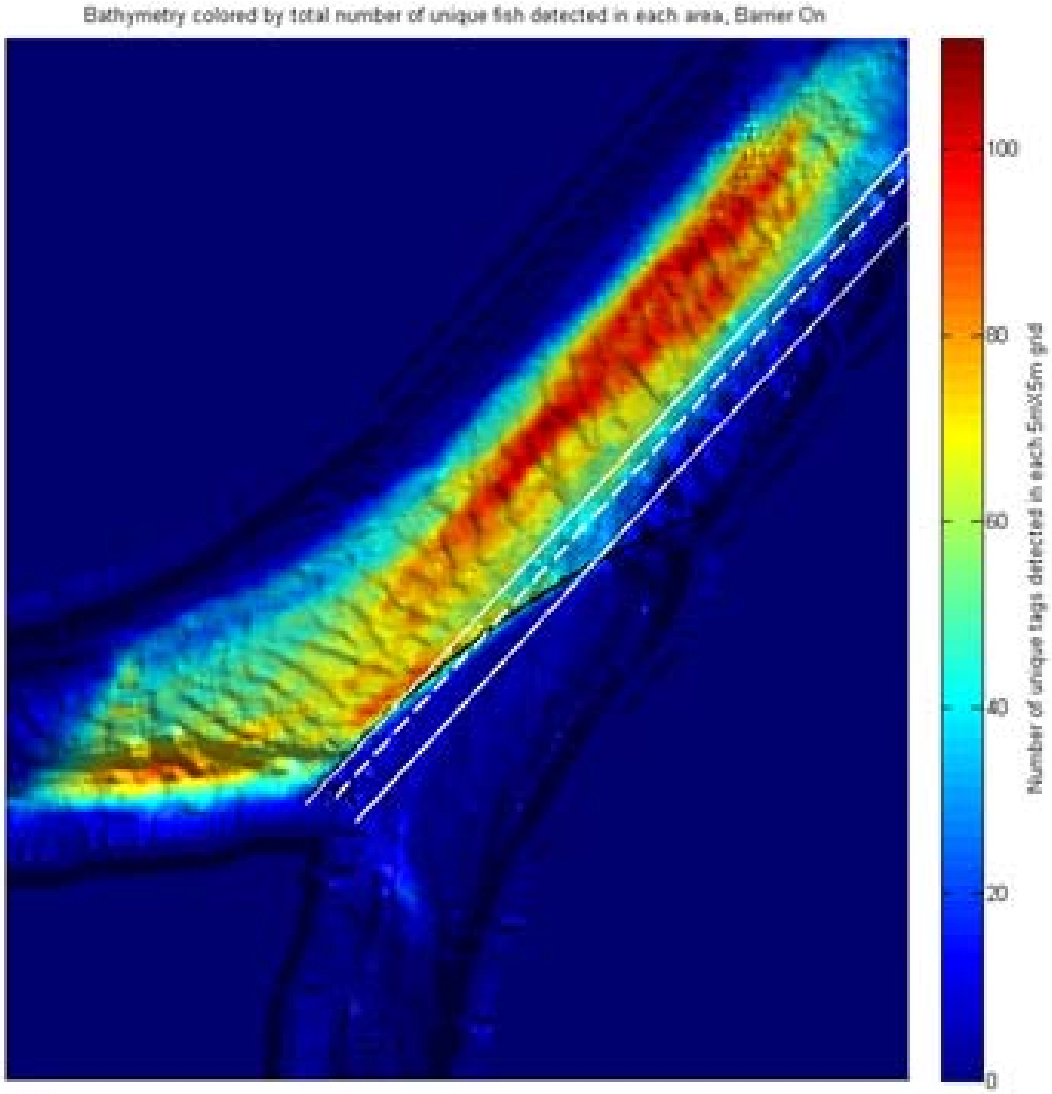

Figure 3.21 – Spatial distribution of tagged juvenile salmon from 2011 BAFF experiment – barrier ON conditions. Warmer colors represent regions of greater fish concentrations.

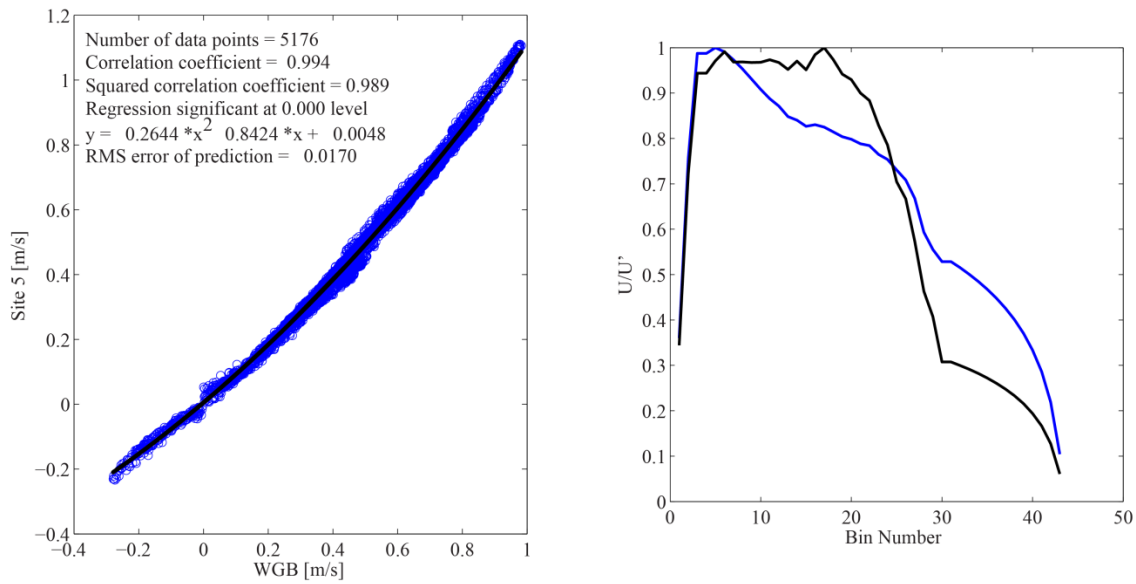

Figure 3.22 (a) 2nd-order polynomial regression of mean cross-sectional velocities and (b) estimated velocity distribution across river (Bin 1 is close to left bank) at Site 5 for downstream conditions (blue line) and upstream conditions (black line). The velocity (U) is normalized by dividing by the cross-section maximum velocity (U').

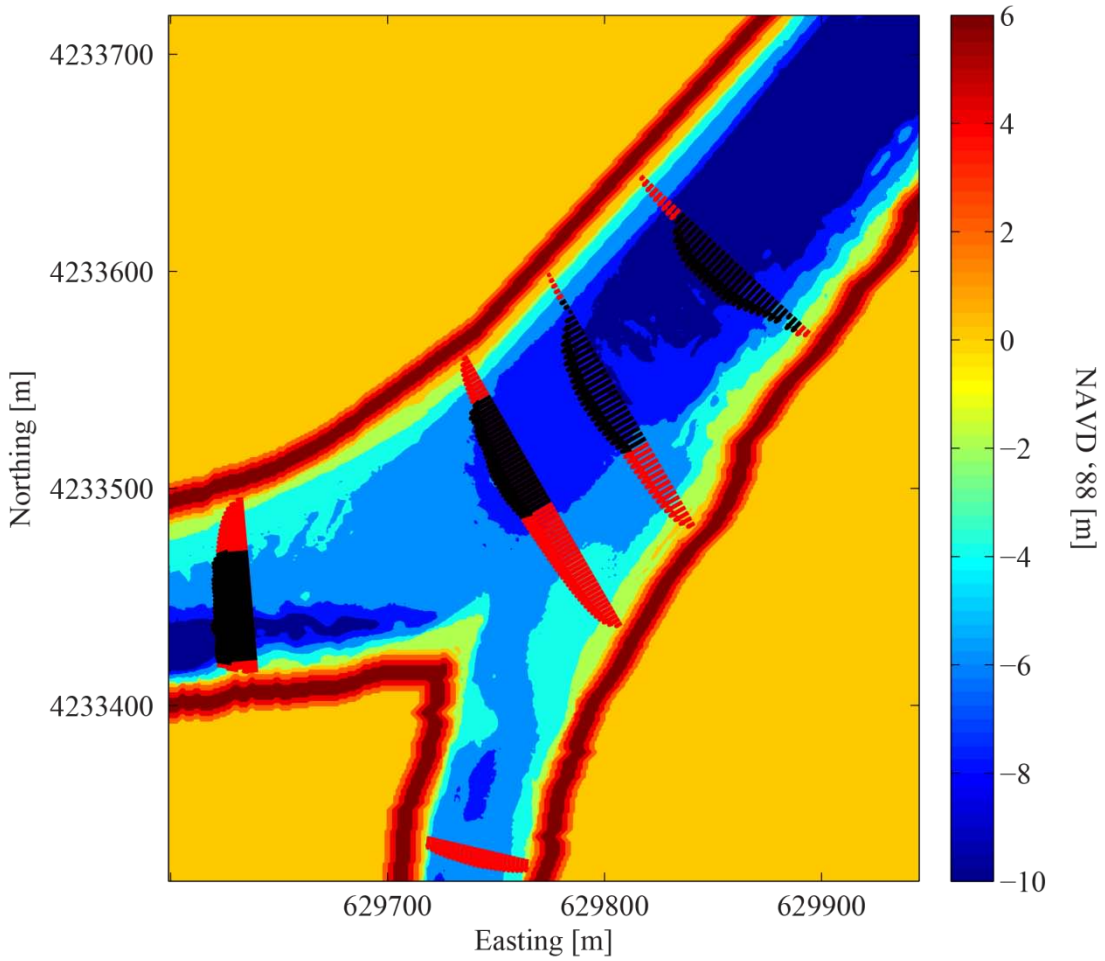

Figure 3.23 Initial velocity vector rotation from measured data (black arrows), and extrapolated velocity vectors and Georgian Slough velocity boundary condition (red arrows); Overlain on bathymetric map of study domain on March 26, 2012 at 0915 PST.

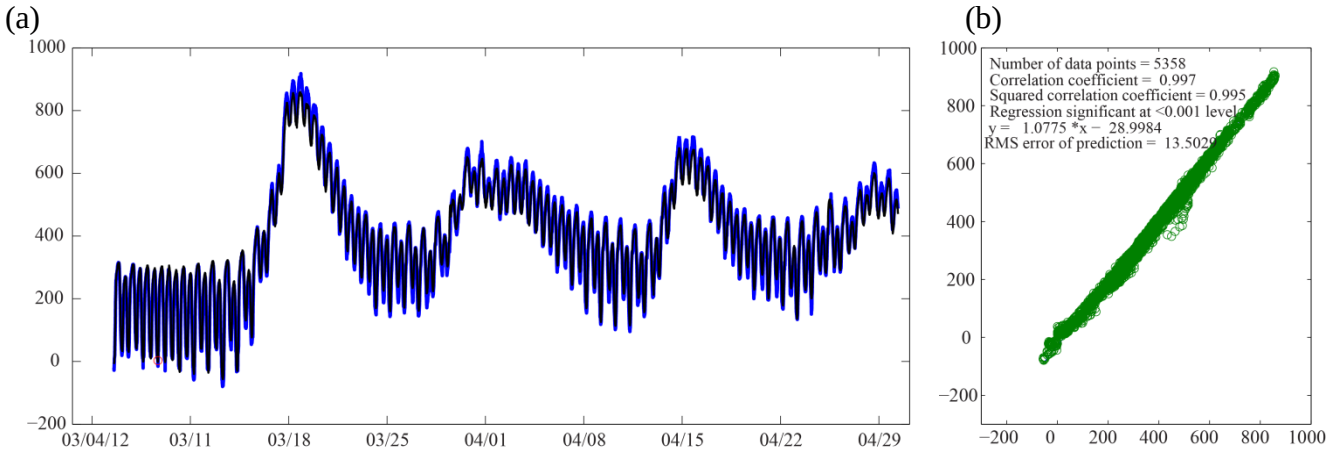

Figure 3.24. (a) Time-series of measured discharge (m^3/s) at Q_A (blue line) and Q_E (black line) and (b) Linear regression of Q_A (m^3/s) versus Q_E (m^3/s) for the study period.

(a) (b)

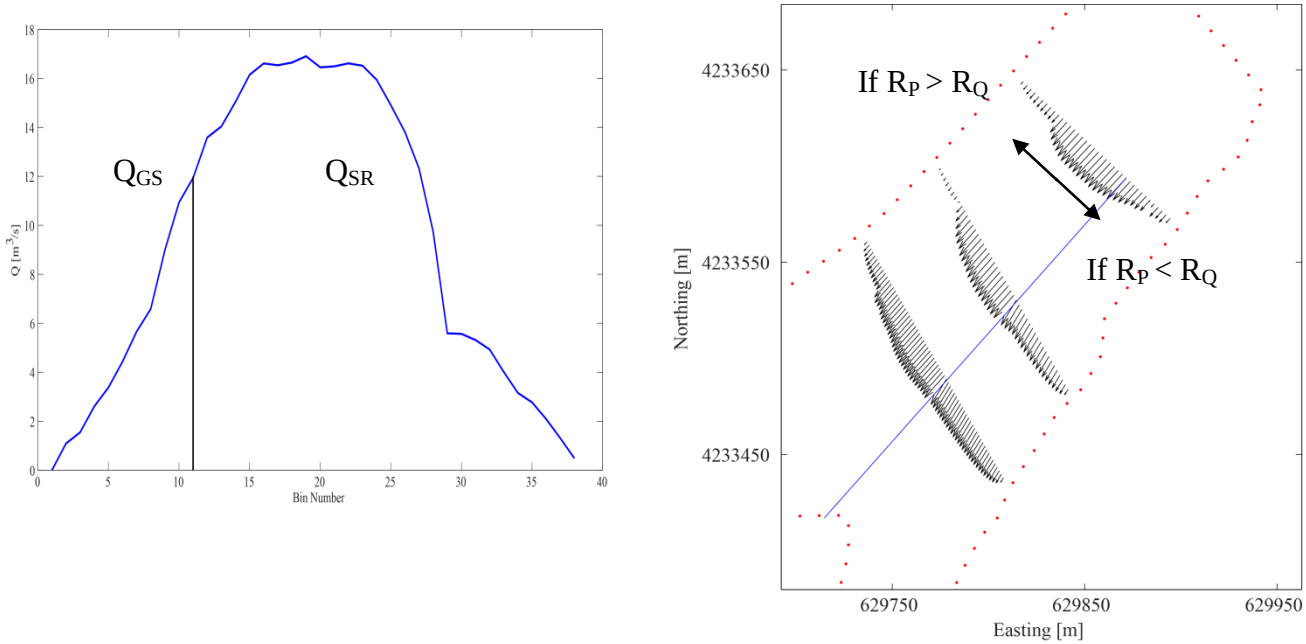

Figure 3.25. (a) Estimated discharge (Q_E) at the first cross section and the ratio of flow at Georgiana Slough (Q_{GS}) and flow down the Sacramento River (Q_{SR}) to determine the C_{SL} (b) The estimated C_{SL} projected downstream and resultant rotation of velocity vectors at Site 2 and 3. The C_{SL} is moved left or right depending on the result of the particle release. On March 26, 2012 at 0915 PST.

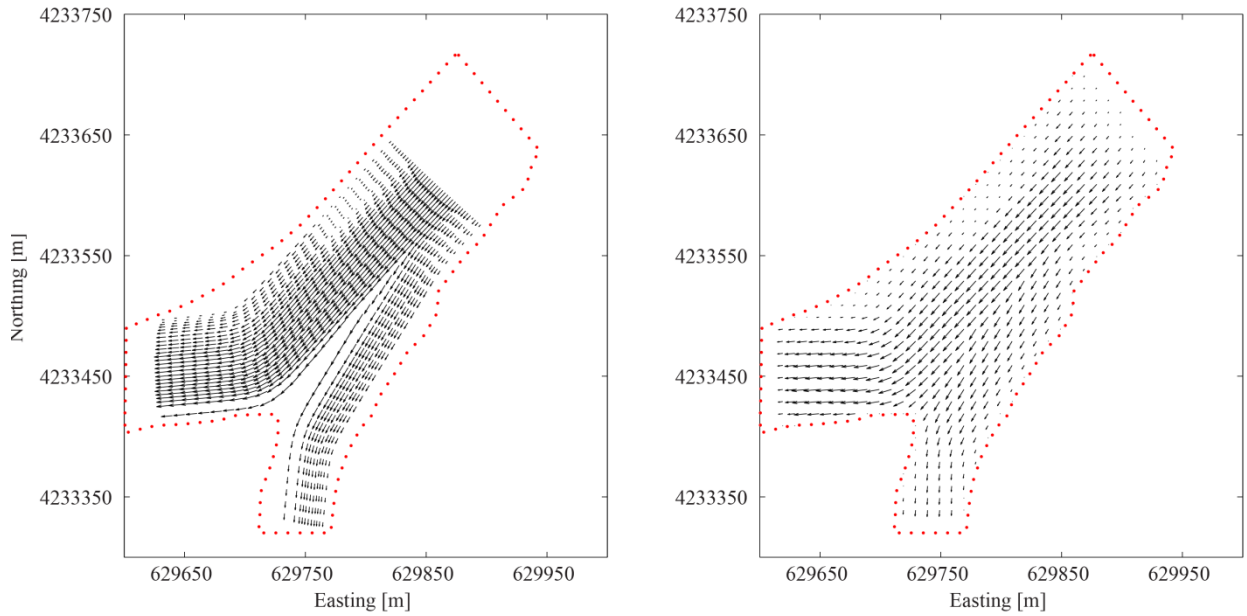

(a) (b)

Figure 3.26 (a) IPLW interpolated velocities after algorithm converges and (b) The resultant grid interpolation. On March 26, 2012 at 0915 PST.

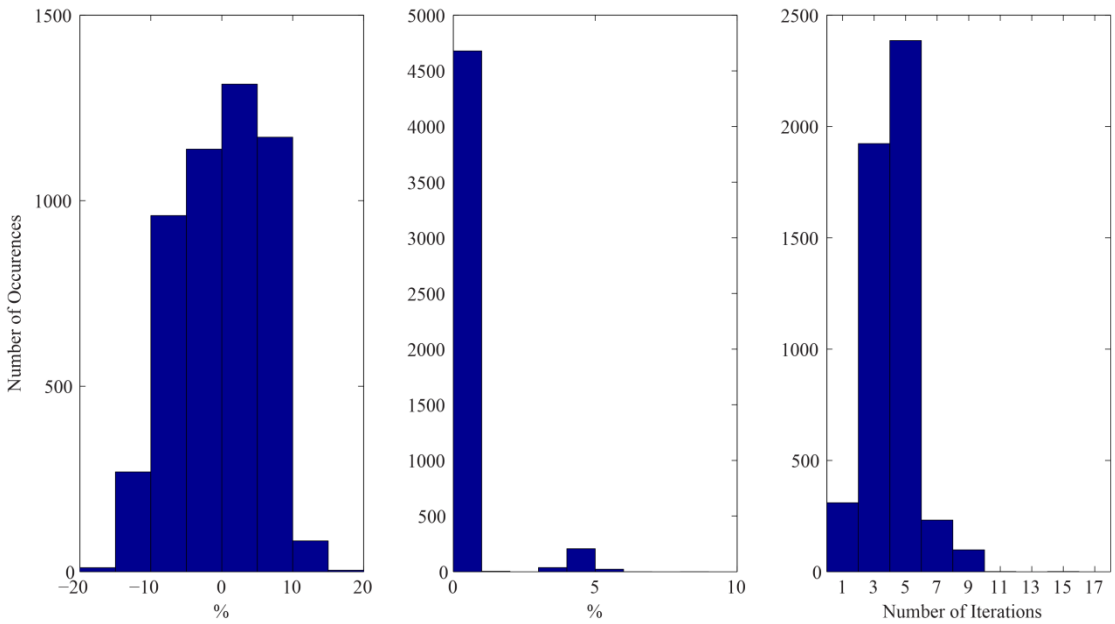

(a) (b) (c)

Figure 3.27 Histograms showing the performance of the LPTA and IPLW interpolation algorithms for n=4795 (a) The percent difference in the ratio of particles (R_P) to the discharge ratio (R_Q) (b) The percentage of particles that move out of the domain when the algorithm converges and (c) The number of iterations needed for a solution to converge.

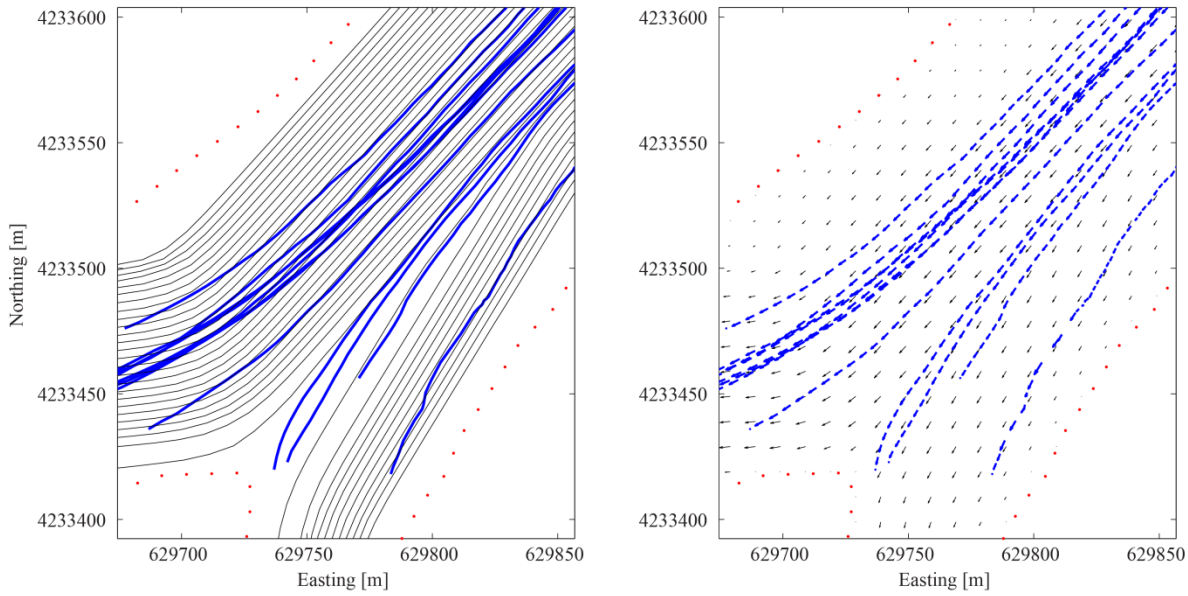

Figure 3.28. Comparison of interpolated data and drifter data for (a) generated particle pathlines (black) and pathlines of drifters (blue) and (b) IPLW interpolated velocities (black arrows) and calculated velocities from drifters (blue arrows). On March 21, 2012 at 1015 PST.

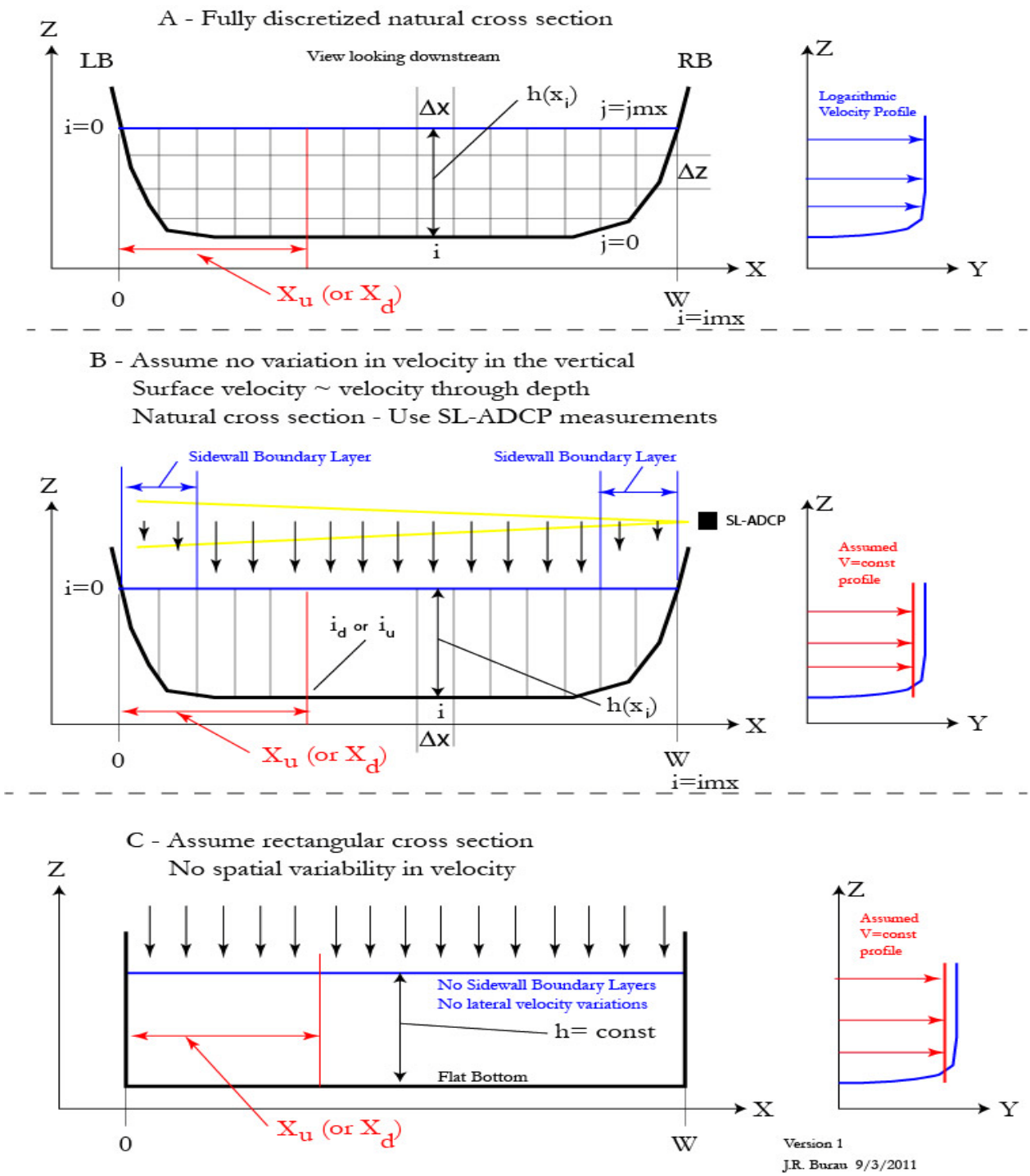

Figure 3.29 - Conceptual drawings of a river cross section (on left) and velocity profile (on right) depicting the various ways in which discharge can be calculated based on an increasing number of assumptions, from A to C.

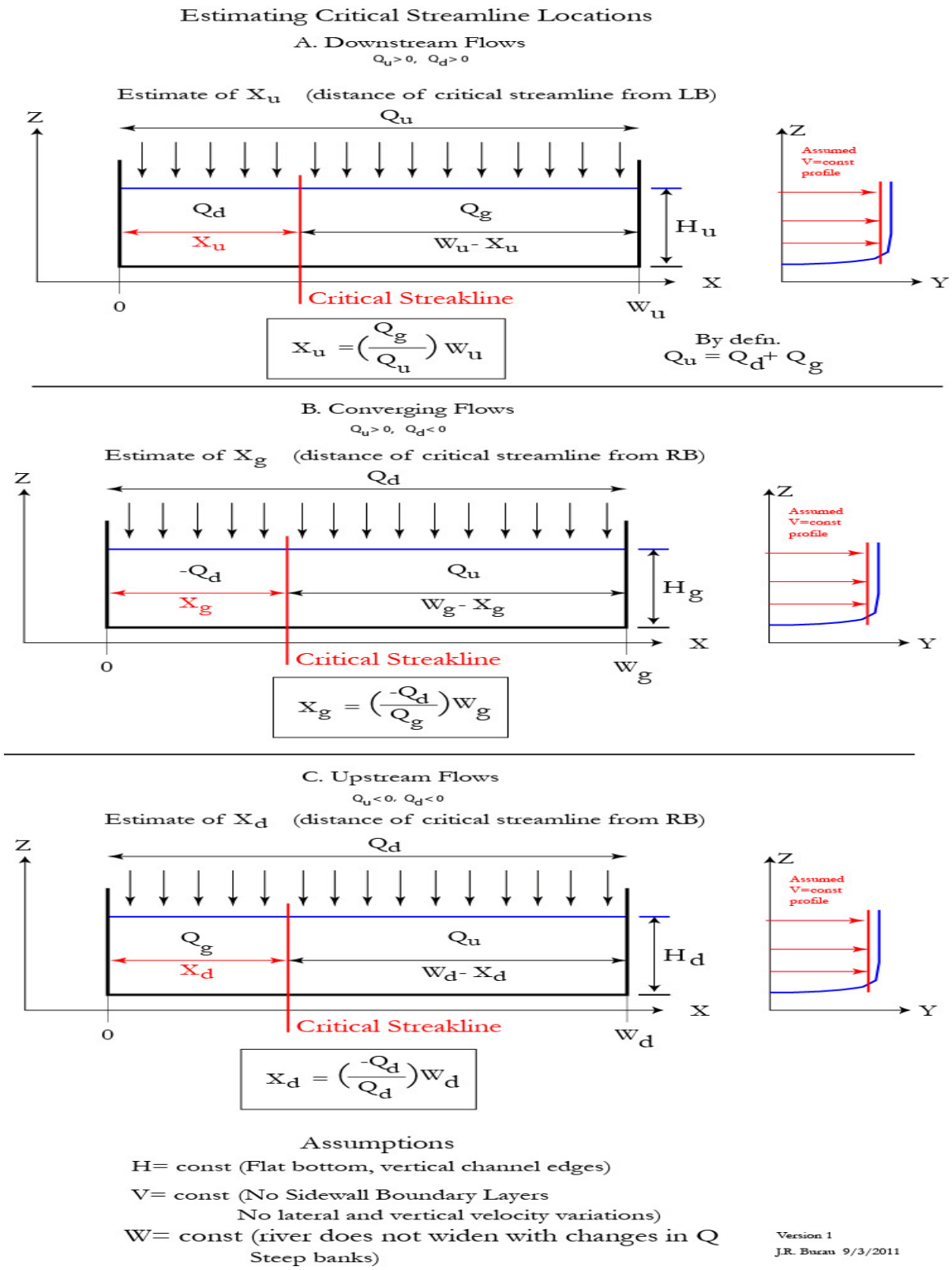

Figure 3.30 – Conceptual drawings of a rectangular river cross section (on left) and velocity profile (on right) depicting the various ways in which discharge can be calculated based on the flow split.

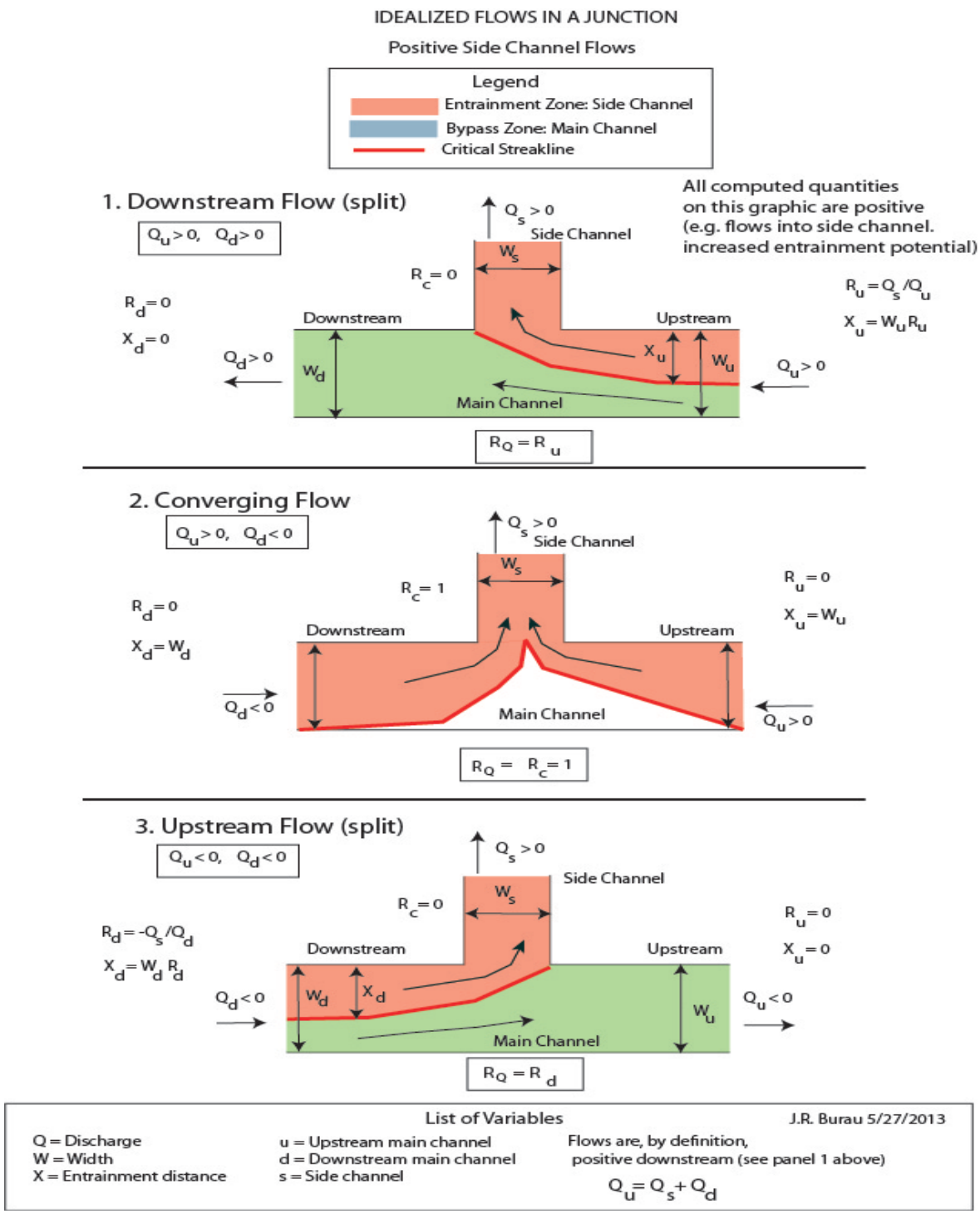

Figure 3.31 – Definition sketch defining the three flow conditions that occur in a tidally forced junction where the water is entering a side channel: (1) downstream flow in the main channel, (2) converging flow, and (3) upstream flow.

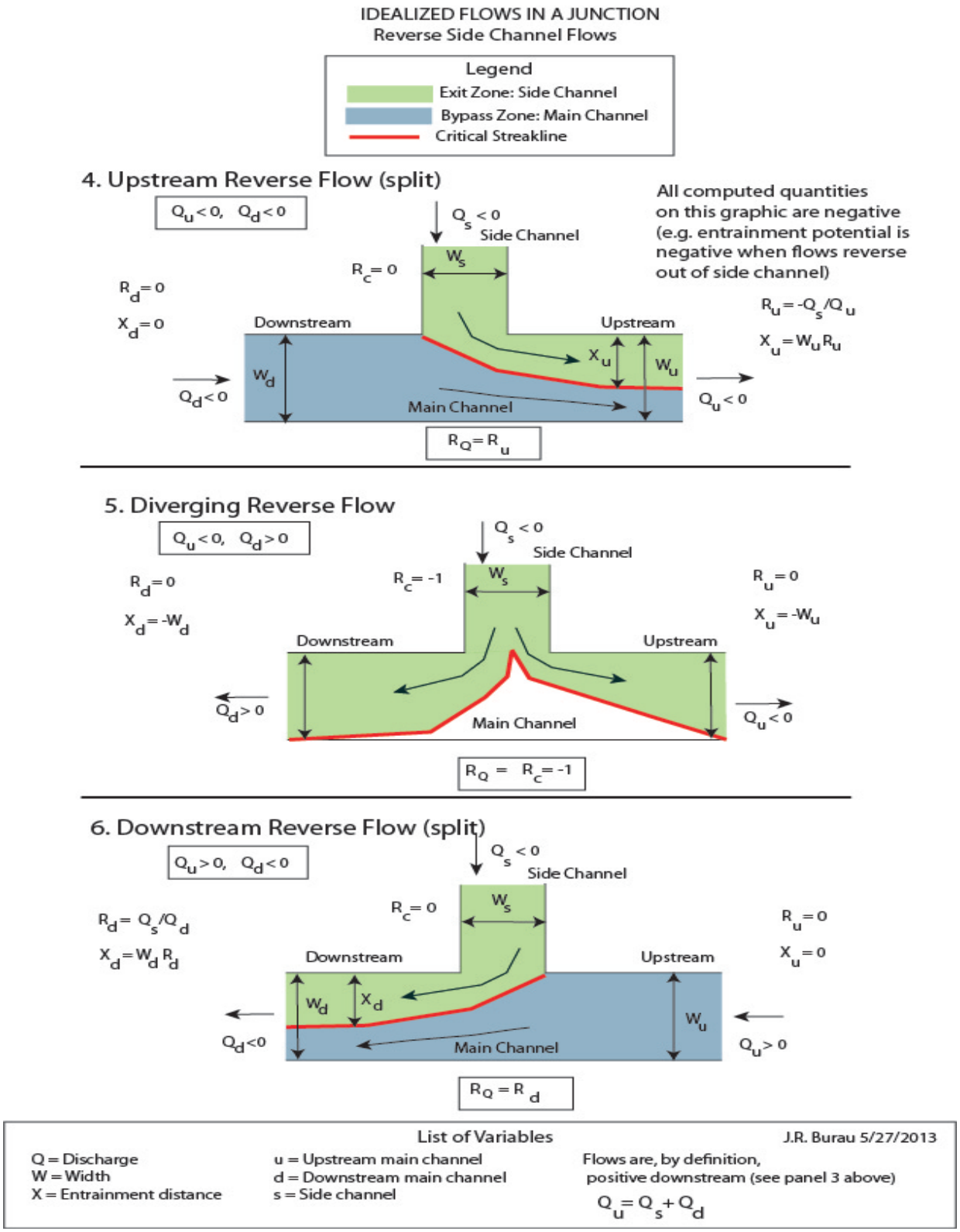

Figure 3.32 - Definition sketch defining the three flow conditions that occur in a tidally forced junction where the water is exiting a side channel: (1) downstream flow in the main channel, (2) converging flow, and (3) upstream flow.

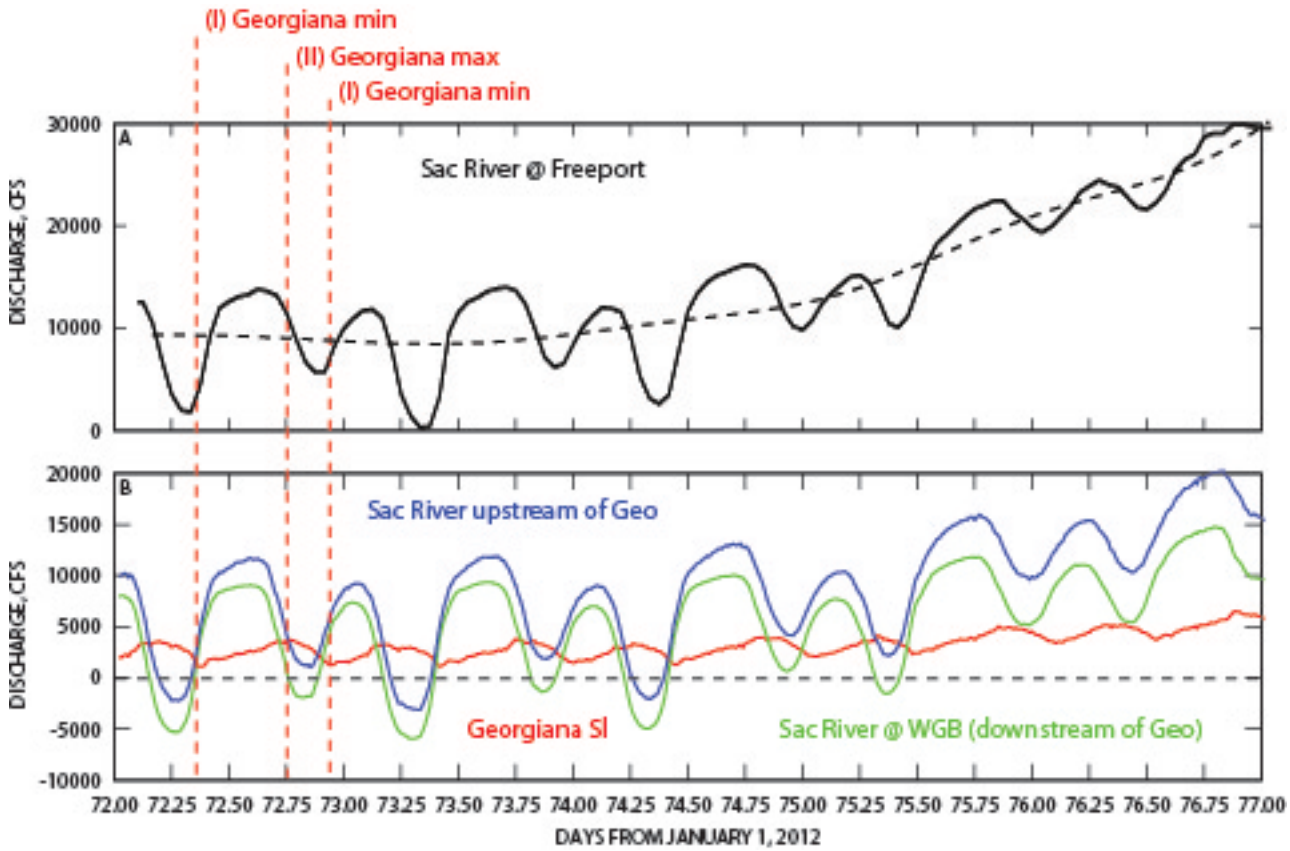

Figure 4.1 – Time series plots of (A) the discharge in the Sacramento River at Freeport (black), (B) the discharge in the Sacramento River upstream, of Georgiana Slough (blue), the Sacramento River downstream of Georgiana Slough (green), and Georgiana Slough (red) during a transition from bi-directional flow to uni-directional flow as the Sacramento River's tidally average discharge increased in 2012.

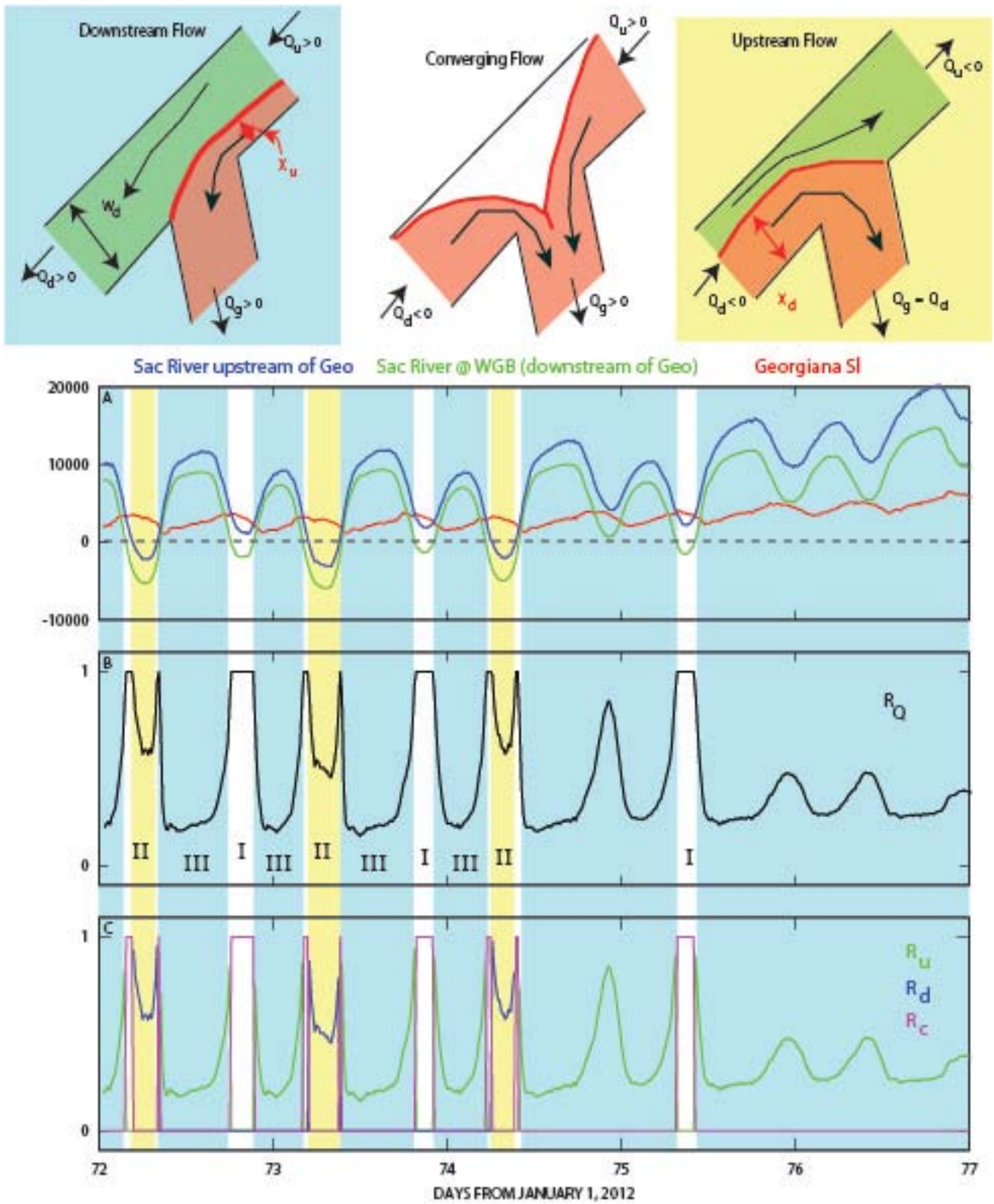

Figure 4.2 – Time series plots of (A) the discharge in the Sacramento River upstream, of Georgiana Slough (blue), the Sacramento River downstream of Georgiana Slough (green),

and Georgiana Slough (red), (B) the total tidal discharge ratio R, and (C) the component discharge ratios R_U (flow entering Georgiana from upstream, green), R_D (flow entering Georgiana from downstream, blue) and R_C (converging flow into Georgiana) during a transition from bi-directional flow to uni-directional flow as the Sacramento River's tidally average discharge increased in 2012. The upper portion of the diagram gives the color coding for the various flow states (light blue for downstream flow, white for converging flow and yellow for reversing flow. During reversing conditions it is clear the flows in the junction cycle through all three of the flow states. In particular the switch between states on either side of converging flow conditions can be quite rapid – condition II above.

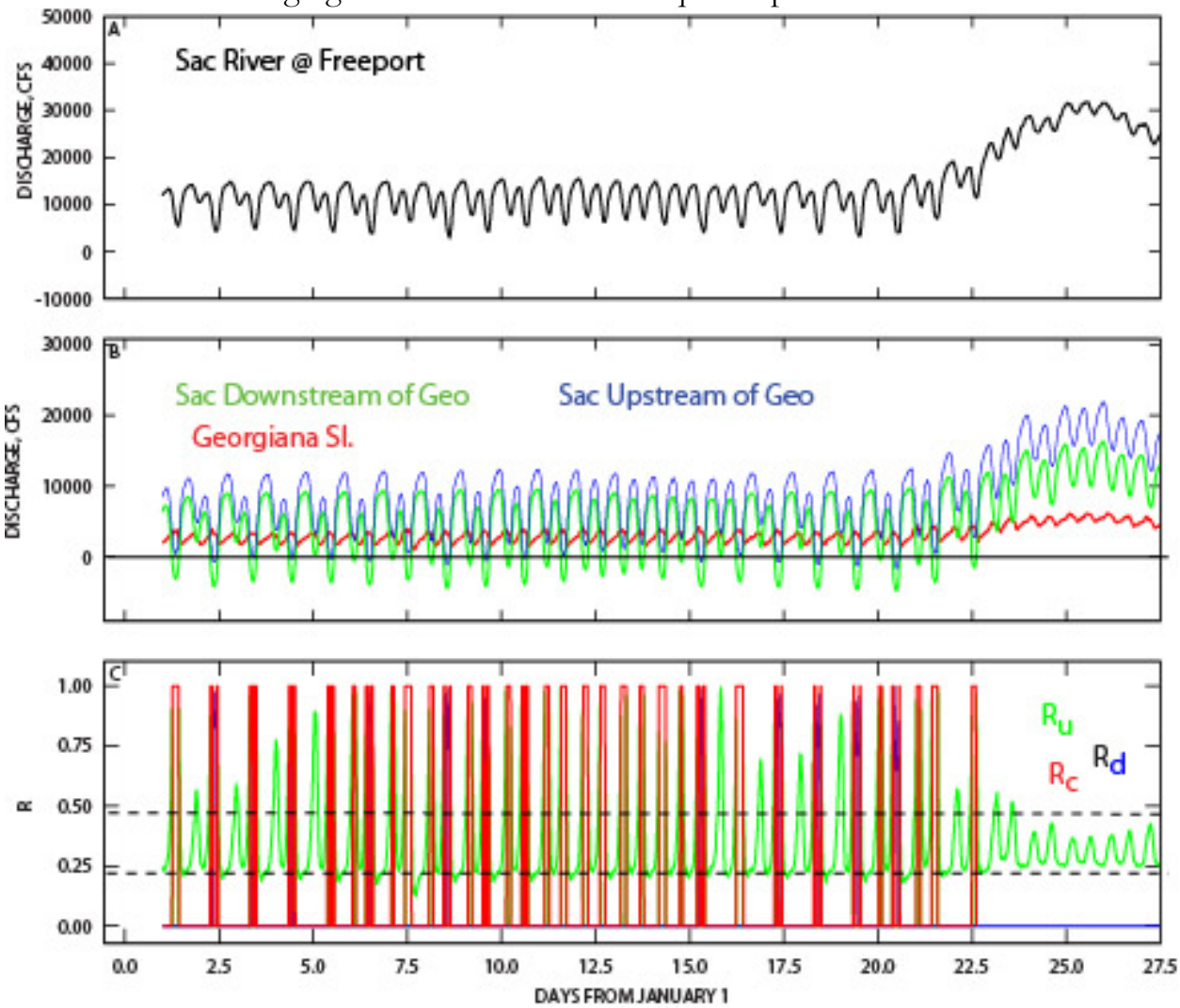

Figure 4.3 – Time series plots of (A) the measured discharge in the Sacramento River at Freeport, (B) the measured discharge in the Sacramento River upstream of Georgiana Slough (blue), the Sacramento River downstream of Georgiana Slough (green), and Georgiana Slough (red), (C) the component discharge ratios R_U (flow entering Georgiana from upstream, green), R_D (flow entering Georgiana from downstream, blue) and R_C (converging flow into Georgiana).

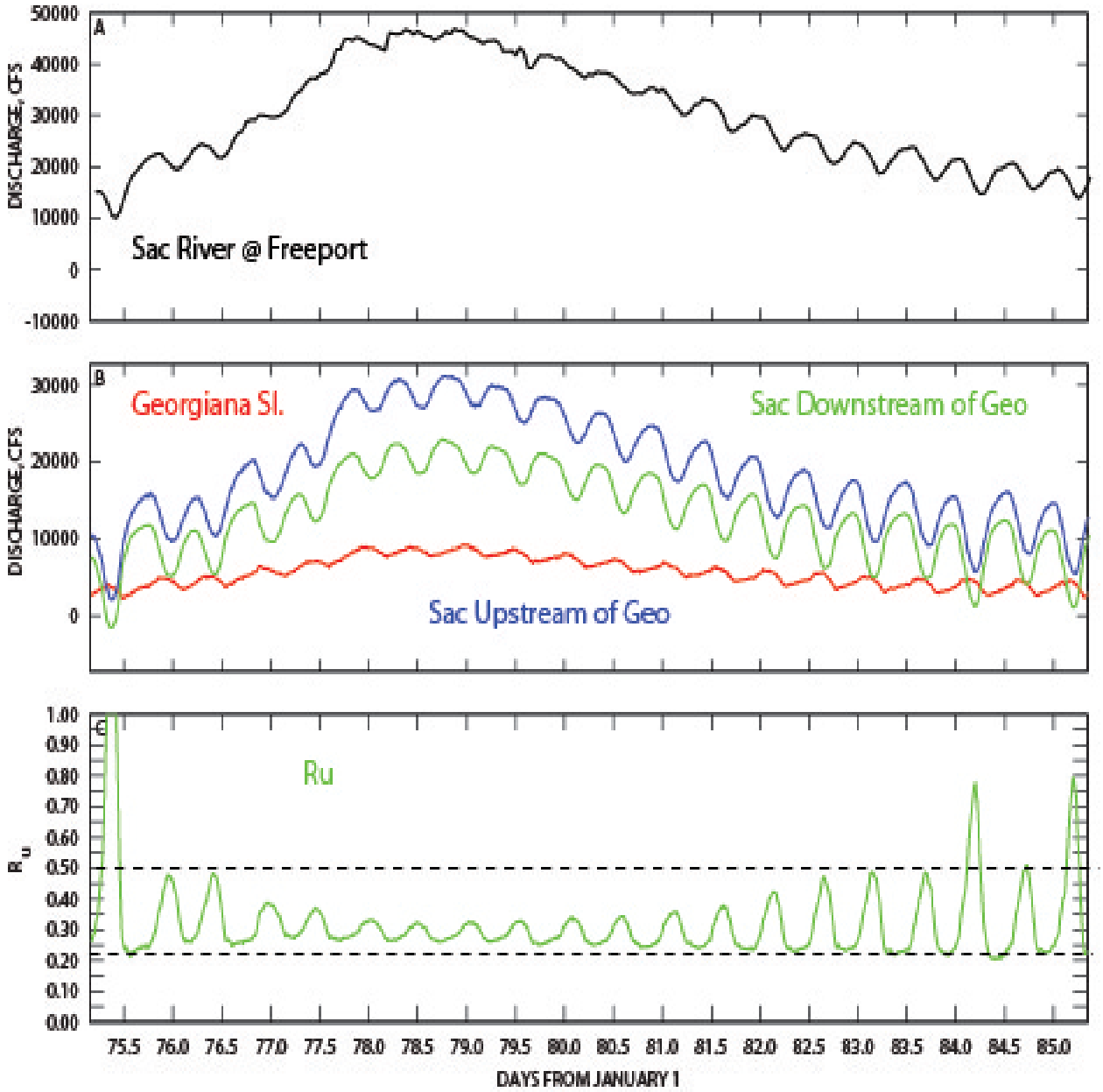

Figure 4.4 - Time series plots of (A) the measured discharge in the Sacramento River at Freeport, (B) the measured discharge in the Sacramento River upstream of Georgiana Slough (blue), the Sacramento River downstream of Georgiana Slough (green), and Georgiana Slough (red), (C) the component discharge ratio R_U (flow entering Georgiana from upstream, green.

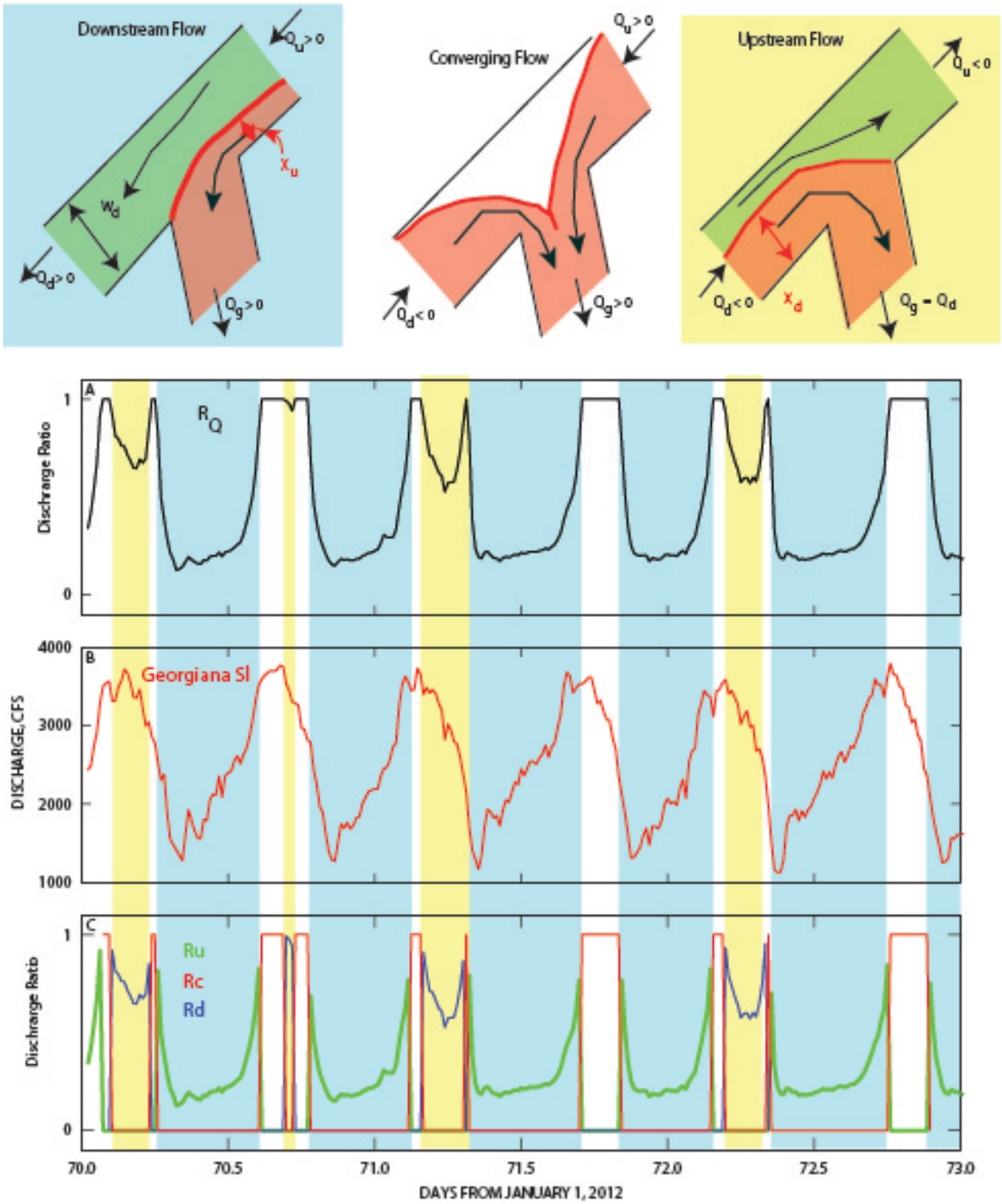

Figure 4.5- Time series plots of (A) the total discharge ratio, R, (B) the discharge in Georgiana Slough, and (C) the component discharge ratios R_U (flow entering Georgiana

from upstream, green), R_D (flow entering Georgiana from downstream, blue) and R_C (converging flow into Georgiana) during low Sacramento River flow period.

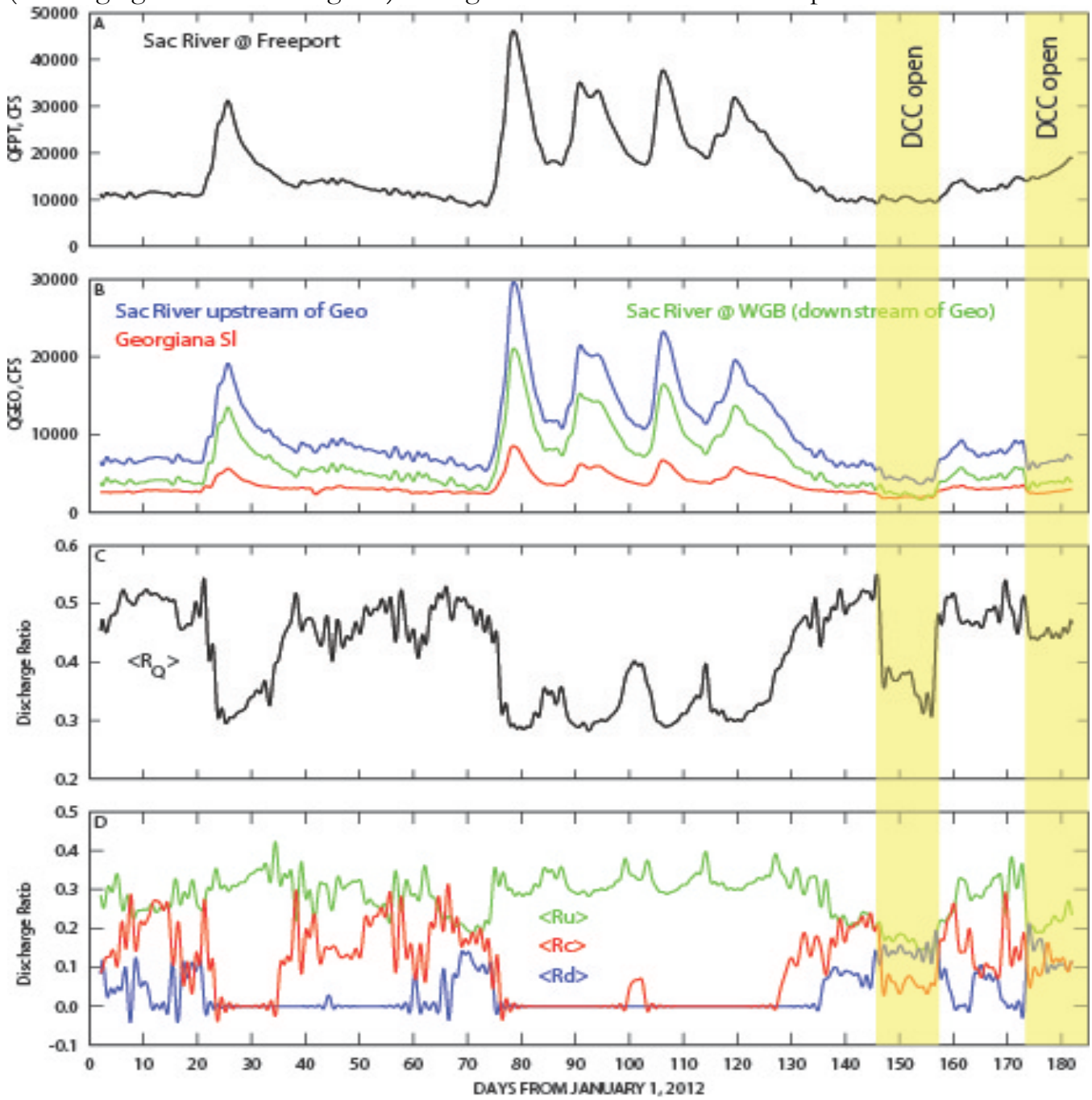

Figure 4.6 – Time series of (A) the tidally averaged flow in the Sacramento River at Freeport, (B) tidally averaged discharge in the Sacramento River upstream of Georgiana Slough (blue), the Sacramento River downstream of Georgiana Slough (green), and Georgiana Slough (red), (C) the tidal timescale total discharge ratio, R_Q, (D) the tidal average component discharge ratios R_U (flow entering Georgiana from upstream, green), R_D (flow entering Georgiana from downstream, blue) and R_C (converging flow into Georgiana).

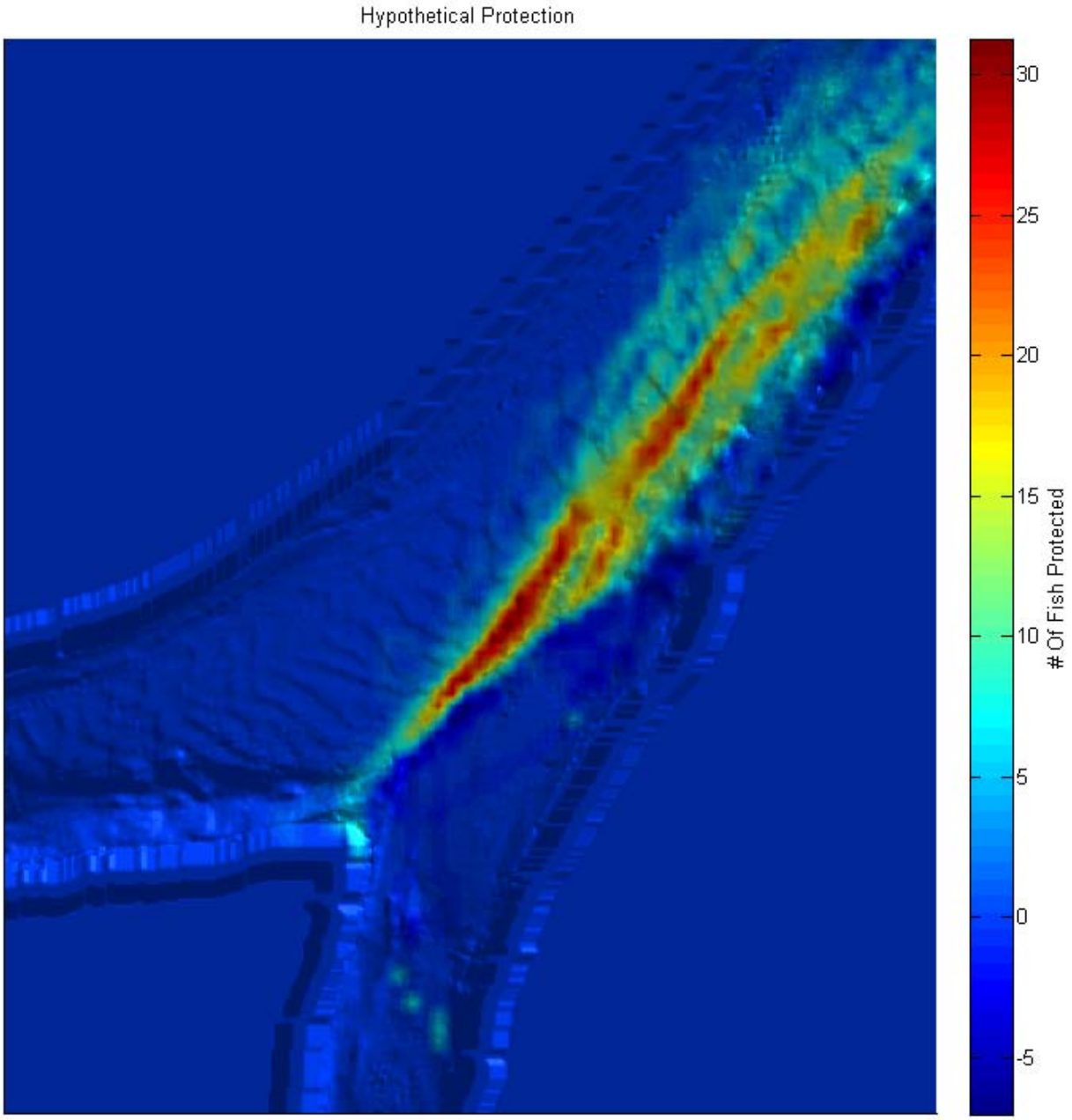

Figure 5.1 – The horizontal spatial difference between barrier OFF and ON conditions which represents the behavioral response of out-migrating salmon to the BAFF. The reduction in entrainment into Georgiana Slough involved those fish that were moved to river right across the streakline.

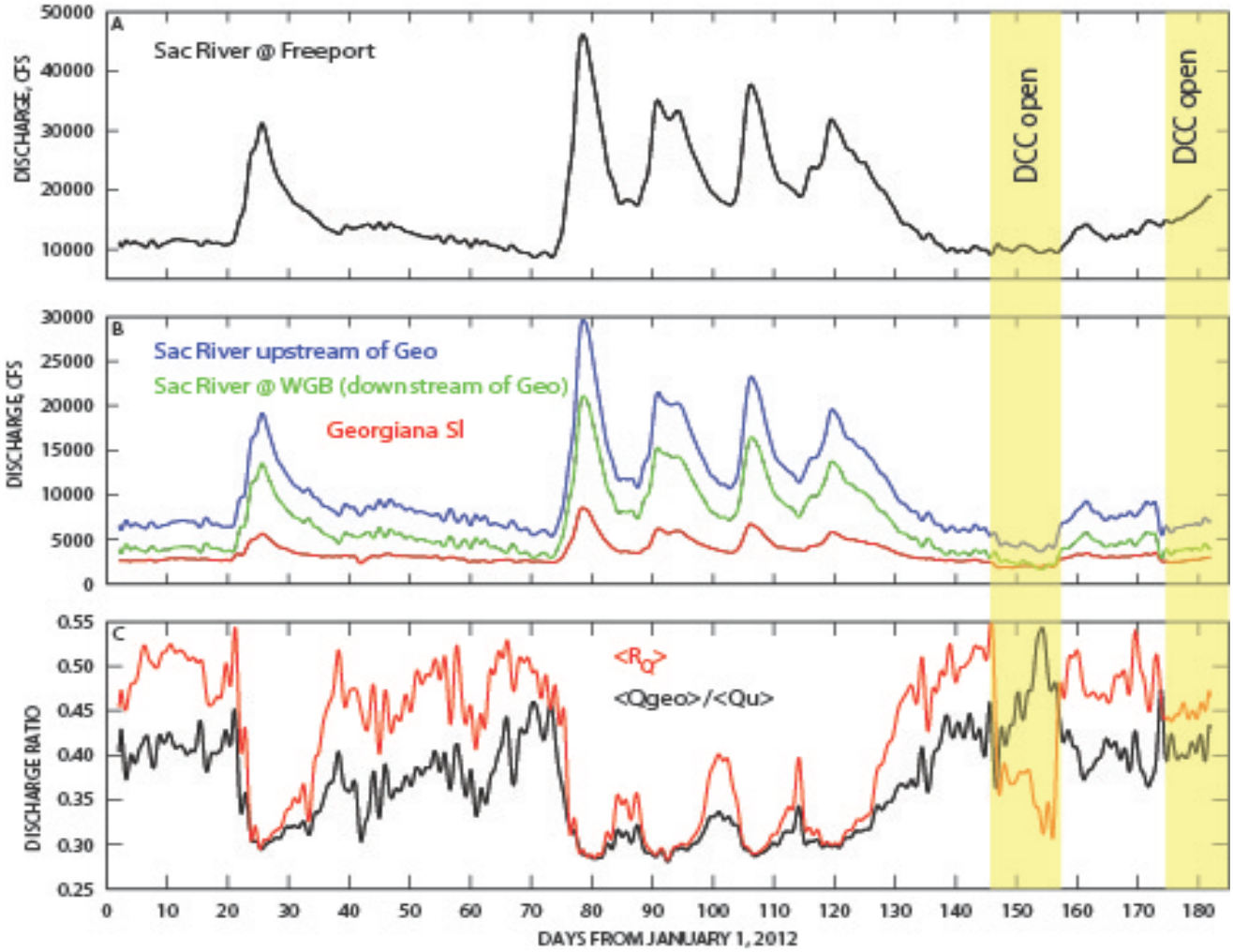

Figure 5.2 – Time series plots of (A) the tidally-averaged discharge in the Sacramento River at Freeport, (B) the tidally averaged discharge in the Sacramento River upstream of Georgiana Slough (blue), the Sacramento River downstream of Georgiana Slough (green), and in Georgiana Slough (red), (C) the tidal average of the total discharge ratio $< R_Q >$ (red), the ratio of the tidal average of the discharge in Georgiana Slough divided by the discharge in the Sacramento River upstream of Georgiana Slough (black).

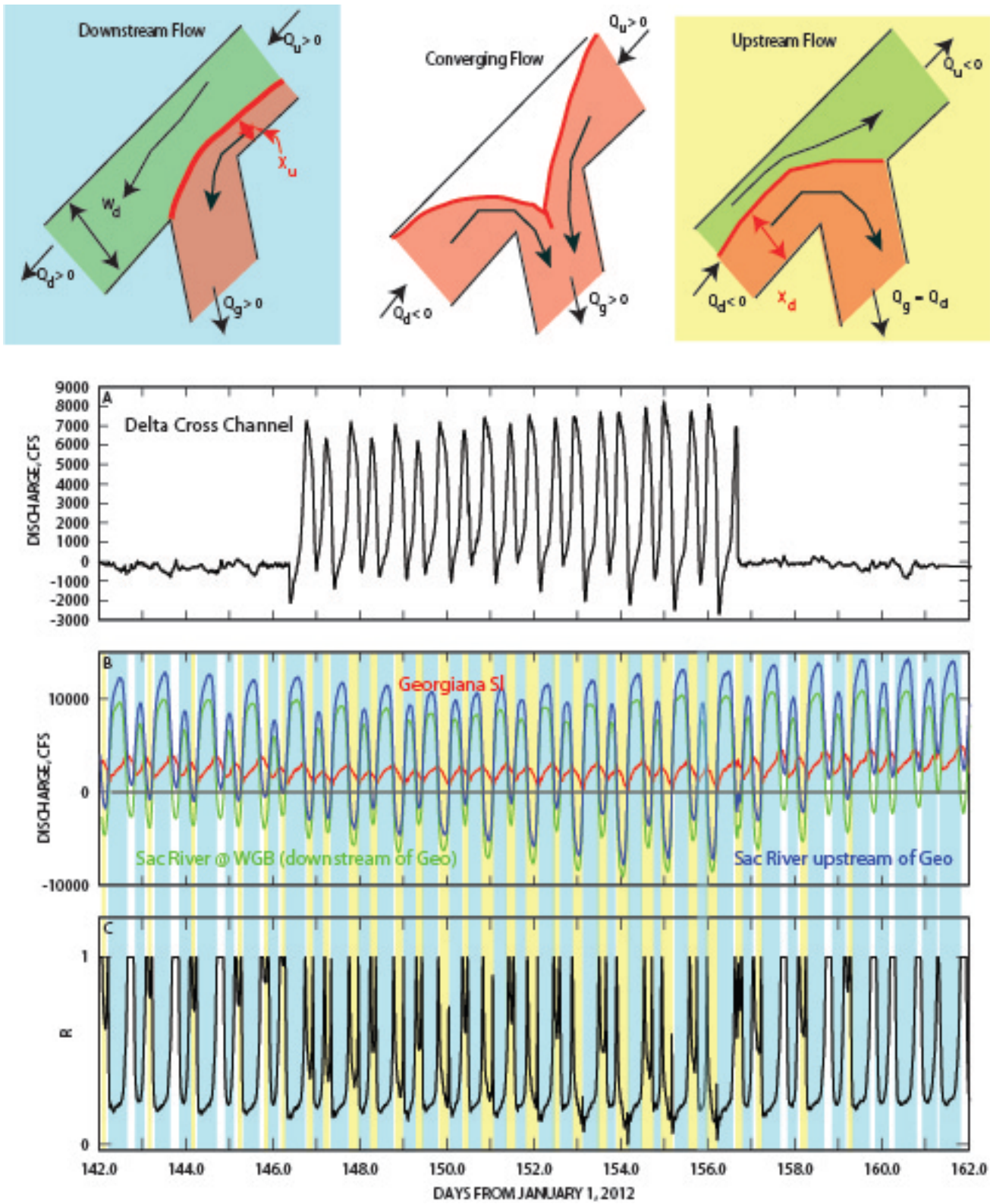

Figure 5.3 – Time series plot of the (A) discharge in the Delta Cross Channel (the gates are closed when the discharge is zero – in this plot up to day 147 and after day 157), (B) the discharge in the Sacramento River upstream, of Georgiana Slough (blue), the Sacramento

River downstream of Georgiana Slough (green), and Georgiana Slough (red), (C) the total discharge ratio, R_Q. The upper portion of the diagram gives the color coding for the various flow states (light blue for downstream flow, white for converging flow and yellow for reversing flow. The effect of closing the DCC gates on Georgiana is to dramatically reduce the period of converging flows in favor of creating flows that bypass the slough and flow upstream and into the DCC. The effect on the tidally averaged flows in Georgiana of closing the gates is fairly minimal, yet the effect on the tidal exchanges in fairly dramatic – an almost complete reduction in converging flows!

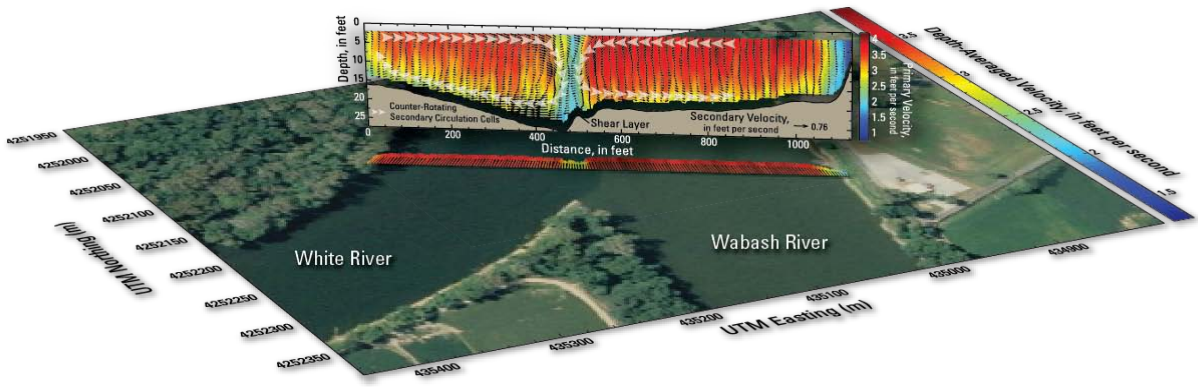

Figure 5.4 - Depth-averaged velocity and primary and secondary velocities (Rozovskii definition) in the confluence of the White and Wabash Rivers along the Illinois and Indiana border, January 12, 2008. Produced in VMT using data from a TRDI 1200 KHz Rio Grande ADCP (Courtesy of USGS, VMT webpage http://hydroacoustics.usgs.gov/movingboat/VMT/VMT.shtml). This image shows that secondary currents can occur in junctions as the flows change direction to enter each channel in the junction. Once the streaklines begin to curve in a junction secondary circulation creates down-welling that can occur at the horizontal location of the critical streakline making it more difficult to move fish across the streakline once fish enter the junction and the particle streaklines begin to curve, another reason upstream behavioral barriers may be preferable..

APPENDIX G

2012 GEORGIANA SLOUGH NON-PHYSICAL BARRIER STUDY
DETERMINATIONS OF OVER-BARRIER OR UNDER-BARRIER PASSAGE OF
ACOUSTICALLY TAGGED FISH

2012 Georgiana Slough Non-Physical Barrier Study

Determinations of Over-Barrier or Under-Barrier Passage of Acoustically Tagged Fish

Methods

At the Sacramento River/Georgiana Slough junction in 2012, hydrophones were deployed in a configuration that allowed two methods of determining vertical positions (elevations) of tagged fish near the BAFF. The first method was the traditional method of deploying surface and bottom hydrophones in a configuration that allowed calculation of a three dimensional position for each tag transmission that occurred as a tagged fish passed the site. The position was based on tag signal arrival time differences between 4 hydrophones arranged such that at least one hydrophone was not in the same plane as that defined by the other three. Significant improvements in the 2012 array design compared to the 2011 study included floating hydrophone mounts that allowed for maximum vertical separation between surface and bottom hydrophones. Positioning tags in three dimensions would not have been expected to produce accurate results in areas away from the BAFF, since in 2012 there were no hydrophones (deep or shallow) deployed mid-river away from the BAFF. However, near the BAFF there were deep and shallow hydrophones deployed at regular intervals to allow three dimensional positioning for those fish that were near the BAFF.

The second method used to find elevations of tagged fish near the BAFF was the comparison of tag signal arrival times from pairs of hydrophones positioned directly above and below each other. Tag signals from tags that went over the BAFF would arrive at the surface hydrophone first, while those from tagged fish that went under the BAFF would arrive at the bottom hydrophone first. Figure __ shows an example of tagged fish transmissions (tag code 3246.17, on March 17, 2012, between 12:27:28 and 12:30:01 PDT) as the tag passed by a co-located pair of surface/bottom hydrophones (HD 207and 208). The upper series of returns, shown in red, are from surface hydrophone 207 and are above (arrived before) those of bottom hydrophone 208, shown in blue. This indicates that for most of this time period, the tag was nearer the surface hydrophone than the bottom hydrophone. Figure __ shows another example (tag code 2679.12, on March 31, between 15:24:09 and 15:26:50 PDT) where the upper series of returns, shown in blue, are from bottom hydrophone 208 and are above (arrived before) those of the surface hydrophone 207, shown in red. This indicates that for most of this time period, the tag was nearer the bottom hydrophone than the surface hydrophone.

By calculating the elevation difference of co-located pairs of hydrophones (based on the bottom mounted hydrophone elevation, surface hydrophone mount depth, and Sacramento River stage height), and using the two dimensional Easting/Northing (X/Y) positions of tagged fish, the elevations of tagged fish were calculated for each fish that crossed the BAFF line.

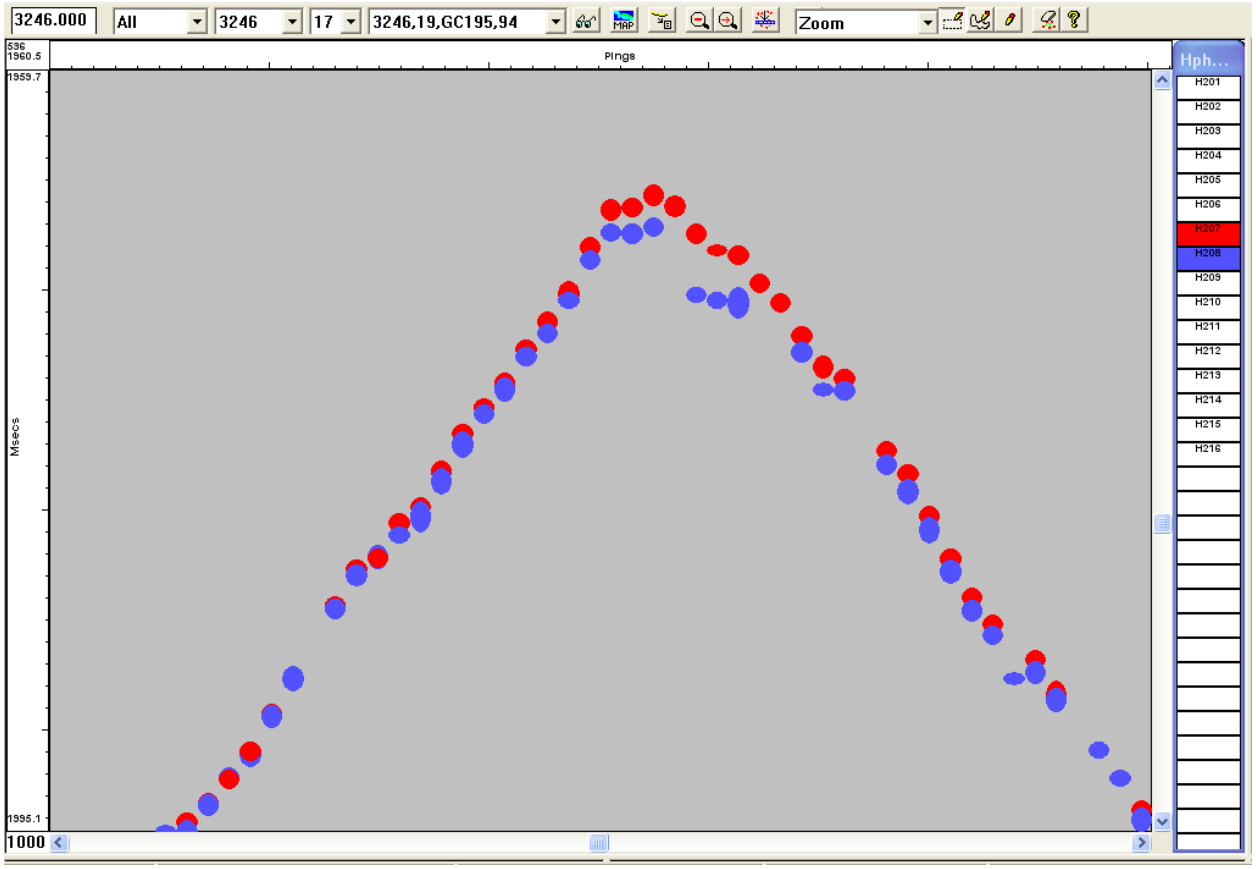

Figure __. Tag signals detected on hydrophones 207 and 208 from tag 3246.17 on March 17, 2012, between 12:27:28 and 12:30:01 PDT, showing signal arrival times that indicate this tag was nearer to the surface hydrophone (HD 207) than to the bottom hydrophone (HD 208).

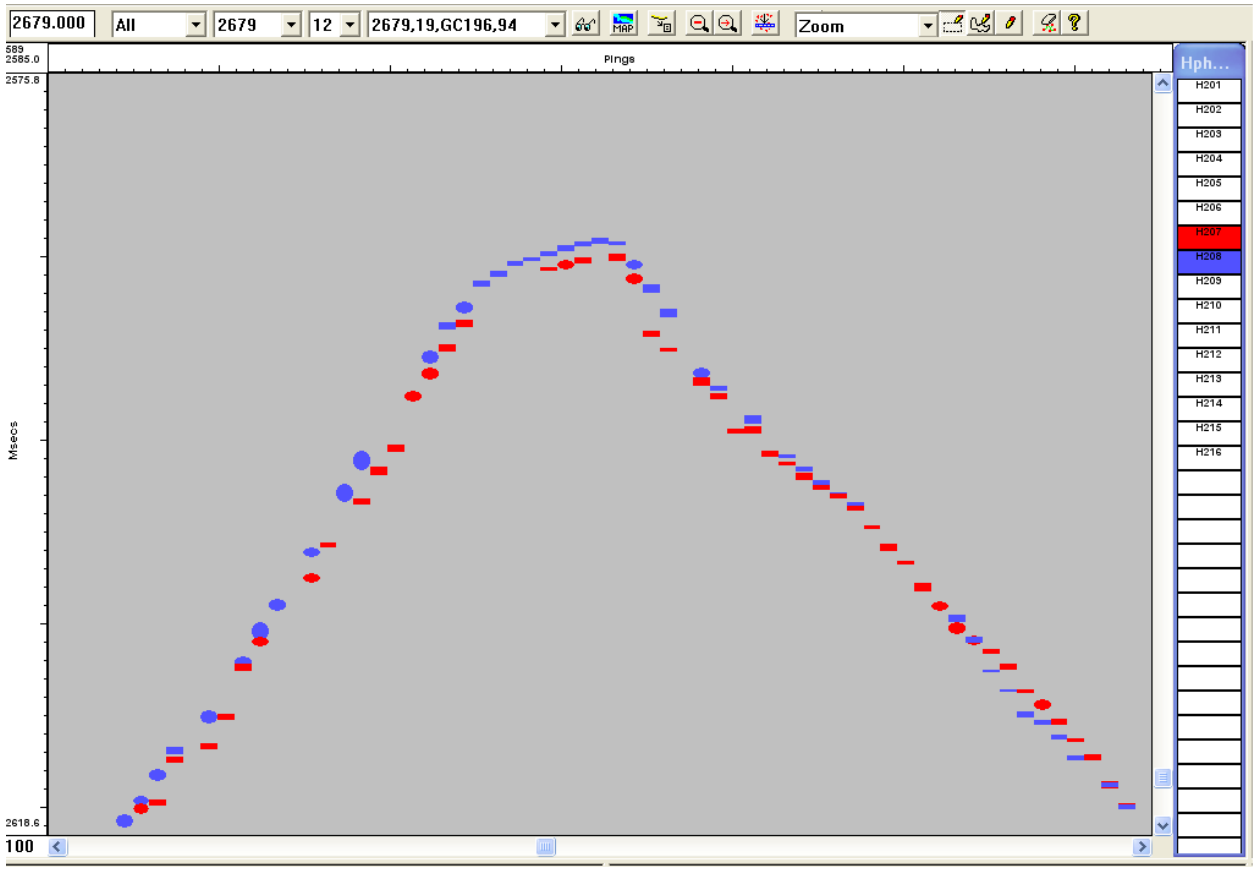

Figure __. Tag signals detected on hydrophones 207 and 208 from tag 2679.12 on March 31, between 15:24:09 and 15:26:50 PDT, showing signal arrival times that indicate this tag was nearer to the bottom hydrophone (HD 208) than to the surface hydrophone (HD 207).

Tagged fish sometimes did not cross the BAFF line directly, but swam along the BAFF line before crossing over the line, and continuing downstream into Georgiana Slough. During this time, they often crossed and re-crossed the defined BAFF line more than once. The BAFF line was defined by straight lines between support pile locations, representing the location of the BAFF frame structure. The position of the bubble curtain produced by the BAFF moved as the flow and river stage height changed. For this reason, the determination of whether the fish passed over or under the BAFF frame was made using only that data from the time period when the cross-product of the BAFF line and the fish position indicated that the tagged fish was consistently upstream of the BAFF, then consistently downstream of the BAFF. Time periods when a tagged fish was moving along the BAFF, causing alternating upstream and downstream values of the BAFF cross-product determinations, were not used for determining whether the fish passed over or under the BAFF frame. In addition, for arrival time elevation calculations, co-located pairs of hydrophones were selected on the same side of the BAFF as the tag X/Y position.

Both arrival time elevation data and 3D position data were displayed and evaluated in EonFusion ™ for each tag that crossed the BAFF line. Determinations of whether the tagged fish went over the BAFF frame or under the BAFF frame were made based on the elevations of the track positions when the tagged fish approached the BAFF, crossed over it, and then continued downstream. Tagged fish whose 3D track and/or arrival time results were unclear (due to lack of hydrophone detections), or were within one (1) meter of the elevation of the bottom of the BAFF frame when they crossed the line were designated as unknown.

Results

A total of 243 tagged fish exhibited tracks that crossed the BAFF line, and entered Georgiana Slough. A summary of the operational status of the BAFF at the time these tagged fish crossed the BAFF line is shown in Table __. Determinations of whether tagged fish passed under the BAFF frame or over the BAFF frame were made for those fish that passed the BAFF line when the BAFF was on, off, or operating in a possibly compromised condition (usually caused by imperfect bubble curtain appearance). These determinations were made using both methods described above. Table __ summarizes the results of the two methods for determining how the tagged fish passed the BAFF.

BAFF Operational Status	Number of Tagged Fish that Crossed BAFF line
Off	147
On	69
Compromised	17
During Removal	7
Removed	2
Discarded (During BAFF Switch)	1

Table __. BAFF operational status when tagged fish crossed the BAFF line.

	Both Techniques Agree			Arr. Time Unknown		3D Track Unknown		Techniques Disagree	
				3D Track	3D Track	Arr. Time	Arr. Time	Arr. Time Under	Arr. Time Over
	Under	Over	Unknown	Under	Over	Under	Over	3D Track Over	3D Track Under
BAFF On	15	15	10	7	3	4	11	1	3
BAFF Off	30	27	19	24	8	5	19	2	13
BAFF Compromised	5	4	1	2	1	0	3	1	0
TOTALS:									
	Under	Over	Unknown						
BAFF On	27	32	10						
BAFF Off	61	67	19						
BAFF Compromised	8	8	1						
(TOTALS uses Arrival Time when techniques disagree, or when 3D Tracks are Unknown)									

Table ___. Determinations of vertical location of passage of 233 tagged fish that crossed the BAFF line at Georgiana Slough, 2012.

Figure __ shows an example EonFusion ™ representation of the 3D track and arrival time elevations of tagged fish 2868.01, designated as passing under the BAFF. Figure __ shows the same view for tagged fish 2406.26, designated as passing over the BAFF. Figure ___ shows the track of tagged fish 2091.26 which crossed the BAFF line, but only after swimming along it for 3.5 minutes. Fish 2091.26 crossed the BAFF line above the elevation of the bottom of the BAFF frame.

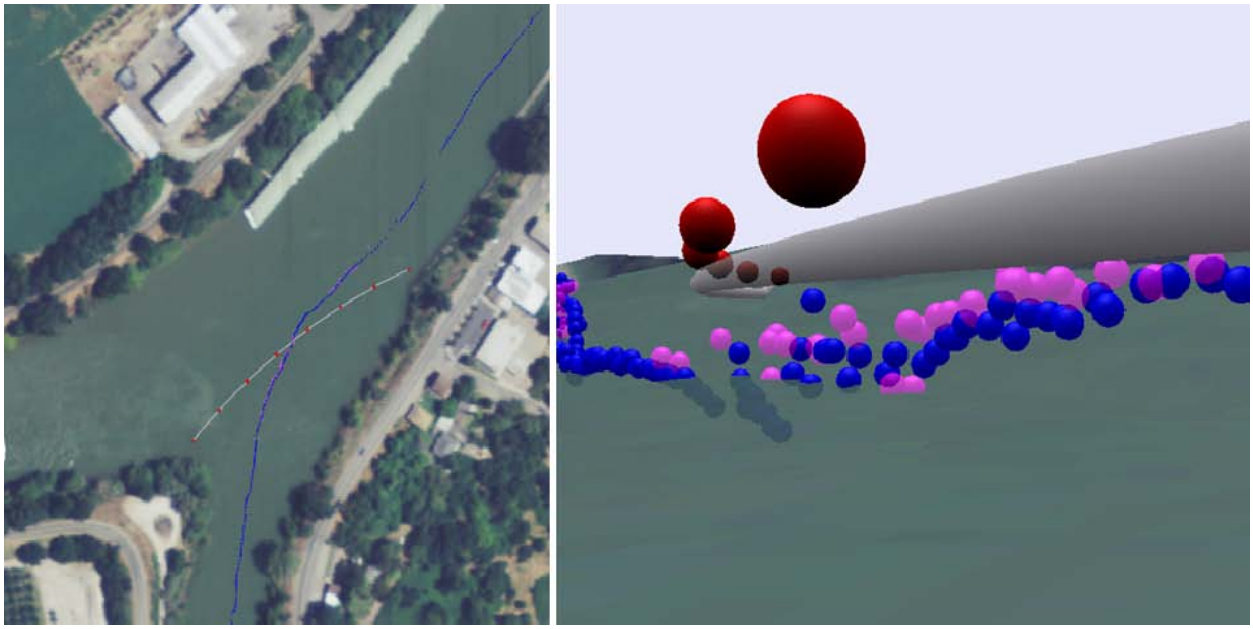

Figure ___. Tag 2868.01 passing below the BAFF frame elevation on April 15, 2012 at 18:12:36 PDT (BAFF operating). Blue spheres are 1m diameter tag position estimates from three dimensional track, pink spheres are 1m diameter elevation estimates from paired hydrophone arrival time measurements.

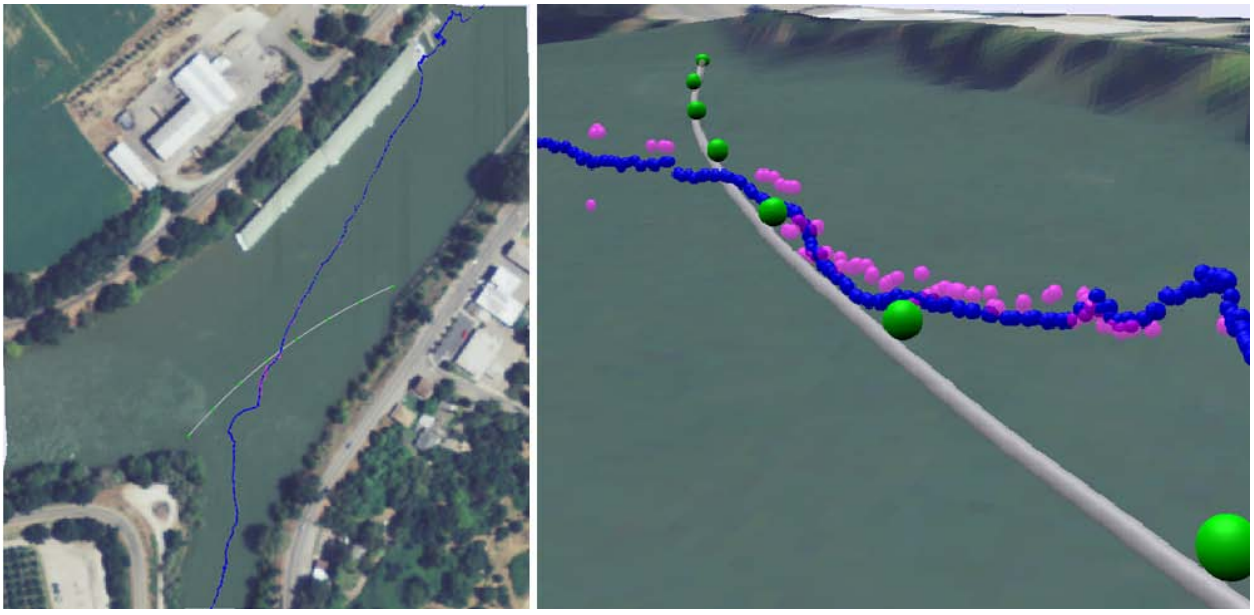

Figure ___. Tag 2406.26 passing above the BAFF frame elevation on April 20, 2012 at 21:10:24 PDT (BAFF not operating). Blue spheres are 1m diameter tag position estimates from three dimensional track, pink spheres are 1m diameter elevation estimates from paired hydrophone arrival time measurements.

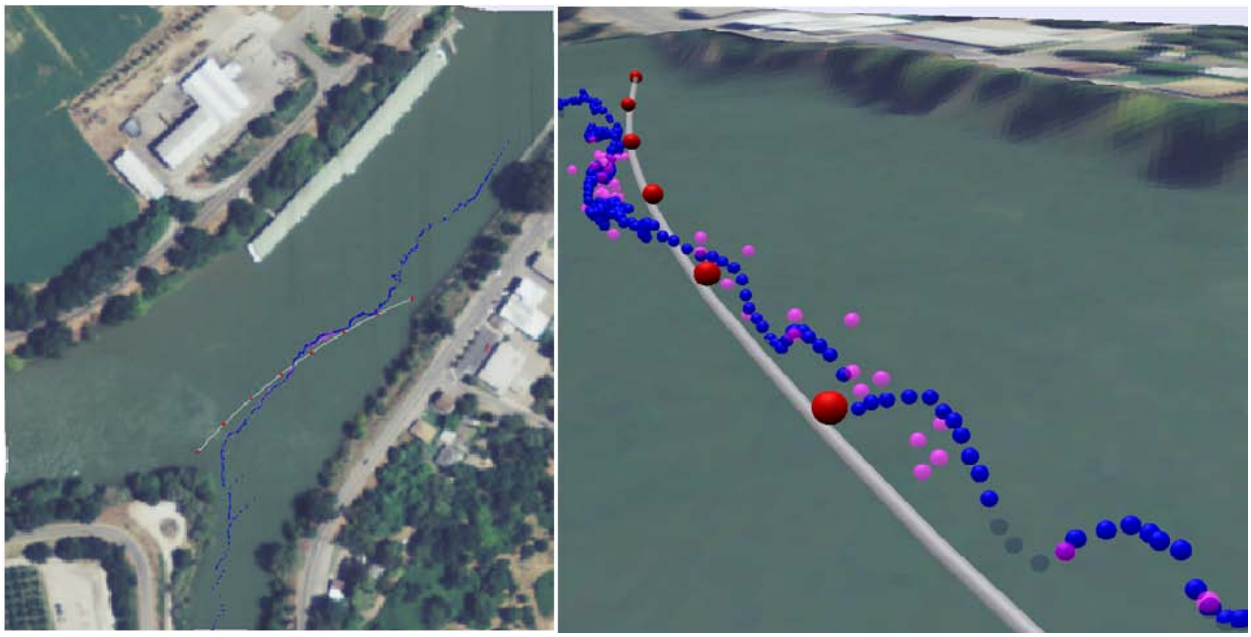

Figure ___. Tag 2091.26 moving along the BAFF frame for 3.5 minutes, then passing over the BAFF frame elevation on April 19, 2012 at 23:26:12 PDT (BAFF operating). Blue spheres are 1m diameter tag position estimates from three dimensional track, pink spheres are 1m diameter elevation estimates from paired hydrophone arrival time measurements.

Figures ___and ___ compile the results from the 243 fish that passed over the BAFF line as EonFusion ™ plots of fish tracks and elevation estimates for BAFF ON, BAFF OFF, and BAFF Compromised conditions. In both Figures, the color of each position indicates its vertical location: green indicates above the BAFF, yellow indicates within 1m (plus or minus) of the BAFF, and red indicates below the BAFF frame.

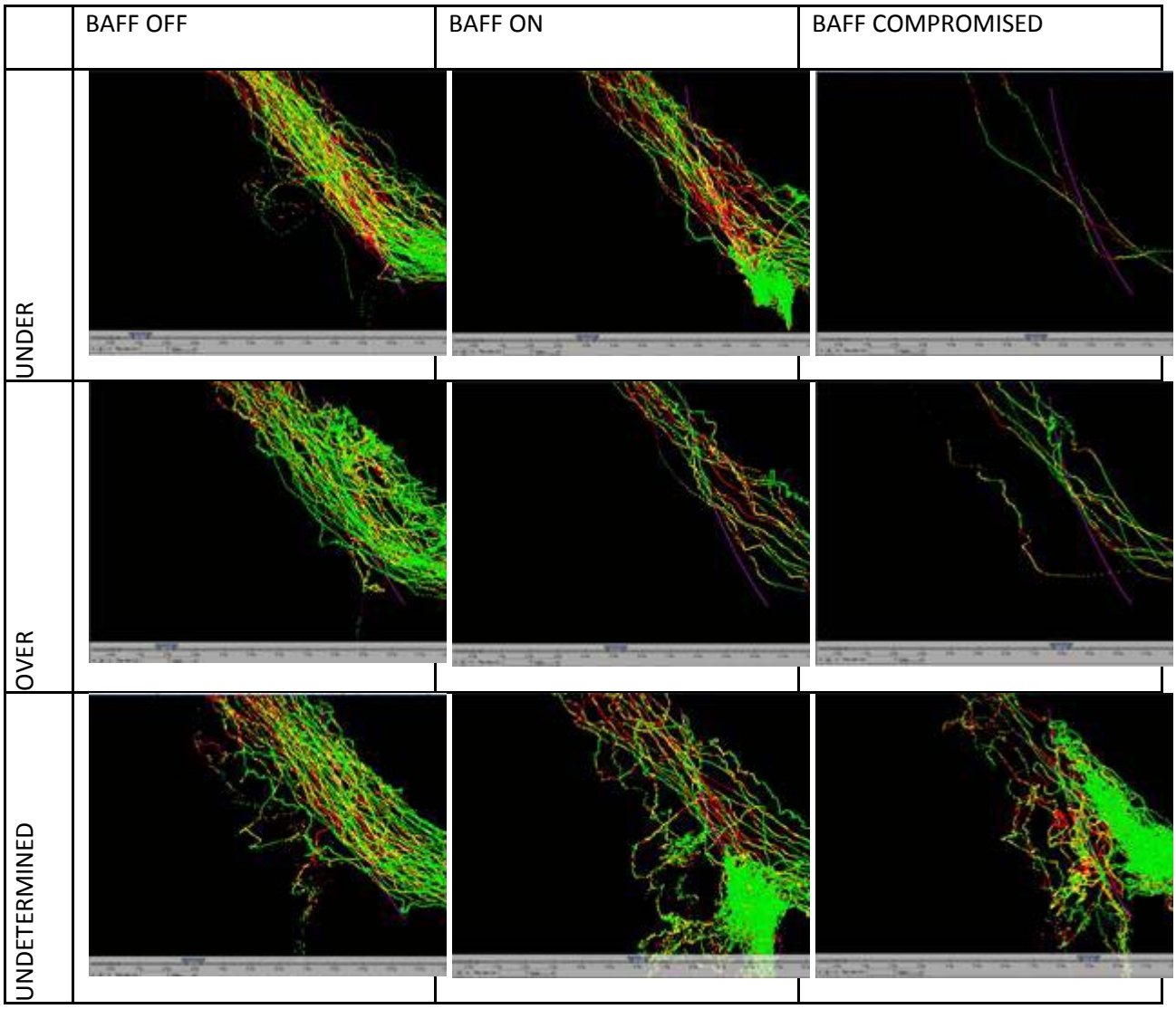

Figure ___. Over/under plots from HTI 3D tracks for BAFF Off, BAFF On, and BAFF Compromised conditions, Georgiana Slough, 2012.

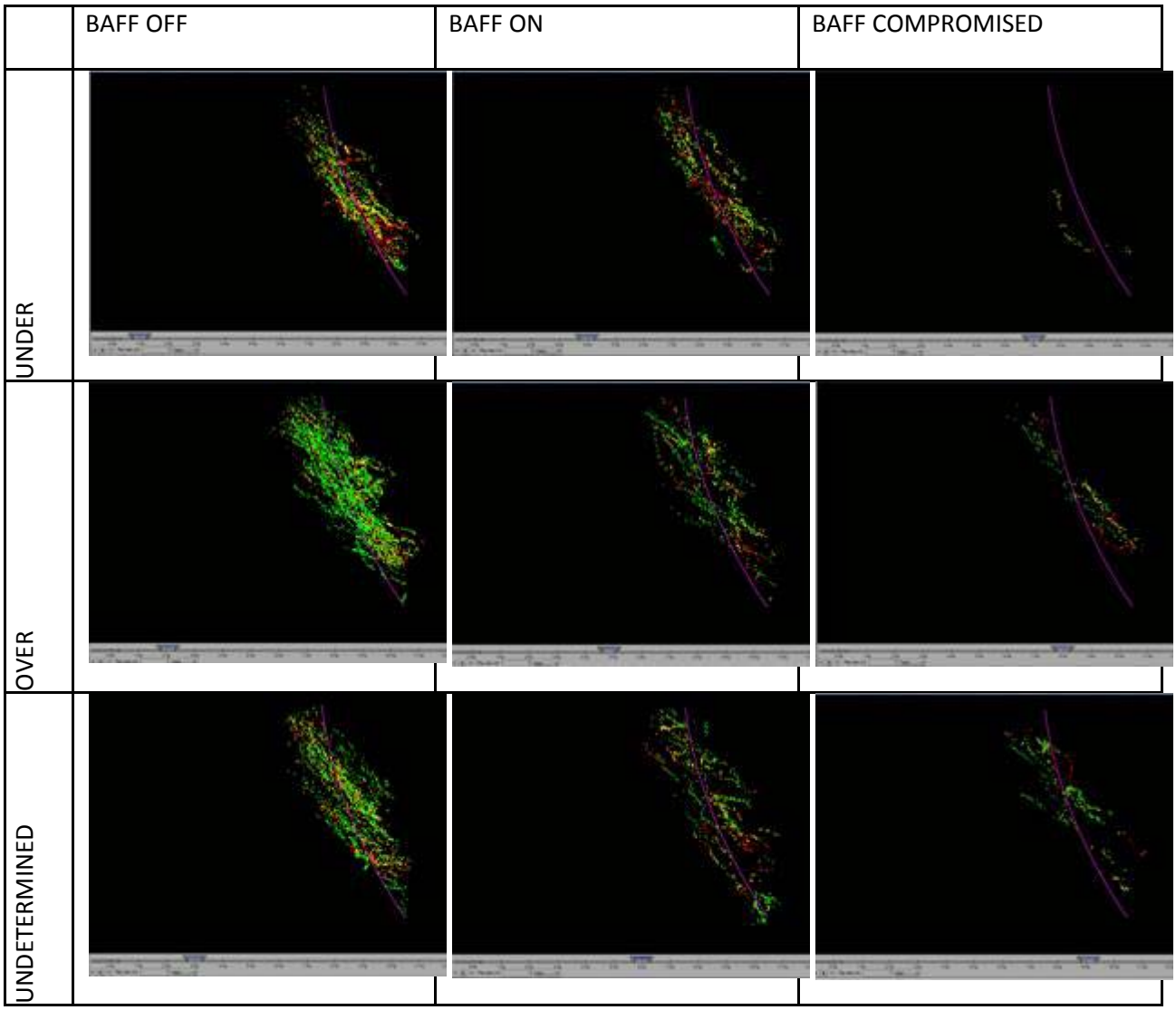

Figure ___. Over/under plots from HTI 3D tracks (arrival time method) for BAFF Off, BAFF On, and BAFF Compromised conditions, Georgiana Slough, 2012.

APPENDIX H

2012 GEORGIANA SLOUGH NON-PHYSICAL BARRIER STUDY
ANALYSES OF TAGGED FISH RELEASED BY THE SACRAMENTO
REGIONAL COUNTY SANITATION DISTRICT

Analyses of Tagged Fish Released by the Sacramento Regional County Sanitation District

Introduction

In addition to the fish released explicitly for the BAFF study, the telemetry network detected acoustically-tagged late-fall Chinook salmon that were released by the Sacramento Regional County Sanitation District (SRCSD) to evaluate their response to the Sacramento Regional Wastewater Treatment Plant (SRWTP). Here, we make use of this additional data by analyzing migration routing and survival as described in Sections 3.5 and 3.6 of the project report. Specifically, fish released by the SRCSD arrived at the junction when the BAFF was on and off, and also while the BAFF was being removed, and after it was completely removed. Our goals were to assess whether migration routing or survival differed between the period when the BAFF structure was in place but not operated (off) versus the period after the BAFF structure was completely removed from the river.

Generalized Linear Models of Fish Entrainment

Methods

Telemetry data were analyzed using logistic regression models following the methods described in Section 3.5 of this report. Fish released by the SRCSD arrived at the junction when the BAFF was on, off, being removed, and completely removed. We performed two model selection analyses: one that compared periods of BAFF on and BAFF off, and the other that compared BAFF off with the BAFF removed.

Results

River Conditions and BAFF Operation

Fish releases from the SRWTP started on the 18th of April 2012 and continued until the 2nd of May 2012. A total of 302 fish were released; of these 190 fish were detected at the study area; this result showed that 37.1% of Chinook juveniles released never arrived at the GS study site. This percentage includes fish that were eaten, fish that moved upstream and used another route, and tags that failed.

Of the fish that arrived in the array 58 were classified as eaten upstream and four never exited the array, leaving 128 fish for the analyses. Of these 128 fish, 22 entered the array when the BAFF was off, 48 entered the array when the BAFF was on, 34 entered the area when the BAFF was being removed, and 24 entered the array when the BAFF was no longer in place (Figure H-1,Table H-1). Of the 128 fish used in the analyses, only 14 were entrained into Georgiana Slough.

Results were consistent with previous findings in Section (X-x). A lower percentage of fish entered Georgiana Slough when the BAFF was on (Table H-1). Only 6% of the fish that encountered the BAFF in the on state entered Georgiana Slough, whereas 23% of the fish that encountered the BAFF in the off

state were entrained into Georgian Slough (Table H-1). Interestingly, only 8% of the fish entering the study area after the BAFF had been completely removed were entrained into Georgiana Slough, 15 percentage points lower than the percentage of fish that were entrained into Georgiana Slough when the BAFF was off.

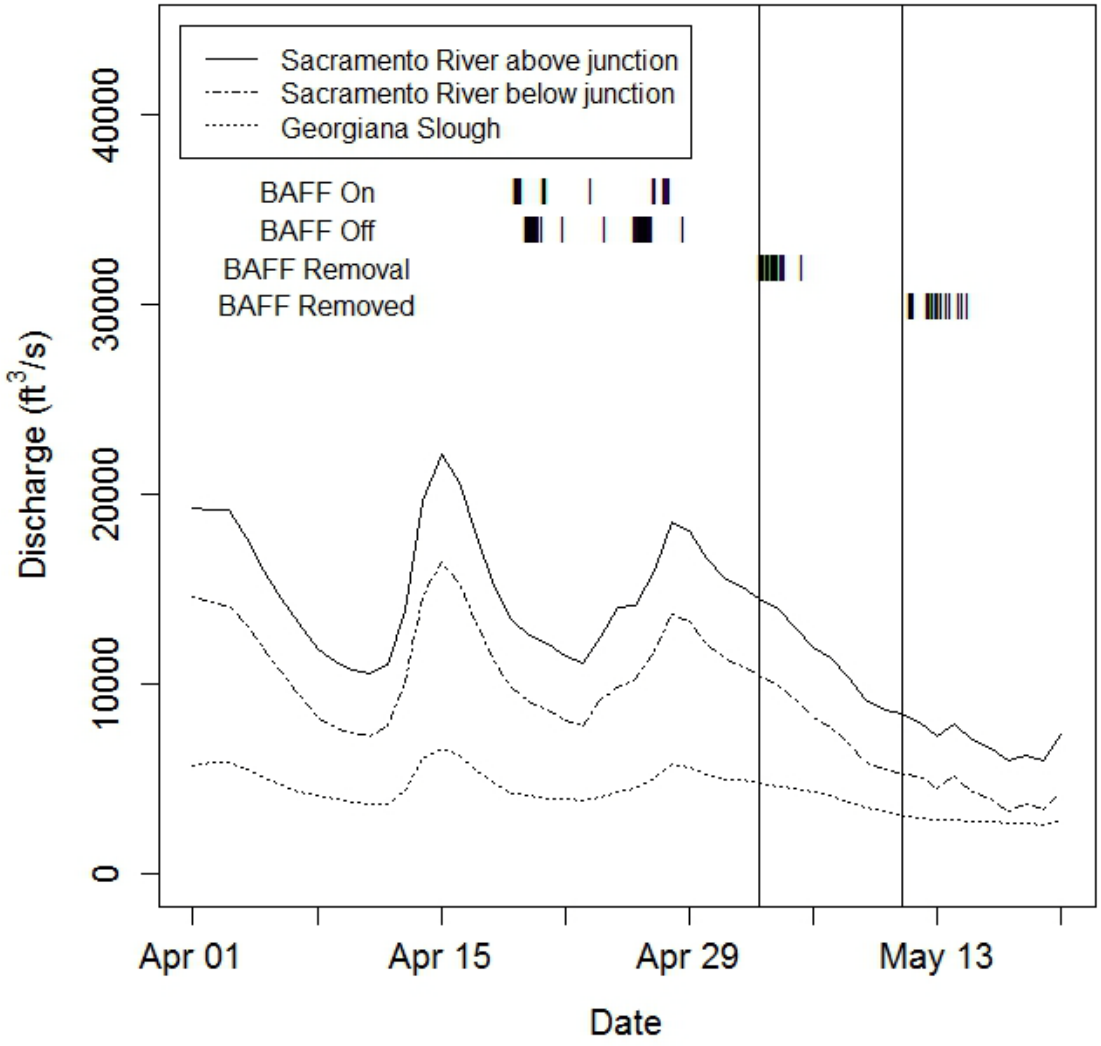

Notes: The small vertical hash marks indicate the presence of a fish in the study area and the status of the BAFF. The two vertical lines indicate the time at which removal of the BAFF began and the time at which the BAFF had been completely removed.

Figure H-1 River discharge for the Sacramento River and Georgiana Slough with arrival times of fish and BAFF status.

Table H-1 Numbers and percentages of SRCSD fish entering each route during all BAFF operational states				
	Off	**On**	**Removal**	**Removed**
Sacramento River	17 (77%)	45(94%)	30 (88%)	22 (92%)
Georgiana Slough	5(23%)	3(6%)	4 (12%)	2 (8%)

Model Selection

BAFF On Compared to BAFF Off

Model selection results for the comparison of BAFF on and BAFF off suggested that BAFF operation (B) was the best explanatory variable of entrainment when comparing all single-variable models (Table H-2). However over all models the intercept-only model, which estimates a single mean entrainment probability, was the best fitting model (Table H-2). The intercept-only model was followed closely by the single variable model that included *B* (Table H-2). All other variables considered were not supported by BIC criteria. Models including interactions did not provide a better fit to the data than the single variable model.

Table H-2
Model Selection Results for Logistic Regression Expressing the Probability of juvenile Chinook Entering Georgiana Slough as a Function of Covariates For BAFF Off and BAFF On States

Model	Group	Number of Variables	NLL	BIC	Group ΔBIC	Overall ΔBIC
*B + S + B * S*	1	3	21.24	59.47	0	5.47
*B + X + B * X*	1	3	22.19	61.38	1.91	7.38
*B + Q + B * Q*	1	3	22.23	61.45	1.98	7.45
B + S + Q + X + D	3	5	21.21	67.9	0	13.9
B + S + Q + D	4	4	21.34	63.92	0	9.92
B + S + X + D	4	4	21.46	64.17	0.25	10.17
B + Q + X + D	4	4	21.66	64.57	0.65	10.57
B + S + Q + X	4	4	22.12	65.49	1.58	11.49
S + Q + X + D	4	4	23.75	68.75	4.83	14.75
B + S + D	5	3	21.51	60.01	0	6.01
B + Q + D	5	3	21.87	60.74	0.73	6.74
B + S + X	5	3	22.21	61.42	1.41	7.42
B + S + Q	5	3	22.24	61.46	1.45	7.46
B + Q + X	5	3	22.43	61.86	1.84	7.86
B + X + D	5	3	22.64	62.27	2.26	8.27
S + X + D	5	3	23.81	64.61	4.6	10.61
Q + X + D	5	3	23.89	64.78	4.77	10.78
S + Q + D	5	3	24.25	65.5	5.48	11.5

Table H-2 Model Selection Results for Logistic Regression Expressing the Probability of juvenile Chinook Entering Georgiana Slough as a Function of Covariates For BAFF Off and BAFF On States						
Model	Group	Number of Variables	NLL	BIC	Group ΔBIC	Overall ΔBIC
S + Q + X	5	3	24.39	65.78	5.77	11.78
B + S	6	2	22.28	57.3	0	3.3
B + Q	6	2	22.6	57.95	0.65	3.95
B + D	6	2	22.67	58.09	0.79	4.09
B + X	6	2	22.96	58.67	1.37	4.67
X + D	6	2	24.22	61.19	3.89	7.19
S + D	6	2	24.25	61.25	3.95	7.25
S + X	6	2	24.4	61.54	4.24	7.54
Q + D	6	2	24.41	61.57	4.27	7.57
Q + X	6	2	24.47	61.68	4.38	7.68
S + Q	6	2	24.76	62.27	4.97	8.27
B	7	1	23.01	54.52	0	0.52
D	7	1	24.52	57.54	3.02	3.54
X	7	1	24.57	57.63	3.11	3.63
S	7	1	24.78	58.05	3.53	4.05
Q	7	1	24.86	58.22	3.7	4.22
Intercept only	7	0	24.88	54	0	0

We selected the single variable model that included BAFF operation as the final model given the purpose of the study and similar support by model selection criteria (Table H-5). The coefficient for the BAFF operation (*B*) suggested that entrainment into Georgiana Slough would decrease when the BAFF was turned on, which is consistent with results from the 2011 study and the 2012 study described in previous sections of this report. Predicted probability of entrainment into Georgiana Slough when the BAFF was off was 0.23 and 0.06 when the BAFF was on.

Table H-3 Parameter Estimates for the Best-Fit Model for juvenile Chinook Salmon			
Variable	Parameter Estimate	Standard Error	95% Confidence Interval
Intercept (Off)	-1.224	0.509	-2.336, -0.296
B	-1.484	0.784	-3.156, 0.023
Notes: Variables defined as follows: *B* = BAFF operation (Off = 0, On=1). The reference group for the intercept is *B* = off.			

BAFF Off compared to BAFF removed

Model selection for the comparison of BAFF off and BAFF removed suggested that the intercept-only model provided the best fit to the data followed by BAFF operation (*B,* Table H-4). Single-variable models including river discharge (*Q*), streakline (*S*), and cross-stream position (*X*) were supported similarly by BIC, but all received less support than *B*. We were not able to include the day-night variable (*D*) due to inadequate sample size. No fish entered Georgiana Slough at night when the BAFF was off, nor did they enter Georgiana Slough at night after the BAFF had been removed.

Table H-4
Model Selection Results for Logistic Regression Expressing the Probability of juvenile Chinook Entering Georgiana Slough as a Function of Covariates For BAFF Off and BAFF Removed States

Model	Group	Number of Variables	NLL	BIC	Group ΔBIC	Overall ΔBIC
*B + S + B * S*	1	3	18.08	51.47	0	8.41
*B + X + B * X*	1	3	18.38	52.08	0.62	9.02
*B + Q + B * Q*	1	3	18.44	52.2	0.73	9.14
B + S + Q + X	4	4	18.34	55.82	0	12.76
B + S + X	5	3	18.34	51.99	0	8.93
B + Q + X	5	3	18.39	52.09	0.1	9.03
B + S + Q	5	3	18.58	52.47	0.48	9.41
S + Q + X	5	3	18.8	52.92	0.93	9.86
B + X	6	2	18.44	48.36	0	5.3
B + Q	6	2	18.59	48.67	0.3	5.61
B + S	6	2	18.6	48.68	0.32	5.62
S + Q	6	2	19.05	49.59	1.22	6.53
Q + X	6	2	19.17	49.82	1.46	6.76
S + X	6	2	19.56	50.61	2.25	7.55
B	7	1	18.68	45.01	0	1.95
Q	7	1	19.3	46.26	1.25	3.2
S	7	1	19.58	46.82	1.81	3.76
X	7	1	19.6	46.85	1.85	3.79
Intercept only	7	0	19.62	43.06	0	0

We present parameter estimates from the single-variable model that included BAFF operation (Table H-5). The coefficient for BAFF operation (*B*) suggested that entrainment into Georgiana Slough decreased after the BAFF was removed. Greater percentages of fish entered Georgiana Slough when the BAFF was

off versus when the BAFF was removed. The estimated probability of entering Georgiana slough when the BAFF was off was 0.23 and 0.08 after the BAFF was removed.

Table H-5
Parameter Estimates for the Best-Fit Model for juvenile Chinook Salmon

Variable	Parameter Estimate	Standard Error	95% Confidence Interval
Intercept (Off)	-1.224	0.509	-2.336, -0.296
B	-1.174	0.897	-3.202, 0.487

Notes:

Variables defined as follows: *B* = BAFF operation (Off = 0, Removed=1). The reference group for the intercept is *B* = off.

Discussion

Given the small sample size available for this analysis, it is not surprising that simpler models with few covariates were selected over more complex models. In short, cross-stream position and river discharge were not deemed important by model selection owing to small sample size and a limited range of conditions to which fish were exposed. Nonetheless, our comparison of BAFF on and BAFF off was consistent with the results from the 2011 and 2012 BAFF studies.

The comparison between BAFF off and BAFF removed time periods yielded results that were somewhat unexpected. A greater proportion of fish entered Georgiana Slough when the BAFF was off and in place, as opposed to when the BAFF was completely removed. However, it is important to note that this effect was not strong enough to be selected over the intercept-only model due to small sample size. Furthermore, differences between BAFF off and BAFF removed may have been caused by differences in environmental conditions rather than effects of the BAFF structure. For example, river discharge declined after the BAFF was removed, which may have influenced entrainment probabilities (Figure H-1). Because this analysis was not designed to control for confounding effects of treatment and environmental conditions, assigning causal mechanisms to our findings should be avoided.

Route Entrainment and Survival Models of SRCSD Fish

Methods

Two alterations were made to determinations from the Fish Fates Conference. First, fish that were classified as "Predation unknown" at the Fish Fates Conference were assumed to have been live tagged salmonids, and their determination was changed to "Not Eaten". Second, the BAFF operation status of "Potentially Impaired" was changed to "On". Fish that were within the study area when the BAFF state was changed were eliminated from the analyses. In total 69 SRCSD fish were used for comparisons of BAFF on and BAFF off treatments and 46 fish were used for the comparison between BAFF off and BAFF removed treatments. In order to utilize the same model used for the main study, we set survival from release to the study area to one. This allowed us to make comparisons of BAFF off and BAFF removed treatments.

Results

Detection probabilities of fish entering the array were high. Detections probabilities were all perfect except for the downstream Sacramento River nodes (Tables H-6, H-7, H-8, H-9). Site S_2 had the lowest detection probabilities for both comparisons. A greater proportion of fish arrived at the array during BAFF on treatments than when the BAFF was off (ω_{on} = 0.68). Approximately equal proportions of fish passed through the array after the BAFF had been removed and when the BAFF was off ($\omega_{removed}$ = 0.52). The probability of entering Georgiana Slough ($\Psi_{G,on}$) was 0.016 with the BAFF on and 0.088 with the BAFF off (Table H-10). The probability of entering Georgiana Slough ($\Psi_{G,removed}$) was 0.083 with the BAFF removed (Table H-11).

We found little difference in survival between BAFF on and BAFF off. Differences between survival for BAFF on and BAFF off treatments were small for fish migrating through the Sacramento River. For Georgiana Slough, we observed differences between BAFF on and BAFF off, but confidence intervals were extremely wide for BAFF off and could not be estimated for BAFF on because all 3 fish survived (Table H-10).When the BAFF was removed survival was very low in Georgian Slough (0.500), but only two fish entered Georgiana Slough after the BAFF was removed, which led to large confidence intervals for this estimate (0.038 to 0.962). Otherwise, survival was similar among routes and BAFF states.

Discussion

As with the previous findings in this study and the 2011 study, the BAFF influenced route entrainment. While the BAFF was on, fewer fish entered Georgiana Slough. In addition fewer fish entered Georgiana Slough after the BAFF had been removed than when the BAFF was off. However there were temporal differences in conditions that may have led to this result, such as different flows and cross-stream positions of fish entering the study area.

Survival estimates were consistent with previous estimates in this study for the Sacramento River, but survival from the array to the downstream Georgiana Slough nodes was affected by very low sample

size. Survival estimates ranged from 1.0 to 0.5 between treatments. Evidence of this can be found in the confidence intervals for these survival estimates.

Table H-6
Detection History Frequencies Used in the Mark-Recapture Model to Estimate Survival, Detection, and Route-Entrainment Probabilities for SRCSD Late-Fall Chinook Salmon Released in Spring 2012 for BAFF On/Off Operations

Model	Detection History Overall	Frequency
Overall model	*1 0 S*	0
	1 0 G	0
	1 Soff 0	4
	1 Soff S	13
	1 Son 0	12
	1 Son S	32
	1 Goff 0	1
	1 Goff G	4
	1 Gon 0	0
	1 Gon G	3
Sacramento double array model	*S1 0*	1
	0 S2	0
	S1 S2	44
Georgiana double array model	*G1 0*	0
	0 G2	0
	G1 G2	7

Table H-7 Detection History Frequencies Used in the Mark-Recapture Model to Estimate Survival, Detection, and Route-Entrainment Probabilities for SRCSD Late-Fall Chinook Salmon Released in Spring 2012 for BAFF Off/Removed Operations		
Model	Detection History Overall	Frequency
Overall model	*1 0 S*	0
	1 0 G	0
	1 Soff 0	4
	1 Soff S	13
	1 Sremoved 0	3
	1 Sremoved S	19
	1 Goff 0	1
	1 Goff G	4
	1 Gremoved 0	1
	1 Gremoved G	1
Sacramento double array model	*S1 0*	4
	0 S2	1
	S1 S2	27
Georgiana double array model	*G1 0*	0
	0 G2	0
	G1 G2	5

Table H-8 Estimates of Detection Probabilities and Standard Errors for All Telemetry Stations for acoustically monitored SRCSD Late-Fall Chinook Salmon Released in Spring 2012 for BAFF On/Off Operations		
Station	Detection Probability	Standard Error
P_1	1.000	NA
P_S	1.000	NA
P_{S1}	1.000	NA
P_{S2}	0.978	0.022
P_G	1.000	NA
P_{G1}	1.000	NA
P_{G2}	1.000	NA
Notes: P_S and P_G are the overall detection probabilities calculated from estimates of each detection location detection probability (P_{S1}, P_{S2} and P_{G1}, P_{G2}, respectively). Estimates with NA for the standard error indicate that the detection probability was set to 1.0 because all fish were detected.		

Table H-9
Estimates of Detection Probabilities and Standard Errors for All Telemetry Stations for acoustically monitored SRCSD Late-Fall Chinook Salmon Released in Spring 2012 for BAFF Off/Removed Operations

Station	Detection Probability	Standard Error
P_1	1.000	NA
P_S	0.995	0.005
P_{S1}	0.964	0.035
P_{S2}	0.871	0.060
P_G	1.000	NA
P_{G1}	1.000	NA
P_{G2}	1.000	NA

Notes:
P_S and P_G are the overall detection probabilities calculated from estimates of each detection location detection probability (P_{S1}, P_{S2} and P_{G1}, P_{G2}, respectively). Estimates with NA for the standard error indicate that the detection probability was set to 1.0 because all fish were detected.

Table H-10
Survival and Route Entrainment Probabilities for BAFF On/Off Operations for Late-Fall Juvenile SRCSD Chinook Salmon released in Spring 2012

BAFF Operation	Reach/Route	Survival Probability ($S_{h,n}$)		Route Entrainment Probability ($\Psi_{h,n}$)	
		Estimate (SE)	95% CI	Estimate (SE)	95% CI
NA	Release to Array	1	NA	NA	NA
On	Sacramento River	0.727(0.067)	0.585, 0.844	0.936 (0.036)	0.843, 0.984
Off		0.765 (0.103)	0.535, 0.920	0.773 (0.089)	0.574, 0.912
On	Georgiana Slough	1	NA	0.064 (0.036)	0.016, 0.157
Off		0.800 (0.179)	0.372, 0.987	0.227 (0.089)	0.088, 0.426

Notes:
Survival was estimated from the start line of the array to peripheral hydrophones located in either the Sacramento River or Georgiana Slough. Confidence intervals (CIs) were estimated with profile likelihood methods. SE = Standard Error

Table H-11
Survival and Route Entrainment Probabilities for BAFF Off/Removed Operations for Late-Fall Juvenile Chinook Salmon Released in Spring 2012

BAFF Operation	Reach/Route	Survival Probability ($S_{h,n}$)		Route Entrainment Probability ($\Psi_{h,n}$)	
		Estimate (SE)	95% CI	Estimate (SE)	95% CI
NA	Release to Array	1	NA	NA	NA
Removed	Sacramento River	0.868 (0.074)	0.686, 0.970	0.917 (0.056)	0.764, 0.986
Off		0.768 (0.103)	0.537, 0.925	0.773 (0.089)	0.574, 0.912
Removed	Georgiana Slough	0.500 (0.354)	0.038, 0.962	0.083 (0.056)	0.014, 0.236
Off		0.800 (0.179)	0.372, 0.987	0.227 (0.089)	0.088, 0.426

Notes:
Survival was estimated from the start line of the array to peripheral hydrophones located in either the Sacramento River or Georgiana Slough. Confidence intervals (CIs) were estimated with profile likelihood methods. SE = Standard Error